9-2006

Structural Analysis of the Rigidizable Inflatable Get-Away-Special Experiment

Anna E. Gunn-Golkin

STRUCTURAL ANALYSIS OF THE RIGIDIZABLE INFLATABLE GET-AWAY-SPECIAL EXPERIMENT

THESIS

Anna E. Gunn-Golkin, Second Lieutenant, USAF

AFIT/GA/ENY/06-S01

DEPARTMENT OF THE AIR FORCE
AIR UNIVERSITY

AIR FORCE INSTITUTE OF TECHNOLOGY

Wright-Patterson Air Force Base, Ohio

AFIT/GA/ENY/06-S01

STRUCTURAL ANALYSIS OF THE RIGIDIZABLE INFLATABLE GET-AWAY-SPECIAL EXPERIMENT

THESIS

Presented to the Faculty

Department of Aeronautics and Astronautics

Graduate School of Engineering and Management

Air Force Institute of Technology

Air University

Air Education and Training Command

In Partial Fulfillment of the Requirements for the

Degree of Master of Science in Astronautical Engineering

Anna E. Gunn-Golkin, B.S.

Second Lieutenant, USAF

September 2006

AFIT/GA/ENY/06-S01

STRUCTURAL ANALYSIS OF THE RIGIDIZABLE INFLATABLE GET-AWAY-SPECIAL EXPERIMENT

Anna E. Gunn-Golkin, B.S.
Second Lieutenant, USAF

Approved:

Dr. Richard G. Cobb (Chairman)	date
Dr. Michael L. Heil (Member)	date
Maj Eric D. Swenson (Member)	date

Abstract

The purpose of this research was to validate the structural integrity of the Rigidizable Inflatable Get-Away-Special Experiment (RIGEX) and make appropriate improvements to the design, motivated by static and dynamic analysis results. RIGEX is designed to advance the use of rigidizable inflatable structures in the space environment by providing three sets of on-orbit test data on the structural characteristics of three thermoplastic composite tubes. This thesis discusses the RIGEX structural analysis. The term structural analysis refers to the development of a detailed finite element model and the tests for which the model was used. The finite element model provided an acceptable estimation of RIGEX's natural frequencies, the structural integrity of the fastener system, the maximum stress seen by the aluminum primary structure, and the maximum possible displacements at various locations around the RIGEX structure for various load conditions. These three analyses motivated numerous design changes, which are discussed in detail in this thesis. The analysis process was repeated following each design change until all structural integrity and design criteria were met. In addition to the structural analysis and associated design changes, this thesis presents the *as built* RIGEX drawing package and wiring schematic.

The results presented in this thesis are the first step towards passing the structural integrity requirements set forth by the National Aeronautics and Space Administration (NASA) for manned spaceflight. Recommendations of appropriate construction and testing techniques to ensure the actual structure matches the computer model are discussed.

Acknowledgments

I would like to express my sincere appreciation to my thesis advisor, Dr. Richard Cobb, for his support and guidance for the RIGEX project. I would also like to thank Major Eric Swenson for shining some light on finite element analysis. Additionally, the RIGEX project would not be possible without the ongoing support of Mr. Wilbur Lacy and Mr. Jay Anderson. Their insights into laboratory work have kept the RIGEX team safe and successful during all varieties of tests. To the folks at the AFIT shop, especially Jason Vangel, thanks for facilitating countless changes to the RIGEX design. The drawings presented in this thesis really are the final versions, I promise.

Thanks also go to past RIGEX researchers, Jeremy Goodwin and Sarah Helms, for taking the time to answer endless questions and facilitate a smooth transition to the new RIGEX team. Mr. Carson Taylor and Mr. Scott Ritterhouse of the Space Test Program are invaluable to the RIGEX program. They offer wisdom beyond their years in mechanical and electrical systems, and with their continued assistance, the RIGEX program is bound to succeed.

Finally, I'd like to thank my family and friends for their valuable support and encouragement.

Anna E. Gunn-Golkin

Table of Contents

Page

ABSTRACT ..... **IV**

ACKNOWLEDGMENTS ..... **V**

LIST OF FIGURES ..... **IX**

LIST OF TABLES ..... **XII**

LIST OF SYMBOLS AND ABBREVIATIONS ..... **XIII**

I. INTRODUCTION **1**

1.1 Motivation for Rigidizable Inflatable Space Structures 2
1.2 Structural Analysis Motivation and Overview 3
1.3 RIGEX Background 4
1.3.1 John D. DiSebastian (10) *7*
1.3.2 Thomas G. Single (42) *8*
1.3.3 Thomas L. Philley (37) *9*
1.3.4 Raymond G. Holstein (18) *10*
1.3.5 Steven N. Lindemuth (22) *11*
1.3.6 David C. Moody (25) *12*
1.3.7 Chad R. Moeller (24) *12*
1.3.8 Sarah K. Helms (17) *13*
1.3.9 Jeremy S. Goodwin *13*
1.3.10 Canister for All Payload Ejections *14*
1.3.11 ANDE *16*
1.4 Research Objectives 17
1.5 Thesis Summary 18

II. LITERATURE REVIEW **21**

2.1 Historical Examples 22
2.2 Structural Analysis of Get-Away-Special Payloads 24
2.2.1 PANSAT *25*
2.2.2 FEGI *26*
2.2.3 VORTEX *29*
2.3 Literature Review Summary 32

III. METHODOLOGY **33**

3.1 Finite Element Method 33
3.1.1 Finite Element Analysis Process *34*
3.1.2 FEMAP and Nastran Software *38*
3.2 Bolt Analysis Method 41
3.2.1 Determining Bolt Strength – Axial Load *43*
3.2.2 Determining Bolt Strength – Shear Pull-Out of Threads *48*
3.2.3 Determining Bolt Strength – Shear Load *49*
3.2.4 Determining Bolt Strength – Combined Loading *49*
3.2.5 Separation Criteria *50*
3.3 Historical RIGEX Finite Element Models 52
3.4 Methodology Summary 57

IV. RIGEX FINITE ELEMENT AND BOLT ANALYSES AND RESULTS **58**

4.1 Finite Element Analysis Introduction 58
4.2 Finite Element Model Design 59
4.3 Modal Analysis and Results 67
4.4 Static Analysis and Results 69
4.4.1 Loads Transferred through Bolts 70
4.4.2 Impact Avoidance through Translation Analysis 74
4.4.3 Structural Strength Analysis – Aluminum Structure 75
4.5 Bolt Analysis Introduction 76
4.6 Bolt Analysis Assumptions 78
4.7 Bolt Analysis Results and Discussion 79
4.7.1 Constraint Bolt Pattern 79
4.7.2 Y-Axis, X-Axis, and Z-Axis Axially Aligned Bolt Patterns 81
4.7.3 Maximally Loaded Shroud Bolt Pattern 83
4.7.4 RIGEX Subsystem Component Constraint Bolts 84
4.8 Analyses and Results Summary 85

V. RIGEX DESIGN 87

5.2 Design Optimization (Bolts) 88
5.3 Bumpers 90
5.4 Pressure Transducer Mounting Blocks 93
5.5 Computer Mounting Scheme 94
5.6 Power Distribution System 96
5.7 Orbiter Electrical Interface 97
5.7.1 Electrical Connection 98
5.7.2 Space Shuttle Orbiter Electrical Emulator 102
5.8 Mass Properties 104
5.9 RIGEX Design Summary 105

VI. CONCLUSIONS AND RECOMMENDATIONS 106

6.1 Future RIGEX Work 106
6.1.1 Acquisition 106
6.1.2 Assembly 106
6.1.3 Power Distribution System Verification 107
6.1.4 Structural Verification and Environmental Testing 108
6.2 Summary and Conclusions 109

APPENDIX A: BOLT ANALYSIS RESULTS 111

APPENDIX B: BOLT ANALYSIS SPREADSHEET 113

APPENDIX C: MATLAB DATA REDUCTION CODE 119

Code for Finding Maximum Loads at Bolt Locations 119
Code for Finding Maximum Deflection of Shroud and Bumpers 124

APPENDIX D: FINAL DRAWING PACKAGE 127

APPENDIX E: FINAL WIRE ROUTING SCHEMATIC 161

APPENDIX F: CONTAINMENT ANALYSIS 176

F.1 Containment Methodology 176
F.2 Oven Containment 178
F.3 Computer Containment 179

APPENDIX G: PHASE II SAFETY DATA PACKAGE 181

Page

BIBLIOGRAPHY **213**

VITA **218**

List of Figures

Page

Figure 1.3-1: Progression of Thermoplastic Composite Tube Deployment 5
Figure 1.3-2: Visual Summary of RIGEX 7
Figure 1.3-3: Philly's RIGEX Quarter Structure 10
Figure 1.3-4: Folded Sub-Tg Tube (Arrow Indicates Coldest Point – inside Fold) 11
Figure 1.3-5: Canister for All Payload Ejections (5) 15
Figure 1.3-6: RIGEX within CAPE (Cut Away View) (40: 21) 16
Figure 2.1-1: Saturn I Rocket Launching from Cape Canaveral (33) 22
Figure 2.1-2: Spider Beam Assembly on Saturn I 1st Stage (14: 4) 23
Figure 2.2-1: NPS's PANSAT (41) 25
Figure 2.2-2: FEGI's Structural Model (44) 27
Figure 2.2-3: FEGI Strut (23) 28
Figure 2.2-4: VORTEX (46: 3) 29
Figure 3.1-1: The RIGEX Geometry Discretized into Finite Elements 34
Figure 3.1-2: Example Finite Elements (45) 36
Figure 3.1-3: FEMAP and NX Nastran Relations 38
Figure 3.1-4: Breathing Mode with Scale Size 1 40
Figure 3.1-5: Breathing Mode with Scale Size 20 41
Figure 3.2-1: UNJ Thread Tolerances (39) 43
Figure 3.3-1: Structural Yield Locations in Holstein's RIGEX FE Model (18) 54
Figure 3.3-2: FE Representation of the First Mode of Holstein's RIGEX Structure (18) 55
Figure 3.3-3: FE Representation of the First Mode Computed from Helm's FE Model (17) 56
Figure 4.2-1: Shroud Bolt Coordinate System Identification (Top View) 60
Figure 4.2-2: Bolts on the RIGEX Structure 61
Figure 4.2-3: RIGEX FE Model without Shroud, Showing Different Mesh Densities 62
Figure 4.2-4: Conjoined Nodes Holding Two RIGEX Plates Together 63
Figure 4.2-5: Computer Mounting Bracket Locations (Point Mass Represented in FE Model at Center of Each Bracket) 65
Figure 4.2-6: Pressure Cylinders and Bolt Locations on a Partial RIGEX FE Model 66
Figure 4.2-7: Final RIGEX Finite Element Model 67
Figure 4.3-1: Relative Deformation at RIGEX First Natural Frequency (185 Hz) – Stress Contours 68
Figure 4.3-2: Relative Deformation at RIGEX Second Natural Frequency (198 Hz) – Stress Contours 68
Figure 4.3-3: Relative Deformation at RIGEX Third Natural Frequency (304 Hz) – Stress Contours 69
Figure 4.4-1: Coarse Mesh RIGEX FE Model (17) 71
Figure 4.4-2: Final RIGEX FE Model 71
Figure 4.4-3: Oven Proximity to Shroud 74

Figure 4.4-4: Maximum Stress on Aluminum 76
Figure 5-1: RIGEX Structural Design Evolution (10 and 15) 87
Figure 5.3-1: Holstein's Snubber Design (17) 91
Figure 5.3-2: Goodwin's Bumper Design (15) 92
Figure 5.3-3: As Built Bumper Design and Arrangement 93
Figure 5.4-1: Three Pressure Transducers for Nitrogen Gas Tanks 94
Figure 5.4-2: Three Pressure Transducers for Thermoplastic Composite Tubes 94
Figure 5.5-1: Computer Mounting Scheme 95
Figure 5.6-1: Power Distribution Unit Concept 96
Figure 5.6-2: Power Distribution Plate 97
Figure 5.7-1: RIGEX/Orbiter Interface Cable Routing 99
Figure 5.7-2: J1 and J2 Cables 99
Figure 5.7-3: Connector Hole Cover Assembly 101
Figure 5.7-4: Connector Hole on CAPE Mounting Plate 101
Figure 5.7-5: Connector Holes on RIGEX Experiment Top Plate 101
Figure 5.7-6: Emulator Electrical Schematic 103
Figure 5.7-7: Emulator Physical Design 103
Figure 5.8-1: Coordinate System 105
Figure D-1: CAPE Mounting Plate View 1 128
Figure D-2: CAPE Mounting Plate View 2 128
Figure D-3: CAPE Mounting Plate View 3 129
Figure D-4: Experiment Top Plate View 1 130
Figure D-5: Experiment Top Plate View 2 130
Figure D-6: Experiment Top Plate View 3 131
Figure D-7: Experiment Top Plate View 4 131
Figure D-8: Large Rib with Computer View 1 132
Figure D-9: Large Rib with Computer View 2 133
Figure D-10: Large Rib with Computer View 3 134
Figure D-11: Large Rib without Computer View 1 135
Figure D-12: Large Rib without Computer View 2 136
Figure D-13: Small Rib with Pin Puller View 1 137
Figure D-14: Small Rib with Pin Puller View 2 138
Figure D-15: Small Rib without Pin Puller View 1 139
Figure D-16: Small Rib without Pin Puller View 2 140
Figure D-17: Oven Mounting Plate View 1 141
Figure D-18: Oven Mounting Plate View 2 141
Figure D-19: Oven Mounting Plate View 3 142
Figure D-20: Oven Mounting Plate View 4 142
Figure D-21: Oven Mounting Plate View 5 143
Figure D-22: Oven Mounting Plate View 6 143
Figure D-23: Oven Mounting Plate View 7 144
Figure D-24: Bottom Rectangular Plate 145
Figure D-25: Inflation Mounting Plate 146
Page
Figure D-26: Oven Bracket Piece 1 147
Figure D-27: Oven Bracket Piece 2 148

Figure D-28: Stabilizing Feet 149
Figure D-29: Lifting Handles 150
Figure D-30: Shroud 151
Figure D-31: Bumper 152
Figure D-32: Power Distribution Plate 153
Figure D-33: Experiment Pressure Transducer Mounting Block Piece 1 154
Figure D-34: Experiment Pressure Transducer Mounting Block Piece 2 155
Figure D-35: Nitrogen Tank Pressure Transducer Mounting Block Piece 1 156
Figure D-36: Nitrogen Tank Pressure Transducer Mounting Block Piece 2 157
Figure D-37: Solenoid Mounting Block 158
Figure D-38: Computer Mounting Plate 159
Figure D-39: Connector Hole Cover 160
Figure E-1: Definition of RIGEX Bay Numbers 161
Figure E-2: Power Distribution Plate 162
Figure E-3: Oven Relay Circuit 162
Figure E-4: Oven Circuit Explanation 163
Figure E-5: Oven Circuit 163
Figure E-6: Pin Puller 1 164
Figure E-7: Pin Puller 2 164
Figure E-8: Pin Puller 3 165
Figure E-9: Transformers and Piezoelectric Patches 166
Figure E-10: Solenoids 167
Figure E-11: Nitrogen Gas Tank Pressure Transducer 168
Figure E-12: Experiment Pressure Transducer 168
Figure E-13: Accelerometer Thermocouple and LED Explanation 169
Figure E-14: Experiment Bay 3 170
Figure E-15: Structure Thermocouple 171
Figure E-16: Cameras 171
Figure E-17: Computer Bay Wire Routing Totals 172
Figure E-18: Experiment Bay 1 Wire Routing Totals 172
Figure E-19: Experiment Bay 2 Wire Routing Totals 173
Figure E-20: Experiment Bay 3 Wire Routing Totals 173
Figure E-21: Oven Mounting Plate Wire Routing Totals 174
Figure E-22: Oven Wire Routing Totals 174
Figure E-23: Wire Routing within PC-104 Computer 175

List of Tables

Page
Table 1. List of Components Included as Point Masses 64
Component 64
Table 2. List of Limit Loads (6) 70
Table 3. Maximum Loads from FEA of RIGEX Structure under Limit Loads 73
Table 4. Constraint Bolt Margins with Full Torque Range (456-616 in-lbs) 80
Table 5. Constraint Bolt Separation Margin with Limited Torque Range (506-563 in-lbs) 81
Table 6. Y-Axis Axial Bolt Margins 59-73 in-lbs Torque Range 81
Table 7. X-Axis Axial Bolt Margins 59-73 in-lbs Torque Range 82
Table 8. Z-Axis Axial Bolt Margins 60-74 in-lbs Torque Range 82
Table 9. Shroud Bolt Margins 36-44 in-lbs Torque Range 83
Table 10. RIGEX Fastener Locations and Types 90
Table 11. Structural Verification and Environmental Testing Requirements 108
Table A1. Computer to CMP Bolts: Torque Range 141-173 in-lbs 111
Table A2. CMP to Rib Bolts: Torque Range 63-69 in-lbs 111
Table A3. Power Distribution Plate to Rib: Torque Range 62-67 in-lbs 111
Table A4. Ovens to Oven Mounting Plate: Torque Range 61-75 in-lbs 112
Table A5. Oven Mounting Brackets to Oven Mounting Plate: Torque Range 60-75 112
Table B1. PASS/FAIL and Torque Overview 113
Table B2. All Inputs (Bolt) 114
Table B3. All Inputs (From FEMAP) 114
Table B4. Preload Calculations 115
Table B5. Strength Criteria 116
Table B6. Cross Sectional Area Calculations for Thread Shear 117
Table B7. Stiffness Calculations 117
Table B8. Separation Criteria 118
Table D1. Drawing List 127

List of Symbols and Abbreviations

Symbol or Abbreviation – Definition

ΔL_b – Change in Bolt Length

ΔL_j – Change in Joint Length

Δt – Change in Temperature

$\{\phi_i\}$ – Eigenvectors (Mode Shapes)

$\varnothing$ – Stiffness Parameter

ρ – Coefficient of Thermal Expansion

ω – Natural Frequency

λ_i – Eigenvalues

A - Ampere

A_c – Area of Equivalent Cylinder for Joint Representation

Al – Aluminum

AS – Aerospace Standard

A_{si} – Shear Area of Internal Threads

A_t – Tensile Stress Area

AWG – American Wire Gauge

C – Celsius

CAD – Computer Aided Design

CAPE – Canister for All Payload Ejections

CDR – Critical Design Review

CHUG – CAPE Hardware Users Guide

CMP – Computer Mounting Plate

CRES – Corrosion Resistant Stainless Steel

D_B – Bolt Head Diameter

D_e – Major Diameter of Internal Threads

D_e^{bsc} – Basic Major Diameter

D_H – Untapped Bolt Hole Diameter

DoD – Department of Defense

DOF – Degrees of Freedom

E – Modulus of Elasticity

{f} – Vector of Applied Forces

F – Fahrenheit

FE – Finite Element

FEA – Finite Element Analysis

FEGI – Field Emission Get-Away-Special Investigation

FEMAP – Finite Element Modeling and Post-Processing Software

F_{su} – Ultimate Shear Strength

F_{tu} – Ultimate Tensile Strength

F_{ty} – Tensile Yield Strength

g – Gravitational Acceleration

GAS – Get-Away-Special

Hz - Hertz

I – Moment of Inertia

in – inch

IVT – Interface Verification Test

JSC – Johnson Space Center

[K] – System Stiffness Matrix

kg - Kilogram

K_{typ} – Typical Nut Factor

kΩ – kilo-ohm

l – Length

lb – Pound

LED – Light Emitting Diode

L_g – Grip Length

L_e – Length of Thread Engagement

[M] – Mass Matrix

m – Meter

MPa – Mega-Pascal

MSFC – Marshall Space Flight Center

N – Newton

n – Loading Plane Factor

NAS – National Aerospace Standard

NASA – National Aeronautics and Space Administration

n_o – Threads per Inch

NPS – Naval Postgraduate School

NSTS – National Space Transportation System

P – Maximum Axial Bolt Load

Pa – Pascal

PANSAT – Petite Amateur Navy Satellite

P_{As} – Axial Load Allowable Due to Thread Shear

P_{At} – Axial Load Allowable Due to Tension

P_{Aty} – Tensile Yield Allowable

P_b – Axial Bolt Load

PDP – Power Distribution Plate

P_{thr}^{neg} – Negative Thermal Load

P_{thr}^{pos} – Positive Thermal Load

P_{sep} – Bolt Separation Load

PZT – Piezoelectric Transducer Patch

R_a – Ratio of Axial Load to Axial Load Allowable

Rad – Radian

RFQ – Request for Quote

RIGEX – Rigidizable Inflatable Get-Away-Special Experiment

R_s – Ratio of Shear Load to Shear Load Allowable

s – Second

SDRC – Structural Dynamics Research Corporation

SEP – Systems Engineering Process

SF – Safety Factor

SF_{sep} – Separation Factor of Safety

STD – Standard

STP – Space Test Program

STS – Space Transportation System

SVP – Structural Verification Plan

T - Total Joint Thickness

TD_e – Tolerance on Major Diameter of External Threads

TE_i – Tolerance on Pitch Diameter of Internal Threads

T_g – Glass Transition Temperature

T_{max} – Maximum Torque Applied

T_{min} – Minimum Applied Torque

{u} – Displacement Vector

VORTEX – Vortex Ring Transit Experiment

w – Weight or load

STRUCTURAL ANALYSIS OF THE RIGIDIZABLE INFLATABLE GET-AWAY-SPECIAL EXPERIMENT

I. Introduction

The Department of Defense is becoming increasingly reliant on space technology. Global navigation, weather prediction, and communications have already been transformed through the use of satellites, and the demand for increased space capabilities is in no way waning.

Yet, despite advances in technology and space concepts, the potential uses of the space environment remain limited by launch capabilities. Space lift performance remains modest, constrained by mass and volume. Even the newest Evolved Expendable Launch Vehicles, commissioned by the Air Force to be built by Boeing and Lockheed Martin, have payload envelopes that cannot accommodate larger concept payloads. The Delta IV Heavy is limited to 28,947 lb into geosynchronous transfer orbit, and the Atlas V Heavy can carry only 27,889 lb to that orbit. The Delta IV and Atlas V are further limited by fairing size, of 16.7 ft and 17.7 ft diameter respectively (20). A space structure cannot exceed the volume lift capabilities of these rockets without including some way of altering its own shape once on orbit. Such on-orbit deployment generally calls for expensive and complex mechanisms, which add weight and risk.

Rigidizable inflatable materials offer a path to bypass launch vehicle volume and weight limits by allowing large structures to fold up tightly for launch. Once on orbit, the small, folded package would be subjected to a pressure and inflated. The structure would

take on the form it needs to function as a space asset and then rigidize in its deployed (operational) configuration. The additional payload mass added by the inflation system is small when compared to a similar mechanical deployment system, and an inflation system has fewer possible failure modes than a complex mechanism. By constructing space structures from rigidizable-inflatable materials, payload volume and weight can be cut tremendously, allowing increases in satellite size and capability without requiring greater space lift capabilities.

1.1 Motivation for Rigidizable Inflatable Space Structures

Since Sputnik first orbited the Earth in 1957, space launch has always been an expensive endeavor, limited by the cost of lifting large objects into space. Once a space lift asset is developed, its payloads are limited by the size of the launch vehicle fairing and the mass that its rockets can boost to the prescribed orbit. Inflatable structures have the potential to reduce spacecraft mass and physical dimensions, and in so doing, reduce both payload and launch costs or allow additional capability to be added as a result of the volume and weight savings. Over the last several decades, inflatable structure concepts have been developed and tested, producing enough data to show their potential to provide a low-cost, low-weight alternative to conventional space hardware, with high mechanical packing efficiency and deployment reliability (13). An inflatable structure is one that can be launched into space in its uninflated configuration and then deployed once in orbit by pressurized gas to its intended geometry. On a purely inflatable structure, the pressurization must remain intact to maintain structural stiffness. Unfortunately, due to material imperfections and micrometeorites, small leaks are unavoidable (19). Due to

these leaks, a pressurized gas reserve would be necessary to maintain proper inflation, which would add weight and complexity to the system. Such a large gas reserve would likely negate the mass and volume advantages theoretically offered by an inflatable system.

A solution to this gas leakage problem comes in the form of rigidization. A rigidizable inflatable structure solidifies after inflation, making continued gas pressurization unnecessary. Rigidization reduces mass and volume by eliminating large and costly pressure tanks. Most rigidizable inflatable materials have relatively high strength and stiffness for their mass and uninflated volume, thus they are able to provide structural support for space payloads at a fraction of the classical launch cost.

In order to use rigidizable inflatable structure technology on operational satellites, such technology must first be proven effective in the space environment. Some inflatable structures have flown previously in space. An aluminum laminate inflatable rigidizable has flown as a structural component on a satellite, but all other inflatable rigidizable technologies are yet untested in space (21). Thus, RIGEX will be flown as another step towards the advancement of rigidizable inflatable structures for space. RIGEX will serve as a proof test for tube deployability as well as act as a tool for developing the predictability of rigidizable inflatable structural properties in the space environment.

1.2 Structural Analysis Motivation and Overview

As RIGEX is slated for flight on the space shuttle orbiter, its safety and structural integrity are of the utmost concern to NASA. Structural requirements and criteria way beyond what would normally be expected for basic structural integrity have to be met,

thus a detailed analysis of the structural design of the RIGEX payload was completed to fulfill NASA requirements for launch. NASA must have confidence in the accuracy of analyses that reveal the structure's properties in order to approve its flight on a crewed vehicle.

The first step in RIGEX structural analysis involved developing a structural model. Two models had been previously designed but one was outdated (it did not reflect the current RIGEX design) and the other lacked the detail required for a comprehensive analysis. Finite element modeling techniques were used to build the model in NX Nastran for Finite Element Modeling and Post-Processing (FEMAP) Version 9.0 software. Next, an eigenvalue analysis was done on the RIGEX finite element (FE) model to solve for its first three natural frequencies. Finally, a set of static analyses were executed in order to assess the maximum internal loads seen by the structural bolts. All three steps (developing a RIGEX FE model, modal and static analysis of the FE model, and bolt analysis) were completed to validate the integrity of the RIGEX structural design before construction could begin. The following chapters detail the processes taken and the results obtained from each set of analysis.

1.3 RIGEX Background

The RIGEX program is designed to test the modal properties and deployment capability of an inflatable rigidizable tube in the space environment and then compare that data to similar ground tests. By comparing the two data sets, an algorithm for tube performance prediction can be developed, which is an important step towards furthering the employment of inflatable rigidizable technologies in space. The inflatable rigidizable

tubes, also referred to as thermoplastic composite tubes, are composed of a proprietary three ply carbon fiber composite, designated L5 by their manufacturer, L'Garde Inc (42, 3-2). L5 is designed to remain rigid below a given glass transition temperature (T_g). Above the T_g, which is 125º Celsius (C) for L5, the composite becomes malleable. Thus, when a pressure is added above the T_g, the tube can inflate from its folded, launch configuration, into a straight tube, which could be used in the construction of large space structures. Conceptually, tube inflation and rigidization is shown in Figure 1.3-1.

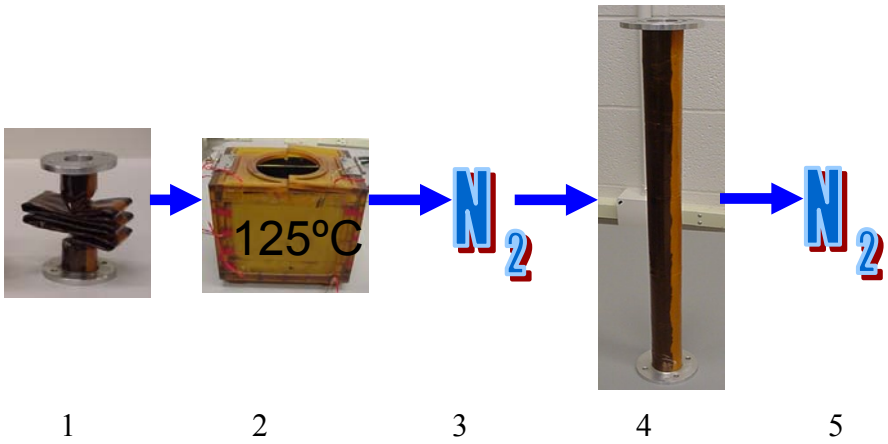

Figure 1.3-1: Progression of Thermoplastic Composite Tube Deployment

1. Folded tube – Sub-T_g Temperature
2. Tube is heated in RIGEX Oven to at least 125º C
3. Nitrogen gas pressure is added to tube
4. Tube inflates, cools, and solidifies (without the need for continued gas pressure)
5. Nitrogen gas is vented

Mounted in the Canister for All Payload Ejections (CAPE) in the space shuttle orbiter, RIGEX will test three of these thermoplastic composite tubes. In three identical, redundant tests, each of these tubes will be independently heated, inflated with gaseous nitrogen (N_2), and rigidized. The N_2 will then be vented and the tubes will be mechanically excited with Piezoelectric Transducer patches (PZTs). An accelerometer

will record the vibration data while a digital camera records the inflation process. The experiment will be recovered with the return of the orbiter for data analysis.

The design and layout of RIGEX is shown in Figure 1.3.2. The experiment is fitted with 8 lifting handles that will be used for ground movement and must be removed before flight. Once these handles are removed, the experiment will be fastened to the CAPE via thirty-two ¼-28 bolts on the CAPE mounting plate. The CAPE mounting plate is a 1.5 inch thick aluminum disk that is considered perfectly rigid with respect to CAPE for all analyses. RIGEX will run off of space shuttle power, and will be controlled via the S-13 switch inside the orbiter's crew compartment. Two large wire bundles will run from the RIGEX power distribution plate (PDP) to the orbiter, and they will be routed through the connector cover atop the CAPE mounting plate. The entire experiment will be encapsulated by a containment shroud. If a thermoplastic composite tube were to break during reentry or landing, the shroud would protect the CAPE from damage. Within the experiment there are four bays of similar proportion. The bays are separated by four ribs. Three of the bays contain identical hardware: a thermoplastic composite tube within an oven, a camera, two LEDs, a heater, a pin puller to release the oven's latching mechanism, and appropriate instrumentation. The fourth bay holds the PC-104 flight computer which will command the experiment, interface with the orbiter, and serve as a data acquisition system. The rectangular area, between the four bays, houses three nitrogen pressure tanks along with other necessary inflation system hardware.

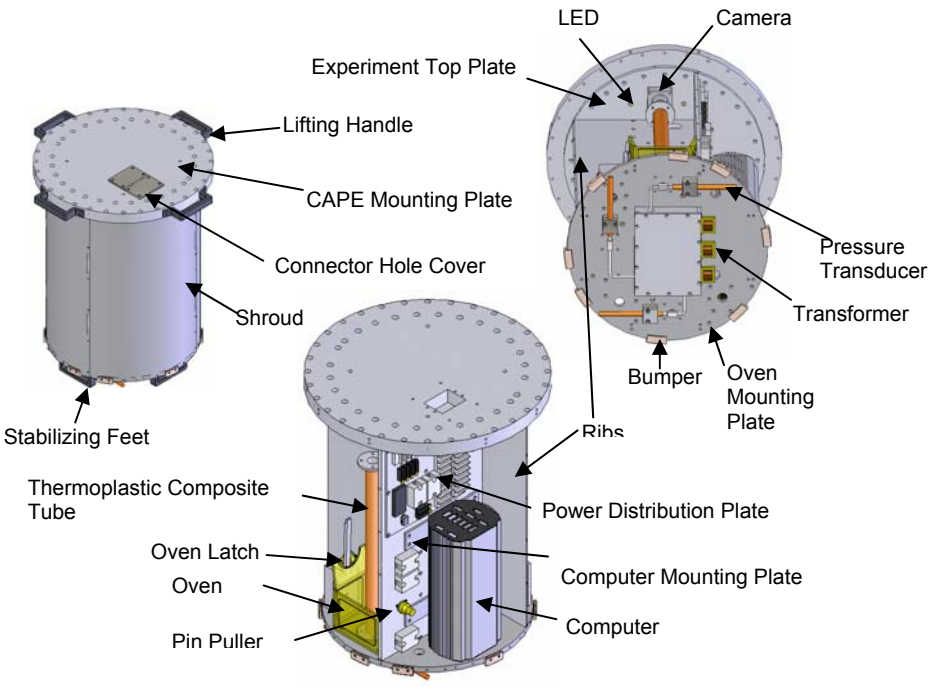

Figure 1.3-2: Visual Summary of RIGEX

Since the inception of the RIGEX program in 2001, nine theses have been written on its development, testing, and analysis. Starting with a broad systems engineering approach to payload development and continuing through detailed design and analysis, the content of these theses is briefly discussed in the following paragraphs.

1.3.1 John D. DiSebastian (10)

In 2001, the RIGEX project was born in John D. DiSebastian's thesis. His thesis outlined RIGEX's preliminary design as well as the systems engineering process used to achieve that design. In his thesis, DiSebastian discussed various systems engineering processes (SEP) that can be used in space system design, and he concluded that the NASA SEP was the best framework for RIGEX. Using the NASA SEP, he defined the

four aspects of the young project: the mission statement, objectives, requirements and constraints. The mission statement for RIGEX, which would drive all future development, is: "To verify and validate ground testing of inflation and rigidization methods for inflatable space structures against a zero-gravity space environment" (10, xi). Based on the correlation between ground and zero-gravity space environment results, an analytic model will be developed to predict how rigidizable inflatable space structures will behave in space.

DiSebastian also went through a generalized selection process to define the components that would be used for the structure, computer, instrumentation, and power distribution. The next step for DiSebastian was design, in which he created a preliminary RIGEX structure in a computer design package. His design adhered to the physical requirements as defined for the Get-Away-Special (GAS) Canister, in which RIGEX was originally designed to fly. The GAS Canister had no way of providing power to the RIGEX and had a smaller payload envelope than the Canister for All Payload Ejections, which the experiment is currently slated to fly in. While the program has changed significantly since 2001, DiSebastian's thesis laid the groundwork for further design and development by providing preliminary analysis and operations concepts.

1.3.2 Thomas G. Single (42)

Thomas G. Single followed DiSebastian on the project by analyzing the thermoplastic composite tubes to be tested on RIGEX. The mission statement put forth by DiSebastian called for ground testing of the rigidizable inflatable tubes to serve as a basis for comparison for the tubes in the zero-gravity space environment. Single's

analyses serve as a preliminary ground test. Through experimental vibration testing, he determined the natural frequencies of vibration and the damping ratios of the tubes. He then excited the deployed and rigidized tubes in both ambient and vacuum conditions using Piezoelectric Transducers. He found that simplified beam bending theory provides a reasonable estimate for the first few modes. He also demonstrated the variation of frequency and damping under vacuum for various temperature conditions. In conditions as close to the space environment as could be simulated in the AFIT lab, Single found the first tube bending mode at 51 Hertz (Hz) and the second and third at 62 and 231 Hz respectively. Single demonstrated that the tube's damping decreases in a vacuum.

1.3.3 Thomas L. Philley (37)

Lee Philley added to Single's ground test data by constructing and testing a RIGEX prototype, including new thermoplastic composite tubes. Most of Philley's tests were conducted on the RIGEX quarter-structure (Figure 1.3-3), which included a rigidizable inflatable tube, inflation hardware, an oven and a camera. Philley's quarter structure was sized to fit in the AFIT vacuum chamber.

Figure 1.3-3: Philly's RIGEX Quarter Structure

Through his testing, Philley concluded that insulation was needed on the heater boxes to prevent heat loss. He also found that gravity significantly affected tube deployment. The operational concept of RIGEX was validated through Philley's work, thus allowing the program to proceed. Philley also provided a new set of ground test data for tube deployment and vibration testing, by exciting new tubes in a variety of configurations.

1.3.4 Raymond G. Holstein (18)

Raymond Holstein developed the first RIGEX finite element model and conducted both analytical analyses and physical tests on RIGEX's response to vibration. Holstein developed FEMs in the finite element analysis (FEA) software ABAQUS for a rigidizable inflatable tube, the quarter structure which Philley used for tube deployment

testing, and the RIGEX prototype model. From these FEMs, Holstein derived expected stresses on the structure at the GAS Canister limit loads. He also ran a FEA to show RIGEX's expected normal modes. Using the GAS canister requirements and constraints as a guide, Holstein developed and implemented a test plan to find the structure's true natural frequencies. While some of Holstein's analytical and experimental results did not match very well (the structure was actually modeled in a backwards configuration), he provided other RIGEX engineers with a working range of expected natural frequencies. Holstein's data allowed the team to proceed with RIGEX development and motivated changes in structural thickness and fastener choice.

1.3.5 Steven N. Lindemuth (22)

In his time at AFIT, Steven Lindemuth constructed a set of GAS Canister RIGEX flight hardware for a single experiment bay, including the 400 psig pressure system. He also determined the heating profile over the surface of the inflation tubes. The heating profile data simplifies the temperature sensing requirements, as it identified the tube's coldest point (Figure 1.3-4). Once the coldest point reached the T_g, the tube can be inflated with no fear of faulty deployment due to incomplete heating.

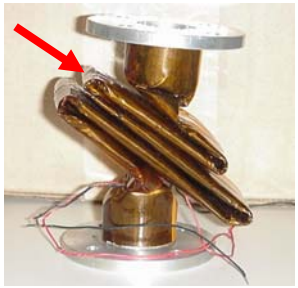

Figure 1.3-4: Folded Sub-Tg Tube (Arrow Indicates Coldest Point – inside Fold)

Lindemuth also identified locations where the pressure system interfered with tube inflation, motivating design modifications. Furthermore, he identified probable leak points within the inflation system, mostly due to the transition from high to low pressure. The large pressure transition is no longer a major issue, as the storage pressure has been reduced from 400 psig to sea level ambient, discussed in Section 1.3.7.

1.3.6 David C. Moody (25)

David Moody, an electrical engineer, designed the first RIGEX computer control and power distribution system. His system design involved two processors. The first processor would control the flow of the experiment and data collection from the pressure transducers, the accelerometers, and the thermocouples. The second computer processor drives image collection from the digital cameras. Moody also developed data analysis software to be used during and after the experiment. His design of the power distribution system was dependant on the autonomous nature of the GAS Canister RIGEX, which required internal 30V battery cells. The power distribution system has also undergone great changes, as RIGEX is now powered and controlled from within the space shuttle orbiter.

1.3.7 Chad R. Moeller (24)

Chad Moeller's thesis research focused on improving the pressurization system and validating the thermoplastic composite tube's cooling profile. The most notable of his pressure system modifications was increasing the volume of the nitrogen gas tank and reducing its internal pressure to ambient, thus substantially reducing the impact of

leakage. During Moeller's tenure, NASA's GAS Canister program was discontinued, replaced by CAPE. The canister switch provoked many changes in the RIGEX design, as the payload envelope, mass requirements, and electrical interface had all changed.

1.3.8 Sarah K. Helms (17)

Sarah Helms focused her thesis research on vibration testing and development of a rudimentary RIGEX structural model. She ran extensive vibration tests on an oven to ensure that it would survive launch and remain functional after exposure to orbiter vibration profiles. While the vibration test was not an acceptance test for the oven hardware, the test allowed RIGEX development to proceed with confidence that the oven would not become a failure mode. She also tested for and found the natural frequencies of the RIGEX engineering model. From the natural frequency test, she was able to validate a finite element modeling methodology for a RIGEX style structure. Helms also oversaw and processed documentation required for RIGEX to fly in CAPE and finalized the RIGEX inflation system design.

1.3.9 Jeremy S. Goodwin

Jeremy Goodwin began the RIGEX detailed design process using the SolidWorks software package. In so doing, he created Draft A of the drawings required for structural fabrication. In addition to resizing most structural components to better fit CAPE, his design included the addition of a containment shroud to protect CAPE should any part of RIGEX break. Goodwin's design also included an updated electrical architecture, moving from an internal battery to the orbiter power supply. His post-thesis work

included creating a thermal model and programming an interface verification test (IVT) as required by NASA to ensure RIGEX is correctly installed within the orbiter prior to launch.

1.3.10 Canister for All Payload Ejections

The Canister for All Payload Ejections (CAPE) is one of the newest space payload envelopes. Developed by Muniz Engineering Incorporated, in cooperation with the Department of Defense (DoD) Space Test Program (STP), CAPE replaces the discontinued Get-Away-Special Canisters. The CAPE is primarily a small-satellite ejection system; however its can be used for payloads intended to make the round trip journey to space and back. CAPE (Figure 1.3-5) is a canister within the space shuttle cargo bay that provides structural support for its payload during flight and an electrical conduit for orbiter interface. Offering three methods of payload mounting, directly to the CAPE lid, directly to the CAPE, and an Ejectable Internal Cargo Unit, the CAPE system can be mounted in payload bay locations 3 through 13, depending on payload weight and center-of-gravity requirements (5, 6). The payload bay locations are numbered from 1 to 13 from forward (closest to the crew cabin) to aft (1).

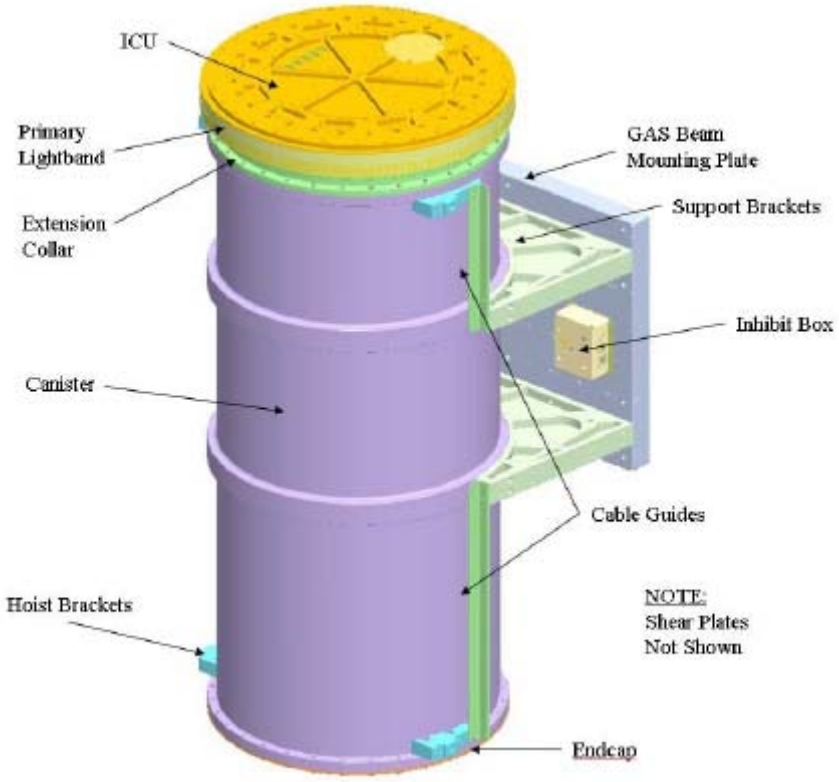

Figure 1.3-5: Canister for All Payload Ejections (5)

Made of 6061-T6 Aluminum, the CAPE is basically a cylinder that attaches to the old Get-Away-Special beams on the orbiter sidewall. RIGEX attaches to CAPE via its CAPE mounting plate. The CAPE mounting plate duals as a lid for the CAPE structure (Figure 1.3-6).

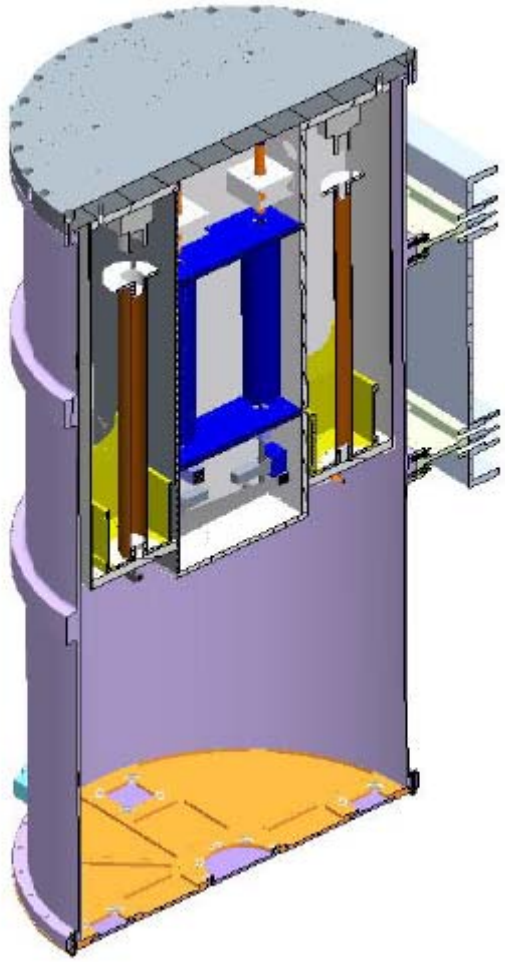

Figure 1.3-6: RIGEX within CAPE (Cut Away View) (40: 21)

1.3.11 ANDE

The first payload slated to be launched in the CAPE is designated STP-H2. CAPE's primary payload will be the Atmospheric Neutral Density Experiment (ANDE), slated to fly on STS-116 in December 2006. ANDE was designed by a team of scientists and engineers at the Naval Research Laboratory to study the Earth's atmosphere from Low Earth Orbit (LEO) by monitoring total atmospheric density at 400 kilometers (36). ANDE will be flown in two parts. ANDE Part I, flying on CAPE, is an experiment of two spheres: the Mock ANDE Active sphere and the Fence Calibration sphere. It will be

used to help validate CAPE's operation and to acquire basic atmospheric data. ANDE Part II will fly on a later orbiter mission and will be fully functional and operational. The successful flight and retrieval of the CAPE after its first mission is critical for a timely launch of RIGEX on STS-123 in December 2007.

1.4 Research Objectives

Since the inception of the RIGEX program, each thesis has been motivated by the same mission, developed by DiSebastian: "To verify and validate ground testing of inflation and rigidization methods for inflatable space structures against a zero-gravity space environment" (10: 1-9).

Program changes have slightly altered the RIGEX objectives, but otherwise, these goals conceived in DiSebastian's 2001 thesis, have remained the same (10):

Primary Objective:

- Design a Canister for All Payload Ejections experiment to collect data on space rigidized structures for validation of ground testing methods.

Secondary Objectives:

- Return inflated/rigidized structures to laboratory for additional testing.
- Enable application of rigidized structures to operational space systems.
- Implement systems engineering principles into the experiment's design.

While the aforementioned mission and objectives motivates the entire RIGEX project, the primary research objective of this thesis is to validate the structural integrity of the RIGEX design through analysis. Structural integrity validation is necessary, not only for mission success, but also for the safety of the space shuttle orbiter and its crew.

The analysis includes the construction of a detailed finite element model, which was used to determine the structure's likely natural frequencies. The FE model was also used to determine the maximum stress, the transferred loads and the displacement at critical locations throughout the structure. Using the loads data, a comprehensive bolt analysis method was developed and applied to each major bolt pattern and to the fasteners securing the larger subsystem components.

The results of the structural analysis motivated design changes that would strengthen the structure and make its components more easily accessible in the assembly and testing phases. The structure was also optimized to ease construction and testing. This thesis, therefore, addresses the finalization of the RIGEX detailed design and presents the as-built drawing package, along with a finalized wiring schematic and RIGEX wire routing map.

Once the structure is completely assembled, there will be no way to see inside RIGEX to ensure each of the components is functioning properly. Furthermore, on the orbiter, the only feedback the crew will have that RIGEX is functioning is a single three-position display. Therefore, the final objective of this thesis was to develop a method of verification of RIGEX functionality for *blind* ground testing and for orbiter integration tests.

1.5 Thesis Summary

This thesis provides a comprehensive structural analysis and a final design description for the Rigidizable Inflatable Get-Away-Special Experiment. Chapter I provided the motivation and background for the RIGEX project.

Chapter II presents a literature review. The review details historical examples of structural analyses in the aerospace industry and provides examples of structural analyses executed on Get-Away-Special Experiments. While the review is not all-inclusive of aerospace structural analysis techniques, it offers insight into the diverse approaches and levels of detail with which similar problems can be solved.

Chapter III provides the methodology for the RIGEX structural analysis. The methodology includes a discussion of the finite element method as well as a bolt strength and separation analysis algorithm. It also presents previous RIGEX finite element models.

Chapter IV presents analyses and results, including the design of the detailed RIGEX finite element model, the modal analysis to determine RIGEX's fundamental frequency, the static analysis to determine the maximum stress, the loads transferred through bolts, and the translation of critical RIGEX components at limit loads. Chapter IV also discusses the analysis and results for the limit load performance of RIGEX structural bolts and for those bolts holding large subsystem components to the structure. The final result of the RIGEX bolt analysis is an acceptable torque range for each bolt pattern.

Chapter V discusses RIGEX design changes as motivated by analysis, component availability, and construction and testing needs. A final mass properties analysis and the orbiter electrical interface are also presented. A design for the space shuttle orbiter emulator is also included, with which a current draw profile for the experiment will be determined.

Chapter VI discusses recommendations for future RIGEX work and offers conclusions drawn from the content of this thesis.

II. Literature Review

Launching a payload into orbit is a risky and expensive endeavor. If a payload suffers physical damage during ascent, its scientific, commercial, or military objectives, as well as the financial and personal investment in its development and fabrication, may be lost. Thus, before the payload structure is even fabricated, analysis must show the structure will remain structurally sound under the worst static and dynamic conditions possible during flight. Such analysis will identify weaknesses in the structure and allow them to be corrected before the payload is built. Using the prevention approach to spacecraft construction saves time and money and is a key step towards ensuring that manifestation of the payload's objectives will not be hindered by flight load damage.

A thorough spacecraft structural analysis prior to fabrication is of the utmost importance to any flight program. The first requirement, before any structural analysis may take place, is the "determination of and subsequent adherence to, a coordinate system" (48: 34). Once the payload's coordinate system is defined, all models must be analyzed with respect to that coordinate system, and that system must be clocked appropriately with that of the launch container or vehicle. From that point, structural analysis can range from static analysis involving loads and moments applied to a free body diagram, to a fine-mesh finite element analysis with static and dynamic loads applied and analyzed through a high power computer. Many of these analysis techniques are discussed in the following Sections.

2.1 Historical Examples

Accomplishing a thorough structural analysis prior to spacecraft operation has been an important requirement since the early days of the space program. Before the introduction of high speed computing, stress analyses were conducted with hand calculations, applying the displacement method of analysis for statically indeterminate structures (38). The first Apollo launch vehicle, the Saturn I, underwent such an analysis prior to its employment. Launched first on October 27, 1961, the Saturn I rocket, Figure 2.1-1, had three stages. The Saturn I's first stage was an arrangement of one Jupiter rocket liquid propellant tank, surrounded by four Redstone liquid propellant tanks and four Redstone liquid oxygen tanks, all powered by eight H-1 engines, totaling 1.2 million pounds of thrust (33).

Figure 2.1-1: Saturn I Rocket Launching from Cape Canaveral (33)

In the development of the Saturn I rocket for the Apollo program, a structural analysis was performed to ensure the cluster of 9 liquid propellant tanks and 8 rocket engines would hold together throughout the entire flight, especially under the critical loads experienced at the point of maximum aerodynamic pressure. The primary component that held these nine tanks together is the *Spider Beam Assembly*. The *Spider Beam Assembly* is visible in red at the top of the stack shown in Figure 2.1-2.

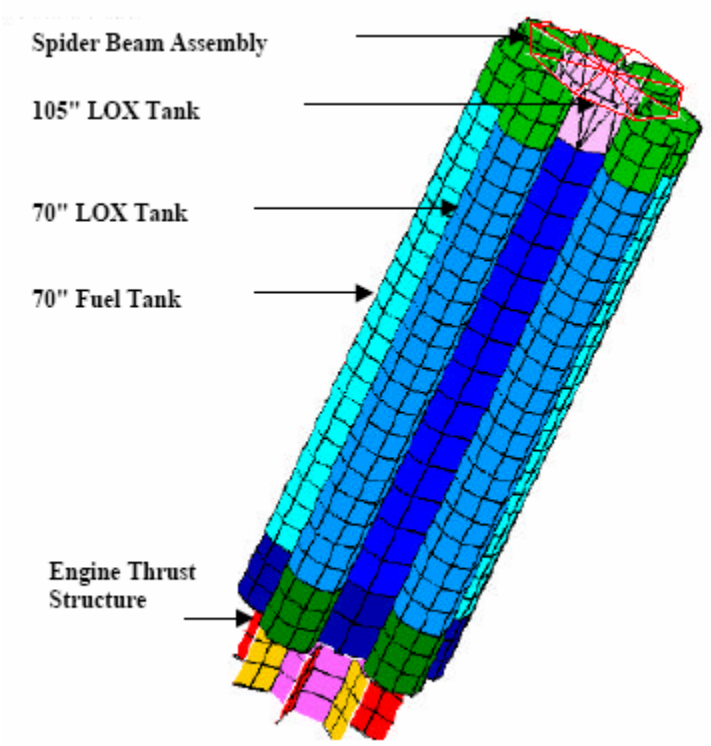

Figure 2.1-2: Spider Beam Assembly on Saturn I 1st Stage (14: 4)

Structural analysis of the *Spider Beam* during Saturn I development involved "the judicious selection of segmented free body cuts through the redundant booster structure to expose points to which internal reaction forces were applied to achieve static equilibrium" (14: 5). As in any structural analysis, assumptions had to be made to

minimize redundants. The Saturn I engineers assumed that no shear load could be transferred across the Spider Beam Assembly, nor could any torque be transmitted from one beam to another within the Spider Beam Assembly. Using the method of virtual work, the deflection of the edges of the spider beam could be compared to the deflection at its center. All of these relative displacements allowed for the development of a stiffness matrix, from which a static and dynamic analysis can be derived (14).

Despite the intensity of work required to complete a by-hand structural analysis, as described above, it is not accurate enough for the NASA engineers. While the analysis lead the engineers to think that their rocket had a chance of surviving launch, it was not an adequate acceptance mechanism to prove the rocket operational (33). Thus, in the space program up to and through the Apollo era, structural static and dynamic tests were performed at Marshal Space Flight Center (MSFC). These tests were very costly and often resulted in structural failure that had not been predicted, thus expensive and time consuming redesigns and retests were necessary.

2.2 Structural Analysis of Get-Away-Special Payloads

Today, advances in structural analysis techniques and software packages, along with increases in computing power, have increased accuracy so much that static and dynamic tests to loads at or above safety factor requirements are not always necessary. In order to fly aboard the space shuttle orbiter, in any capacity, a payload's structure must be verified. A verified structure is one that meets structural strength, fracture control, and fastener requirements.

2.2.1 PANSAT

Designed by the Naval Postgraduate School (NPS), the Petite Amateur Navy Satellite (PANSAT) Hitchhiker Ejectable was made to provide radio message relays via spread spectrum techniques (Figure 2.2-1) (41). PANSAT was originally designed for flight aboard the orbiter in a GAS canister, but program changes forced it to fly on the orbiter's pallet ejection system. Before PANSAT could be successfully launched aboard STS-95, NASA required that it undergo a thorough structural analysis, motivated by both mission success and safety.

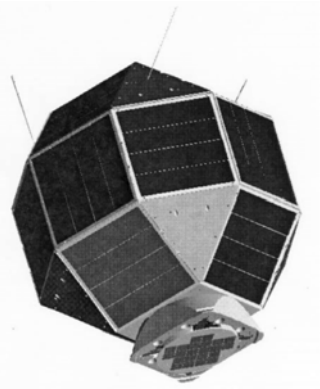

Figure 2.2-1: NPS's PANSAT (41)

PANSAT's structural verification plan included ensuring structural and fastener strength. The Navy engineers modeled and analyzed PANSAT using the Structural Dynamics Research Corporation (SDRC) finite element modeling and analysis tools (41). The FE model was validated by comparing the model to tests on a prototype structure and ensuring that the results correlated within an acceptable margin of error. Then, using the FE model, a structural strength analysis was performed that showed that stresses resulting from expected static loads could be considered low risk. A fastener analysis was then

performed on the load-bearing fasteners. The analysis was done by multiplying the maximum expected loads at the constraint point by the maximum moment arm, multiplied by the weight of the components and a 2.0 factor of safety. Analysis showed that all constraint bolts would hold assuming the bolts were constructed properly. Thus, a representative quantity of bolts, of size #10 or greater, was tested at NPS for compliance, to ensure they would perform as expected (41).

2.2.2 FEGI

The Field Emission Get Away Special Investigation (FEGI) is undergoing design by Penn State University and University of Michigan to test a field emitter array electron emission device in the space environment. The FEGI team hopes to flight-qualify their field emitter array so that it can be used in future payloads (44). While the field emitter array drives the mission, the science and engineering proof necessary for flight qualification cannot be completed if the structure fails during flight. Therefore FEGI is undergoing a detailed structural verification. The requirements for FEGI were motivated by the orbiter's launch profile and the mounting of the GAS canister, in which it was originally designed to fly. These requirements necessitate that the structure withstand loads of "10 g in the x-, y-, and z-axes with an ultimate factor of safety greater than 2.0 and a yield factor of safety greater than 1.5" (43: 5).

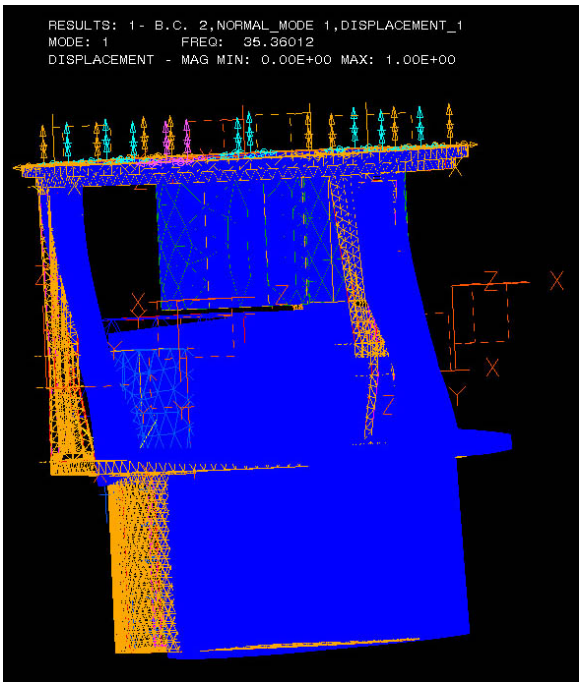

Figure 2.2-2: FEGI's Structural Model (44)

In their structural analysis, the FEGI team made assumptions to simplify the problem and reduce computational time. The approach they used for fastener analysis was to simulate a welded joint location within their finite element analysis software. They also determined the payload's center-of-gravity by creating a volume specific density for each part, rather than using a singular lumped mass. Finally, they considered all nonstructural components to have one-tenth the stiffness of the 6061-T6 aluminum that the primary structure was constructed from. Using SDRC I-DEAS Version 9.0, the FEGI engineers applied the 10g load scenarios and found that the maximum stress exceeded the 183 Mega-Pascal (MPa) allowed by their 1.5 factor of safety (Figure 2.2-2). Thus the structure did not meet the NASA structural requirements and needed further modification before flight. The structure also failed the fundamental frequency

requirement of 35 Hertz (Hz) or greater. The I-DEAS analysis revealed the first natural mode to be 32.2 Hz. The team decided that shortening the struts (Figure 2.2-3) would be an appropriate fix.

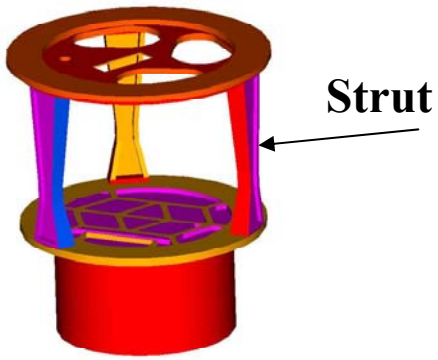

Figure 2.2-3: FEGI Strut (23)

Finally, FEGI is undergoing a fastener analysis. The FEGI analysis team included bolt holes in their I-DEAS finite element model, and modeled the bolts as welds, surrounding those holes. They found that the sharp edges on their structure around these holes caused a stress singularity in their finite element model, which created an obvious failure before they even included the details of the fasteners. The FEGI team decided that, in addition to a strut redesign, an improved finite element model to better show the load distribution pattern was needed (43). Further design and analysis of the FEGI payload is ongoing as they await flight reassignment after the cessation of the GAS canister program (23).

2.2.3 VORTEX

While FEGI is a GAS canister payload that is still undergoing development, the Vortex Ring Transit Experiment (VORTEX) is an example of one that has already successfully flown on the space shuttle orbiter. Designed by the University of Michigan Students for the Exploration and Development of Space, VORTEX (Figure 2.2-4) was flown on STS-89 in January 1998, and again on STS-88 in December 1998. The purpose of VORTEX was to study the propagation of a vortex ring through a liquid/gas interface in the space environment (46: 3). Like all other space science experiments, the primary structure allowed the VORTEX to fly safely and carry out its mission.

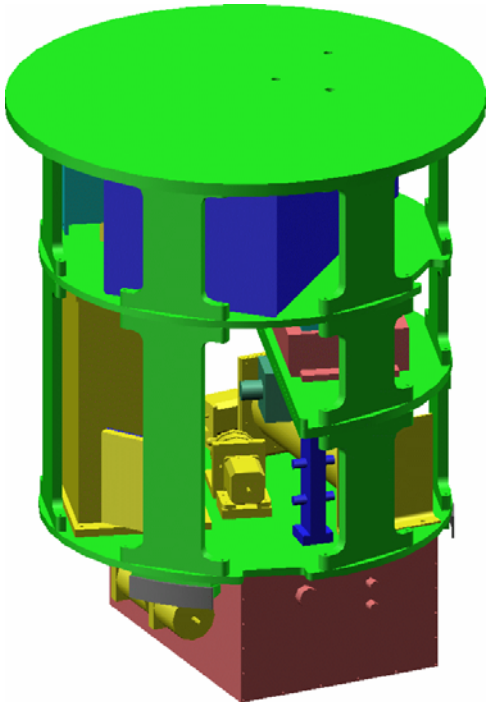

Figure 2.2-4: VORTEX (46: 3)

Designed to fly in the GAS canister, the VORTEX structure was made of two and a half shelves, connected by I-beams spaced equally around the full shelves. The

structure needed to be analyzed to ensure it would be able to successfully endure all aspects of spaceflight, including a second trip to space (its mission objectives were not met on the first flight due to powering issues).

In their analysis, the VORTEX team modeled all components as concentrated point masses at their centers-of-gravity. Additionally, they did not take into account any thermal gradients, as they considered thermal loading negligible. Finally, their broadest assumption was modeling the payload as a simple beam for analysis of loads applied to the top and bottom plates (47: 11). To determine the loads at different locations around the structure under limit load conditions, the VORTEX engineers used simple beam theory, modeling the structure as a beam of constant stiffness "with one end rigidly fixed at the (GAS interface plate) and the other end simply supported at the bumper location" (47: 13). Using brute force in their hand calculations, the team found the shear loads, normal loads, and bending moments at each major component throughout the structure. They then ensured that the yield and ultimate stresses of the component materials were greater than those induced by the shear, normal, and bending loads.

A fastener analysis was also completed on constraint fasteners for all experiment boxes that weighed more than five pounds. They determined the distribution of axial loads between fasteners by

$$L_{Ti} = \frac{Ml_i}{\sum l_i^2} + \frac{F_n}{n} \tag{1}$$

and the shear loads by

$$L_{Si} = \frac{F_S}{n} \tag{2}$$

where L_s are the tension and shear load, M is the moment of the load, l is the arm from the bolt axis to the component's center-of-gravity, F_s are the normal and shear load components and n is the number of bolts over which the load is distributed (Vortex). Note that these symbols differ in Equations 1 and 2 from those in the remainder of this thesis.

Finally, the VORTEX team conducted a fundamental frequency analysis, using the equation for a hinged beam (47: 26)

$$F_i = \frac{15.4}{2\pi}\sqrt{EIg/wl^4} \tag{3}$$

where E is the modulus of elasticity in tension, I is the moment of inertia, g is gravitational acceleration, w is the uniform load along the structural element, and l is the length of the structural material. They found that their first natural frequency was 64 Hz, well above the 35 Hz minimum required for flight in a GAS canister.

Overall, the team completed a structural analysis that was accepted by Goddard Space Flight Center, thus allowing the VORTEX payload to fly on two separate space shuttle missions.

2.3 Literature Review Summary

Chapter II discussed the importance of a thorough structural analysis for an aerospace project and the evolution of structural analysis techniques through the years. While detailed computer based structural analyses have only been feasible in the past few decades, rudimentary structural analysis has always been an important tool in identifying potential problems in structural integrity under limit loading conditions. Chapter II also demonstrated that structural analysis approaches can vary greatly. Three GAS canister payloads (FEGI, VORTEX, and PANSAT) were all held to the same structural strength and fundamental frequency requirements, but none of their development teams approached the analysis the same way. Likewise, due to the employment of the new CAPE payload envelope, as well as the ever evolving safety criteria for flight aboard the space shuttle orbiter, the methodology discussed in the following chapter for the RIGEX structural analysis differs significantly from that discussed in this literature review.

III. Methodology

Finite element analysis (FEA) is among the NASA and STP approved structural verification methods (17). FEA is used to validate the structural design's reaction to limit loads and to determine the structure's natural frequencies. A FE model of RIGEX is constructed, from which solutions for the first natural frequency of vibration and the structure's response to sixty-four limit load scenarios are found. Solutions from the limit load FEA are used as inputs in a comprehensive bolt strength and separation analysis. While FEA has been accomplished by past RIGEX researchers as a developmental tool, a highly detailed analysis of the final RIGEX design was still required to obtain the level of accuracy required for the bolt strength and separation analysis.

3.1 Finite Element Method

R. Courant originally developed finite element analysis in 1943 while using the Ritz method of numerical analysis to analyze a hollow shaft. Without the aid of computers, FEA was such a tedious task that it was originally used only to verify a design already completed or to determine why a structure had failed (7). Throughout the next few decades, great strides were made towards expanding the usability and usefulness of FEA. Analysis techniques began evolving to incorporate better algorithms, utilizing the Galerkin and Rayleigh-Ritz methods (45). Computer speed has also improved, thus allowing these increasingly more complex analyses to be accomplished faster. With these advances, FEA became a tool used throughout the breadth of engineering. To accomplish a finite element analysis, the geometric structure being

analyzed is divided, or discretized, into very small, yet finite (versus infinitesimally small) elements (Figure 3.1-1).

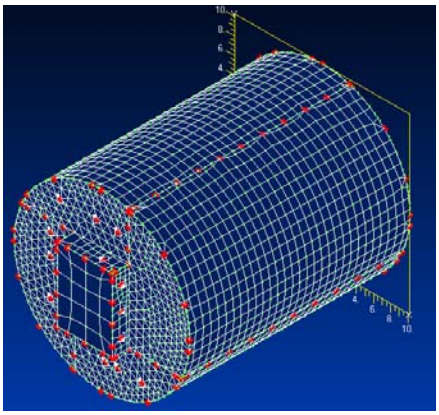

Figure 3.1-1: The RIGEX Geometry Discretized into Finite Elements

3.1.1 Finite Element Analysis Process

The first step in FEA is to classify the problem at hand. Classification is the process of planning out the analysis and establishing an understanding of the problem's conditions. While classifying the FE problem, the engineer must determine if the problem is linear and whether it is static or dynamic. The refinement of the mesh and the level of model detail must also be resolved (45).

The linearity of the FE problem is dependent on both geometric and material properties. A model is nonlinear with respect to geometry if the displacement of a structure is large in relation to its smallest dimension, and a model is nonlinear with respect to material if the yield limit of that material is surpassed. If either type of nonlinearity arises, a nonlinear FEA should be accomplished for more accurate results (4).

Whether the analysis is static or dynamic often determines how detailed the model must be. A modal characterization, which is to determine the natural frequencies of the structure, requires dynamic analysis. There should be significantly more FE degrees of freedom (DOF) in a FE model than eigenpairs computed (typically at least 100 times). For example, if the first three normal modes of a given structure are needed, the FE model must have at least 300 FE DOF for accurate eigensolutions. Static FEA can require a much finer discretization (resulting in many more FE DOF) than a dynamic analysis if accurate loading or stress solutions are required at specific locations on the model.

Choosing the proper dimensionality of the analysis for the given geometry is the next step in planning a FEA. One, two, or three dimensional elements (Figure 3.1-2) can be used. The lowest element dimensionality that results in accurate solutions should be employed (45). An example of such a simplification is in modeling plates. While a physical plate has three dimensions, it is very thin, thus solutions computed using two dimensional elements are often just as or more accurate than solutions computed using three dimensional elements.

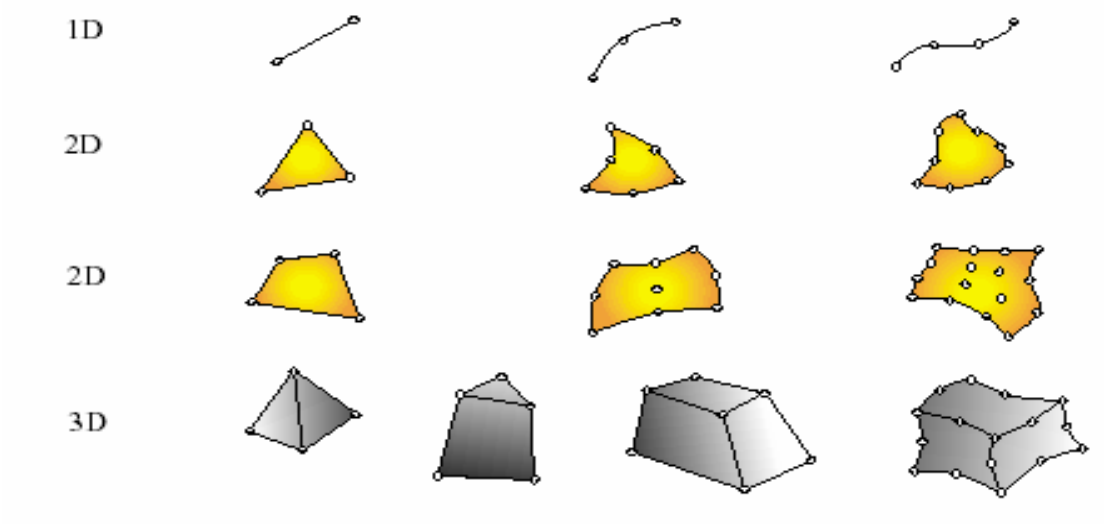

Figure 3.1-2: Example Finite Elements (45)

Once the dimensionality of the FEA is determined, a finite element model must be designed. The FE model is an analytical idealization of the physical structure. While FE models can be very accurate, the geometry, material properties, loads, and boundary conditions used in FEA are not a perfect representation of the physical structure. Therefore, the responsibility lies with the engineer to ensure that solutions computed using the FEA show accurate solutions to the problem at hand (7). The model geometry is either drawn in a stand alone computer aided design (CAD) software package then imported into the FEA software, or model geometry is drawn using the FEA pre-processor software.

Adding material properties is the next step in FE model development. Material properties include assigning thickness to two-dimensional geometries, as well as defining the Young's modulus, Poisson's ratio, shear modulus, coefficient of thermal expansion,

conductivity, specific heat, heat generation factor, mass density, damping, and stress limits.

Once developed, the model geometry must be discretized into (finite) elements. Referred to in FE software packages as *applying a mesh*, discretization determines the accuracy of the results. A fine mesh will produce better results than a coarse mesh, but it will also significantly increase computational time. Therefore, to decrease computational time, a coarse mesh is often used over flat, non critical parts of the geometry. A fine mesh is typically applied around fasteners and other areas where a high level of accuracy is required.

After meshing, the FE model is ready for loads and boundary conditions to be applied. Loads can come in many forms, including point loads, distributed loads, pressure, angular accelerations, and temperature differentials. Loads can be applied at one location, along an edge or surface, or throughout the entire body. For static analysis, a rigid boundary condition must also be applied to prevent the model from accelerating (infinite displacement). Like loads, boundary conditions can be applied to a single location up through the entire body and can prevent movement in any combination of the degrees-of-freedom.

Solutions can be computed after the FE model has been meshed and the loads and boundary conditions have been applied. Most FE software packages complete analysis by reading in all inputs and then returning displacement, rotation, internal load, stress and strain solutions. The solutions can be viewed numerically or visually interpreted through a post-processor. The frequency response of the structure can also be computed.

3.1.2 FEMAP and Nastran Software

The software package called Finite Element Modeling and Post-processing, FEMAP, is a pre- and post-processing tool that allows the user to visualize the problem's geometry, loads, and constraints both before and after analysis. FEMAP integrates a CAD package, in which the user can build a structure to a level of detail specific to the planned FEA. The user can build, mesh, and apply appropriate loads and constraints to the geometry, after which FEMAP writes the model to a text file. NX Nastran reads the text model file written by FEMAP and then computes a solution, which is written to a NX Nastran output file. FEMAP then reads the output file and post-processes it, allowing the user to see the solution (Figure 3.1-3). FEMAP displays the results which allow the user to interpret the structure's response to various loads and accelerations. While FEMAP provides ease of user interface and a good tool for result interpretation, NX Nastran actually computes solutions for the finite element analysis.

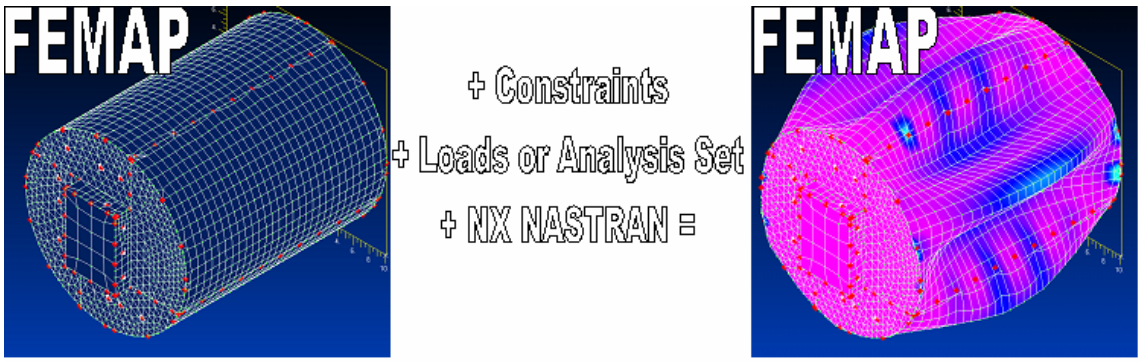

Figure 3.1-3: FEMAP and NX Nastran Relations

NX Nastran has a wide range of computational analysis capabilities, including linear statics, normal modes, buckling, heat transfer, aeroelasticity, and transient

response. Linear static analysis and modal analysis were used to evaluate the design of the RIGEX structure.

In linear static analysis, the matrix of displacements **u** is computed from

$$\mathbf{Ku} = \mathbf{f} \tag{4}$$

where the matrix of input loads **f** is supplied by the user. NX Nastran generates the stiffness matrix **K** based on user supplied geometry and material properties. NX Nastran then computes the displacement matrix **u** by inverting the stiffness matrix. The displacement matrix **u** can be used in computing stress, strain, and internal loads.

In normal modes analysis, also referred to as eigenvalue analysis, NX Nastran computes the natural frequencies (from eigenvalues) and mode shapes (related to eigenvectors) from the stiffness and mass of the structure. A natural frequency is a resonant frequency at which an object vibrates freely after being subjected to a disturbance or an initial condition. Without adequate damping, a structure excited at one of its natural frequencies will begin to resonate. The amplitude of vibration may increase to the point of structural damage.

The eigenvectors ϕ_i and eigenvalues λ_i are computed from the generalized eigenvalue problem

$$\left[\mathbf{K} - \lambda_i \mathbf{M}\right]\phi_i = 0 \tag{5}$$

where ***M*** is the mass matrix. The eigenvectors are related to the mode shape through the FE shape functions. The modes are the structure's motion corresponding to a given

frequency. The structure's natural frequencies are related to the eigenvalues by $\omega_i = \sqrt{\lambda_i}$ where ω_i is measured in radians per second.

Natural frequencies are not a function of the load, and mode shapes are subject to scaling. Each eigenvector dictates the displacement and rotation of each node, or grid point, relative to those around it. The post-processor does not show the magnitude of said displacements and rotations, since there are no actual applied loads in eigenvalue analysis. Thus, post-processor visualizations of the mode shapes can be used to view relative displacements, stresses, and strains, thus allowing the user to identify possible structural deficiencies and stress concentrations. Such visualizations cannot be used as a tool for determining the actual displacement, load, or stress at a given location. FEMAP allows the scale to be varied to enhance visualization of the modal shapes (Figures 3.1-4 and 3.1-5).

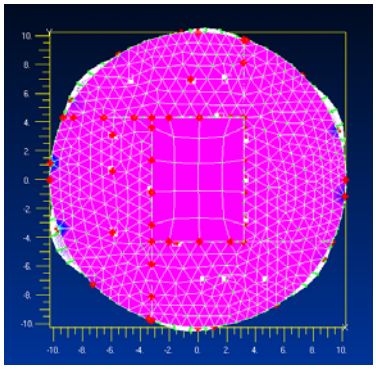

Figure 3.1-4: Breathing Mode with Scale Size 1

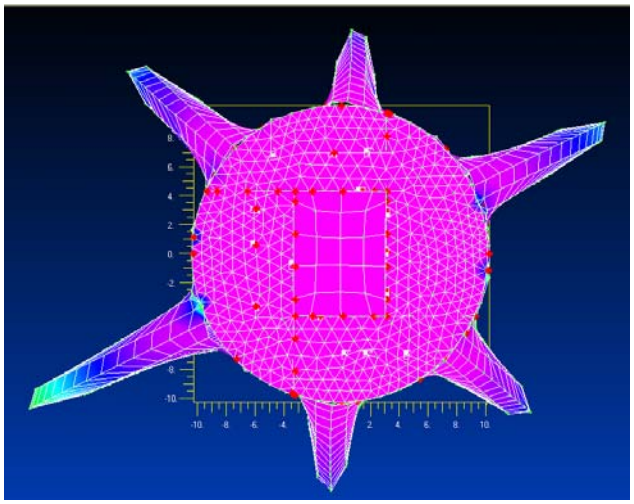

Figure 3.1-5: Breathing Mode with Scale Size 20

The research presented in this thesis uses the Lanczos method of eigenvalue extraction. "The Lanczos method overcomes the limitations and combines the best features of the other methods (of eigenvalue extraction) and it is the best overall method due to its robustness" (12). Compared to other eigenvalue analysis tools, the Lanczos method requires little disk space and is two to ten times faster than the subspace iteration method (7).

3.2 Bolt Analysis Method

Once a static loads FEA is accomplished, the maximum loads transferred through the bolts during flight limit load conditions are derived. The load values at the bolt locations are used as applied shear and axial loads in the bolt analysis discussed below.

The first steps of the bolt analysis are to determine the size and type of bolts to be used at each location. Initial bolt sizes are governed by what would fit easily into a given configuration and allow for ease of insertion and torquing. Bolt choices are limited to

those that comply with National Aerospace Standards (NAS) for corrosion resistant stainless steel (CRES). Being NAS fasteners, the bolts all comply with Aerospace Standard (AS) 8879, which governs UNJ profile screw threads. A UNJ profile, used for aerospace applications, has slightly deeper thread grooves, which increases the integrity of a joint as compared to the standard UN profile.

Based on a bolt's diameter and threads per inch (n_o), AS 8879 reveals the details of a bolt's construction. Important values extracted from AS 8879 include the bolt's major diameter, minor diameter, maximum pitch, and minimum pitch. The major diameter is the bolt's diameter at the crest of the thread, and the minor diameter is measured at the thread root. The pitch diameter is that of a theoretical cylinder that passes through the threads in such a position that the widths of the thread ridges and the thread groves are equal on opposite sides. Other details regarding the bolt's dimensions, including head radius, countersink angle if applicable, and length, were all obtained from the NAS specification for the given bolt type. The tolerance on the major diameter and pitch diameter of the threads is found based on the diagram provided in AS8879 (Figure 3.2-1).

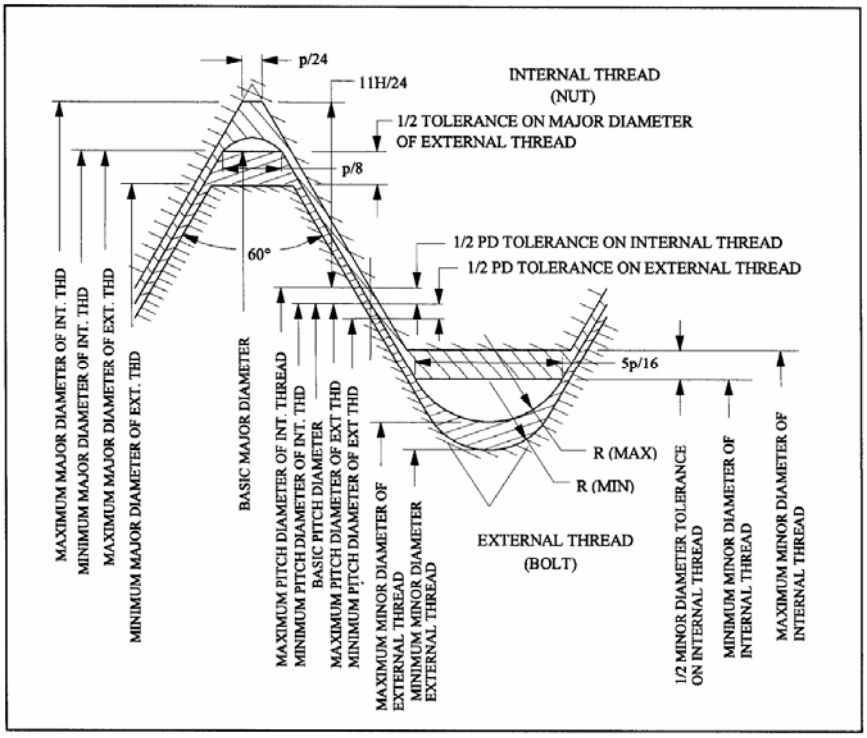

Figure 3.2-1: UNJ Thread Tolerances (39)

Material data on A286 is obtained from MIL-HDBK-5B, which provides the material's ultimate shear and tensile strengths, F_{su} and F_{tu} respectively, along with the modulus of elasticity E (8). Material data is also obtained for the 6061-T6 Aluminum Alloy that is used to construct the RIGEX primary structure. A286 CRES is used for calculations concerning the external threads, and 6061-T6 Aluminum is used for internal thread calculations. Unless otherwise noted, the equations in Section 3.2 are obtained from NSTS 08307, *Space Shuttle Criteria for Preloaded Bolts*.

3.2.1 Determining Bolt Strength – Axial Load

Once an exhaustive list of properties for each type of bolt and taps is developed, the analysis can proceed. The first step is to ensure the cross section of the bolt is large

enough to carry its maximum expected axial load. The first part of the axial bolt load analysis treats the bolt as a slender rod. In order to find the maximum axial load that the bolt can endure, we must find the tensile stress area A_t (in^2) from

$$A_t = 0.7854\left(D_e^{bsc} - \frac{0.9743}{n_o} \right)^2 \tag{6}$$

where D_e^{bsc} (in) is the basic major diameter of the bolt and n_o (in^{-1}) is the number of threads per inch along the bolt. Then, the axial load allowable P_{At} (lb) is computed from

$$P_{At} = A_t F_{tu} \tag{7}$$

where F_{tu} (lb/in^2) is the ultimate tensile strength of the bolt's A286 CRES.

A 2.0 safety factor (*SF*) is used to determine whether the bolt meets the NASA criteria for tensile strength, by satisfying:

$$\frac{P_{At}}{SF \times P} - 1 \geq 0 \tag{8}$$

where P (lb) is the maximum axial load that the bolt would experience at the applied limit loads. If Equation 8 is false, then there are two options. The bolt itself can be replaced with a larger diameter bolt in order to increase its axial load allowable P_{At} or the bolt pattern can be modified to better distribute the load.

The second part of determining if the cross-section of the bolt is large enough to handle the expected loads is to determine the actual axial bolt load. The axial bolt load P_b (lb) includes both the maximum preload applied to the bolt as a locking mechanism PLD_{max} (lb) and the shear due to torquing. The axial bolt load P_b is determined from

$$P_b = PLD_{\max} + n\phi(SF \times P) \tag{9}$$

where n (unit-less) is the loading plane factor, and ϕ (unit-less) is the stiffness parameter. The values of maximum preload PLD_{max}, loading plane factor n, and stiffness parameter ϕ are derived in the following paragraphs.

Determining the maximum preload PLD_{max} requires the input of the maximum torque applied T_{max} (lb*in) to the bolt. Along with the minimum applied torque T_{min}, the actual value for T_{max} is unknown at this stage of the analysis. To get the analysis started, an initial estimate of T_{max} is used, based on average torque values as published in NASA MSFC-STD-486B (35). The initial estimate of T_{max} remains until the entire analysis algorithm is established, and then T_{max} is allowed to vary in order to ensure all criteria are met with maximized safety margins.

Computing the maximum preload also requires determining the uncertainty Γ (unit-less) for torque measurement. Since the bolt is unlubricated, a conservative estimate is Γ=±35%. A conservative estimate is also used for the typical nut factor K_{typ} (unit-less), which is 0.2 for an unlubricated bolt with a steel-to-aluminum interface.

Finding the expected thermal load P_{thr} (lb) is the last step required in developing the preload equation. The thermal load analysis is based on Bickford's text *An Introduction to the Design and Behavior of Bolted Joints*. The positive thermal load is found from

$$P_{thr}{}^{pos} = \frac{A_t E}{L_e}\left(\Delta L_j - \Delta L_b\right) \tag{10}$$

where E (lb/in^2) is the material's modulus of elasticity, and L_e (in) is the length of the thread engagement. The changes in length of the joint or the bolt ΔL_i (in), subscript j or b respectively, due to a change in temperature is

$$\Delta L_i = \rho_i L_g \Delta T \tag{11}$$

where ΔT (ºF) is the temperature range for positive thermal expansion and ρ ($ºF^{-1}$) is the coefficient of thermal expansion. ΔT assumes that RIGEX will be constructed at room temperature (70º F) and that the maximum temperature RIGEX could experience in orbit is 165º F. The coefficient of thermal expansion ρ is found in the charts of MIL-HDBK-5H and is based on metal type of and temperature range (8).

By using conservative estimates for uncertainty and the typical nut factor, along with employing an initial estimate for maximum applied torque based on historical data, and by finding the maximum positive thermal load a bolt would be expected to endure, the maximum preload is determined from

$$PLD_{\max} = \frac{(1+\Gamma)T_{\max}}{K^{typ} D} + P_{thr}^{\ pos} \tag{12}$$

where D (in) is the basic major diameter of the external threads.

The only steps that remain in computing axial bolt load (Equation 9) involve distributing the applied load forces over the entire bolt. Loads are seldom applied to a single point in a bolted joint. While a detailed stress analysis of the bolt itself would be necessary to determine where on the bolt the load is actually applied, the load can be conservatively estimated using loading planes (1: 442). Therefore, a loading plane factor is developed for each joint. The loading plane factor is the ratio of the thickness of joint material loaded in compression to the total thickness. For the RIGEX analysis, a value of 0.5 is used as an estimate of the actual loading plane factor in order to greatly simplify the problem. Using 0.5 is recommended by both the STP engineers and Bickford (1: 450).

In order to compute axial bolt load P_b from Equation 9, the stiffness parameter ϕ is found from

$$\phi = \frac{K_b}{K_b + K_j} \tag{13}$$

where is the bolt stiffness, K_b (lb/in) is

$$K_b = \frac{A_t E_b}{L_e} \tag{14}$$

and the joint stiffness, K_j (lb/in) is

$$K_j = \frac{A_c E_j}{T} \tag{15}$$

where T (in) is the total thickness of the joint, and A_c (in^2) is the cross-sectional area of the equivalent cylinder used to represent the joint (1: 151-153).

Since the diameter of the RIGEX joint (generally a large panel of 6061-T6 Al) is significantly greater than the diameter of the bolt, A_c is computed from

$$A_c = \frac{\pi}{4}\left[\left(D_B + \frac{T}{10}\right)^2 - D_H{}^2\right] \tag{16}$$

where D_B (in) is the diameter of the bolt head and D_H (in) is the diameter of the untapped hole (1: 152). Equation 16 analytically represents the joint as a cylinder and finds that cylinder's cross sectional area.

All variables needed to solve for the axial bolt load P_b in Equation 9 are now available. Once the axial load is obtained, the load must meet NASA's second *Minimum Cross-Section of Bolt* safety criteria for axial loading:

$$\frac{PA_t}{P_b} - 1 > 0 \tag{17}$$

The maximum input torque, T_{max}, is varied until Equation 17 is true.

3.2.2 Determining Bolt Strength – Shear Pull-Out of Threads

The second major step in the bolt analysis method is to determine if the threads will shear away from the bolt or tap. The shear pull-out of threads analysis includes two criteria,

$$\frac{P_{As}}{SF \times P} - 1 \geq 0 \tag{18}$$

and

$$\frac{P_{As}}{P_b} - 1 > 0 \tag{19}$$

which require that the load on the bolt, computed in the FEA, does not exceed the axial load allowable of bolt due to thread shear P_{As} (lb) for the given bolt (32).

The shear load allowable is computed from

$$P_{As} = A_{si} F_{su} \tag{20}$$

where A_{si} (in^2) is the shear area of the internal threads on the RIGEX structure. The internal threads are used since 6061-T6 Aluminum is weaker than A286 CRES. A_{si} is computed from

$$A_{si} = \pi L_e D_e \left[0.875 - 0.57735 n_o \left(T_{De} + T_{Ei} \right) \right] \tag{21}$$

where D_e (in) is the major diameter of the internal threads, T_{De} (in) is the tolerance on the major diameter of the external threads, and T_{Ei} (in) is the tolerance on the pitch diameter of the internal threads, as derived from Figure 3.2-1.

If Equation 18 is false, the bolt or bolt pattern must be altered to either increase the allowable load or better distribute the applied loads. If Equation 19 is false, the input maximum torque T_{max} can be adjusted until Equation 19 becomes true. If any adjustments are made, it must be verified that Equations 8 and 17 are still true.

3.2.3 Determining Bolt Strength – Shear Load

Shear load V (lb) on the bolt due to limit loads, as determined in the FEA, must not exceed the shear load allowable V_A (lb) defined by

$$V_A = A_m F_{su} \tag{22}$$

where A_m is the minor diameter area (in^2) (11).

To ensure that the bolt will remain intact at maximum shear loading,

$$\frac{V_A}{SF \times V} - 1 \geq 0 \tag{23}$$

must be satisfied (32).

3.2.4 Determining Bolt Strength – Combined Loading

It is rare that a bolt would encounter either an axial or shear load without the other. It is more likely that during ascent, the orbiter will dynamically excite the RIGEX structure resulting in simultaneous shear and axial loads on the bolts. Therefore, analysis must show that the bolts will not fail under maximum combined loads.

The ratio of axial load to axial load allowable R_a (unit-less) must be determined. To ensure the most conservative R_a is used, the maximum of three choices is selected (32):

$$R_a = \max\left\{\frac{SF \times P}{P_{At}}, \frac{P_b}{P_{At}}, \frac{PLD_{\max}}{P_{At}}\right\} \tag{24}$$

The ratio of shear load to shear load allowable R_s (unit-less) is found from

$$R_s = \frac{SF \times V}{V_A} \tag{25}$$

The bolt will be able to withstand maximum combined loading if

$$\frac{1}{R_a^{\,2} + R_s^{\,3}} - 1 > 0 \tag{26}$$

is true. If Equation 26 is false, the bolt, bolt pattern, or preload must be adjusted to either strengthen the bolt or reduce the load it must carry.

3.2.5 Separation Criteria

The final criterion which drives the torque values is preloaded bolt separation. If a bolt's locking torque is not large enough, the joint it secures could separate, thus driving the bolt into the nonlinear regime of material properties, which must be avoided.

The first step in bolt separation analysis is to determine the load at which bolt separation could first occur P_{sep} (lb) from

$$P_{sep} = P \times SF_{sep} \tag{27}$$

where SF_{sep} (unit-less) is the separation factor of safety. SF_{sep} is 1.2, as required by Table II in NASA-STD-5001, *Structural Design and Test Factors of Safety for Spaceflight Hardware*.

A value for the minimum applied torque T_{min} (lb*in) is also necessary in the bolt separation analysis, as joint separation is most likely to occur at minimum preload. In a method similar to that used to derive an initial estimate for T_{max}, based on average torque

values as published in NASA MSFC-STD-486B, an initial estimate for T_{min} is selected. While T_{min} will be varied in order to make the bolt separation criterion

$$\frac{PLD_{\min}}{(1-n\phi)P_{sep}} - 1 \geq 0, \tag{28}$$

true by driving the minimum preload PLD_{min}, the hypothetical T_{min} offers a realistic starting value.

The other values necessary to compute the minimum preload include the prevailing torque T_p (lb*in). The prevailing torque is required to initiate rotation of the bolt due to its locking device (patchlock, Heli-Coil, or locknuts). An expected negative thermal load, P_{thr}^{neg} (lb), is also determined. P_{thr}^{neg} is found using the same method as P_{thr}^{pos} (Equations 10 and 11), but with a different temperature range. After being constructed at room temperature, 70ºF, the minimum temperature the bolts may encounter in orbit is -75ºF; therefore the new ΔT would be -145ºF. Additionally, "most preloaded joints experience some amount of preload loss, due to plastic deformation and/or vibration" (32: 3-8). The preload loss P_{loss} (lbs) must be accounted for in order to define an accurate minimum preload. Thus, based on historical engineering data for metal-to-metal contact throughout the joint thickness, the expected preload loss would be five percent of the maximum preload:

$$P_{loss} = 0.05 \times PLD_{\max}. \tag{29}$$

Finally, compilation of data allows for the calculation of the minimum preload from

$$PLD_{\min} = \frac{(1-\Gamma)(T_{\min} - T_p)}{K^{typ} D} + P_{thr}^{neg} - P_{loss}. \tag{30}$$

To ensure joint separation will not occur, the minimum preload found in Equation 30 must satisfy Equation 28. If Equation 28 is not satisfied, the minimum applied torque must be raised.

The axial loading P_b (lb) must also not exceed the tensile yield allowable P_{Aty} (lb)

$$P_b = PLD_{\min} + n\phi P_{sep} \geq P_{Aty} \tag{31}$$

where the tensile yield allowable is

$$P_{Aty} = F_{ty} A_t \tag{32}$$

where F_{ty} is the tensile yield strength of the bolt material. If Equation 31 is satisfied, the analysis will remain linear. If Equation 31 is false, the minimum applied torque T_{min} must be raised.

Once the minimum preload is such that it satisfies both Equations 28 and 31, a check must be done to ensure the minimum preload does not exceed the maximum preload value determined earlier. If an acceptable torque range is not obtainable, the bolt type or pattern must be adjusted to better distribute the expected loads.

Having now fully developed the methodology for the finite element and bolt analyses, the analyses may occur. But first, the two earlier versions of the RIGEX FEMs will be reviewed to better understand the importance of a new, detailed analysis.

3.3 Historical RIGEX Finite Element Models

Previously, two RIGEX FE models were developed and analyzed. These two models served their purpose as developmental tools, guiding choices for material selection and fastening techniques. However, the two FE models were no longer

acceptable for flight verification purposes as they reflect a previous RIGEX design and do not contain the level of detail necessary to obtain accurate load data at bolt locations.

The first RIGEX FE model was developed and analyzed by Holstein. For his FE model, Holstein imported his Pro-E structural design into the ABAQUS FEA program. Holstein's FE model was developed from a RIGEX configuration designed to fly in a Get-Away-Special canister. The primary structure is comprised completely of 0.25" thick 6061-T6 aluminum plates, which the original RIGEX team had planned to weld together. Only twenty-four #10-32 bolts were included in this design to attach RIGEX to the experiment mounting plate in the GAS canister.

Holstein's FE model was designed for structural verification of flight load limits and to determine the structural fundamental frequency (17, 30). For flight in the GAS canister, a payload would need to meet a 2.0 factor of safety in analytical analysis to avoid physical hardware testing. Therefore, Holstein applied a 20 g load to all three axes of his FE model and performed the subsequent structural strength analysis. The welded joints in his model had three points of high stress concentration (Figure 3.3-1). Those locations were later proven accurate by Helms during a random vibration test, where constraint bolts (filling in for a welded joint on the RIGEX engineering model) sheared in half at those weakened locations.

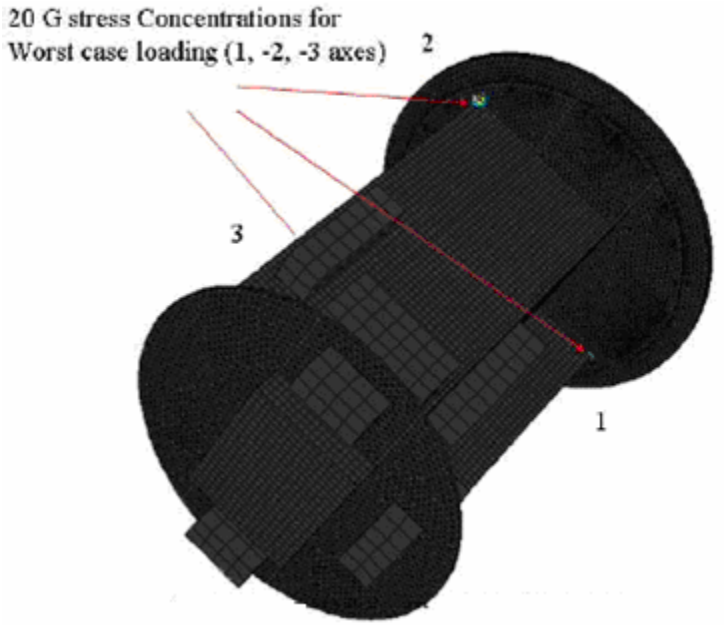

Figure 3.3-1: Structural Yield Locations in Holstein's RIGEX FE Model (18)

Holstein also performed an eigenvalue analysis of the structure using the Lanczos method in order to show that RIGEX's first natural frequency was above the required 35 Hz (Figure 3.3-2). His analysis revealed a first natural frequency of 148 Hz. Unfortunately, the RIGEX structure and the structural analysis requirements have changed drastically since Holstein published his thesis, thus his FEA and accompanying results are no longer valid.

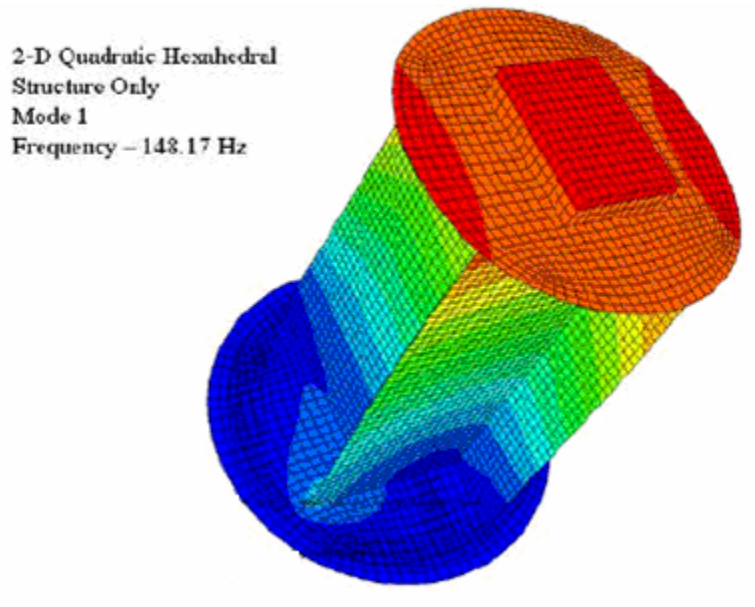

Figure 3.3-2: FE Representation of the First Mode of Holstein's RIGEX Structure (18)

Helms created the second RIGEX FE model. Her FE model was developed in FEMAP and reflected the changes in the RIGEX structure that had been made since Holstein's RIGEX work. These design changes included thicker structural plates secured by bolts instead of welds, as NASA strongly discouraged the use of welds. To fly aboard the orbiter, all welds must be x-rayed and certified, a time and money consuming process which could be avoided by employing bolts as fasteners instead of welds. Helms also included a limited number of RIGEX subsystem components in her FE model. These components were modeled as point masses and were placed at their estimated locations, as exact locations had not yet been determined. As there was no RIGEX structure available to determine the actual natural frequency, Helms relied on vibration data from the old engineering model to develop a FE model design methodology. She was able to design a FE model that closely matched the actual natural frequency of the engineering

model and then updated that model to reflect the current (as of her analysis) design. Helms computed an eigensolution from the updated RIGEX FE model to determine if the structure's first natural frequency exceeded 50 Hz, as required to fly in CAPE. Using Nastran as the FE software, Helms computed the first natural frequency of the structure to be 242 Hz, far exceeding the minimum requirement (Figure 3.3-3).

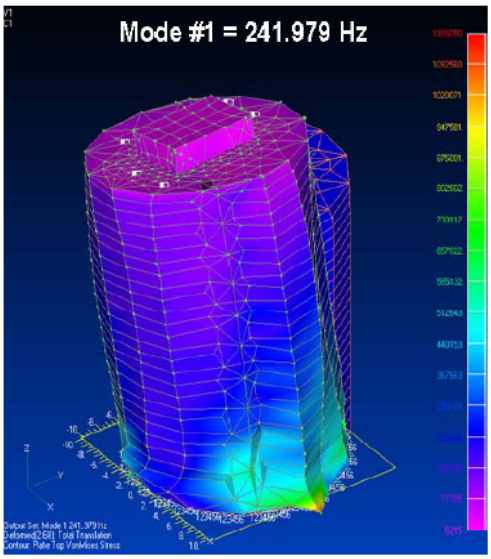

Figure 3.3-3: FE Representation of the First Mode Computed from Helm's FE Model (17)

While Helm's FE model, with just over 6000 FE DOF, closely resembles the current RIGEX configuration, the mesh needed to be refined for a more accurate stress analysis at key bolt locations. Additionally, enough changes have been made to the RIGEX design to warrant the creation of a completely new FE model.

3.4 Methodology Summary

Chapter III discussed the methodology developed for the RIGEX finite element analysis and bolt strength and separation analysis. Chapter III also presented previous RIGEX finite element analyses to show the motivation for the creation of a more detailed and accurate finite element model with which to execute the FE and bolt analyses. The next chapter will present the RIGEX finite element and bolt analyses and results.

IV. RIGEX Finite Element and Bolt Analyses and Results

4.1 Finite Element Analysis Introduction

Finite element analysis is an important tool in the structural design and development of any space payload. The detailed RIGEX structural model, or finite element model, was developed to provide a computational means for natural frequency identification and structural strength verification of the RIGEX design. FE results for the RIGEX structure paired with physical hardware testing is mandated by NASA and STP to ensure that RIGEX is structurally compatible with the space shuttle orbiter (54). Additionally, the paired analysis will be used to show that the combined CAPE/RIGEX payload will meet all of its mission objectives when subjected to space shuttle orbiter flight loading conditions (6).

The RIGEX FE model, or structural model, is used to show that the structure will exceed the minimum first natural frequency requirement as dictated in the CAPE Hardware Users Guide (CHUG) (5). The FE model is also used to meet the analytical requirements for the structural strength verification as outlined in the CHUG. Structural strength will be assessed by applying 64 unique maximum loading combinations to the model. These 64 load combinations, provided by STP in the SVP, include expected static and random vibration load factors for a sidewall mounted payload. The loads are used in a FE static analysis to ensure that the loads transferred through fasteners do not exceed their allowable limits plus a factor of safety. A maximum stress analysis will also be performed for the entire structure using the 64 limit load combinations. Static analysis is

also used to determine material deflections, thus relieving fear of the RIGEX structure damaging the CAPE or its own scientific hardware during flight.

4.2 Finite Element Model Design

The first step in designing the new RIGEX finite element model was to classify the problem the FE model would be used to solve. The FE model would be a tool used to accurately estimate the first natural frequency of the RIGEX structure and to conduct a structural strength analysis under 64 different possible limit loads. For static loads analysis, the FE model must be finely discretized near bolt locations.

FE model development began in FEMAP by creating sketches of the structural plates. Plates were chosen for the model instead of solid elements based on the analysis presented in Helms' thesis (17). The NX Nastran FEA tool did not present very accurate results when Helms used solid elements to model the RIGEX engineering model, due to the very thin nature of the structural components. When modeling the GAS canister RIGEX design in FEMAP, Helms was able to better emulate the actual response when using 2-dimensional plate elements. Furthermore, Helms showed that vent and cable holes within the structure have only a slight affect in mass and stiffness reduction (17: 84). These holes are omitted from the structural plates in the new RIGEX FE model. Despite the non-conservative omission of small holes, the FE model is still an accurate representation of the actual RIGEX structure due to the conservative nature of all other assumptions. As an actual RIGEX structure is not available to validate the FE model, adhering to the design methodology proven by past RIGEX research was accepted as the best available tool for ensuring the accuracy of the new FE model.

Once the plates (including the RIGEX experiment top plate, oven mounting plate, four ribs, two pressure system mounting plates, and a bottom plate) (Figure 1.3-2) were drawn and properly dimensioned in FEMAP, the shroud was created by extruding two semi-circles from the oven mounting plate up to the experiment top plate.

Eight coordinate systems would be needed in order to complete the bolt analysis, as the loads transferred along the axial length of the bolt would need to be identified. The global coordinate system aligns with the x, y, and z-axes of the RIGEX structure, which is collinear with the CAPE axes. The global coordinate system would suffice for every bolt with its axis aligned with a RIGEX axis. The bolts placed at odd angles to secure the shroud, however, would need their own coordinate systems. Thus, seven additional coordinate systems (Figure 4.2-1) were placed around the shroud; lining up with the fourteen shroud attachment planes.

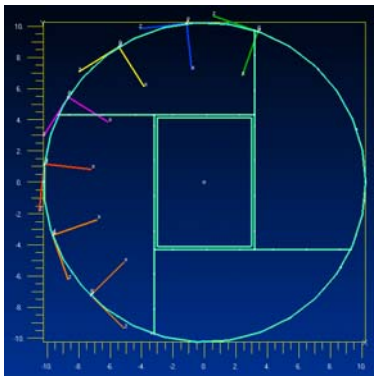

Figure 4.2-1: Shroud Bolt Coordinate System Identification (Top View)

After adding the seven coordinate systems to the plate structure, bolt locations were placed as points on the structure, shown in Figure 4.2-2. The bolt locations served as a guide for creating a mesh. The results of the bolt strength and separation analyses

motivated changes in bolt pattern design. The changes were then fed back into the FE model, which then provided new result data for bolt analysis. This iterative process provides a high level of confidence that the final design will perform nominally.

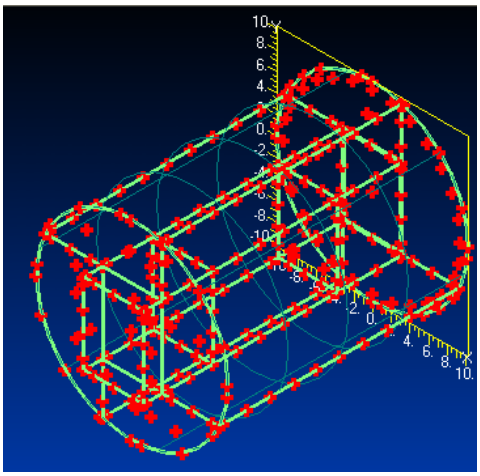

Figure 4.2-2: Bolts on the RIGEX Structure

The next step in FE model development was to assign material properties for each plate. The material properties include Young's modulus, Poisson's ratio, shear modulus, coefficient of thermal expansion, conductivity, specific heat, heat generation factor, mass density, damping, and the stress limits for 6061-T6 Aluminum. The properties also include plate thickness. Assigning an appropriate plate thickness (0.375" for the ribs, 0.675" for the oven mounting plate and experiment top plate, 0.25" for the pressure system mounting plates and bottom plate, and 0.075" for the shroud) allows the two-dimensional FE plates to represent thin, three-dimensional aluminum plates.

Because the FE model will be used for both static and dynamic analyses, a fine mesh was chosen around critical bolt locations, and a relatively coarse mesh was applied to flat, uniform surfaces (Figure 4.2-3). A custom mesh was developed to implement a

fine mesh at the required locations. Using a custom mesh pattern also allows for the creation of nodes at the point masses and at the points that represent bolts. Further mesh refinement was not required on the flat, uniform surfaces of the FE model because the FE model already exhibits 37,512 FE DOF: far more than required for an accurate estimate of the first normal mode.

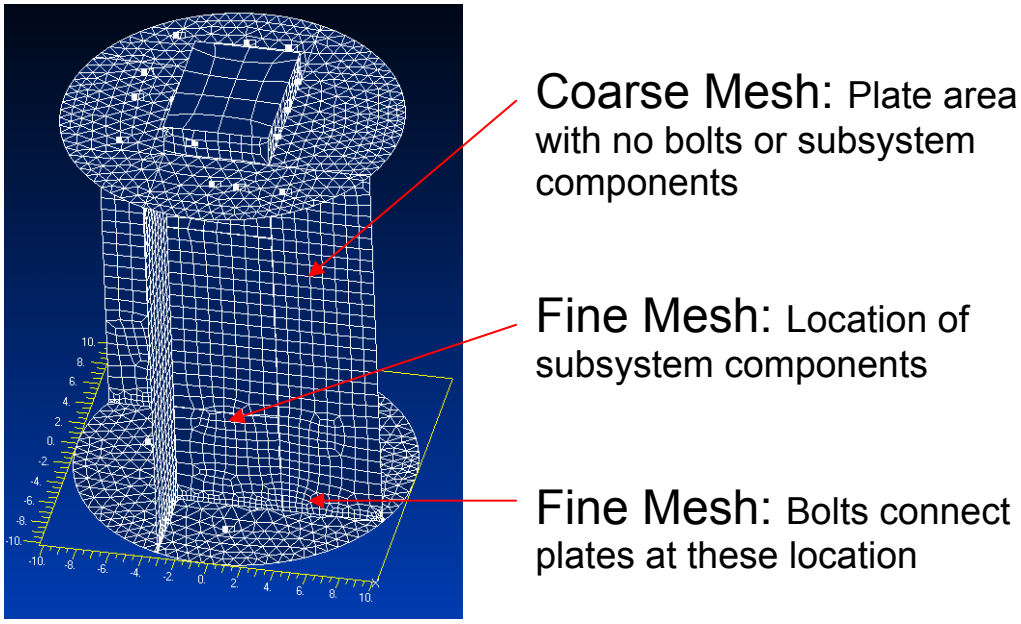

Figure 4.2-3: RIGEX FE Model without Shroud, Showing Different Mesh Densities

Figure 4.2-6 shows that the RIGEX plates were meshed individually. The mesh on each plate was carefully modified to maximize the node quantity around critical bolts and subsystem components. After each plate was meshed, node numbers at bolt locations were recorded. Once an adjoining plate was meshed, a search for coincident nodes was executed. Due to the fine nature of the mesh, not all nodes considered coincident by FEMAP (within a 0.004 inch radius) were actually meant to be coincident. Thus, the results of the coincident node query were cross-checked with the list of bolt/node

locations. All coincident nodes at bolt locations were then selected and conjoined, thus simulating a bolt holding the two plates together at the appropriate location (Figure 4.2-4).

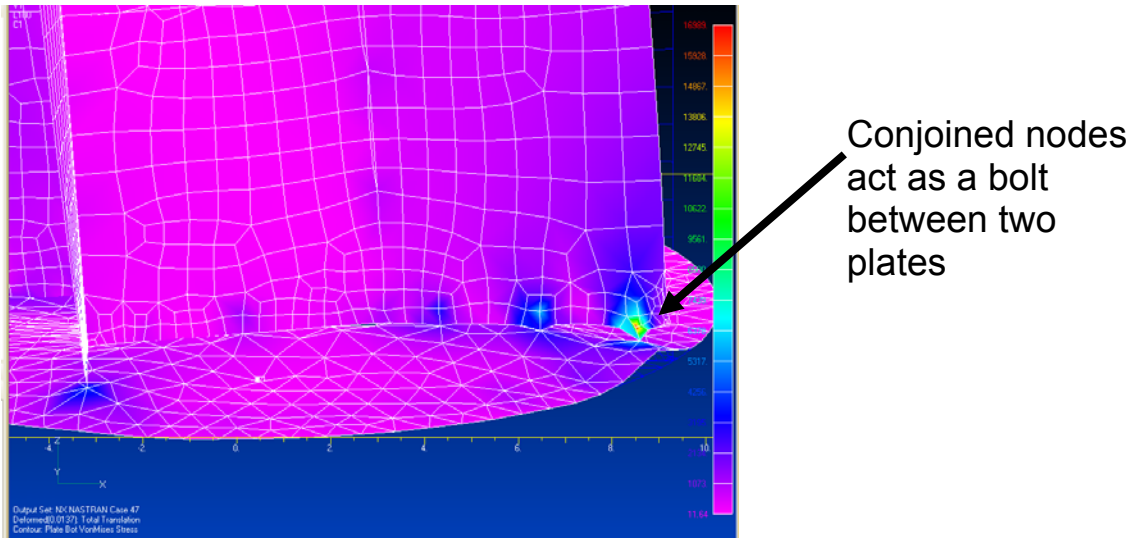

Figure 4.2-4: Conjoined Nodes Holding Two RIGEX Plates Together

The RIGEX subsystem components mounted on the plates were placed at propositioned FEMAP geometry points, which were added at the proper location prior to meshing. The custom mesh ensured a node would be located coincident to the geometry point. The subsystem components were treated as single point masses at the midpoint location of their mounting bolts. A list of the point masses applied to the FE model is in Table 1.

Table 1. List of Components Included as Point Masses

Component	Quantity	Mass per Unit (kg)
Power Relay	3	0.10
Transformer	3	0.15
Pressure Cylinder Mount	3	0.38
Oven Bracket	3	0.73
Oven	3	1.25
Computer	1	5.94
Camera	3	0.28
Power Distribution Plate	1	2.18

Incorporating component masses as point masses is a conservative estimate for two reasons. The point mass represents both the subsystem component and a single bolt that adheres it to the structure. For all of these components, at least two bolts and as many as four bolts are used in constraint, thus there is at least a factor of safety of two built in before the analysis even begins. The dynamic analysis is also conservative, as point masses decrease structural stiffness, thus decreasing the expected natural frequencies. In reality, many of the subsystem components have a large surface contact area with the RIGEX structure, and could serve to increase its stiffness. The only exception to the single point mass rule is the computer, which was modeled as two point masses. Each of the computer point masses is located at the midpoint of the two

computer mounting brackets (Figure 4.2-5), which better reflects the actual mass distribution of this large component.

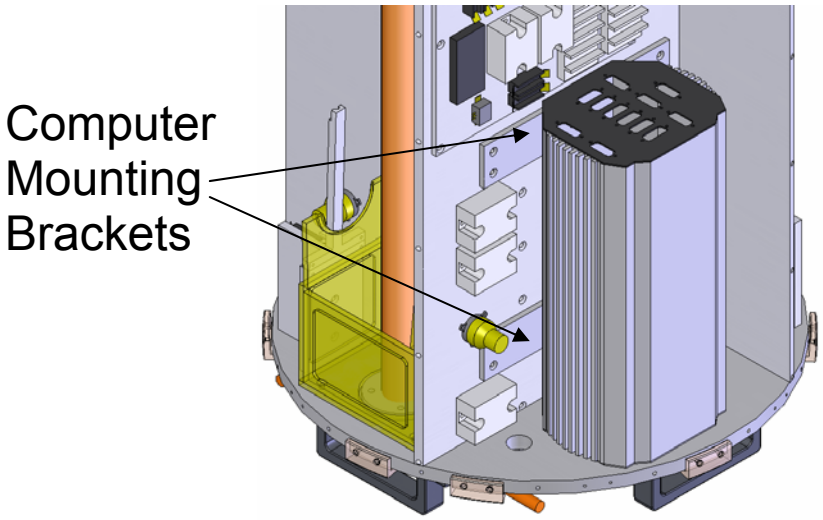

Figure 4.2-5: Computer Mounting Bracket Locations (Point Mass Represented in FE Model at Center of Each Bracket)

The only subsystem components not modeled as point masses were the three nitrogen pressure cylinders. These three tanks were modeled accurately as tube elements because they are attached to two distinct locations on the two pressure system mounting plates, and their material properties are well known (Stainless Steel) (Figure 4.2-6).

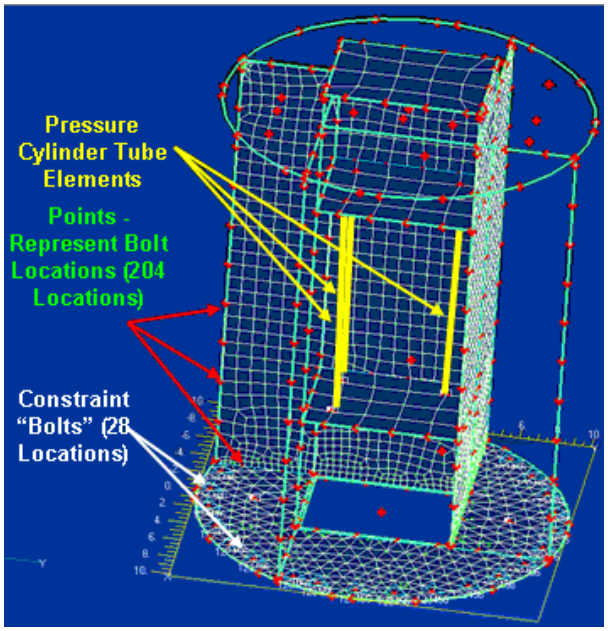

Figure 4.2-6: Pressure Cylinders and Bolt Locations on a Partial RIGEX FE Model

After the RIGEX FE model was meshed and the 408 bolt node locations combined into 204 single nodes acting as bolts, the FE model was ready for boundary conditions. The RIGEX FE model includes only the RIGEX experiment top plate, and not the 1.5 inch thick piece of aluminum that is the CAPE mounting plate (reference Figure 1.3-2). For the purposes of RIGEX structural analysis, the CAPE mounting plate is considered perfectly rigid with respect to the CAPE structure. Therefore, the only constraints for the RIGEX FE model are 28 completely constrained nodes (zero displacement and rotation for all six degrees of freedom) that represent the 28 constraint bolts holding the RIGEX experiment top plate to the CAPE mounting plate (Figure 4.2-6). The addition of these 28 constraints signifies the completion of RIGEX FE model development (Figure 4.2-7).

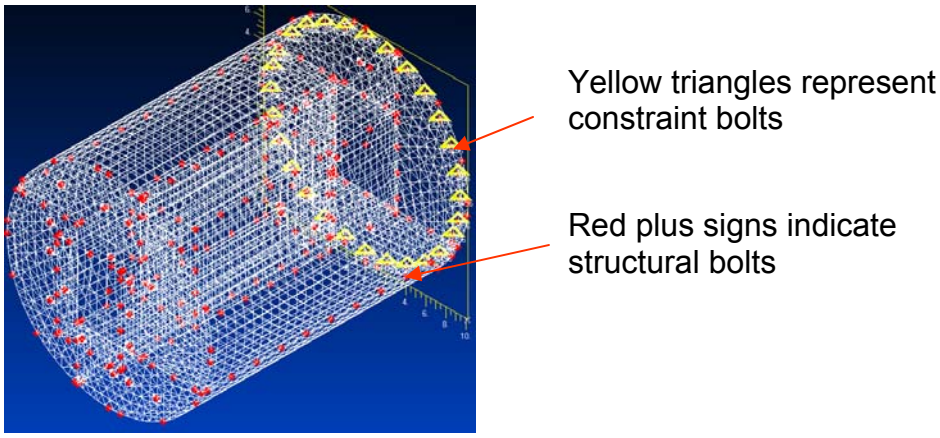

Figure 4.2-7: Final RIGEX Finite Element Model

4.3 Modal Analysis and Results

An eigen solution for the new RIGEX FE model was completed using the Lanczos solver in NX Nastran to compute the first three modes of vibration. Due to RIGEX's flight location on the space shuttle orbiter, the structure's first natural frequency must exceed 50 Hz (6: 16). The first natural frequency is 185 Hz, which is the first bending mode about the y-axis (Figure 4.3-1). With a margin of 135 Hz, the RIGEX structure is cleared to fly in CAPE without a NASA dynamic model verification test (6:16).

The fundamental frequency's large margin was expected. Since the CAPE is designed to accommodate payloads nearly double RIGEX's size, weight is no longer a critical consideration. With no weight restriction, RIGEX can have thick (3/8 inch) ribs that can easily hold #10-32 bolts, adding to the structural strength. The structural bulk added by the thick ribs, along with the shroud, cause RIGEX to be much stiffer than necessary, and no effort to reduce mass was required.

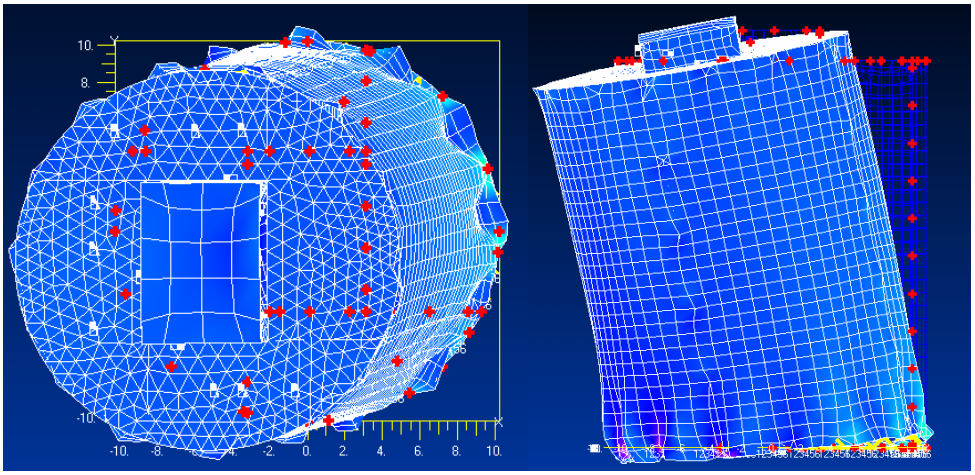

Figure 4.3-1: Relative Deformation at RIGEX First Natural Frequency (185 Hz) – Stress Contours

While only knowledge of the first mode was necessary to meet NASA requirements for flight aboard the orbiter, the second and third mode shapes also provided valuable insight. The second natural frequency, at 198 Hz, bends about the RIGEX x-axis (Figure 4.3-2).

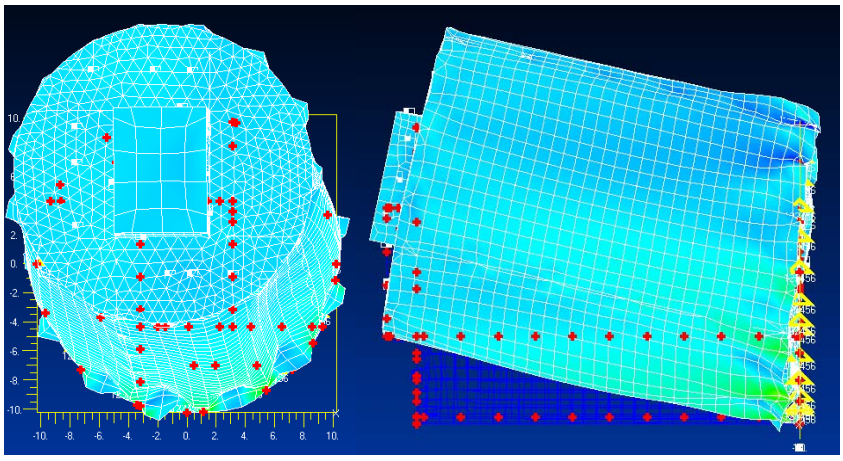

Figure 4.3-2: Relative Deformation at RIGEX Second Natural Frequency (198 Hz) – Stress Contours

The third mode of the RIGEX structure is the shroud breathing mode, which has a natural frequency at 304 Hz (Figure 4.3-3).

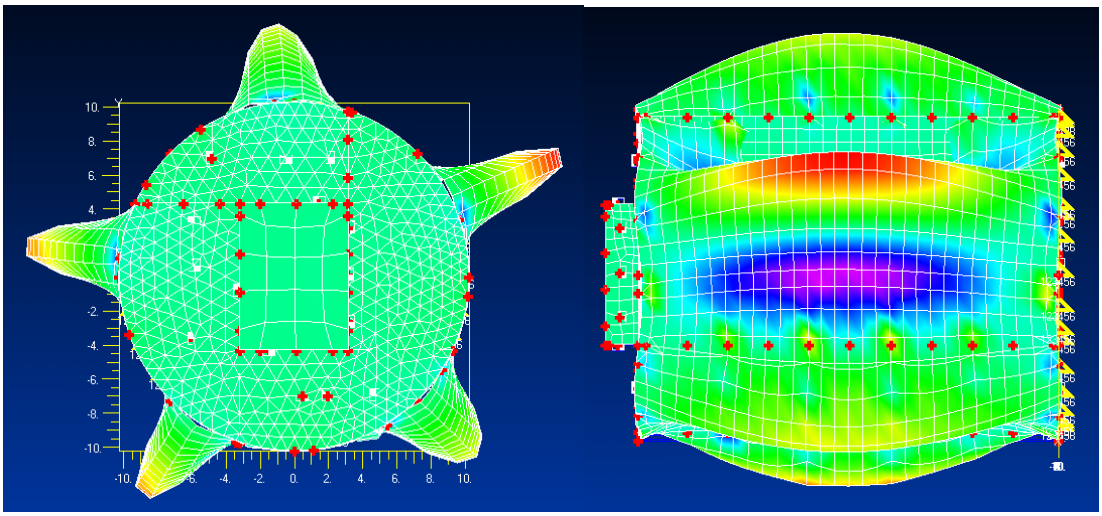

Figure 4.3-3: Relative Deformation at RIGEX Third Natural Frequency (304 Hz) – Stress Contours

4.4 Static Analysis and Results

Sixty-four different static loading cases (specified by NASA) were also analyzed. These sixty-four loads represent the maximum values from Table 2, which is a compilation of limit loads seen by side-wall mounted payloads in the orbiter during the various phases of flight, with an applied factor of safety (6). These maximum static loads were applied to the RIGEX FE model and static solutions were computed to determine the loads that are passed through the RIGEX fasteners. Static solutions were also computed to determine the maximum stress in the RIGEX structure and to determine the deformation of the RIGEX structure during limit load conditions.

Table 2. List of Limit Loads (6)

Flight Event	Load Factor (g)			Angular Acceleration (Rad/s^2)		
	Nx	Ny	N z	Φx	Φy	Φz
Lift-Off	± 7	± 7	± 6	± 195	± 60	± 75
Low Freq. Vibration	± 5.4	± 8	± 5.4			
Combination 1	± 8.8	± 7	± 6	± 195	± 60	± 75
Combination 2	± 7	± 10.6	± 6	± 195	± 60	± 75
Combination 3	± 7	± 7	± 8.1	± 195	± 60	± 75
Landing	± 6	± 7	± 8	± 108	± 34	± 80

Once identified, the 64 different maximum load combinations were assigned to a multiset analysis in FEMAP. A multiset analysis allows the user to compute all loads at each node location for all 64 load cases. As the FE model has 6252 nodes, the NX Nastran output file has 2,400,768 data points (translations along the x, y and z axes and rotations about the x, y and z axis for 64 different load cases at 6252 nodes). Algorithms were developed in Matlab to retrieve, transform, and analyze these data (Appendix C).

4.4.1 Loads Transferred through Bolts

The value of a very detailed finite element analysis is clear while searching for the loads transferred through bolts. Figure 4.4-1 and Figure 4.4-2 juxtapose Helms' coarse mesh FE model with the final RIGEX structural model. It is clear that the fine mesh provides a much more accurate solution for the stresses around structural bolts. While Helm's model excelled at its purpose as an initial dynamic analysis tool, a finer discretization is necessary to identify accurate load and stress concentrations around the RIGEX fasteners.

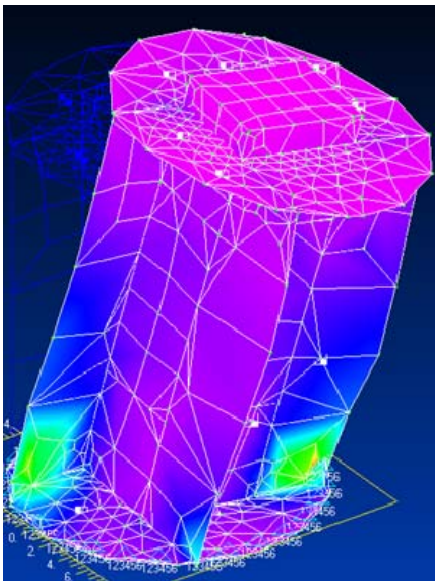

Figure 4.4-1: Coarse Mesh RIGEX FE Model (17)

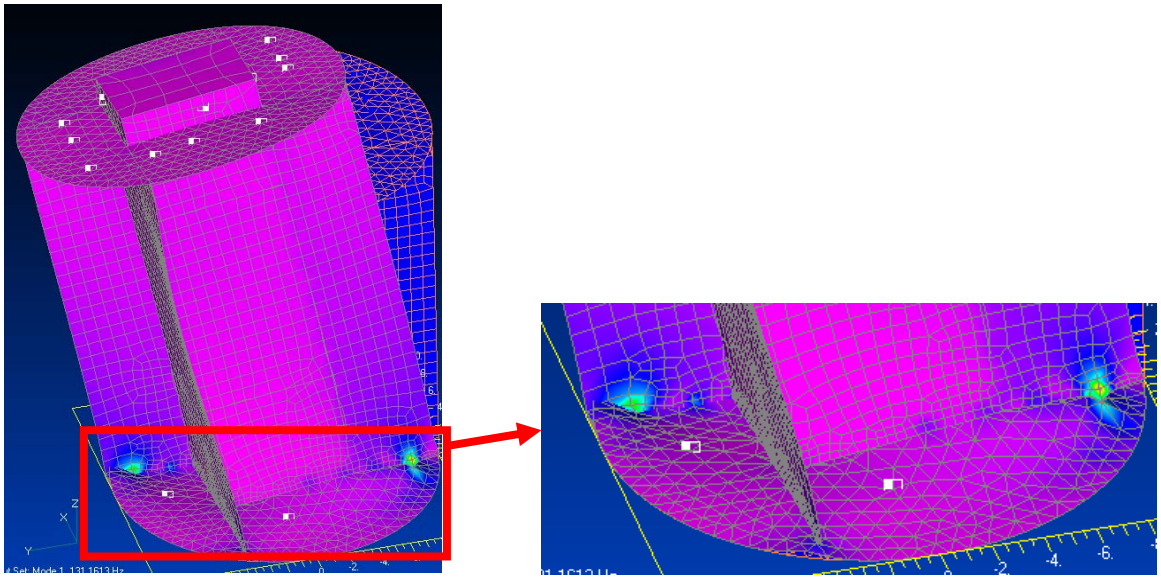

Figure 4.4-2: Final RIGEX FE Model

After NX Nastran found solutions to the multiset load analysis, the first Matlab algorithm retrieved the load values at each of the 204 bolt node locations. Unfortunately, the coordinate systems defined during FE model development could not translate through

to the output data. Thus, the load values at each bolt location were appropriately rotated to reflect the actual orientation of the bolt in order to gain axial and shear load data. The Matlab code then sorted the data into 11 different bolt patterns. The bolt patterns included: constraint bolts, bolts with their primary axis aligned with the global x-axis, bolts with their primary axis aligned with the global y-axis, bolts with their primary axis aligned with the global z-axis, and seven 'shroud' bolt patterns (rotated 173º, 198.71º, 224.42º, 70.16º, 95.87º, 121.58º, and 147.29º about the global z-axis). The load data for the nodes carrying point masses, representing RIGEX subsystem components, were also retrieved. Only the maximum axial and shear load of each bolt pattern or type of point mass (oven, camera, etc.) was reported by the Matlab script. The Matlab data reduction algorithm output 32 data points (Table 3), which were further analyzed per the bolt analysis discussion in Section 3.2.

Table 3. Maximum Loads from FEA of RIGEX Structure under Limit Loads

Location	Value	Force (lbs)
Constraint Bolts	Max Axial	1180.3
	Max Shear	428.4
"Z-axis axial" bolts	Max Axial	2.3
	Max Shear	70.9
"Y-axis axial" bolts	Max Axial	9.1
	Max Shear	115.1
"X-axis axial" bolts	Max Axial	4.9
	Max Shear	145.3
Shroud Coord 1 Bolts	Max Axial	2.6
	Max Shear	26.5
Shroud Coord 2 Bolts	Max Axial	2.7
	Max Shear	28.1
Shroud Coord 3 Bolts	Max Axial	4.7
	Max Shear	32.2
Shroud Coord 4 Bolts	Max Axial	2.5
	Max Shear	13.1
Shroud Coord 5 Bolts	Max Axial	4.34
	Max Shear	24.5
Shroud Coord 6 Bolts	Max Axial	3.0
	Max Shear	21.0
Shroud Coord 7 Bolts	Max Axial	2.2
	Max Shear	18.8
Camera	Max Axial	8.6
	Max Shear	10.6
Computer	Max Axial	84.8
	Max Shear	167.3
Power Distribution Plate	Max Axial	50.4
	Max Shear	85.1
Oven	Max Axial	33.6
	Max Shear	80.0
Oven Mounting Bracket and Latch	Max Axial	20.3
	Max Shear	47.1

4.4.2 Impact Avoidance through Translation Analysis

The large displacements of the breathing mode shown in Figure 4.3-3 raised concern at the Critical Design Review (CDR) that the shroud could impact RIGEX internal components and jeopardize the mission. Thus, the maximum limit load output data was used again to find the maximum possible deflection of the shroud in towards the RIGEX hardware. The ovens were identified as the highest risk area because their corners come closer to the shroud than any other component. Figure 4.4-3 shows a close-up view of the oven-shroud proximity issue. For the impact avoidance analysis, the nodes around the shroud between bolt locations were selected for review, as they exhibited the greatest relative deflections in the eigenvalue analysis.

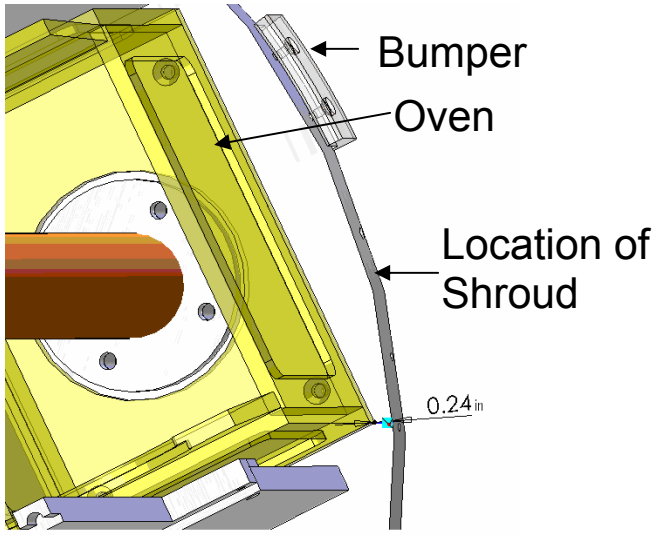

Figure 4.4-3: Oven Proximity to Shroud

It was also necessary to validate that the bumpers would not strike the inside of CAPE, even under maximum loading conditions. While the bumpers are designed to

protect the CAPE from the metal-on-metal damage that would occur if RIGEX struck it, an optimal flight would encompass no contact at all between RIGEX and CAPE. The bumpers are located in seven locations around the RIGEX oven mounting plate, thus the nodes closest to their locations were selected for analysis.

A second Matlab algorithm was developed to sort through the translation data at the critical shroud and bumper node locations. The Matlab code searched through the outputs of all 64 limit load scenarios and rotated the translations appropriately for the given location. The code then selected the maximum inward (towards the oven) and outward (towards CAPE) translations at the appropriate nodes. Analysis results show that the maximum expected deflection by any of the nodes under the limit loads would barely exceed $1/16^{th}$ inch, and therefore would not cause damage to the ovens or CAPE.

4.4.3 Structural Strength Analysis – Aluminum Structure

The Structural Verification Plan (SVP) is a document prepared by STP and AFIT that will ensure RIGEX is compatible with the space shuttle orbiter and that RIGEX will meet all of its mission objectives when subjected to anticipated load conditions (6). Per the SVP, analysis must show that even the worst case stress scenario, induced by the limit loads presented in Table 2, still shows a non-negative margin for yield stress conditions. As the largest stresses were generally seen by the corrosion resistant stainless steel (CRES) bolts, the bolt analysis, discussed in Section 3.2, does much to satisfy this condition. A stress analysis of the RIGEX primary structure from the 64 limit load scenarios shows that the maximum stress on the aluminum structure is 11,957 psi (Figure 4.4-4).

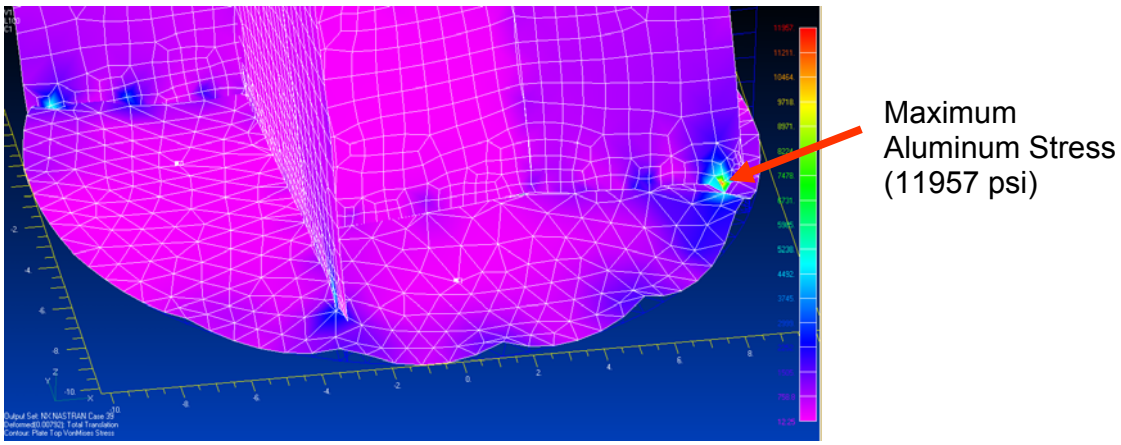

Figure 4.4-4: Maximum Stress on Aluminum

The maximum stress experienced by RIGEX must be at least two times less than the allowable stress for the 6061-T6 Aluminum, shown by

$$\frac{AllowableStress}{(FS)\times ActualStress} - 1 \geq 0 \qquad (33)$$

where *AllowableStress* is 27,000 pounds per square inch (8). With a 2.0 Factor of Safety *FS*, the margin was calculated to be 1.129, and therefore the Aluminum RIGEX structure is compliant with STP and NASA's Structural Strength Criterion. Such a large factor of safety allows RIGEX to fly on the orbiter despite the *analysis only* approach to structural verification.

4.5 Bolt Analysis Introduction

To fly aboard the space shuttle orbiter, a payload's bolts must have at least two locking devices to ensure the joint will not fail in the unique environment of space flight. Preload will serve as the first locking device. On RIGEX, every bolt is assigned a preload, which will be recorded and maintained with a calibrated torque-o-meter style torque wrench. The second locking device for the bolt is dependant on its location and

accessibility on the RIGEX structure. For bolts that will likely need to be removed and retorqued multiple times, a locking helical insert is used. These inserts, produced by the Heli-Coil company, are placed permanently in the tapped hole and serve to protect the internal thread while locking the bolt in place. While these locking helical inserts preserve bolt and tap integrity, they are difficult to install, therefore a simpler locking method called patchlock was adopted for bolts that will be installed once and never removed. Patchlock is a small nylon patch at the threaded end of a bolt which increases the prevailing torque that will be required to initiate rotation. Finally, locknuts are used on easily accessible bolts where the nut will not interfere with experiment hardware.

It is important to determine an adequate preload range to which each set of bolts will be torqued. The lower end of this preload range is governed by preload locking requirements. The preload had to be large enough to create an adequate locking torque. The upper limit of the preload range is governed by the material characteristics of the structure and the fasteners. Over-torquing a bolt could reduce its strength and fastening ability. In order to determine the preload range, a bolt strength and separation analysis was completed in accordance with the NASA document governing preloaded bolts, NSTS 08307, Revision A. Use of safety criteria ensures that any preloaded bolt will exhibit adequate strength and meet a separation factor of safety at limit load (32). The ultimate goal of the bolt analysis was to determine a torque range for each bolt on RIGEX that would comply with the NSTS 08307 criteria.

Often, all criteria could not be met simultaneously with the originally designated bolt; therefore a stronger or larger bolt was called for. Altering bolt size often interfered with the busy RIGEX configuration, thus bolt pattern and component mounting

configuration changes ensued. Per the RIGEX SVP, a factor of safety of 2.0 for ultimate was applied to the strength analysis. As RIGEX is being developed as protoflight hardware, such a large safety factor in analysis allows for space operations without rigorous ground testing.

4.6 Bolt Analysis Assumptions

In the bolt analysis, the following assumptions are made:

- The bolts, locknuts, and Heli-Coils are all in compliance with their applicable NAS and AS. Their dimensions are all within the calculated tolerances for the given thread.
- The tapped holes in the RIGEX structure will have an internal thread in compliance with the UNJ thread standards, per AS8879. UNJ taps will allow UNJ, UNR, and Heli-Coil external threads to fit into the holes and meet the required tolerances.
- The 6061 aluminum plates are considered perfectly uniform solids, in compliance with the specifications for yield and ultimate strength, modulus of elasticity, and coefficient of thermal expansion, as given in MIL-HDBK-5B (8).
- The fastener material (A286 CRES) is considered perfectly uniform and in compliance with the specifications for yield and ultimate strength, modulus of elasticity, and coefficient of thermal expansion, as given in MIL-HDBK-5B (8).
- While each of the RIGEX subsystem components are held to the structure by at least two bolts, the bolt analysis assumes that all but one of those bolts has already failed.
- Prevailing torque for the Heli-Coil inserts is determined from either the minimum locking toque after the 15^{th} cycle (worst case) as derived from MIL-F-18240E (9: 13)

or the maximum locking torques (whichever produces worse margins) as published from Heli-Coil (16: 10).

- Prevailing torque for bolts with patchlock is found from the minimum allowable breakaway torque (worst case) as published in MIL-F-18240E.
- Bolt yield is considered failure for the purposes of the RIGEX mission.
- RIGEX will be built and all bolts will be torqued to their specified preloads at room temperature (70ºF).
- The maximum temperature range of the CAPE canister in orbit is -75º to 165ºF.

4.7 Bolt Analysis Results and Discussion

The process described in Chapter III was repeated for each of the 11 bolt patterns identified in the FEA, as well as for the bolts securing each of the major subsystem components. The results of these analyses are discussed below.

4.7.1 Constraint Bolt Pattern

The constraint bolts are those which hold the RIGEX top plate to the CAPE mounting plate. Originally slated to be ¼-28 A286 CRES, spaced around the top plate in 28 locations at a 9.75" radius, the constraint bolts failed their shear loading strength criteria. As the bolts had not yet been purchased, the logical choice was simply to increase the bolt size, thus increasing the shear load allowable. 3/8-24 A286 CRES bolts meeting NAS 1189 were selected. With the appropriate input values changed to reflect the characteristics of the new, larger bolt, all analyses showed positive safety margins. However, in order to integrate these larger bolts into the RIGEX structure, the bolt pattern radius had to be decreased to 9.5", which prompted a redesign of the CAPE

mounting plate and RIGEX top plate in the SolidWorks design package along with an update to the FE model. Once the FE model was updated, the maximum expected loads were again derived and input into Microsoft Excel spreadsheets for bolt analysis. While the load changed due to the new mounting bolt pattern, the change was not significant enough to induce negative safety margins. Therefore, a worst case scenario constraint bolt was able to pass all established criteria.

The torque range that allows for all positive margins along the constraint bolt pattern when using NAS1351N6-20 bolts is 456 to 616 in-lbs, however, the margins are very small in some cases (Table 4). A more conservative torque range will be used while constructing RIGEX, which will start from the middle of the allowable torque range, plus or minus five percent, which provides for larger margins (Table 5). Using the conservative torque range will help ensure that human error during construction will not force the applied torque outside the acceptable range.

Table 4. Constraint Bolt Margins with Full Torque Range (456-616 in-lbs)

Criteria		PASS/FAIL	Margin
Min Cross-Section of Bolt	*Equation 8*	PASS	4.953

	Equation 17	PASS	0.031
Shear Pull-Out of Threads	*Equation 18*	PASS	4.778
	Equation 19	PASS	0.001
Shear Load	*Equation23*	PASS	1.644
Combined Loads	*Equation26*	PASS	0.005
Separation Criteria	*Equation 28*	PASS	0.004

Table 5. Constraint Bolt Separation Margin with Limited Torque Range (506-563 in-lbs)

Criteria		PASS/FAIL	Margin
Min Cross-Section of Bolt	*Equation 8*	PASS	5.0
	Equation 17	PASS	0.1
Shear Pull-Out of Threads	*Equation 18*	PASS	4.8
	Equation 19	PASS	0.1
Shear Load	*Equation23*	PASS	1.6
Combined Loads	*Equation26*	PASS	0.2
Separation Criteria	*Equation 28*	PASS	0.5

4.7.2 Y-Axis, X-Axis, and Z-Axis Axially Aligned Bolt Patterns

Bolts with their axial direction aligned with the RIGEX coordinate system y-axis, as identified in the finite element analysis, are #10-32 A286 CRES ¾ in long, with a 100º flat head and a patchlock element. These bolts, in conformance with NAS 1189, pass all the required strength and separation criteria when loaded to their limit load as identified in the FEA. When torqued to 66 in-lbs ±7 in-lbs, the y-axial bolts exhibit firmly positive margins, as illustrated in Table 6.

Table 6. Y-Axis Axial Bolt Margins 59-73 in-lbs Torque Range

Criteria		PASS/FAIL	Margin
Min Cross-Section of Bolt	*Equation 8*	PASS	173.8

	Equation 17	PASS	0.1
Shear Pull-Out of Threads	*Equation 18*	PASS	247.6
	Equation 19	PASS	0.5
Shear Load	*Equation23*	PASS	5.9
Combined Loads	*Equation26*	PASS	0.1
Separation Criteria	*Equation 28*	PASS	8.5

The bolts with their axes aligned with the RIGEX x-axis meet the same NAS as those aligned with the y-axis. Although their margins are larger than required when applying the y-axis input torque range (Table 7), that same torque range will be used for the x-axis bolts to standardize RIGEX construction.

Table 7. X-Axis Axial Bolt Margins 59-73 in-lbs Torque Range

Criteria		**PASS/FAIL**	**Margin**
Min Cross-Section of Bolt	*Equation 8*	PASS	324.2
	Equation 17	PASS	0.1
Shear Pull-Out of Threads	*Equation 18*	PASS	461.6
	Equation 19	PASS	0.5
Shear Load	*Equation23*	PASS	4.5
Combined Loads	*Equation26*	PASS	0.1
Separation Criteria	*Equation 28*	PASS	16.7

Bolts along the RIGEX z-axis are that are very similar to those along the x and y axes, only they are ¼ in longer. The length increase is driven by the fact that the z-axial bolts must pass through the oven mounting plate or RIGEX top plate (both 0.675") prior to reaching their threaded hole. Those bolts along the x and y axes only have to pass through a 0.375" ribs. With an input torque range of 60 to 74 in-lbs, these bolts also exhibited positive margins at the limit load (Table 8).

Table 8. Z-Axis Axial Bolt Margins 60-74 in-lbs Torque Range

Criteria		PASS/FAIL	Margin
Min Cross-Section of Bolt	*Equation 8*	PASS	683.3
	Equation 17	PASS	0.1
Shear Pull-Out of Threads	*Equation 18*	PASS	972.2
	Equation 19	PASS	0.5
Shear Load	*Equation23*	PASS	10.2
Combined Loads	*Equation26*	PASS	10.2
Separation Criteria	*Equation 28*	PASS	42.8

4.7.3 Maximally Loaded Shroud Bolt Pattern

A different type of bolt, in compliance with NAS 8402, will hold the RIGEX shroud in place. The NAS 8402 flange button #8-32 bolts, made of A286 CRES, will be fastened in to the ribs, RIGEX top plate and oven mounting plate with a Heli-Coil insert that will allow for ease of removal if repairs or changes are needed within the RIGEX structure. Flange button bolts also have a unique, rounded head with an integrated washer, making them ideal for keeping the external structure clear of catch points (26). An analysis was executed on all 7 shroud bolt patterns, but again, for construction standardization, the torque range for all shroud bolts will be guided by the bolt pattern with the smallest margins. Based on analysis at load limits, an acceptable torque range of 29 to 50 in-lbs was identified, allowing the bolts to comply with all criteria. To ease construction, the recommended torque range for the shroud bolts was reduced to 36-44 in-lbs, producing positive safety margins, as shown in Table 9.

Table 9. Shroud Bolt Margins 36-44 in-lbs Torque Range

Criteria		PASS/FAIL	Margin
Min Cross-Section of Bolt	*Equation 8*	PASS	235.2
	Equation 17	PASS	0.1
Shear Pull-Out of Threads	*Equation 18*	PASS	334.1
	Equation 19	PASS	0.6
Shear Load	*Equation23*	PASS	17.1
Combined Loads	*Equation26*	PASS	0.3
Separation Criteria	*Equation 28*	PASS	58.1

4.7.4 RIGEX Subsystem Component Constraint Bolts

The computer is the heaviest subsystem component on RIGEX, and it is also the only system without redundancy. Therefore, the bolts holding the computer to the structure must not fail or separate, endangering the fragile electronics within. Two separate analyses were performed on the computer bolts. One analysis focused on the bolts that hold the computer to the computer mounting plate (CMP) and the other on the bolts that restrain the computer mounting plate to the structural rib.

The bolts constraining the computer to the CMP are a set of four ¼-28 bolts, conforming to NAS1351N4-24. The analysis produced all positive margins for a torque range of 141-173 in-lbs. A set of eight #10-32 (NAS1189E3P8B) bolts hold the CMP to the rib, and those bolts must be torqued within the range of 63-69 in-lbs to meet all requirements.

The power distribution plate (PDP) is secured to the rib with nine #10-32 bolts. These bolts, also in compliance with NAS1189E3P8B must meet the torque range of 62 to 67 in-lbs.

The bolts constraining the ovens to the oven mounting plate are #10-32, ¾ in long A286 CRES, in compliance with NAS1189E3P12B. These bolts will be torqued to 61 to 75 in-lbs.

Finally, the bolts holding the oven mounting brackets to the oven mounting plate are NAS1189E3P16, or #10-32 A286 CRES 1 inch long. These bolts will be torqued to 67 in-lbs plus or minus 7 in-lbs to meet the required criteria.

Result details for the bolts discussed in Section 4.3.4 are available in Appendix A.

4.8 Analyses and Results Summary

Finite element modeling and analysis are powerful risk mitigation tools that ensure adequate strength of payload design. Based on analysis of the final RIGEX FE model, the expected first normal mode is approximately 185 Hz. Maximum stress on the aluminum structure, maximum loading at all bolt locations, and maximum deflections of the shroud and bumpers were also determined. Analytical FE model documentation, along with future flight model acceptance testing, will provide AFIT and STP with adequate structural verification data for launch. The final RIGEX FE model has been submitted to STP, where it will be integrated with the CAPE and eventually the space shuttle orbiter FE models for detailed integration analysis.

After results were obtained through finite element analysis for the loads transferred through critical RIGEX bolts at limit load conditions, the RIGEX bolt strength and separation analysis could proceed.

While the bolt analysis is only as accurate as the assumptions made, the assumptions were generally very conservative, and therefore the required torque range, as

gleaned from the analysis, is much tighter than required for bolt and locking mechanism integrity. Using a tight range will ease construction, as a small range will not leave a room for error or lack of conformity within the bolt patterns. RIGEX construction can proceed with confidence that the bolts will have adequate strength and a proper separation factor of safety in order to function properly throughout the entire mission profile.

The analysis results form this chapter, as well as other NASA prescribed requirements, have motivated numerous design changes. These changes are discussed in the following chapter.

V. RIGEX Design

RIGEX has undergone many design changes as its mission operation and payload envelope have evolved since the project began in 2000 (Figure 5-1). Now that RIGEX has been manifested on CAPE, construction of the hardware can proceed without fear of needing a major redesign to accommodate a different payload envelope. Therefore, the Drawing Package, Wire Routing Scheme, and fastener and component selection needed to be finalized. The design of RIGEX, initiated by DiSebastian and Goodwin, needed numerous additions and changes to prepare it for flight. Additionally, many changes were made to the design to facilitate the real world problem of component acquisition, as well as to make construction, integration and testing less difficult.

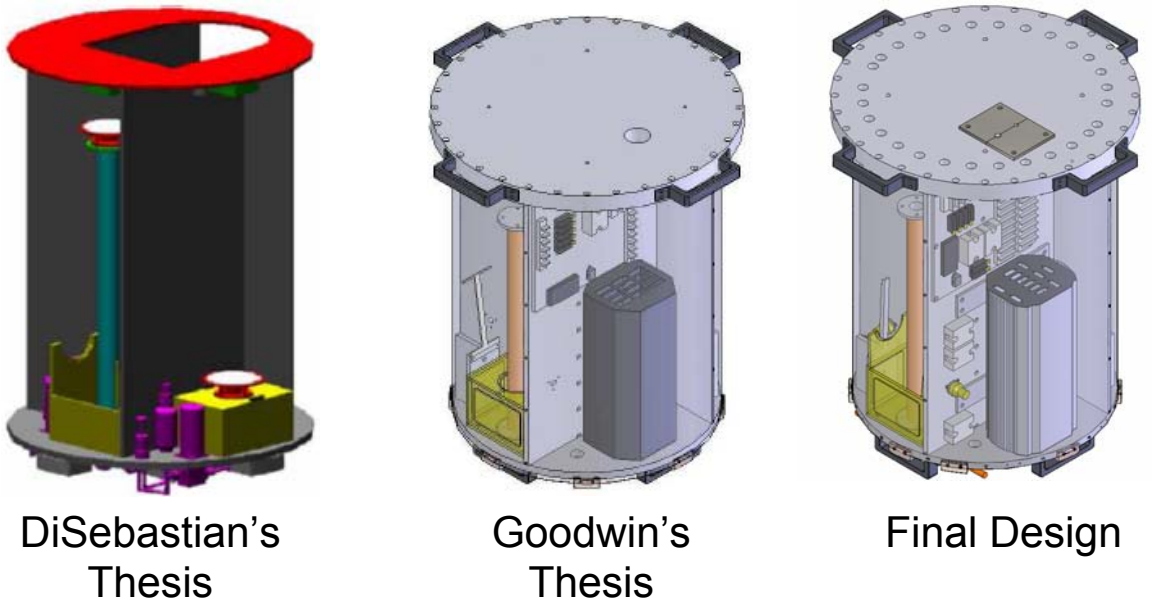

Figure 5-1: RIGEX Structural Design Evolution (10 and 15)

5.2 Design Optimization (Bolts)

At the RIGEX CDR, the RIGEX draft design called for over forty different types of fasteners, all of which needed to comply with different National Aerospace Standards. A unique type of fastening system was used at almost every joint. The quest to acquire such a wide array of bolts proved futile, limited by both expense and availability. Therefore, nearly every joint within the RIGEX structure was redesigned to promote fastener conformity. Unfortunately, the power distribution subsystem components' bolts were constrained to fit through the preexisting holes in those components, so a large variety of bolts was still needed to fill the needs of the numerous electrical parts. Through optimization, the total number of unique fasteners needed nearly halved, from forty at CDR to just twenty-two in the design as submitted for construction (and analyzed in the bolt analysis discussed in this thesis).

The first step in the optimization process involved identifying the NAS approved fastening devices that would meet the NASA requirement of having a locking mechanism (in addition to the applied preload). The fasteners must be manufactured from A286 Corrosion Resistant Stainless Steel (CRES), which was designated by STP as the material of choice for CAPE payloads. Four primary bolt types were identified as meeting these requirements, NAS1189, NAS1351, NAS1351, and NAS8402 bolts. NAS1189 bolts offered a flat head, which would fit a 100 degree countersunk hole (29). NAS1189 bolts are ideal for holding the primary structure together, as bolt heads will not protrude into the experiment bays and interfere with tube deployment. NAS1351 (27) and NAS1352 (28) bolts are very similar to each other, each with socket head caps.

NAS1351 and NAS1352 bolts work well to hold subsystem components in place, and they are a good choice for locations where the structure is too thin for a countersink. NAS8402 bolts serve well in locations that require a nearly flat head, but that cannot accommodate a countersink (26).

Once the bolt types were selected, the locking mechanism was identified. Patchlock was only used for components that did not have a likelihood of being removed often, as that would diminish the patch's locking properties. Heli-Coil inserts were used to lock in components like the shroud, the CAPE mounting plate, the power distribution system, and the computer. These inserts will allow those components to be removed and reinstalled multiple times without wearing the tap in the aluminum structure. Finally, locknuts were selected for components that were attached to a thin structure, such as the oven latch.

The exact bolt size to be used to fasten the various components together was selected next. Multiple Requests for Quote (RFQ) were submitted to fastener vendors for the bolts that would be simplest in a given location, and that had already proven themselves in the bolt strength and separation analyses. Unfortunately, as certificates of compliance* would be needed for these relatively rare NAS bolt types, very few RFQs were returned. Of those that were returned, many vendors were unable to locate all of the fasteners requested for RIGEX. Therefore, the RIGEX design was enhanced to make better use of industry standard fasteners that are readily available. In many instances,

* A certificate of compliance is a formal document provided by the manufacturer or distributor stating that the given component has been constructed to and meets the physical testing requirements as specified in the associated Military Specification (MS) and/or National Aerospace Standard (NAS). In order to fly on a

design modifications involved adding a countersink or counterbore to a bolt thru hole in order to facilitate a more readily available fastener. Design optimization became an iterative process with the FE and bolt analyses. Eventually, the RIGEX fastener choices were able to satisfy both the bolt strength and separation criterion and the list of available NAS fasteners. Table 10 details the final fastener choices.

Table 10. RIGEX Fastener Locations and Types

Location	Thread Type		Size	Threads/Inch	Length (in)	Head Type	Patchlock?
shroud (52)	UNJ	MS21209C0820L	Helicoil #8-32, 2x diameter				
computer mounting plate to rib (8), connector cover assembly to CAPE mounting plate (8)	UNJ	MS21209F1-20L	Helicoil #10-32, 2x diameter		1.5*d		
experiment top plate to CAPE mounting plate (28)	UNJ	MS21209F6-15L	Helicoil 3/8-23 1.5x dia				
bumpers (28)	UNJF-3A	NAS1189E04P8B	#4	40	1/2	Flat	Yes
ribs to ribs, press sys mounting plates and bottom plate (88), oven to oven mounting plate (12), oven bracket piece 1 to piece 2 (9), solenoid mounting block to adjacent rib (6), pressure transducer mounting block (to itself and to rib) (24)	UNJF-3A	NAS1189E3P12B	#10	32	3/4	Flat	Yes
ribs to oven mounting plate and top plate (36), oven bracket to oven mounting plate (12), connector cover assembly to CAPE mounting plate (8)	UNJF-3A	NAS1189E3P16B	#10	32	1	Flat	Yes
PDP to rib (9), computer mounting plate onto rib (8)	UNJF-3A	NAS1189E3P8B	#10	32	1/2	Flat	Yes
pin puller to rib (9), oven hinges (24), oven bracket to oven latch hinge(24)	locknut	NAS1291C04M	#4	40			
experiment tube to oven mounting plate (12), computer to computer mounting plate (4)	locknut	NAS1291C4M	1/4	28			
computer to computer mounting plate (4)	UNRF-3A	NAS1351N4-12	1/4	28	3/4	Socket Cap	No
experiment tubes to oven mounting plate (12)	UNRF-3A	NAS1351N4-24	1/4	28	1 1/2	Socket Cap	No
experiment top plate to CAPE mounting plate (28)	UNJF-3A	NAS1351N6-20	3/8	24	1.25	Socket Cap	Yes
pin puller to rib (9)	UNRC-3A	NAS1352N04-10	#4	40	5/8	Socket Cap	No
oven bracket to oven latch hinge (12), solenoid to solenoid Mounting Block (6)	UNRC-3A	NAS1352N04-8	#4	40	1/2	Socket Cap	No
EMI filter to PDP (4)	UNRC-3A	NAS1352N04LB4	#4	40	1/4	Socket Cap	Yes
terminal blocks (40), fuse block (20), cameras (12)	UNRC-3A	NAS1352N06LB8	#6	32	1/2	Socket Cap	Yes
transformers (6), power relays (10)	UNRC-3A	NAS1352N08LB4	#8	32	1/4	Socket Cap	Yes
computer mounting plate to rib (8)	washer	NAS620C10	#10				
pin puller to rib (18), oven hinges (24), oven bracket to oven latch hinge (24)	washer	NAS620C4	#4				
experiment tube to oven mounting plate (24), computer to computer mounting plate (4)	washer	NAS620C416	1/4				
shroud (52)	UNJC-3A	NAS8402-7	#8	32	4/9	Flange Button	No

5.3 Bumpers

The RIGEX bumpers are designed to protect CAPE from the RIGEX free end. The finite element analysis revealed that flight loads will not cause the free end to displace into CAPE once RIGEX is secured in place, but there is still a chance of metal-

---

NASA crewed space vehicle, all components of a payload must have a certificate of compliance for an

on-metal contact as RIGEX is being installed. The concept of bumpers was introduced originally as *snubbers* in Holstein's thesis (Figure 5.3-1). While both a bumper and a snubber aim to protect the inside of a payload canister, they have one key difference. A snubber is designed to fit tightly against the inside of the canister, preventing vibration. Conversely, a bumper is designed to absorb impact and protect metal surfaces if contact should occur, but it is not intended to ever actually touch the opposing surface. RIGEX bumpers are just like automobile bumpers: they are there for protection, but ideally they will never be used.

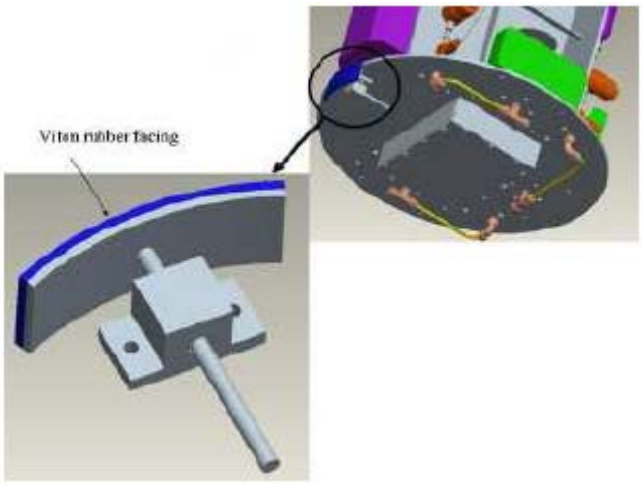

Figure 5.3-1: Holstein's Snubber Design (17)

The snubber concept was altered into a bumper design by Goodwin, who chose to simplify them and construct them from a lightweight, near frictionless plastic, Delrin. Goodwin chose to place 8 bumpers at equal distances around the oven mounting plate, and secure them with #10-32 bolts (Figure 5.3-2).

---

acceptable MS or NAS.

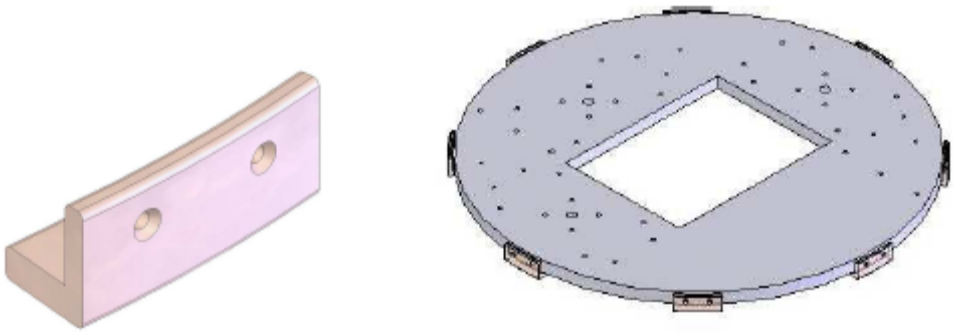

Figure 5.3-2: Goodwin's Bumper Design (15)

The final bumper design required modification. The use of #10 bolts overwhelmed the bumpers, as their caps would protrude from the countersunk hole, thus eliminating the metal-on-metal contact protection. The bolt size was reduced to #4, and a counterbore was added in order to imbed the bolt head deep within the bumper, thus preventing any chance of CAPE contact with the bumper bolts. Furthermore, the bumpers had to be rearranged on the oven mounting plate to deconflict bumper bolt holes with shroud attachment points. Finally, the bumpers themselves were thickened to ¼ inch. Extended bumpers cause RIGEX to protrude slightly into the CAPE Payload Envelope, but this protrusion was accepted at a teleconference with STP as it allows for better CAPE protection.

Based on probable RIGEX into CAPE mounting procedures, the use of only eight bumpers in the configuration below (Figure 5.3-3) was permitted by STP. However, fourteen bumpers will be produced in the event that STP-H2 (ANDE) actions call for a more protected payload in future CAPE missions.

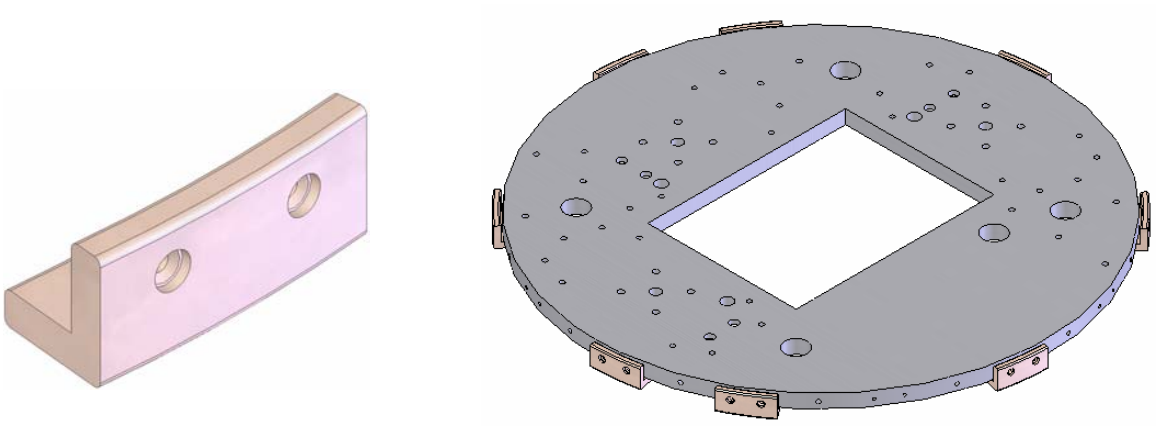

Figure 5.3-3: As Built Bumper Design and Arrangement

5.4 Pressure Transducer Mounting Blocks

RIGEX employs six pressure transducers: three to monitor the pressure in the Nitrogen Gas Tanks and three to record the pressure in the thermoplastic composite tubes as they are being inflated (Figure 5.4-1 and 5.4-2 respectively). These pressure transducers and their backshells can be modeled as 6.5 inch beams that are cantilevered from the inflation system tubing. Valid concern was raised at CDR that such an arrangement would strain the tubing during launch and cause damage or even failure to the pressure transducers. Therefore, a set of pressure transducer mounting blocks was designed to inhibit the transducer's expected vibrations. Each of these blocks contains two pieces: section one which will attach directly to an adjoining rib and section two will be attached to section one once the pressure transducer is installed.

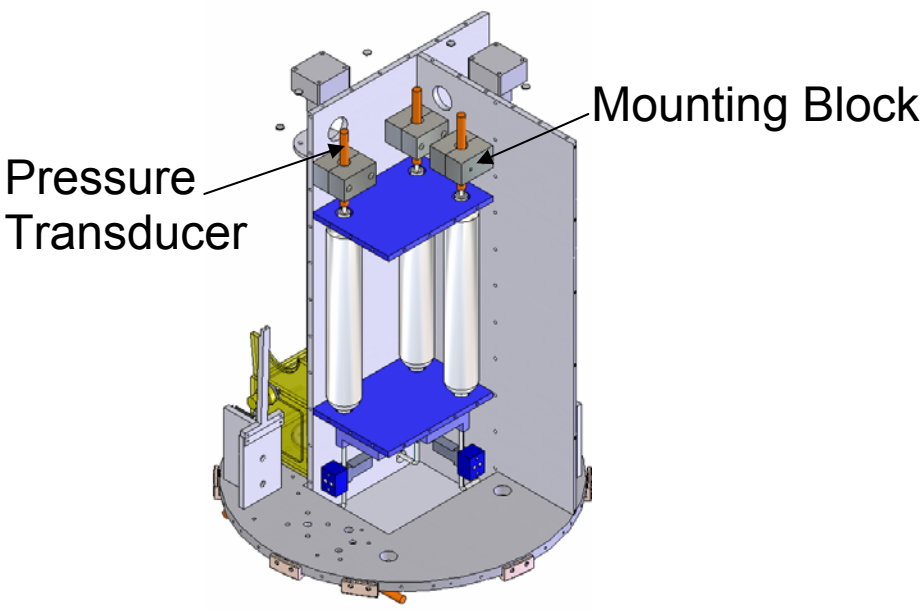

Figure 5.4-1: Three Pressure Transducers for Nitrogen Gas Tanks

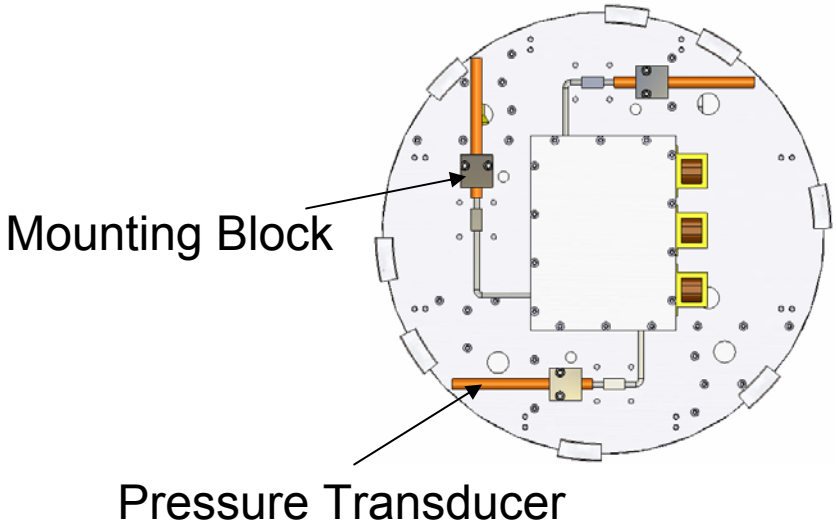

Figure 5.4-2: Three Pressure Transducers for Thermoplastic Composite Tubes

5.5 Computer Mounting Scheme

The computer case was originally designed to be bolted directly to the 13-inch computer rib. Bolting the case directly not only makes it extremely difficult to attach the

computer to the rib during construction, but it becomes impossible to remove the computer for repair or data retrieval without disassembling much of the primary structure, thus wearing at the fastener threads and degrading their locking capability.

Therefore, the computer mounting scheme shown in Figure 5.5-1 was developed. Before the computer is even inserted in the computer container, the computer container will be fastened to the two computer mounting brackets via four ¼-28 bolts and locknuts. Once in place, these four fasteners will never be removed. The computer will then be added into the computer case. At the appropriate stage of assembly, the computer brackets will be attached to the 13-inch computer rib by eight #10-32 bolts that will thread into Heli-Coil inserts already in the rib. These inserts will allow the computer mounting bracket bolts to be removed and reinstalled multiple times without degrading the quality of the joint. The bolts holding the computer mounting brackets to the rib will be easily accessible, therefore the shroud is the only part of RIGEX that will need to be removed in order to access the computer.

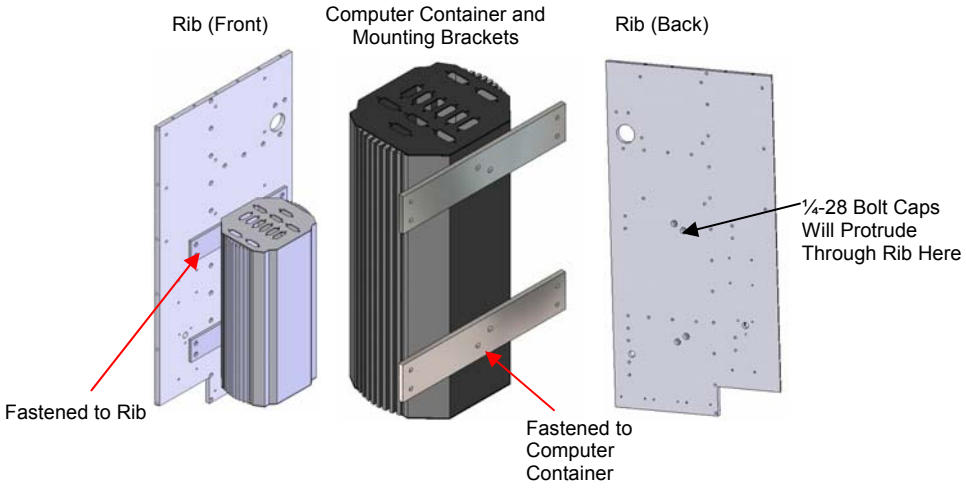

Figure 5.5-1: Computer Mounting Scheme

5.6 Power Distribution System

The power distribution system, the arrangement of its components, and its wiring schematic all required finalization before the NASA/RIGEX Phase II Safety Review (19 September 2006). The original plan for the power distribution system was to house all non-computer electrical components within the power distribution unit (Figure 5.6-1).

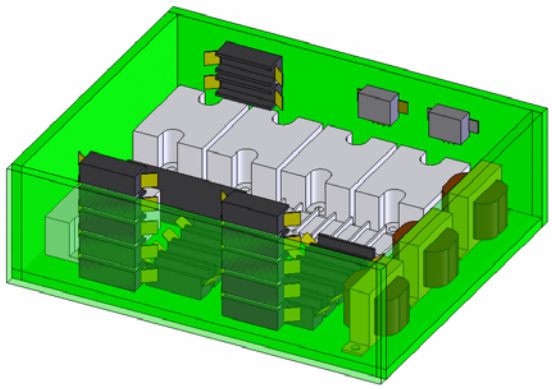

Figure 5.6-1: Power Distribution Unit Concept

The power distribution unit box was very crowded, and wiring would become error prone, thus the power distribution plate (PDP) concept was developed. The PDP would serve as an electrical isolation plate for the components it carried. It would also house only the central power distribution components. Those parts specific to the individual tubes would be dispersed throughout the RIGEX structure to ease wiring. Other power distribution system components were isolated in order to avoid expensive out-gassing testing. The Oven Relays, for example, have unknown outgassing properties. Therefore, they were brought inside the shroud in the Computer Bay, where they could not directly outgas onto either CAPE or the optical equipment in each of the three Experiment Bays. The complete wire routing schematic is available in Appendix E.

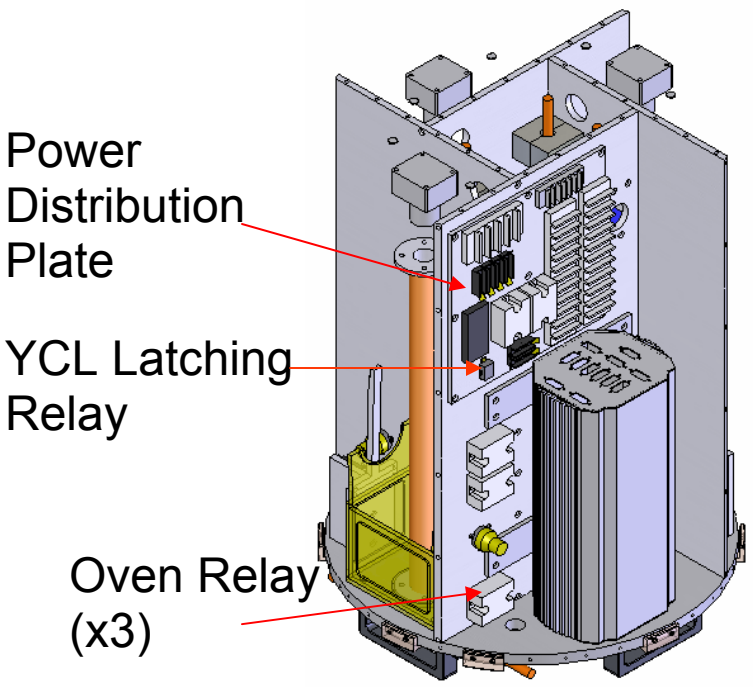

Figure 5.6-2: Power Distribution Plate

5.7 Orbiter Electrical Interface

RIGEX will be powered and controlled from within the space shuttle orbiter. It will interface directly to the orbiter via two pigtail cables. For RIGEX, the two key electrical components within the orbiter are the S13 (UP, NEUTRAL, DOWN) three-way momentary switch and the DS13 three way display (UP, STRIPES, DOWN). When NASA determines an appropriate time for RIGEX operation, an astronaut crew member will hold the S13 switch up until the DS13 display switches from STRIPES to UP. However, DS13 is not tied in directly to S13. DS13 is a feedback display directly triggered by RIGEX that signifies the YCL latching relay (Figure 5.6-2) on the PDP has activated and the system is now accepting shuttle power. At this point, RIGEX also will begin its interface verification test (IVT). The IVT will cycle the major RIGEX

components to test and record their functionality. The data produced by the IVT will be important in determining the cause of any abnormal deployment and vibration data during the actual thermoplastic composite tube tests. During the IVT, DS13 will read UP for approximately 300 seconds, after which it will transition to STRIPES for another 300 seconds. It will then read DOWN for 60 seconds, and when the IVT is finished (approximately 60 seconds later), DS13 will transition back to STRIPES. The entire IVT runs for approximately 720 seconds. After the IVT process, the crew will have a 300 second window in which they can place S13 DOWN and turn the experiment off. Then the actual experiment will begin, and DS13 will read UP for its entirety. Once the experiment is complete, DS13 will show DOWN, at which point it is safe for the crew to move S13 DOWN, thus disengaging the latching relay and cutting RIGEX power.

5.7.1 Electrical Connection

All of the power, feedback and control will be wired from RIGEX directly to the orbiter through two cables, called pigtails (Figure 5.7-1). These two cables will each be wire bundles, designated J1 and J2 (Figure 5.7-2). The six 22 American Wire Gauge (AWG) wires in the J1 bundle will run to and from S13 and DS13, and the three 8 AWG wires in J2 will carry 28 Volts Direct Current (VDC) to and from RIGEX, along with providing a Ground conduit.

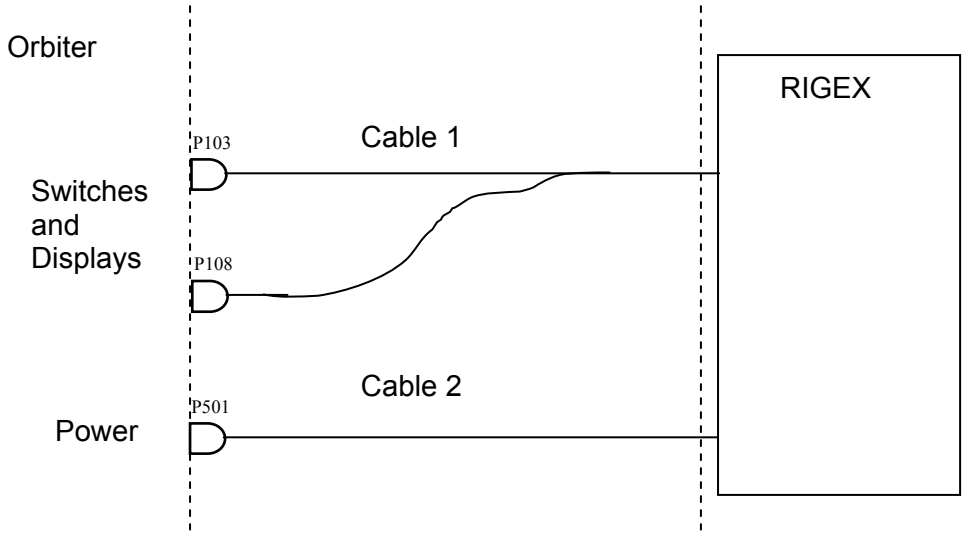

Figure 5.7-1: RIGEX/Orbiter Interface Cable Routing

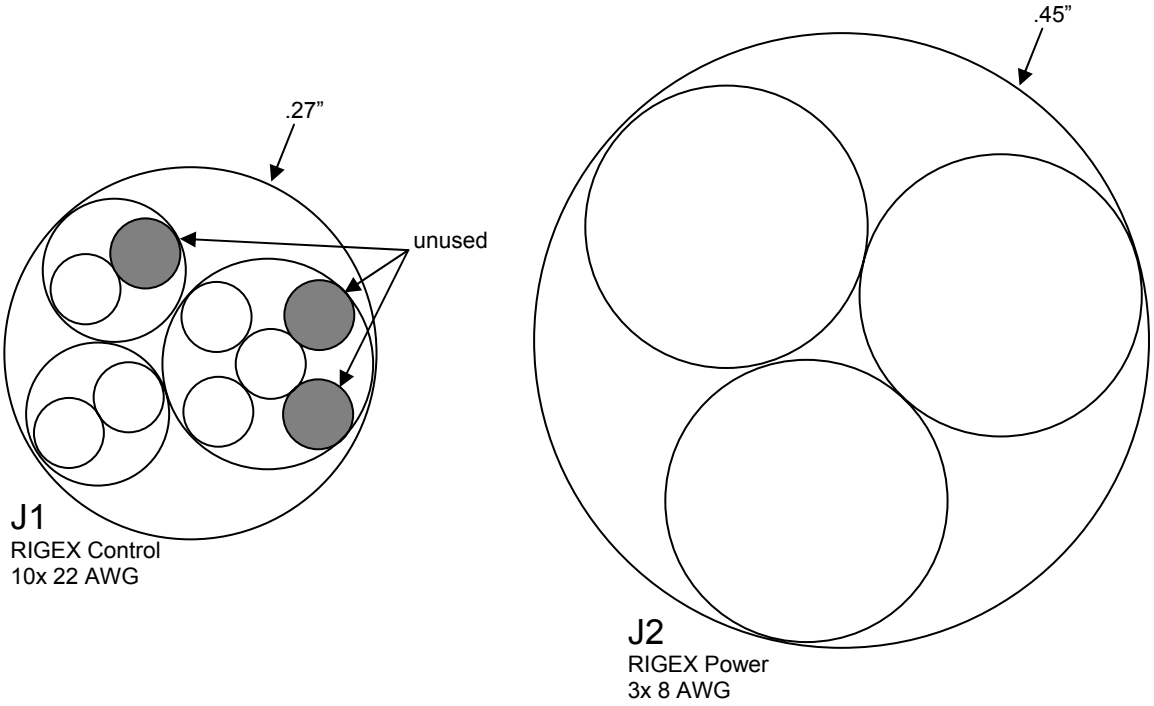

Figure 5.7-2: J1 and J2 Cables

The pigtail nature of the cables simplifies the connector requirements, as the wires will be permanently attached to the RIGEX PDP. From the PDP, the wires will run

all the way to the orbiter, with no intermediate connectors. Therefore, the plugs that will be inserted in the appropriate orbiter socket will be permanently attached to the cables that will, in turn, be permanently attached to RIGEX. Using pigtails opens another configuration issue. The wires will need to travel through both the CAPE mounting plate and the RIGEX experiment top plate on their way from the orbiter to the PDP, but the CAPE mounting plate will need to be removed for shipping, testing and ground handling. A large, unguarded, hole through the CAPE mounting plate through which the connector ends of the wires could feed was ruled out as an option because it does not offer the cable support required at that point and it produces a containment problem. Therefore, the connector hole cover assembly was developed (Figure 5.7-3). This simple, two-piece Assembly will hold the J1 and J2 cables snuggly above the CAPE mounting plate. When the CAPE mounting plate must be removed, the connector hole cover assembly will be removed, thus revealing a hole on the CAPE mounting plate that is large enough for the connectors to pass through (Figure 5.7-4). The cables will remain attached to the PDP through the holes they were originally fed through on the RIGEX experiment top plate (Figure 5.7-5).

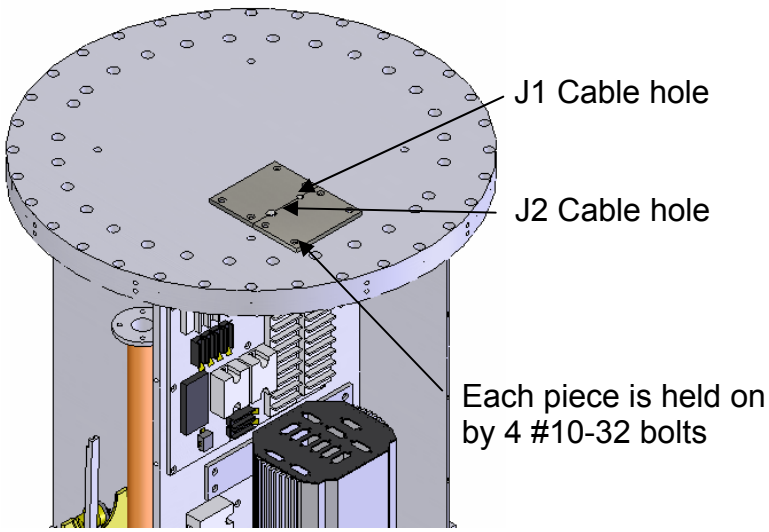

Figure 5.7-3: Connector Hole Cover Assembly

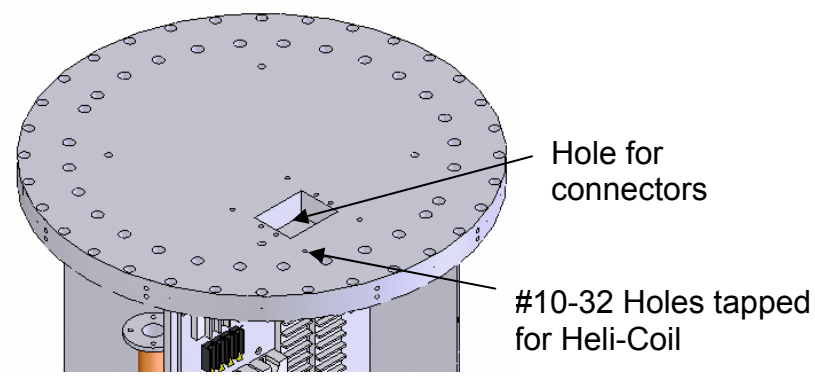

Figure 5.7-4: Connector Hole on CAPE Mounting Plate

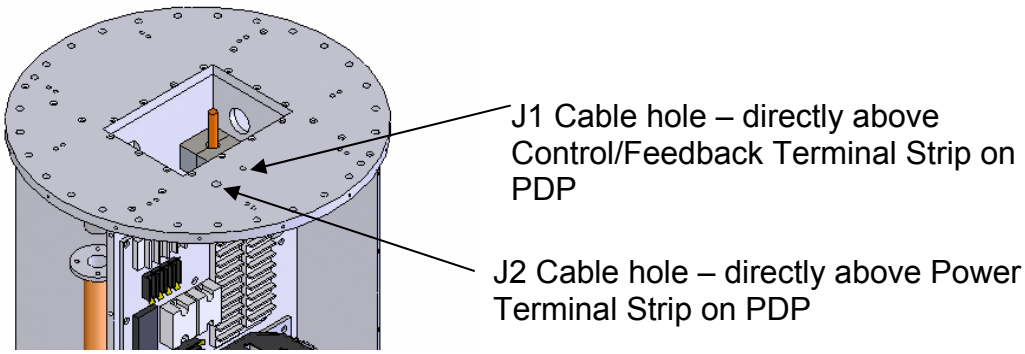

Figure 5.7-5: Connector Holes on RIGEX Experiment Top Plate

5.7.2 Space Shuttle Orbiter Electrical Emulator

In order to determine RIGEX's actual current and power draw during the IVT and the actual experiment, and in order to ensure RIGEX will function as designed with orbiter power, feedback and control, a space shuttle orbiter electrical emulator was developed. The emulator closely mimics the appropriate circuitry on the orbiter, and provides the same DS-13 feedback, as well as projecting current in real time.

The emulator circuit (Figure 5.7-6) mimics the orbiter's momentary S-13 switch, and relies on the YCL latching relay within RIGEX to activate the DS-13 UP and DOWN displays. The differences in circuitry between the emulator and the applicable parts of the actual orbiter are the display type, the fuse, and the ability to monitor more of RIGEX's electrical activity than just whether DS-13 reads UP, DOWN or STRIPES.

The DS-13 display on the orbiter is a relic, as it physically switches from UP, DOWN and STRIPES, causing 35.4 kΩ resistance. The LEDs on the emulator offer almost no resistance, thus a resistor was added to the circuit. A 15 A fuse was also added to the emulator. If a power spike should occur, the easily replaceable fuse would fail before any RIGEX fuse, therefore reducing risk to flight hardware. Finally, methods of monitoring voltage and current draw were designed. A permanent ammeter display is available on the emulator box (Figure 5.7-7) for quick viewing and for monitoring RIGEX outside of the AFIT lab. Banana jacks were also added to the circuit that allow for interface with the LabView computer in the AFIT Lab, which will enable current data recording for in depth analysis and reporting.

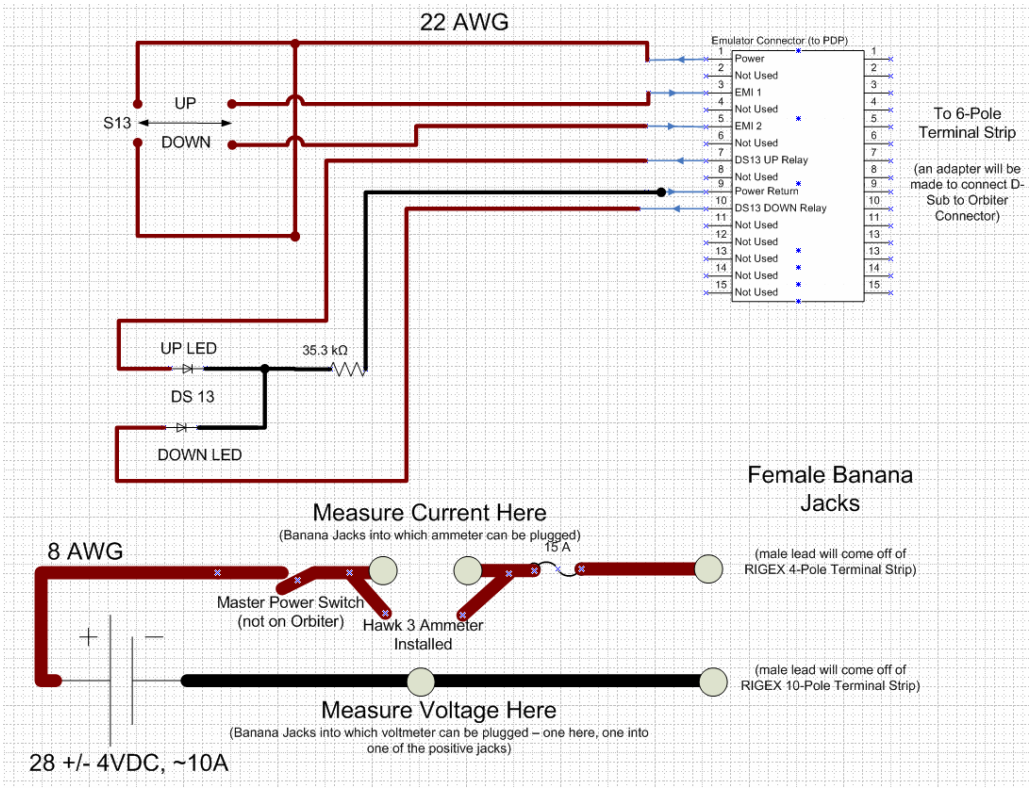

Figure 5.7-6: Emulator Electrical Schematic

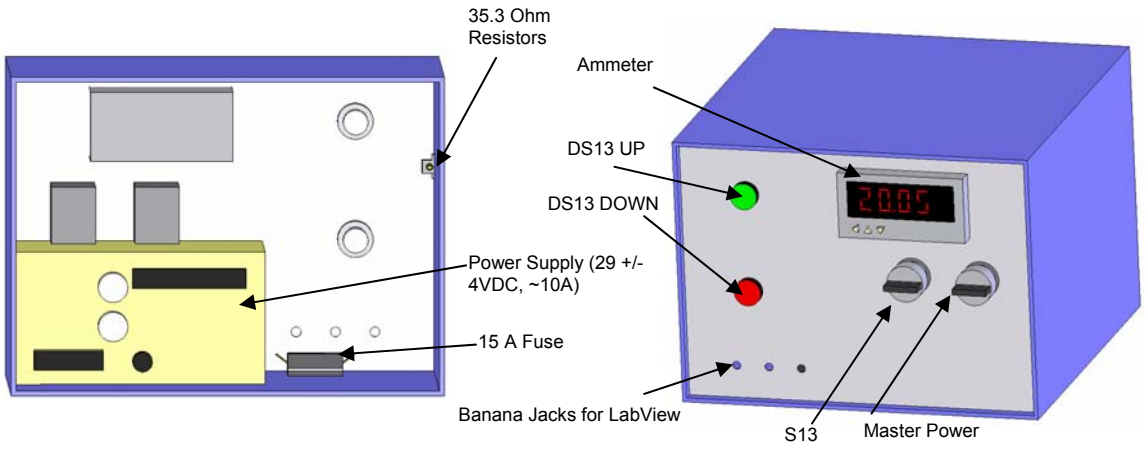

Figure 5.7-7: Emulator Physical Design

Once all RIGEX electrical subsystem components become available for testing, the emulator will be used to establish an expected current profile. Once the entire RIGEX structure is built and the shroud installed, there will be no way to directly observe the subsystem functions. Therefore, the current profile, as revealed from the emulator in laboratory tests, can be compared to current readout on the emulator during functional checks to ensure components are drawing the proper amount of current on queue.

5.8 Mass Properties

The SolidWorks software package makes it easy to determine the mass properties of a well designed assembly. The total mass of the flight assembly (without the lifting handles and stabilizing feet) is expected to be 211 lbs, which does not include fasteners (estimated 15 lbs) or wires and connectors (estimated 10 lbs). The fasteners, wires, and connectors will be distributed relatively equally around RIGEX, although the wires and connectors will favor the positive x-axis. The total expected flight weight is approximately 236 lbs, with a center-of-gravity located at (+0.4, +0.2, +11.7) inches with respect to the coordinate system shown in Figure 5.8-1.

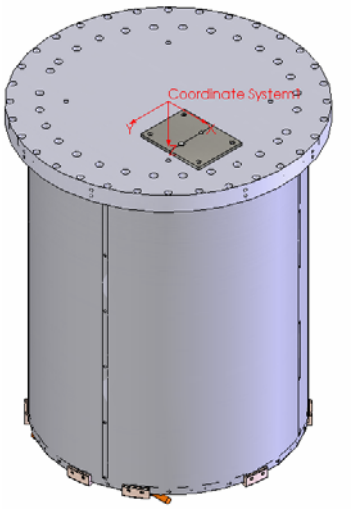

Figure 5.8-1: Coordinate System

5.9 RIGEX Design Summary

The final design, as submitted in this thesis, is the culmination of the efforts of the author and nine other RIGEX researchers. The final RIGEX drawing package is available in Appendix D. The RIGEX structural components are currently undergoing fabrication in the AFIT shop, after which they will be assembled in the RIGEX lab. During assembly, the torque value of every bolt must be recorded and submitted to STP. The RIGEX wiring schematic was also developed and is presented in Appendix E. Once the wiring harness is complete, the space shuttle orbiter electrical emulator will be used to determine the RIGEX current draw profile.

VI. Conclusions and Recommendations

This thesis presents the current status of an ongoing effort to analyze, construct, and test the RIGEX structural and electrical designs. After the submission of this thesis, work will continue by the author and the RIGEX team to prepare for the Phase II Safety Review and to provide STP with a RIGEX electrical current profile for the entirety of the experiment.

6.1 Future RIGEX Work

6.1.1 Acquisition

Although the RIGEX design is finalized, much work remains. First, the acquisition of all necessary RIGEX components must be completed expediently. Difficulties in obtaining the components has delayed the inception of RIGEX primary structure construction and indefinitely postponed the execution of the current draw analysis. The RIGEX parts and materials list must be maintained in real time to reflect those components which have been ordered, those which arrive at AFIT, and those which are changed to accommodate budget and availability.

6.1.2 Assembly

Assembly drawings and procedures will be written by the author prior to the Phase II Safety Review. These drawings and their associated procedures will provide a step-by-step guide to those inheriting the RIGEX project. During the assembly process, special care must be taken to record the torque applied to each bolt, ensuring that is

within the acceptable torque range as identified in the bolt analysis. As there is no official quality control system in place at AFIT, the applied torque must be confirmed by two individuals and entered into the *File to Manage Running Torques* within the RIGEX network folder. The torque management document must be submitted to NASA and STP along with the completed RIGEX. A binder of certificates of compliance must also be created and organized for submission. The binder will include a certificate of compliance for every RIGEX component, both structural and electrical. Finally, once all RIGEX bolts arrive at AFIT, a representative sample of each bolt type must be sent to STP for destructive testing. Testing will verify the bolts' "chemical and mechanical properties to ensure that no mistakes were made and/or shortcuts taken in the manufacturing process" (30: 5). The representative sample will be 2 to 5 bolts, as determined by the *Minimum Sample Sizes Per Lot Size* table in the *JSC Fastener Integrity Testing Program* document.

6.1.3 Power Distribution System Verification

Prior to the integration of the power distribution system onto the assembled RIGEX structure, an expected current draw profile must be obtained. The profile will be developed by attaching the space shuttle orbiter electrical emulator (discussed in Section 5.7.2) to the power and command terminal strips on the power distribution plate and running the experiment (with thermoplastic composite tubes that are for ground test only). It will be easier to run the current draw test, and obtain baseline results, with the RIGEX subsystem components laid out on a table, than it would be to run the test on the fully assembled and electrically integrated RIGEX structure. While the components are in full view and easily accessible, their functionality can be verified visually. The test

will be run again on the integrated structure, but at that time it will be used simply to verify functionality of components that can no longer be directly observed.

6.1.4 Structural Verification and Environmental Testing

Per the CAPE/RIGEX Structural Verification Plan (SVP), the analyses and tests in Table 11 must be accomplished prior to flight (8). Table 11 also indicates whether the test has already been completed. Once the RIGEX structure is built, the RIGEX team must complete random vibration, mass properties, and thermal analyses per the requirements outlined in the SVP.

Table 11. Structural Verification and Environmental Testing Requirements

Qualification Issue	Analysis		Test	
	Required	**Complete**	**Required**	**Complete**
Structural Strength	X	X		
Structural Stiffness	X	X		
Random Vibration	X		X	
Mass Properties	X	X	X	
Thermal	X		X	
Fracture	X	X		
Pressurization/Depressurization	X	X		

Finally, RIGEX will need to undergo thorough Electro-Magnetic Interference (EMI) testing. EMI testing will occur at F2Labs in Burton, Ohio no earlier than November 2007.

6.2 Summary and Conclusions

The completion of this thesis brings RIGEX one step closer to its launch in December 2007 on STS-123. After discussing the development of the final fine mesh FE model with which to conduct accurate analyses, this thesis presented the results of the completed Structural Verification Plan items as required by NASA and STP. Analyses includes the structural strength analysis, which shows that RIGEX's 6061-T6 Aluminum primary structure will not fail under limit load conditions. The structural strength analysis also included developing a methodology for and executing comprehensive bolt strength and separation analyses that validate every RIGEX joint. Results shows that every bolt on RIGEX will have adequate structural strength and exhibit an acceptable safety factor for joint separation at limit loads. Through analysis, this thesis has also shown that RIGEX's structural stiffness exceeds the fundamental frequency requirements outlined in the SVP by 135 Hz. Finally, the as built mass properties for RIGEX are shown in this thesis.

This thesis presents the as built drawings of all RIGEX structural components. These drawings have been submitted and are currently being used in the construction of the RIGEX structure. The electrical schematic and wiring map for the RIGEX power distribution system is also presented.

Designing a data acquisition system for and executing vacuum chamber tests to aid the development of the RIGEX thermal model, working with the RIGEX team to prepare and present the Critical Design Review, and preparing for the Phase II Safety Review have all been excellent opportunities to push RIGEX towards its launch on STS-

123. The RIGEX project has made great progress in the past year towards its ultimate goal of providing valuable structural data regarding the performance of rigidizable inflatable technology in space.

Appendix A: Bolt Analysis Results

Table A1. Computer to CMP Bolts: Torque Range 141-173 in-lbs

Criteria		PASS/FAIL	Margin
Min Cross-Section of Bolt	*Equation 8*	PASS	33.3
	Equation 17	PASS	0.1
Shear Pull-Out of Threads	*Equation 18*	PASS	75.8
	Equation 19	PASS	1.5
Shear Load	*Equation23*	PASS	7.9
Combined Loads	*Equation26*	PASS	0.2
Separation Criteria	*Equation 28*	PASS	4.5

Table A2. CMP to Rib Bolts: Torque Range 63-69 in-lbs

Criteria		PASS/FAIL	Margin
Min Cross-Section of Bolt	*Equation 8*	PASS	17.9
	Equation 17	PASS	0.1
Shear Pull-Out of Threads	*Equation 18*	PASS	16.8
	Equation 19	PASS	0.0
Shear Load	*Equation23*	PASS	3.8
Combined Loads	*Equation26*	PASS	0.2
Separation Criteria	*Equation 28*	PASS	0.9

Table A3. Power Distribution Plate to Rib: Torque Range 62-67 in-lbs

Criteria		PASS/FAIL	Margin
Min Cross-Section of Bolt	*Equation 8*	PASS	30.7
	Equation 17	PASS	0.1
Shear Pull-Out of Threads	*Equation 18*	PASS	28.9
	Equation 19	PASS	0.05
Shear Load	*Equation23*	PASS	8.4
Combined Loads	*Equation26*	PASS	0.2
Separation Criteria	*Equation 28*	PASS	2.1

Table A4. Ovens to Oven Mounting Plate: Torque Range 61-75 in-lbs

Criteria		PASS/FAIL	Margin
Min Cross-Section of Bolt	*Equation 8*	PASS	46.6
	Equation 17	PASS	0.1
Shear Pull-Out of Threads	*Equation 18*	PASS	88.8
	Equation 19	PASS	1.0
Shear Load	*Equation23*	PASS	10.4
Combined Loads	*Equation26*	PASS	0.1
Separation Criteria	*Equation 28*	PASS	4.4

Table A5. Oven Mounting Brackets to Oven Mounting Plate: Torque Range 60-75 in-lbs

Criteria		PASS/FAIL	Margin
Min Cross-Section of Bolt	*Equation 8*	PASS	78.0
	Equation 17	PASS	0.1
Shear Pull-Out of Threads	*Equation 18*	PASS	222.3
	Equation 19	PASS	2.1
Shear Load	*Equation23*	PASS	15.9
Combined Loads	*Equation26*	PASS	0.2
Separation Criteria	*Equation 28*	PASS	9.7

Appendix B: Bolt Analysis Spreadsheet

The bolt analysis was performed in a set of Microsoft Excel spreadsheets. The entire set of spreadsheets for the constraint bolt analysis is included below. The analysis for the other bolt patterns and subsystem component bolts followed a very similar format.

Table B1. PASS/FAIL and Torque Overview

Criteria		**PASS/FAIL**	Margin
Min Cross-Section of Bolt	PAt/(SF*P)-1>0	PASS	4.9529
	PAt/Pb-1>0	PASS	0.031
Shear Pull-Out of Threads	Pas/(SF*P)-1>0	PASS	4.7777
	Pas/Pb-1>0	PASS	0.0007
Shear Load	VA/(SF*V)-1	PASS	1.6441
Combined Loads	(1/(Ra^2+Rs^3))-1>0	PASS	0.0052
Case 1 (Pb < Tesile Yield Allowable)			
Use?	**USE ME**	PASS	0.0042
Separation Criteria	PLDmin/((1-n*ø)*Psep)-1>0		
Case 2 (Pb > Tesile Yield Allowable)		N/A	
Use?	DO NOT USE ME		

NAS #	Size	Threads/In	Length	Head Type
NAS1351N6-20	3/8	24	1 1/4	Standard

Final Torque Values:		Input:
Maximum Torque	Tmax	616 in*lb
Minimum Torque	Tmin	456 in*lb

Construct with torque range: 536 +/- 27 in lbs

Table B2. All Inputs (Bolt)

Term	Symbol	Value	Notes	Units
Basic major diameter of external threads (bolt)	D	0.375		in*lb
Maximum Torque	Tmax	616	starting value per MSFC-STD-486B p28, eventually optimized per criteria	in*lb
Minimum Torque	Tmin	456	""	in*lb
Axial load allowable of bolt due to tension	PAt	14052.5209	A*Ftu	lbs
Ultimate Shear Stress (bolt)	Fs	91000	MIL-HDBK-5H Table 6.2.1.0(b)	lb/in^2
Tensile Stress Area	A	0.087828256	Equation a in the Axial Load Allowable Due to Tension section of Appendix A of NSTS 08307	
Length of thread engagement	Le	0.5625		in
Tolerance on major diameter of threads (external)	TDe	0.0072	(maximum major diameter of screw-minimum major diameter of screw)	
Tolerance on pitch diameter of threads (internal)	TEi	0.0029	(maximum pitch diameter of thread-minimum pitch diameter of thread)	
Allowance on external threads	Ge	0		
Threads/in	no	24		
Bolt modulus of elasticity	Eb	29100000	MIL-HDBK-5H Table 6.2.1.0(b)	lb/in^2
Effective Length of Bolt	Lb	0.5625	An Introduction to the Design and B	in
Yield Allowable	Fty	95000	MIL-HDBK-5-H	lb/in^2
Ultimate Tensile	Ftu	160000		lb/in^2
Maximum Major Diameter of Screw		0.375		in
Minimum Major Diameter of Screw		0.3678		in
Maximum Pitch Diameter of Thread		0.3479		in
Minimum Pitch Diameter of Thread		0.345		in
Ultimate Shear Stress (structure)	Fs	28000	Mechanics of Materials 5th Edition, R.C. Hibbeler	lb/in^2
Prevailing Torque	Tp	80	MSFC-STD-486B	range is 9.5 to 80 per Heli-coil, 80 has the worst effect on margins
Actual Length of Bolt	Lb	1.25		
Bolt Head Diameter	Db	0.694		

Table B3. All Inputs (From FEMAP)

Term	Symbol	Value	Notes	Units
External axial load applied to joint at bolt location due to application of limit load to the structure	P	1180.3	Axial loads from FEMAP	lbs
Bolt shear load resulting from limit load	V	428.3548	Shear loads from FEMAP	lbs
Bolt bending moment resulting from limit load	M	200	Arbitrary Value	
Plastic Bending Factor	Ky	0	Arbitrary Value	
Max Preload K	K	100	Arbitrary Value	
Min Preload K	K	100	Arbitrary Value	

Table B4. Preload Calculations

Term	Symbol	Value	Notes	Units
uncertainty	Γ	0.35	non-lubricated	
typical nut factor	Ktyp	0.2	non-lubricated	
Basic major diameter of exernal threads (bolt)	D	0.375		in*lb
Positive thermal load	Pthrpos	1.97E+03	Bickford p 487	lbs
Negative thermal load	Pthrneg	-1.53E+03	Bickford p 487	lbs
Expected Preload Loss	Ploss	652.9368255	.05*PLDmax	lbs
Max Preload	PLDmax	13058.73651	((1+Γ)*Tmax)/(Ktyp*D)+Pthrpos	
Min Preload	PLDmin	1078.211582	((1-Γ)*(Tmin-Tp))/(Ktyp*D)+Pthrneg-Ploss	
Maximum Torque	Tmax	616	per MSFC-STD-486B p28	in*lb
Minimum Torque	Tmin	456	per MSFC-STD-486B p28	in*lb
Prevailing Torque	Tp	80	independent of preload level	in*lb
Thermal Load Calculations:	Calculated using equations in Bickford page 487			
Tensile Stress Area	A	0.087828256		in^2
Modulus of Elasticity of Bolt	E	29100000		
Length of Bolt	Le	1.25		in
Change in length of joint for -dt	dLj-	-2.24E-03		in
Change in length of joint for +dt	dLj+	1.51E-03		in
Change in length of bolt for -dt	dLb-	-1.59E-03		in
Change in length of bolt for +dt	dLb+	1.08E-03		in
coefficient of thermal expansion of bolt (-75 to 70	rhob-	8.76E-06	Mil-Hdbk-5h	in/in/*f
coefficient of thermal expansion of joint (-75 to 7	rhoj-	1.24E-05	Mil-Hdbk-5h	in/in/*f
coefficient of thermal expansion of bolt (70 to 165	rhob+	9.10E-06	Mil-Hdbk-5h	in/in/*f
coefficient of thermal expansion of joint (70 to 165	rhoj+	1.28E-05	Mil-Hdbk-5h	in/in/*f
Length of Thread Engagement	Le	0.5625		in/in/*f
Change in Temp (positive)	-dt	95		*F
Change in Temp (negative)	+dt	-145		*F
Ft+	Pthrpos	1.97E+03	Bickford p 487	lbs
Ft-	Pthrneg	-2.96E+03	Bickford p 487	lbs
Assuming built at room temp (70 degrees) and the max/min temps it'll experience are: -75 and 165*F respectively				
Thermal Load using Stiffness Equation from Bickford p 488				
Ft+=	1.02E+03			
Ft- =	-1.53E+03			

Table B5. Strength Criteria

Term	Symbol	Value	Notes	Units
Axial load allowable of bolt due to tension	PAt	14052.5209		lbs
bolt strength factor of safety	SF	2	NASA=STD-5001	
External axial load applied to joint at bolt location due to application of limit load to the structure	P	1180.3	Update this value with maximum axial loads from FEMAP	lbs
Bolt axial load resulting from yield, ultimate or joint separation load	Pb	13629.89526	PLDmax+n*ø*(SF*P)	lbs
Stiffness Parameter	ø	0.483909811	Kb/(Kb+Ki)	
Loading-plane factor	n	0.5	Carson Taylor	
Axial load allowable of bolt or nut due to thread shear	PAs	13638.88266	Asi*Fs, use smaller of 2 allowables	lbs
Ultimate Shear Stress (bolt)	Fs	91000	MIL-HDBK-5H Table 6.2.1.0(b)	lb/in^2
Ultimate Shear Stress (structure)	Fs	28000	Mechanics of Materials 5th Edition, R.C. Hibbeler	lb/in^2
Tensile Stress Area	A	0.087828256		in^2
Shear load allowable of bolt	VA	2265.2	Am*Fs	
Bolt shear load resulting from limit load	V	428.3548		
Bolt bending moment resulting from limit load	M	200		
Thread Shear Area	Asi	0.487102952		
Plastic Bending Factor	Ky	0		
		0.167984095	(SF*P)/PAt	
		0.96992528	Pb/PAt	
		0.929280704	PLDmax/PAt	
Ratio of P to PA (greatest of previous 3)	Ra	0.96992528		
Ratio of M to MA	Rb	0	OSS says 0 if no shimming	
Ratio of V to VA	Rs	0.378204838	(SF*V)/VA	
Max Preload K	K	100	Arbitrary (no Rb so K is not relevant)	
Min Preload K	K	100	Arbitrary (no Rb so K is not relevant)	
Minor Diameter Area	Am	0.0809	http://www.efunda.com/designstandards/screws/screwunf.cfm	

Table B6. Cross Sectional Area Calculations for Thread Shear

Term	Symbol	Value	Notes
Shear area of internal threads (since 6061is weaker material)	Asi	0.487102952	pi*Le*De*[.875-.57735*no*(TDe+TEi+Ge)
Length of thread engagement	Le	0.5625	in
Major diameter of internal threads	De	0.375	in
Tolerance on major diameter of threads (external)	TDe	0.0072	2*(maximum major diameter of screw-minimum major diameter of screw)
Tolerance on pitch diameter of threads (internal)	TEi	0.0029	2*(maximum pitch diameter of thread-minimum pitch diameter of thread)
Allowance on external threads	Ge	0	
Threads/in	no	24	

Table B7. Stiffness Calculations

Term	Symbol	Value	Notes	Units
Stiffness of bolt	Kb	4543648.423	(Ab*Eb)/Lb, Bickford	lb/in
Stiffness of joint	Kj	4845804.566	(Ej*Ac)/T, Bickford p 150, Cylinder method	lb/in
Bolt x-sectional area	Ab	0.087828256		in^2
Bolt modulus of elasticity	Eb	29100000	MIL-HDBK-5H Table 6.2.1.0(b)	lb/in^2
Effective Length of Bolt	Lb	0.5625	An Introduction to the Design and Behavior of Bolted Joints, by John H Bickford, Bickford Bickford p 147	in
Joint material modulus of elasticity	Ej	10000000	Mechanics of Materials 5th Edition, R.C. Hibbeler	lb/in^2
cross-sectional area of the equivalent cylinder used to represent the joint length	Ac	0.333149064	Bickford (Eqn 5.21 p 152)	in
total thickness of joint length	T	0.6875	Bickford (actual length of bolt - length of thread engagement)	in
Bolt Head Diameter	Db	0.694	Bolt NAS Spec	in

Diameter of Hole	Dh	0.397	SolidWorks Drawing	in

Table B8. Separation Criteria

Term	Symbol	Value	Notes	Units
Bolt axial load resulting from yield, ultimate or joint separation load	Pb	1420.906832	PLDmin+n*ø*(SF*P)	lbs
Joint Separation Load	Psep	1416.36	P*SFsep	lbs
Joint separation factor of safety	SFsep	1.2		
Yield Allowable	Fty	95000	MIL-HDBK-5-H	lb/in^2
Tensile Yield Allowable	PAty	8343.684283	Fty*At	lbs
Min Preload	PLDmin	1078.211582		

Appendix C: Matlab Data Reduction Code

Code for Finding Maximum Loads at Bolt Locations

```
function [ptid,T,Gpts, conzmaxaxial, conzmaxshear, zmaxaxial, zmaxshear,
ymaxaxial, ymaxshear, xmaxaxial, xmaxshear, maxaxialshroud1,
maxshearshroud1, maxaxialshroud2, maxshearshroud2, maxaxialshroud3,
maxshearshroud3, maxaxialshroud4, maxshearshroud4, maxaxialshroud5,
maxshearshroud5, maxaxialshroud6, maxshearshroud6, maxaxialshroud7,
maxshearshroud7, pressaxial, presssheаr, camaxial, camshear, compaxial,
compshear, pdpaxial, pdpshear, ovenaxial, ovenshear, mountaxial,
mountshear, transaxial,
transshear]=boltfinal(num_lines,pathname,filename,varargin);

%*********************************************************************
***
%
% The shell of this program was written by Dr. Cobb to input a Nastran
text
% file and extract data at given point IDs.
% The file was  modified by 2d Lt Anna Gunn-Golkin to process a load
% data file output from Nastran, rotate those loads to the appropriate
% coordinate frame, and determine the shear and axial loads experienced
by
% the bolts which will be located at each specifically identified grid
% point.
%
% To run this program, open this dir in matlab and type in the
% command window:
% [ptid,T,Gpts, conzmaxaxial, conzmaxshear, zmaxaxial, zmaxshear,
ymaxaxial
% , ymaxshear, xmaxaxial, xmaxshear, maxaxialshroud1, maxshearshroud1,
% maxaxialshroud2, maxshearshroud2, maxaxialshroud3, maxshearshroud3,
% maxaxialshroud4, maxshearshroud4, maxaxialshroud5, maxshearshroud5,
% maxaxialshroud6, maxshearshroud6, maxaxialshroud7, maxshearshroud7,
% pressaxial, presssheаr, camaxial, camshear, compaxial, compshear,
% pdpaxial, pdpshear, ovenaxial, ovenshear, mountaxial, mountshear,
% transaxial, transshear]=boltfinal(****)
%
% **** indicates the number of lines of the input file you want the
% program to search through
%
%*********************************************************************
***

% Pulls specific Nastran output file
fid=fopen('L:\eny students\RIGEX\Bolt Analysis\New
Results\multiset2.f06');
eof=fgetl(fid);
x=0;
finish=[];Gpts=[];
i=1;
ptid=1;
% Finds and stores all Load values at Grip Points
if nargin==0;num_lines=1e10;end % max number of lines to read
```

```
while x < num_lines & isempty(finish);
    x=x+1;
    eof=fgetl(fid);
    if eof ~=-1
     indx=findstr(deblank(eof),'     T3     ');
     finish=findstr(deblank(eof),'END OF JOB');
     grid=findstr(deblank(eof),'GRID');
     if ~isempty(grid)
         if grid(1)==31;
             Gpts = [ Gpts ;str2num(eof(55:62)) str2num(eof(63:70))
str2num(eof(71:78)) ];
         end
     end
    else
        indx=[];
    end
    if ~isempty(indx)
        if strcmp(eof(7:11),'POINT')
            eoblock=0;
            while ~eoblock
                eof=fgetl(fid);
                tmp=str2num(eof(11:14));
                if size(tmp,2)==1
                    ptid(i)=tmp;
                    % Shows location of the load in the 1, 2, and 3
                    % direction within the .txt file
                    T1(i,1)=str2num(eof(29:39));
                    T2(i,1)=str2num(eof(43:54));
                    T3(i,1)=str2num(eof(57:69));
                    i=i+1;
                else
                    eoblock = 1;
                end
            end
        end
    end
end
T=[T1 T2 T3];
disp(sprintf('points extracted %i',i-1));
fclose(fid);


%this finds the shear and axial loads for bolts with axial along the z-
axis
%for non-constraint bolts
alongzaxis=find(ptid==2028 | ptid==2251 | ptid==2612 | ptid==2586 |
ptid==2291 | ptid==2624 | ptid==4314  | ptid==340 | ptid==280 |
ptid==3453 | ptid==2479 | ptid==2487 | ptid==2328 | ptid==2320 |
ptid==2302 | ptid==2369 | ptid==2362 | ptid==519 | ptid==2578 |
ptid==1047 | ptid==2566 | ptid==6038 | ptid==6044 | ptid==523 |
ptid==6927 | ptid==6957 | ptid==7218 | ptid==5974 | ptid==5971 |
ptid==7141 | ptid==4239 | ptid==6848 | ptid==2671 | ptid==26681 |
ptid==2294);
zmaxaxial=max(abs(T3(alongzaxis,:)));
shearz=sqrt(dot(max(T1(alongzaxis,:)),max(T1(alongzaxis,:)))+dot(max(T2(
alongzaxis,:)),max(T2(alongzaxis,:))));
zmaxshear=max(shearz);
```

```
%this finds the shear and axial loads for bolts with axial along the z-
axis
%for 'constraint' bolts
conalongzaxis=find(ptid==2344 | ptid==2199 | ptid==2238 | ptid==2240 |
ptid==2249 | ptid==2256 | ptid==2273 | ptid==2275 | ptid==2287 |
ptid==2311 | ptid==2313 | ptid==2329 | ptid==2354 | ptid==2386 |
ptid==2433 | ptid==2438 | ptid==2442 | ptid==2459 | ptid==2463 |
ptid==2465 | ptid==2525 | ptid==2538 | ptid==2541 | ptid==2548 |
ptid==2550 | ptid==2574 | ptid==2575 | ptid==2584);
conzmaxaxial=max(abs(T3(conalongzaxis,:)));
conshearz=sqrt(dot(max(T1(conalongzaxis,:)),max(T1(conalongzaxis,:)))+do
t(max(T2(conalongzaxis,:)),max(T2(conalongzaxis,:))));
conzmaxshear=max(conshearz);


%this finds the shear and axial loads for bolts with axial along the y-
axis
alongyaxis=find(ptid==16 | ptid==17 | ptid==18 | ptid==34 | ptid==2740 |
ptid==2742 | ptid==62 | ptid==63 | ptid==64 | ptid==2677 | ptid==3374 |
ptid==3371 | ptid==4211 | ptid==3365 | ptid==4205 | ptid==2868 |
ptid==2865 | ptid==3034 | ptid==3037 | ptid==3042 | ptid==4187 | ptid==7
| ptid==6633 | ptid==6627 | ptid==41 | ptid==6243 | ptid==6249 |
ptid==73 | ptid==72 | ptid==71 | ptid==5127 | ptid==6150 | ptid==5133 |
ptid==5136 | ptid==5139 | ptid==5142 | ptid==6259 | ptid==6608 |
ptid==6606 | ptid==6692 | ptid==6649 | ptid==5148 | ptid==4247 |
ptid==4253 | ptid==4259 | ptid==8656 | ptid==8482 | ptid==4277 |
ptid==5100 | ptid==5094 | ptid==5088 | ptid==5082 | ptid==5076 |
ptid==5070);
ymaxaxial=max(abs(T2(alongyaxis,:)));
sheary=sqrt(dot(max(T1(alongyaxis,:)),max(T1(alongyaxis,:)))+dot(max(T3(
alongyaxis,:)),max(T3(alongyaxis,:))));
ymaxshear=max(sheary);

%this finds the shear and axial loads for bolts with axial along the x-
axis
alongxaxis=find(ptid==5980 | ptid==5986 | ptid==5998 | ptid==5992 |
ptid==6004 | ptid==6010 | ptid==8203 | ptid==8038 | ptid==7864 |
ptid==2643 | ptid==2637 | ptid==2631 | ptid==4748 | ptid==4847 |
ptid==4855 | ptid==4858 | ptid==4543 | ptid==4528 | ptid==5940 |
ptid==5943 | ptid==5946 | ptid==4405 | ptid==4233 | ptid==5949 |
ptid==36 | ptid==5185 | ptid==5183 | ptid==39 | ptid==2 | ptid==5842 |
ptid==5820 | ptid==5 | ptid==5760 | ptid==5671 | ptid==5618 | ptid==5627
| ptid==5537 | ptid==5527 | ptid==2702 | ptid==2699 | ptid==2696 |
ptid==2693 | ptid==2690 | ptid==2687 | ptid==5116 | ptid==5119 |
ptid==68 | ptid==5125 | ptid==48 | ptid==47 | ptid==46 | ptid==45 |
ptid==4222 | ptid==4225 | ptid==3385 | ptid==4231 | ptid==14 | ptid==13
| ptid==12 | ptid==11);
xmaxaxial=max(abs(T1(alongxaxis,:)));
shearx=sqrt(dot(max(T2(alongxaxis,:)),max(T2(alongxaxis,:)))+dot(max(T3(
alongxaxis,:)),max(T3(alongxaxis,:))));
xmaxshear=max(shearx);

%this finds the shear and axial loads for bolts holding on the camera
cambolts=find(ptid==2281 | ptid==2512 | ptid==2403);
camaxial=max(abs(T3(cambolts,:)));
shearcam=sqrt(dot(max(T1(cambolts,:)),max(T1(cambolts,:)))+dot(max(T2(ca
mbolts,:)),max(T2(cambolts,:))));
```

```
camshear=max(shearcam);

% this finds the shear and axial loads for bolts holding on the
% pressure transducers
pressbolts=find(ptid==6956 | ptid==7076 | ptid==7175);
pressaxial=max(abs(T3(pressbolts,:)));
shearpress=sqrt(dot(max(T1(pressbolts,:)),max(T1(pressbolts,:)))+dot(max
(T2(pressbolts,:)),max(T2(pressbolts,:))));
pressshear=max(shearpress);

%this finds the shear and axial loads for bolts holding on the oven
%mounting bracket
mountbolts=find(ptid==6880 | ptid==7183 | ptid==7103);
mountaxial=max(abs(T3(mountbolts,:)));
shearmount=sqrt(dot(max(T1(mountbolts,:)),max(T1(mountbolts,:)))+dot(max
(T2(mountbolts,:)),max(T2(mountbolts,:))));
mountshear=max(shearmount);

%this finds the shear and axial loads for bolts holding on the oven
%mounting bracket
ovenbolts=find(ptid==6894 | ptid==7063 | ptid==7171);
ovenaxial=max(abs(T3(ovenbolts,:)));
ovenshear=sqrt(dot(max(T1(ovenbolts,:)),max(T1(ovenbolts,:)))+dot(max(T2
(ovenbolts,:)),max(T2(ovenbolts,:))));
shearoven=max(ovenshear);

%this finds the shear and axial loads for bolts holding on the computer
compbolts=find(ptid==5390 | ptid==5287);
compaxial=max(abs(T1(compbolts,:)));
shearcomp=sqrt(dot(max(T2(compbolts,:)),max(T2(compbolts,:)))+dot(max(T3
(compbolts,:)),max(T3(compbolts,:))));
compshear=max(shearcomp);

%this finds the shear and axial loads for bolts holding on the PDP
pdpbolts=find(ptid==5614);
pdpaxial=max(abs(T1(pdpbolts,:)));
shearpdp=sqrt(dot(max(T2(pdpbolts,:)),max(T2(pdpbolts,:)))+dot(max(T3(pd
pbolts,:)),max(T3(pdpbolts,:))));
pdpshear=max(shearpdp);

%this finds the shear and axial loads for bolts holding on the
transformers
transbolts=find(ptid==5300 | ptid==5261 | ptid==5272);
transaxial=max(abs(T1(transbolts,:)));
sheartrans=sqrt(dot(max(T2(transbolts,:)),max(T2(transbolts,:)))+dot(max
(T3(transbolts,:)),max(T3(transbolts,:))));
transshear=max(sheartrans);


%These are the rotation matrices for the 7 shroud bolt coordinate
systems
rad=pi/180;
theta1=173*rad;
theta2=198.71*rad;
theta3=224.42*rad;
theta4=70.16*rad;
theta5=95.87*rad;
```

```
theta6=121.58*rad;
theta7=147.29*rad;
ROT1=[cos(theta1) sin(theta1) 0; -sin(theta1) cos(theta1) 0; 0 0 1];
ROT2=[cos(theta2) sin(theta2) 0; -sin(theta2) cos(theta2) 0; 0 0 1];
ROT3=[cos(theta3) sin(theta3) 0; -sin(theta3) cos(theta3) 0; 0 0 1];
ROT4=[cos(theta4) sin(theta4) 0; -sin(theta4) cos(theta4) 0; 0 0 1];
ROT5=[cos(theta5) sin(theta5) 0; -sin(theta5) cos(theta5) 0; 0 0 1];
ROT6=[cos(theta6) sin(theta6) 0; -sin(theta6) cos(theta6) 0; 0 0 1];
ROT7=[cos(theta7) sin(theta7) 0; -sin(theta7) cos(theta7) 0; 0 0 1];

%This rotates the shroud bolts and then finds the max axial and shear
loads

shroud11=ROT1*(T(ptid==6770,:))';
shroud12=ROT1*(T(ptid==8208,:))';
shroud13=ROT1*(T(ptid==6728,:))';
shroud14=ROT1*(T(ptid==2087,:))';
shroud1=abs([shroud11 shroud12 shroud13 shroud14]);
maxaxialshroud1=max(shroud1(1,:));
maxshearshroud1=(sqrt(dot(max(shroud1(2,:)),max(shroud1(2,:)))+dot(max((
shroud1(3,:))),max(shroud1(3,:)))));

shroud21=ROT2*(T(ptid==2123,:))';
shroud22=ROT2*(T(ptid==8199,:))';
shroud23=ROT2*(T(ptid==9179,:))';
shroud24=ROT2*(T(ptid==9180,:))';
shroud2=abs([shroud21 shroud22 shroud23 shroud24]);
maxaxialshroud2=max(shroud2(1,:));
maxshearshroud2=(sqrt(dot(max(shroud2(2,:)),max(shroud2(2,:)))+dot(max((
shroud2(3,:))),max(shroud2(3,:)))));

shroud31=ROT3*(T(ptid==2117,:))';
shroud32=ROT3*(T(ptid==6758,:))';
shroud33=ROT3*(T(ptid==6800,:))';
shroud34=ROT3*(T(ptid==8213,:))';
shroud35=ROT3*(T(ptid==2105,:))';
shroud36=ROT3*(T(ptid==9185,:))';
shroud3=abs([shroud31 shroud32 shroud33 shroud34]);
maxaxialshroud3=max(shroud3(1,:));
maxshearshroud3=(sqrt(dot(max(shroud3(2,:)),max(shroud3(2,:)))+dot(max((
shroud3(3,:))),max(shroud3(3,:)))));

shroud41=ROT4*(T(ptid==6794,:))';
shroud42=ROT4*(T(ptid==8201,:))';
shroud43=ROT4*(T(ptid==2111,:))';
shroud44=ROT4*(T(ptid==6752,:))';
shroud4=abs([shroud41 shroud42 shroud43 shroud44]);
maxaxialshroud4=max(shroud4(1,:));
maxshearshroud4=(sqrt(dot(max(shroud4(2,:)),max(shroud4(2,:)))+dot(max((
shroud4(3,:))),max(shroud4(3,:)))));

shroud51=ROT5*(T(ptid==6788,:))';
shroud52=ROT5*(T(ptid==8205,:))';
shroud53=ROT5*(T(ptid==9185,:))';
shroud54=ROT5*(T(ptid==2105,:))';
shroud5=abs([shroud51 shroud52 shroud53 shroud54]);
maxaxialshroud5=max(shroud5(1,:));
```

```
maxshearshroud5=(sqrt(dot(max(shroud5(2,:)),max(shroud5(2,:)))+dot(max((
shroud5(3,:))),max(shroud5(3,:)))));

shroud61=ROT6*(T(ptid==8195,:))';
shroud62=ROT6*(T(ptid==8196,:))';
shroud63=ROT6*(T(ptid==2099,:))';
shroud64=ROT6*(T(ptid==9175,:))';
shroud6=abs([shroud61 shroud62 shroud63 shroud64]);
maxaxialshroud6=max(shroud6(1,:));
maxshearshroud6=(sqrt(dot(max(shroud6(2,:)),max(shroud6(2,:)))+dot(max((
shroud6(3,:))),max(shroud6(3,:)))));

shroud71=ROT7*(T(ptid==8198,:))';
shroud72=ROT7*(T(ptid==6776,:))';
shroud73=ROT7*(T(ptid==2093,:))';
shroud74=ROT7*(T(ptid==9177,:))';
shroud7=abs([shroud71 shroud72 shroud73 shroud74]);
maxaxialshroud7=max(shroud7(1,:));
maxshearshroud7=(sqrt(dot(max(shroud7(2,:)),max(shroud7(2,:)))+dot(max((
shroud7(3,:))),max(shroud7(3,:)))));
```

Code for Finding Maximum Deflection of Shroud and Bumpers

```
function [maxbumpa, maxbumpb, maxbumpc, maxbumpd, maxbumpe, maxbumpf,
maxbumpg]=maxdeflection(num_lines,pathname,filename,varargin);
%*****************************************************************
***
%
% The shell of this program was written by Dr. Cobb to input a Nastran
text
% file and extract data at given point IDs.
% The file was  modified by 2d Lt Anna Gunn-Golkin to process a
translation
% data file output from Nastran, rotate those translations to the
appropriate
% coordinate frame, and determine maximum 'inward' and 'outward'
% deflections
%
% To run this program, open this dir in matlab and type in the
% command window:
% [maxbumpa, maxbumpb, maxbumpc, maxbumpd, maxbumpe, maxbumpf,
maxbumpg]=maxdeflection(****)
%
% **** indicates the number of lines of the input file you want the
% program to search through
%
%*****************************************************************
***

fid=fopen('L:\eny students\RIGEX\Bolt Analysis\Max Deflection at
Bumpers\trans000.f06');
eof=fgetl(fid);
x=0;
finish=[];Gpts=[];
i=1;
ptid=1;
```

```
if nargin==0;num_lines=1e10;end % max number of lines to read
while x < num_lines & isempty(finish);
    x=x+1;
    eof=fgetl(fid);
    if eof ~=-1
     indx=findstr(deblank(eof),'     T3     ');
     finish=findstr(deblank(eof),'END OF JOB');
     grid=findstr(deblank(eof),'GRID');
     if ~isempty(grid)
         if grid(1)==31;
             Gpts = [ Gpts ;str2num(eof(55:62)) str2num(eof(63:70))
str2num(eof(71:78)) ];
         end
     end
    else
        indx=[];
    end


    if ~isempty(indx)
        if strcmp(eof(7:11),'POINT')
            eoblock=0;
            while ~eoblock
                eof=fgetl(fid);
                tmp=str2num(eof(11:14));
                if size(tmp,2)==1
                    ptid(i)=tmp;
                    T1(i,1)=str2num(eof(29:39));
                    T2(i,1)=str2num(eof(43:54));
                    T3(i,1)=str2num(eof(57:69));
                    i=i+1;
                else
                    eoblock = 1;
                end
            end
        end
    end
end
T=[T1 T2 T3];
disp(sprintf('points extracted %i',i-1));
fclose(fid);

%These are the rotation matrices for the 7 bumper coordinate systems
rad=pi/180;
thetaa=211.6*rad;
thetab=185.9*rad;
thetac=160.5*rad;
thetad=134.4*rad;
thetae=108.7*rad;
thetaf=83.015*rad;
thetag=57.305*rad;
ROTa=[cos(thetaa) sin(thetaa) 0; -sin(thetaa) cos(thetaa) 0; 0 0 1];
ROTb=[cos(thetab) sin(thetab) 0; -sin(thetab) cos(thetab) 0; 0 0 1];
ROTc=[cos(thetac) sin(thetac) 0; -sin(thetac) cos(thetac) 0; 0 0 1];
ROTd=[cos(thetad) sin(thetad) 0; -sin(thetad) cos(thetad) 0; 0 0 1];
ROTe=[cos(thetae) sin(thetae) 0; -sin(thetae) cos(thetae) 0; 0 0 1];
ROTf=[cos(thetaf) sin(thetaf) 0; -sin(thetaf) cos(thetaf) 0; 0 0 1];
ROTg=[cos(thetag) sin(thetag) 0; -sin(thetag) cos(thetag) 0; 0 0 1];
```

```
%This rotates the bumper locations and finds the max deflection there

bumpa1=ROTa*(T(ptid==6761,:))';
bumpa2=ROTa*(T(ptid==6760,:))';
bumpa3=ROTa*(T(ptid==6803,:))';
bumpa4=ROTa*(T(ptid==6802,:))';
bumpa=abs([bumpa1 bumpa2 bumpa3 bumpa4]);
maxbumpa=max(bumpa(1,:))

bumpb1=ROTb*(T(ptid==6766,:))';
bumpb2=ROTb*(T(ptid==6767,:))';
bumpb3=ROTb*(T(ptid==6809,:))';
bumpb4=ROTb*(T(ptid==6808,:))';
bumpb=abs([bumpb1 bumpb2 bumpb3 bumpb4]);
maxbumpb=max(bumpb(1,:))

bumpc1=ROTc*(T(ptid==6773,:))';
bumpc2=ROTc*(T(ptid==6731,:))';
bumpc3=ROTc*(T(ptid==7305,:))';
bumpc4=ROTc*(T(ptid==9165,:))';
bumpc=abs([bumpc1 bumpc2 bumpc3 bumpc4]);
maxbumpc=max(bumpc(1,:))

bumpd1=ROTd*(T(ptid==6778,:))';
bumpd2=ROTd*(T(ptid==6779,:))';
bumpd3=ROTd*(T(ptid==6736,:))';
bumpd4=ROTd*(T(ptid==9102,:))';
bumpd=abs([bumpd1 bumpd2 bumpd3 bumpd4]);
maxbumpd=max(bumpd(1,:))

bumpe1=ROTe*(T(ptid==6785,:))';
bumpe2=ROTe*(T(ptid==6784,:))';
bumpe3=ROTe*(T(ptid==6743,:))';
bumpe4=ROTe*(T(ptid==6742,:))';
bumpe=abs([bumpe1 bumpe2 bumpe3 bumpe4]);
maxbumpe=max(bumpe(1,:))

bumpf1=ROTf*(T(ptid==6791,:))';
bumpf2=ROTf*(T(ptid==6792,:))';
bumpf3=ROTf*(T(ptid==6749,:))';
bumpf4=ROTf*(T(ptid==6750,:))';
bumpf=abs([bumpf1 bumpf2 bumpf3 bumpf4]);
maxbumpf=max(bumpf(1,:))

bumpg1=ROTg*(T(ptid==6796,:))';
bumpg2=ROTg*(T(ptid==6797,:))';
bumpg3=ROTg*(T(ptid==6754,:))';
bumpg4=ROTg*(T(ptid==6755,:))';
bumpg=abs([bumpg1 bumpg2 bumpg3 bumpg4]);
maxbumpg=max(bumpg(1,:))
```

Appendix D: Final Drawing Package

Table D1 is a list of all RIGEX drawings as submitted to the Wright Patterson Air Force Base Shop for construction. The drawings for each part listed in Table D1 are below. They represent the *As Built* drawings for the RIGEX primary and secondary structure.

Table D1. Drawing List

Part Description	Main Drawing #
CAPE Mounting Plate	RIGEX-2006-1
Experiment Top Plate	RIGEX-2006-2
Large Rib with Computer	RIGEX-2006-3
Large Rib	RIGEX-2006-4
Small Rib with Pin Puller	RIGEX-2006-5
Small Rib	RIGEX-2006-6
Oven Mounting Plate	RIGEX-2006-7
Bottom Rectangular Plate	RIGEX-2006-8
Inflation Mounting Plate	RIGEX-2006-9
Oven Bracket - Piece 1	RIGEX-2006-10
Oven Bracket - Piece 2	RIGEX-2006-11
Oven Latch	RIGEX-2006-12
Stabilizing Feet/Lifting Handles	RIGEX-2006-13
Top Plate Lifting Handles	RIGEX-2006-14
Shroud	RIGEX-2006-15
Bumper	RIGEX-2006-16
Power Distribution Plate	RIGEX-2006-17
Pressure XDCR Mounting - Piece 1	RIGEX-2006-18
Pressure XDCR Mounting - Piece 2	RIGEX-2006-19
Solenoid Mounting Block	RIGEX-2006-20
Storage Tank Pressure XDCR Mounting - Piece 1	RIGEX-2006-21-1
Storage Tank Pressure XDCR Mounting - Piece 2	RIGEX-2006-22-1
Computer Mounting Plate	RIGEX-2006-23-1
Connector Hole Cover	RIGEX-2006-24-1

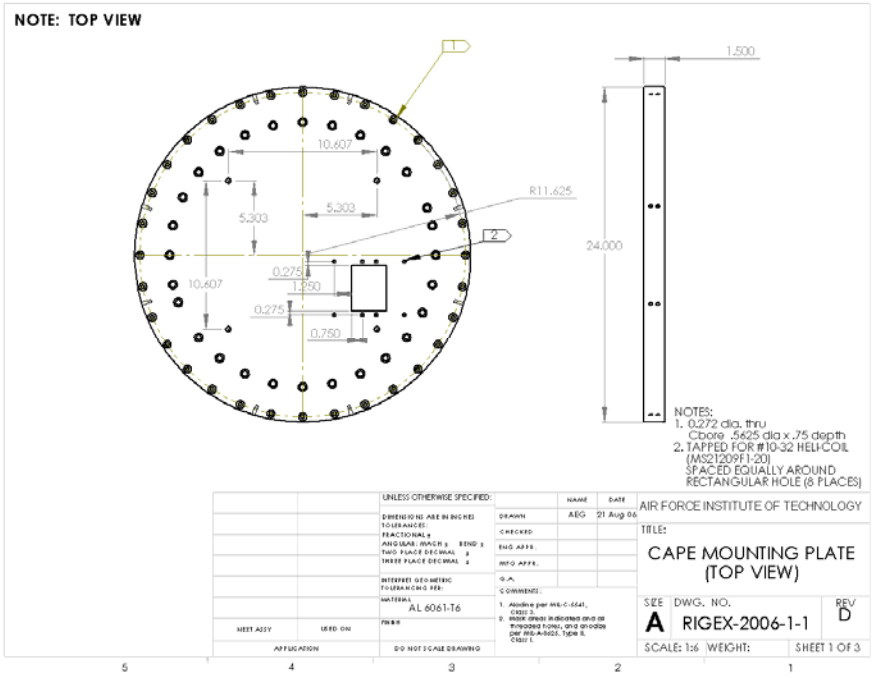

Figure D-1: CAPE Mounting Plate View 1

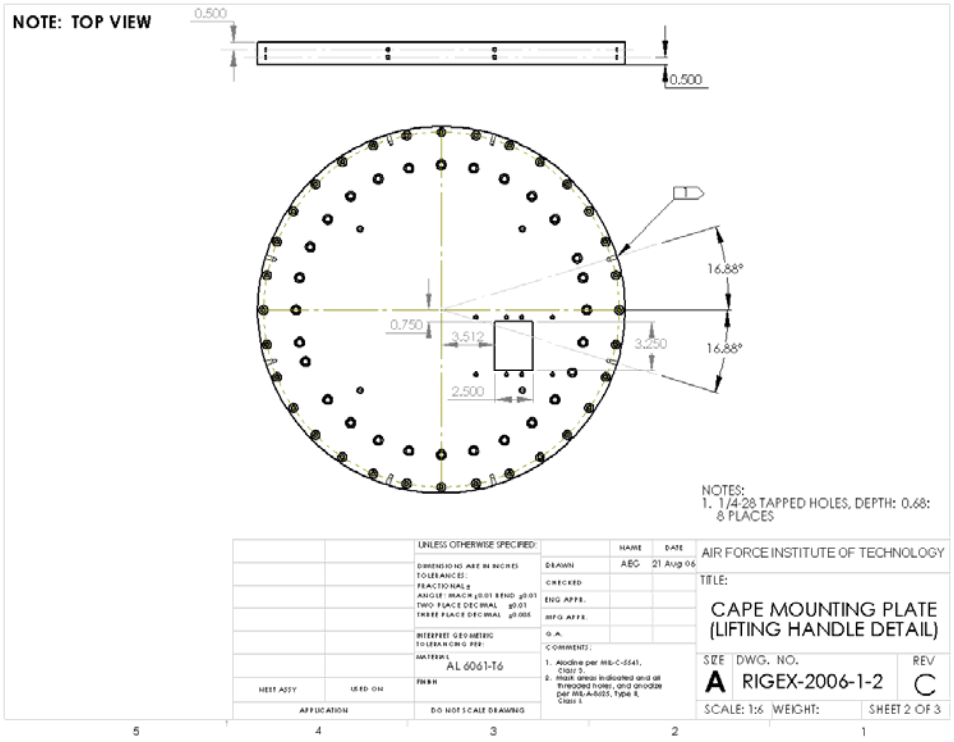

Figure D-2: CAPE Mounting Plate View 2

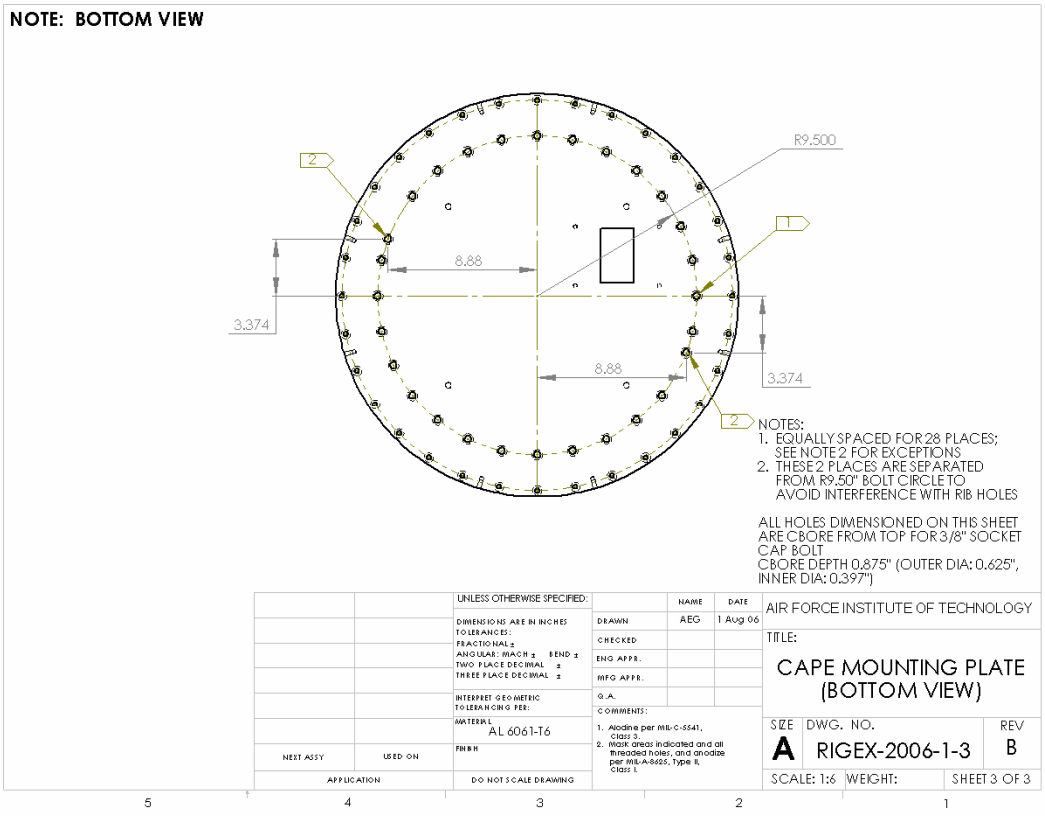

Figure D-3: CAPE Mounting Plate View 3

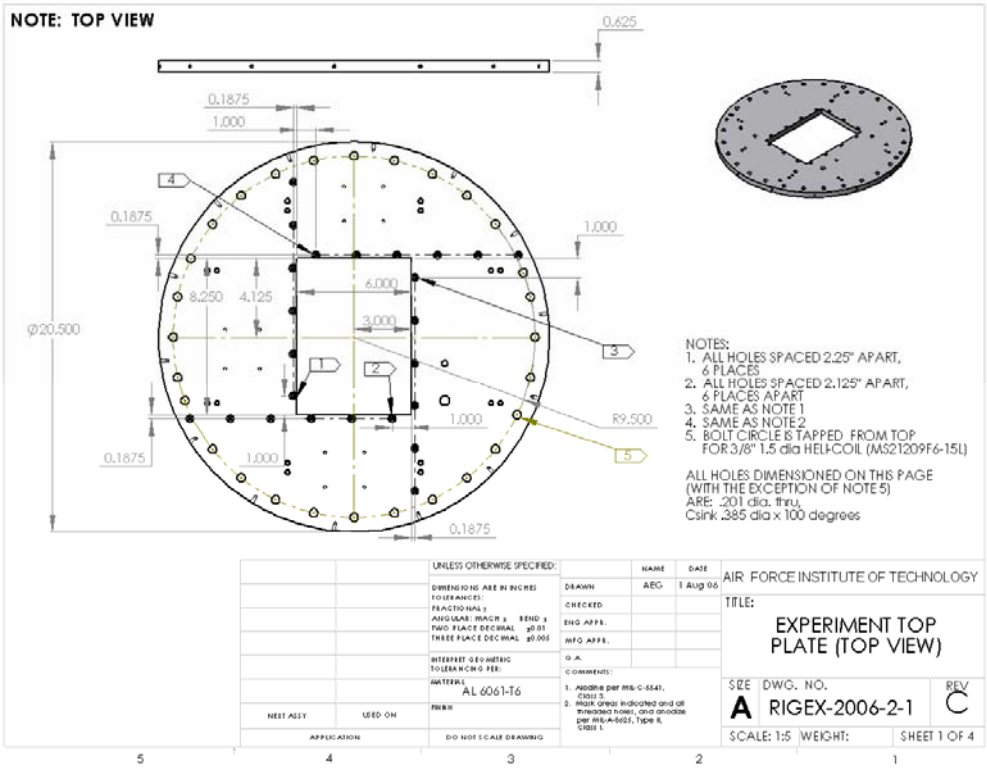

Figure D-4: Experiment Top Plate View 1

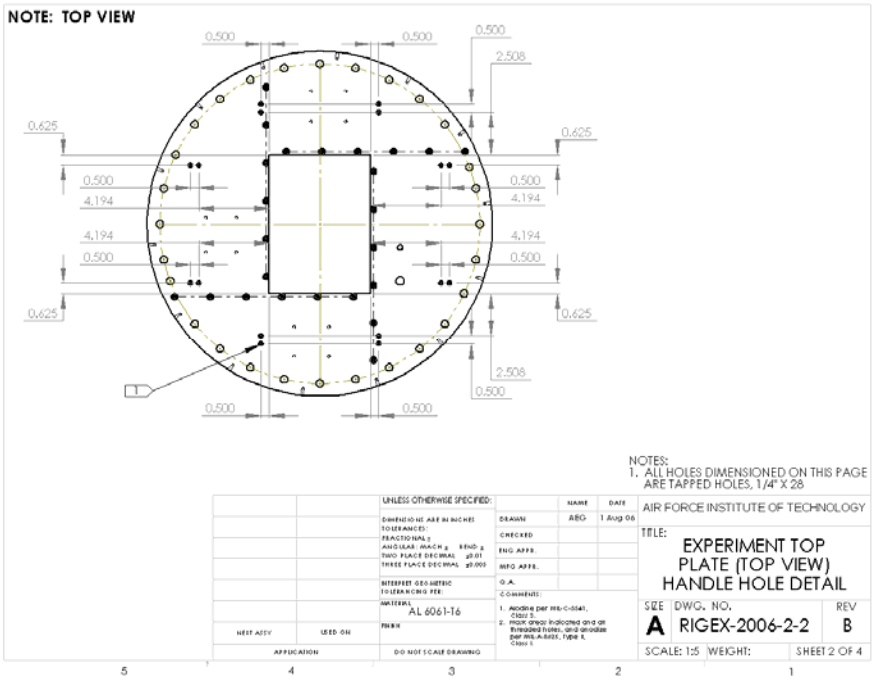

Figure D-5: Experiment Top Plate View 2

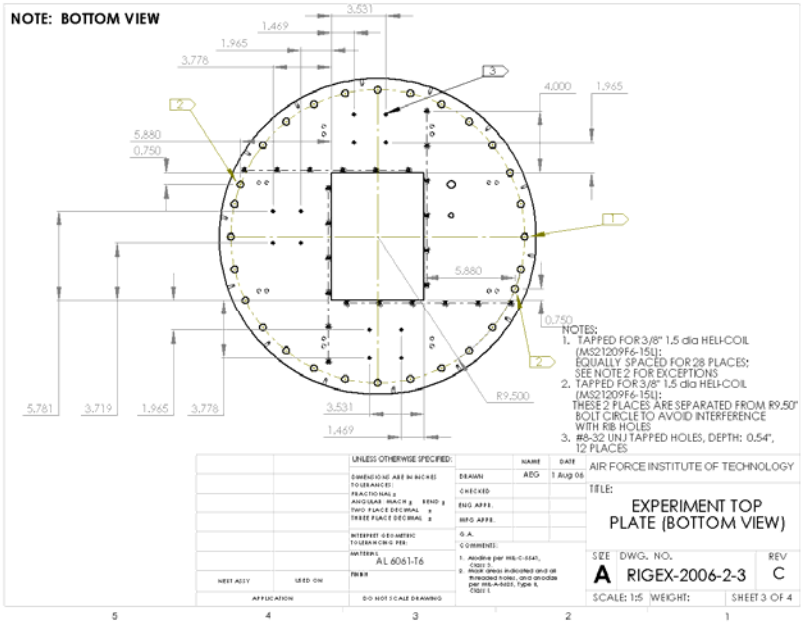

Figure D-6: Experiment Top Plate View 3

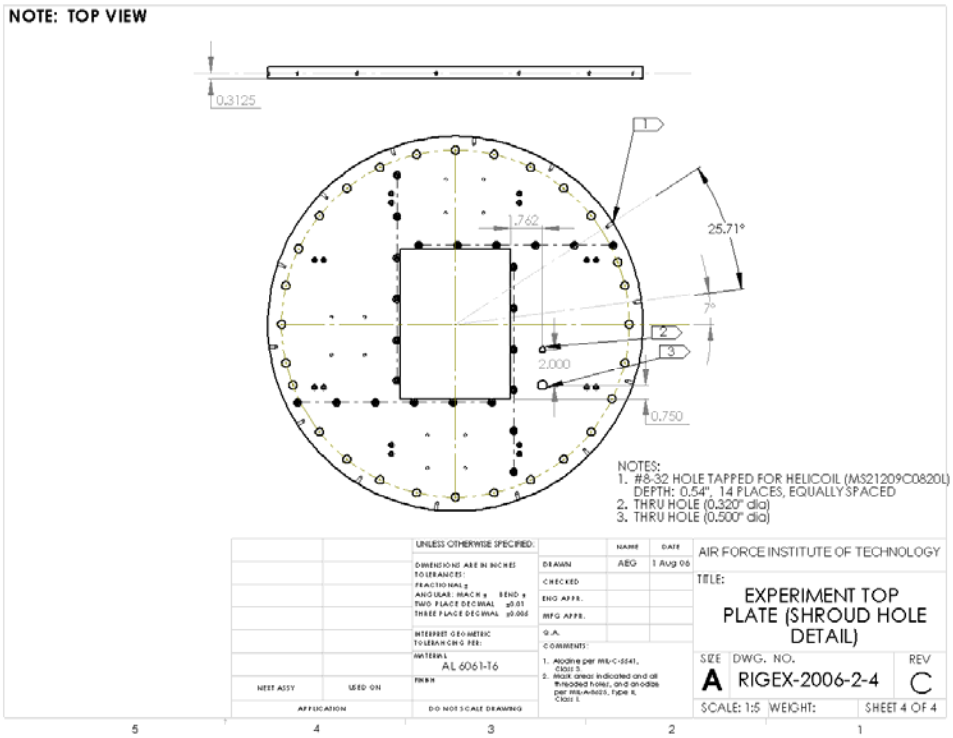

Figure D-7: Experiment Top Plate View 4

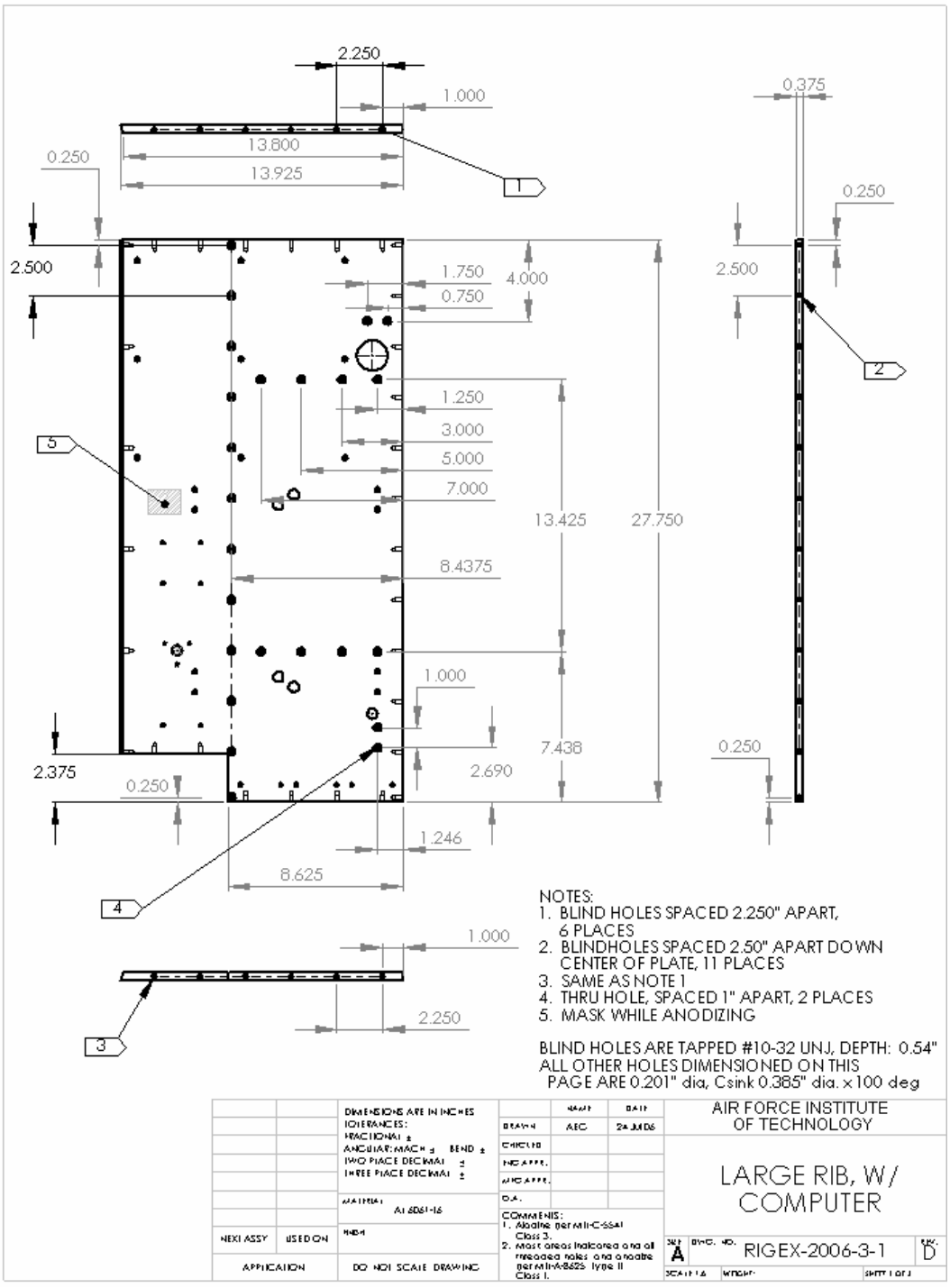

Figure D-8: Large Rib with Computer View 1

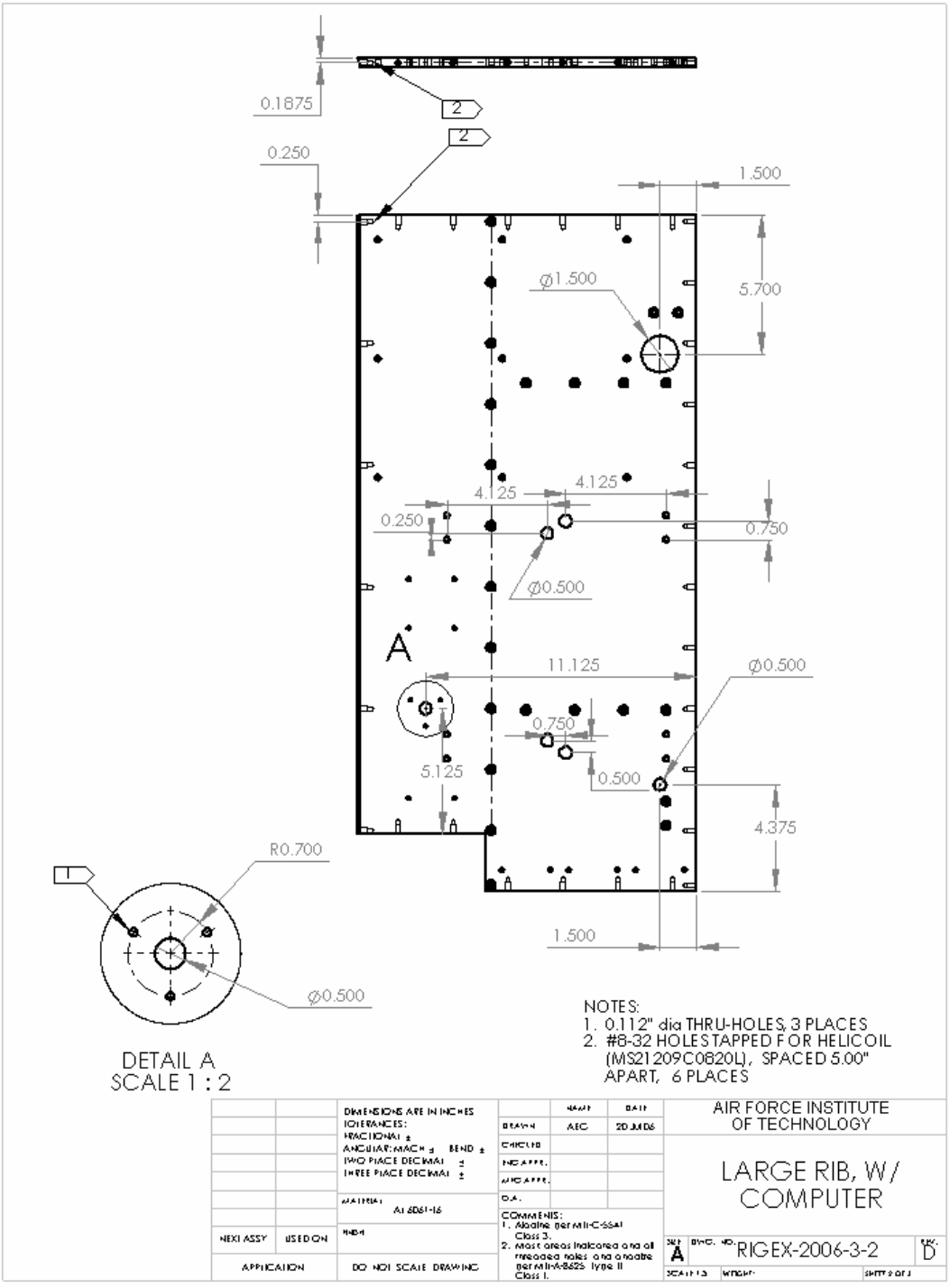

Figure D-9: Large Rib with Computer View 2

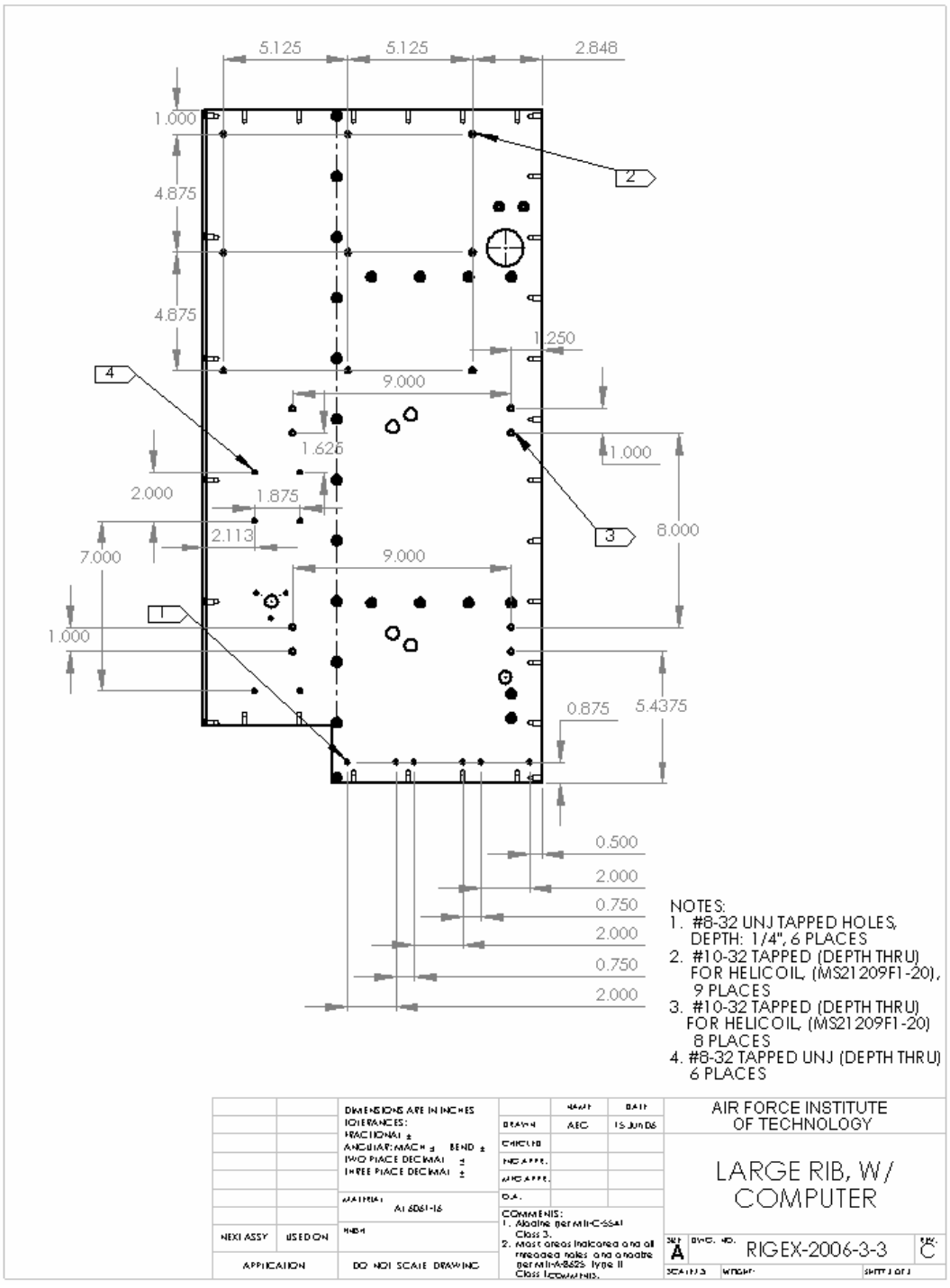

Figure D-10: Large Rib with Computer View 3

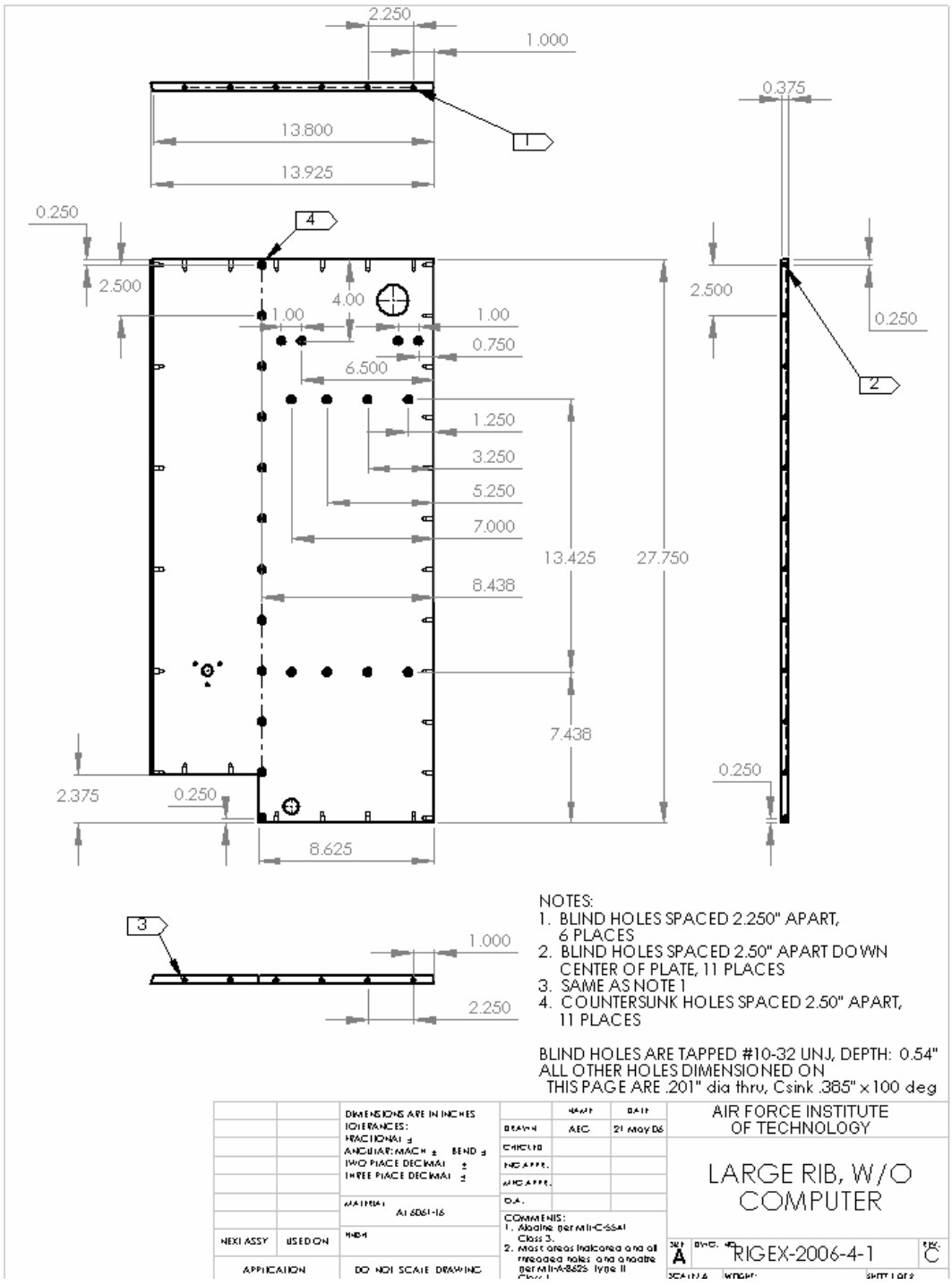

Figure D-11: Large Rib without Computer View 1

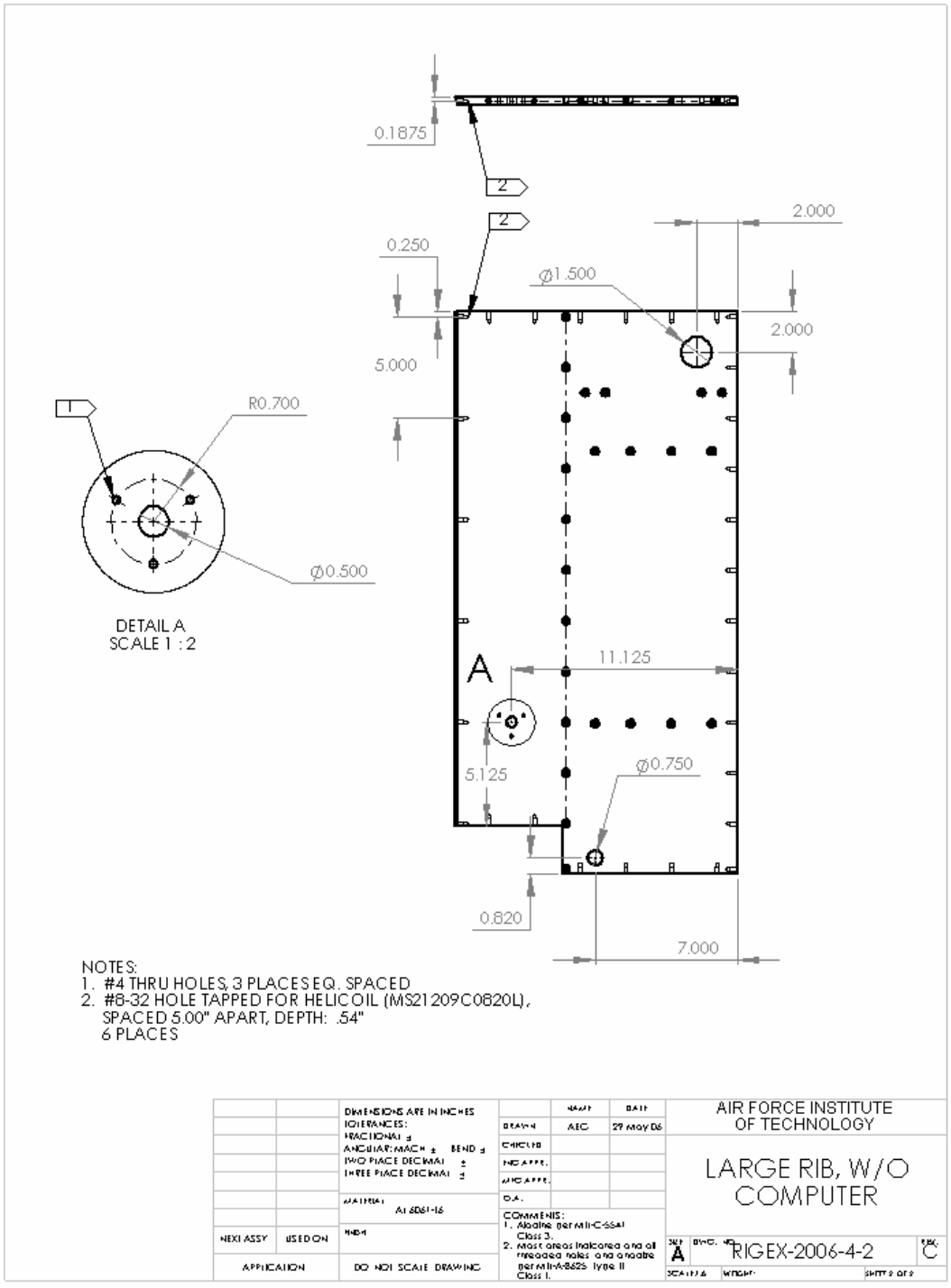

Figure D-12: Large Rib without Computer View 2

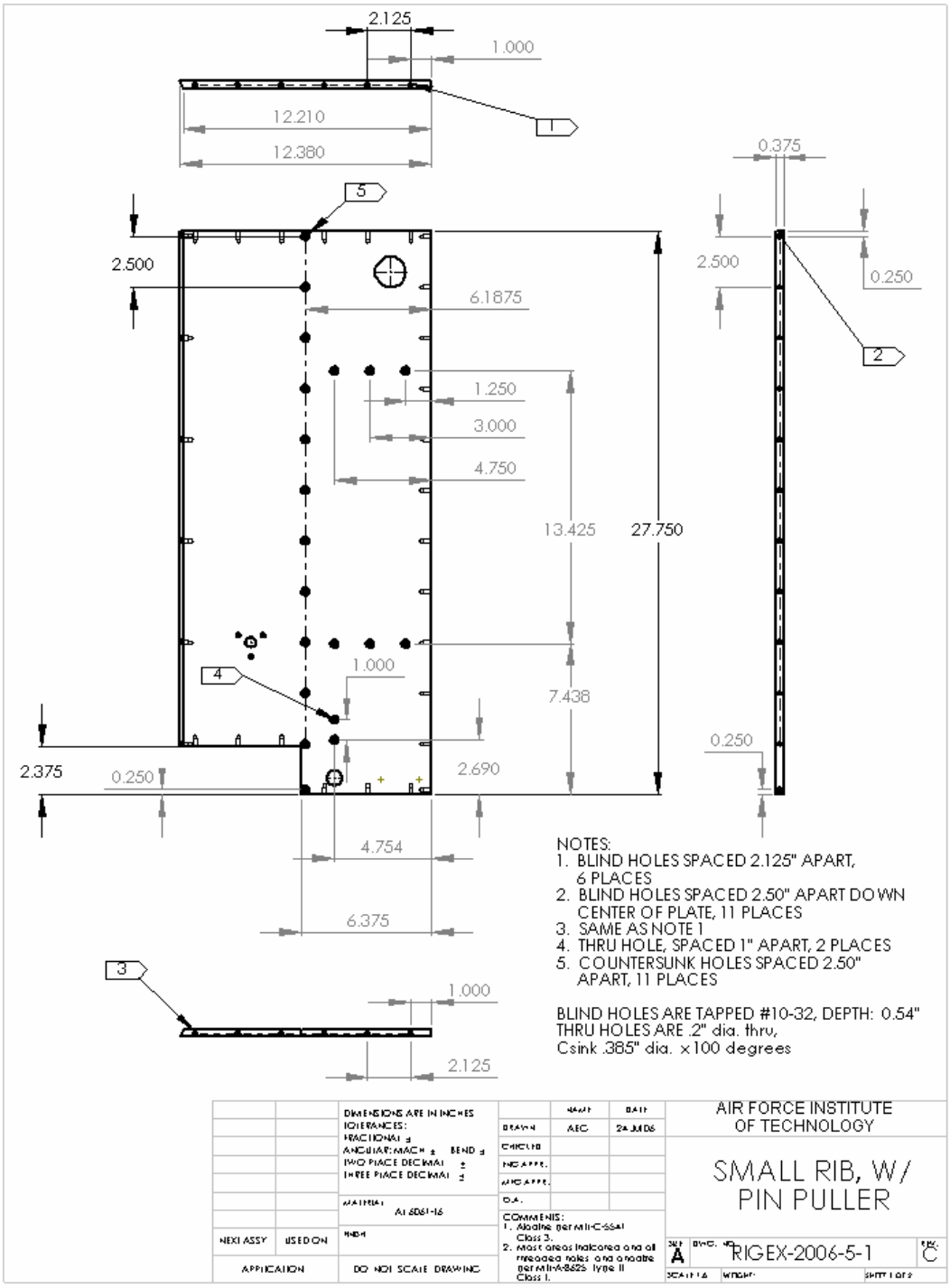

Figure D-13: Small Rib with Pin Puller View 1

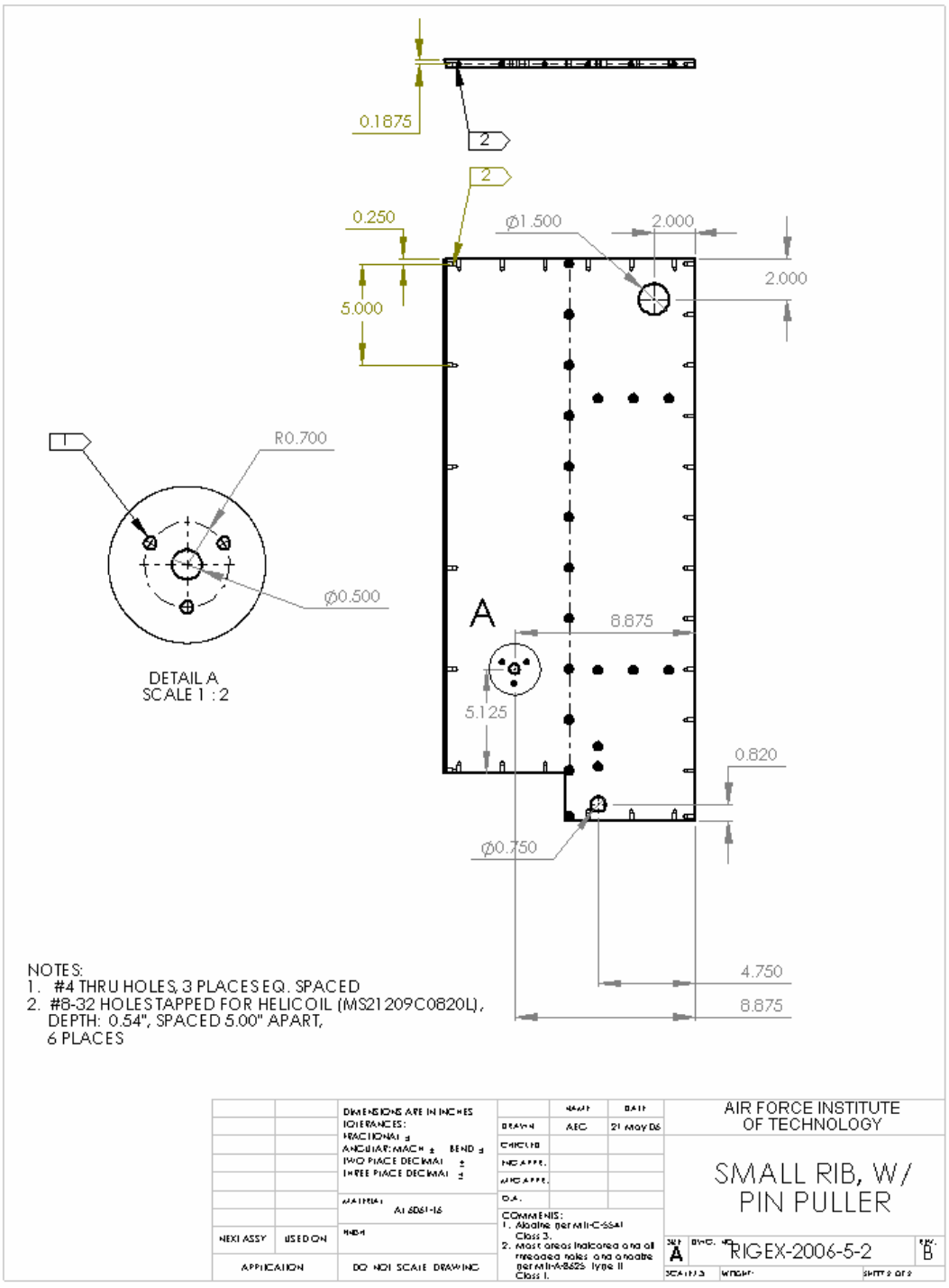

Figure D-14: Small Rib with Pin Puller View 2

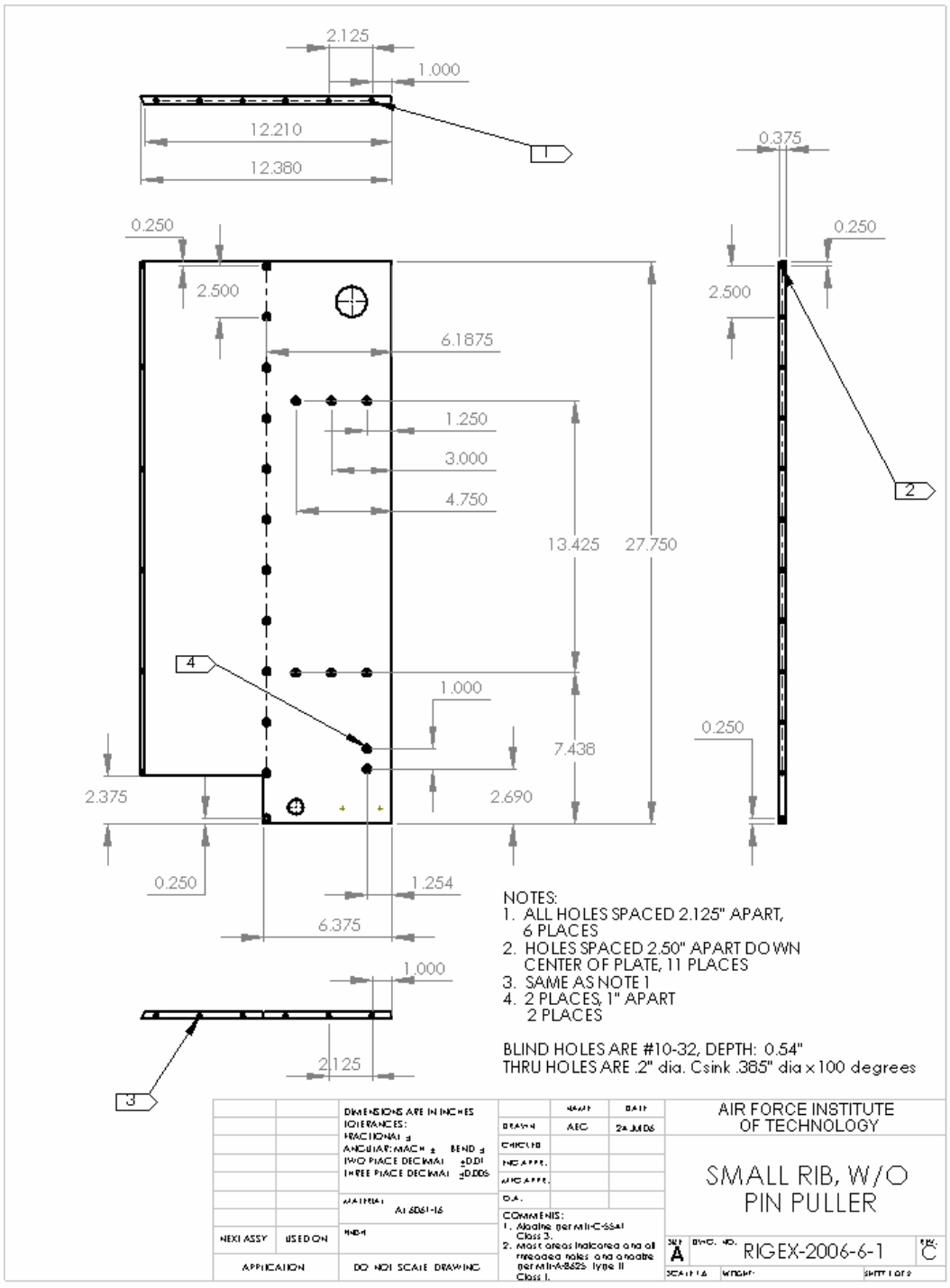

Figure D-15: Small Rib without Pin Puller View 1

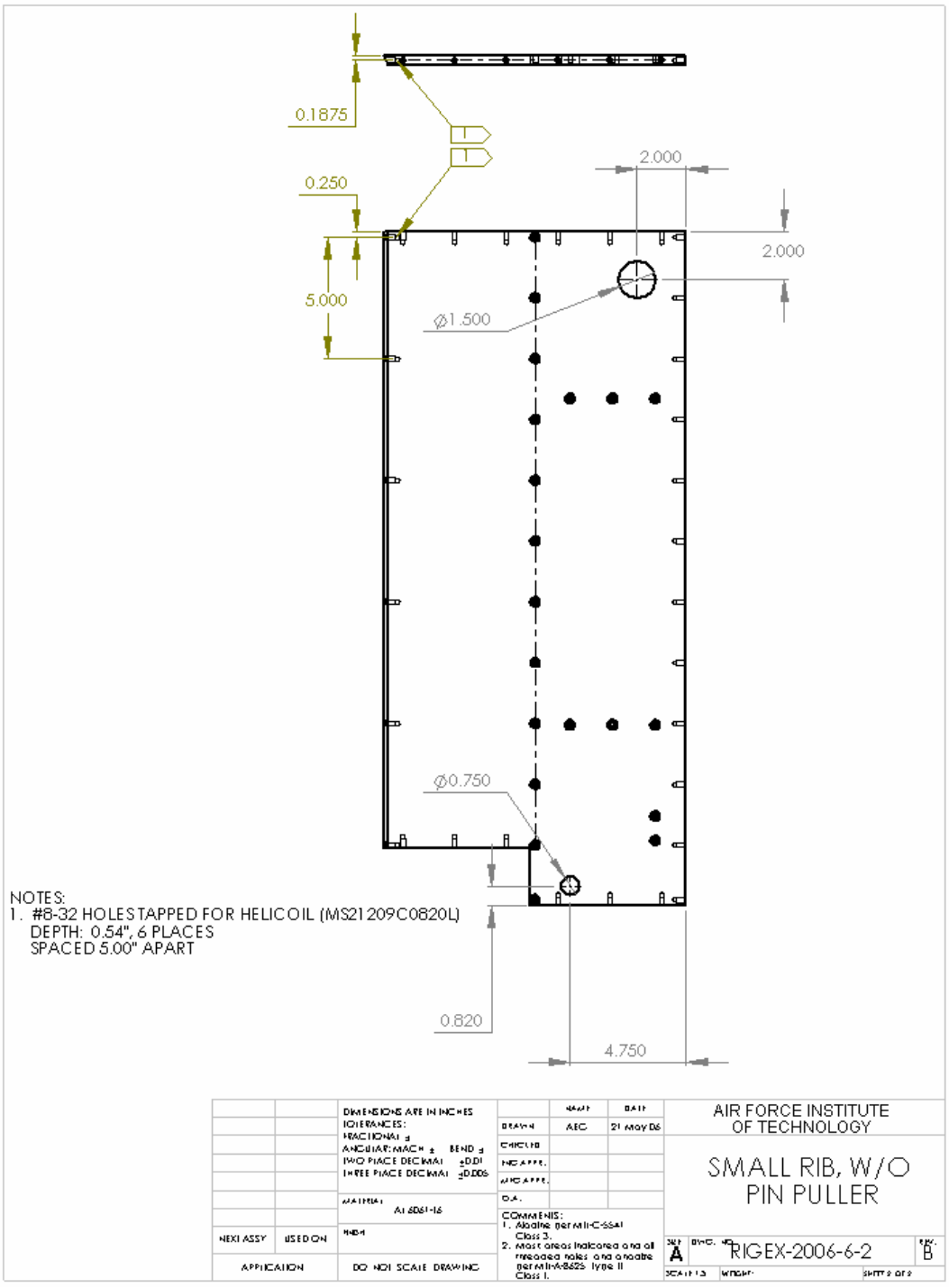

Figure D-16: Small Rib without Pin Puller View 2

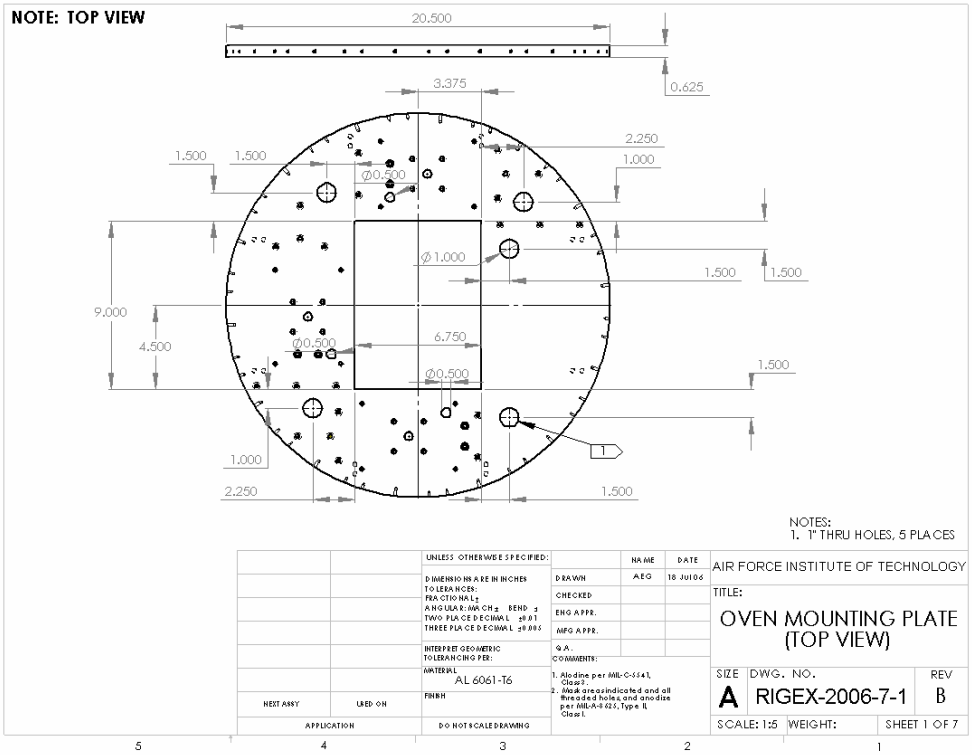

Figure D-17: Oven Mounting Plate View 1

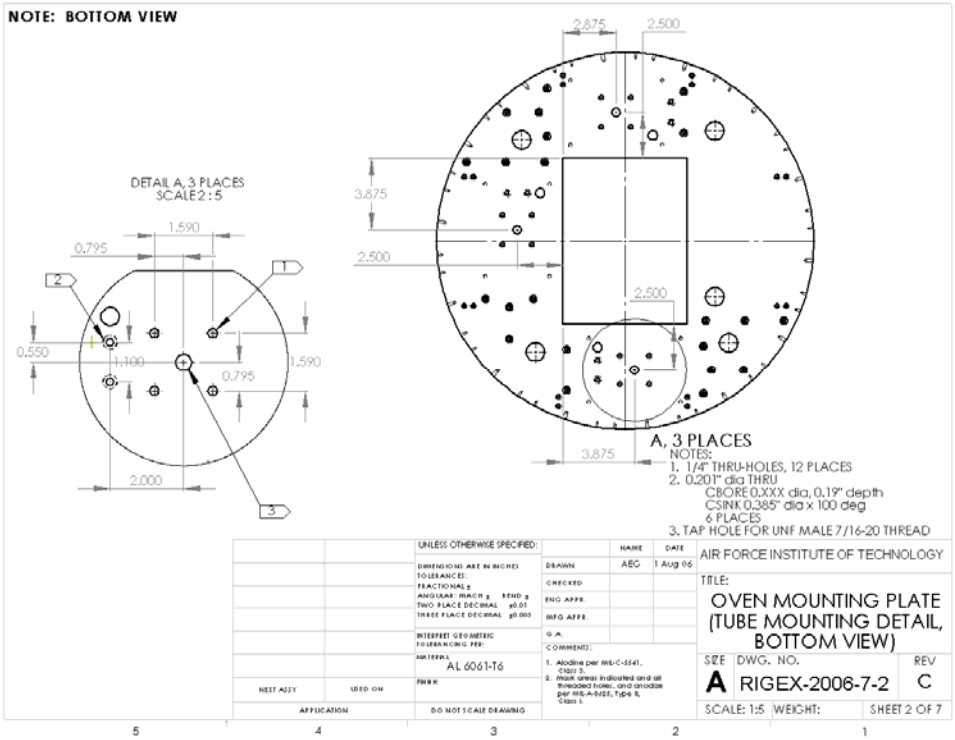

Figure D-18: Oven Mounting Plate View 2

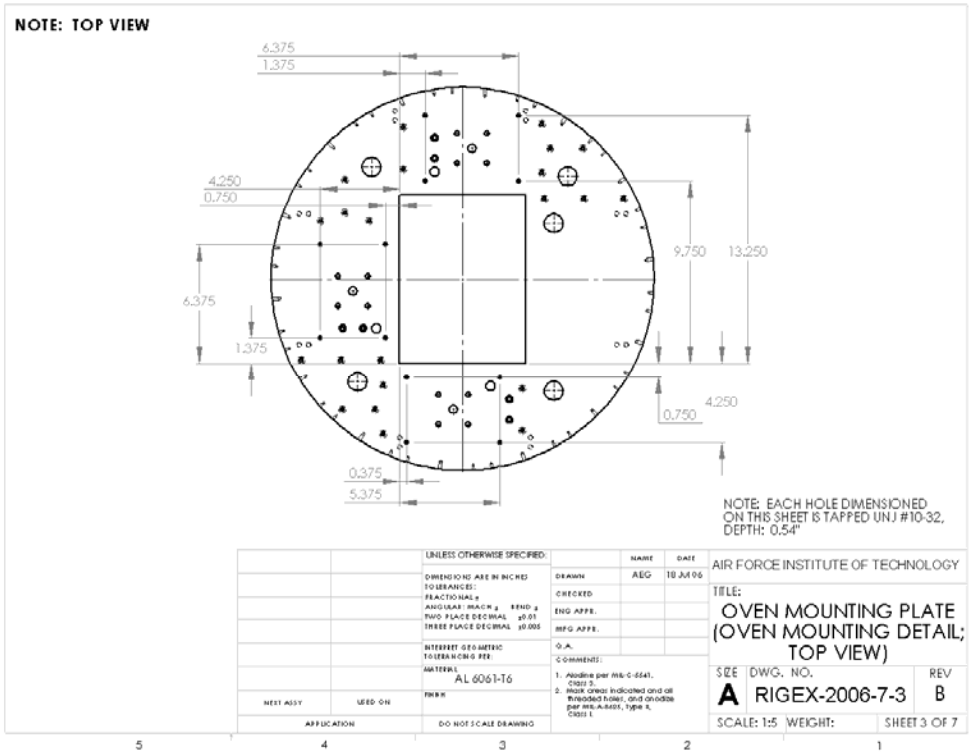

Figure D-19: Oven Mounting Plate View 3

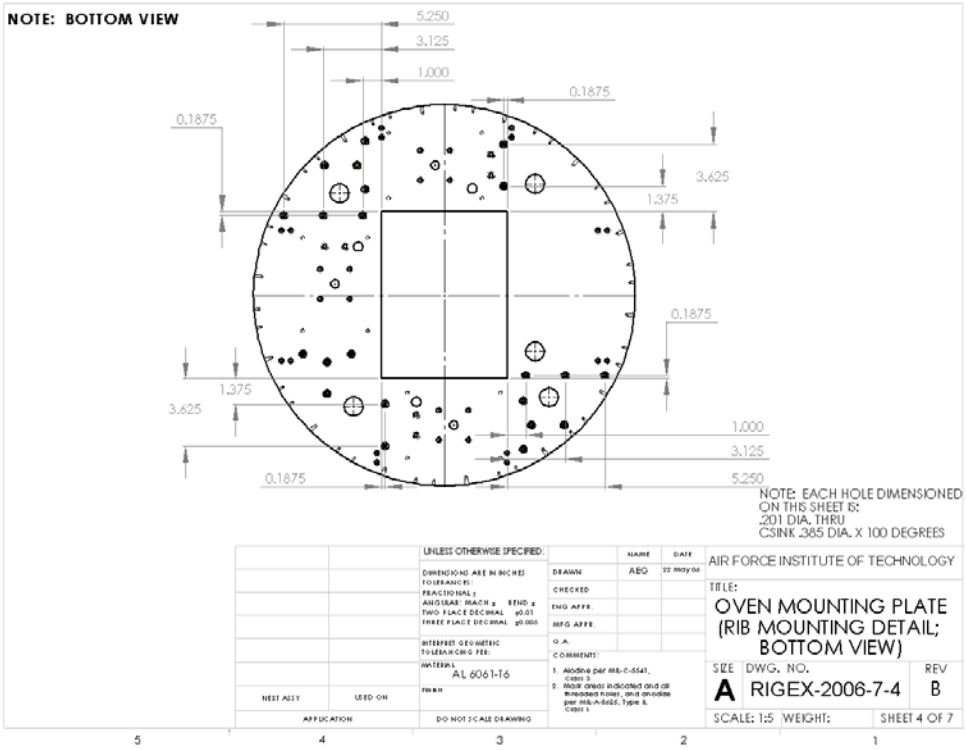

Figure D-20: Oven Mounting Plate View 4

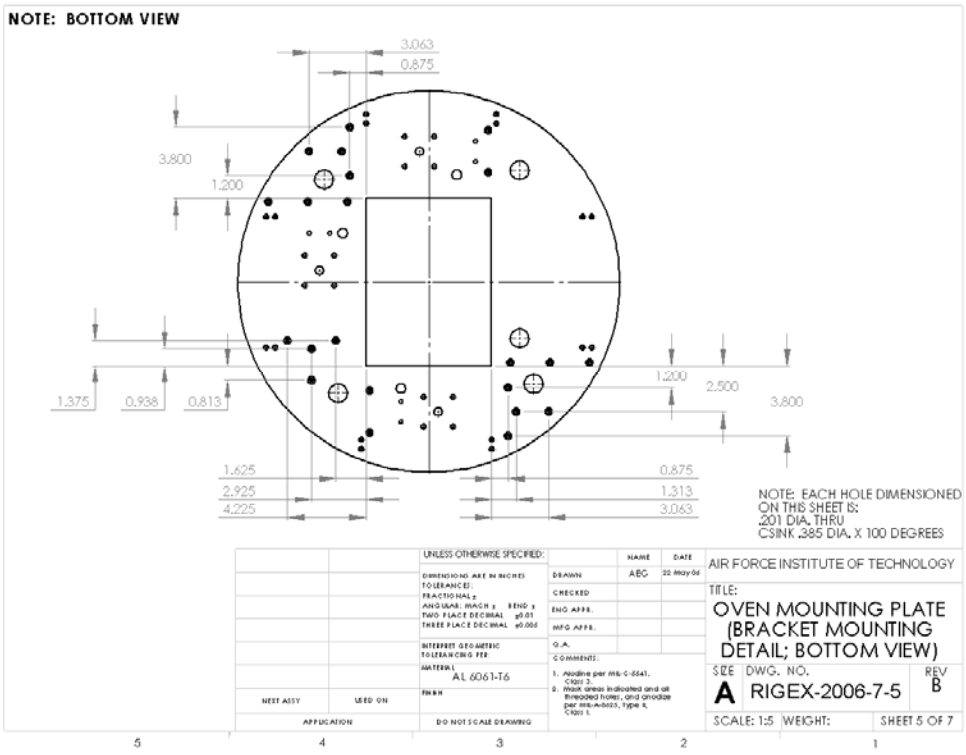

Figure D-21: Oven Mounting Plate View 5

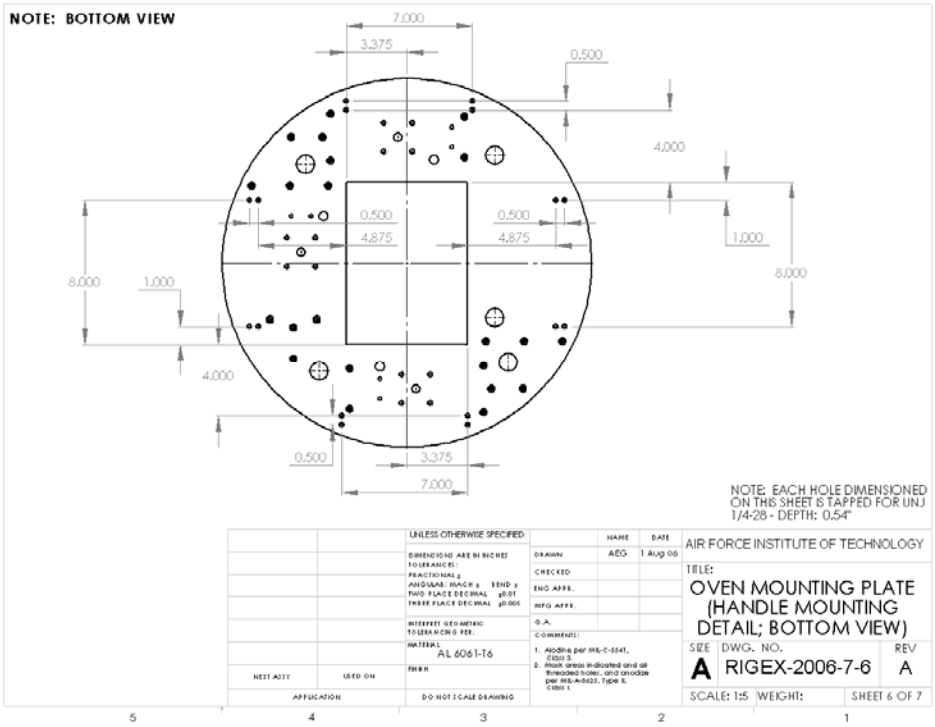

Figure D-22: Oven Mounting Plate View 6

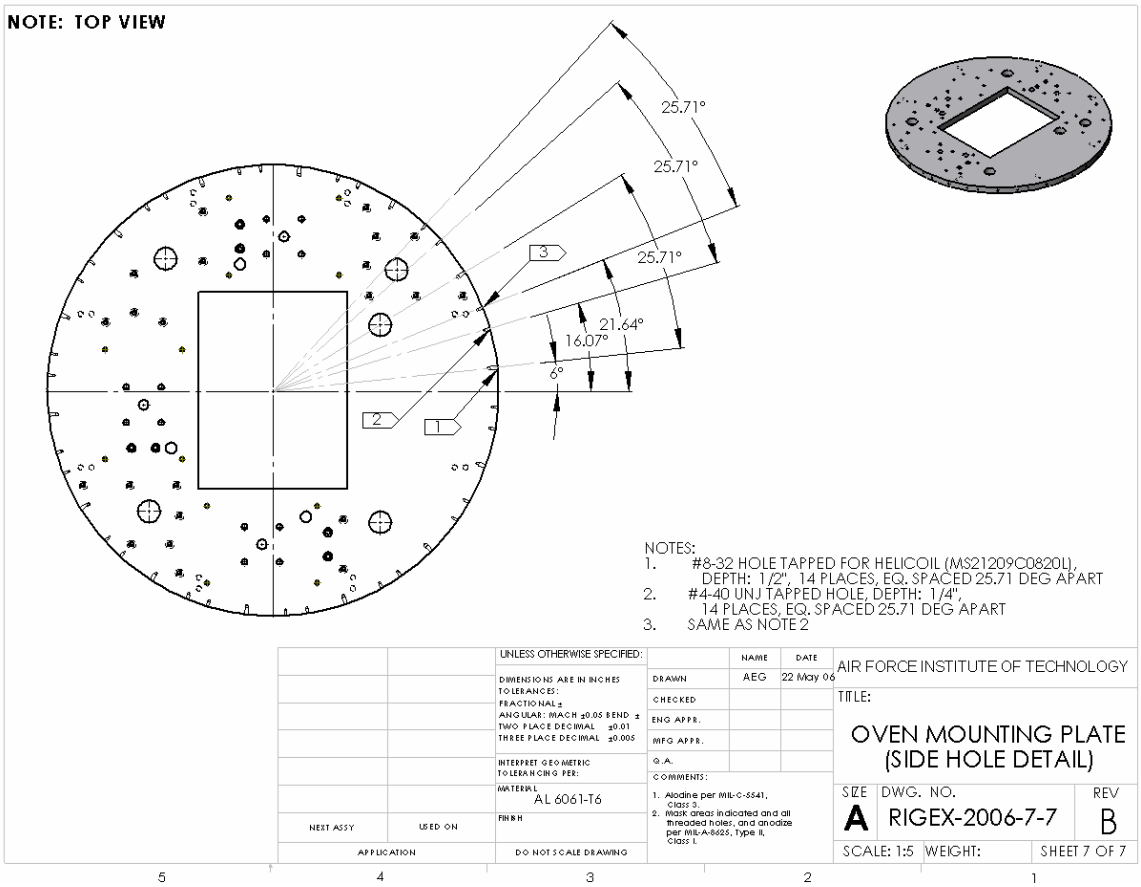

Figure D-23: Oven Mounting Plate View 7

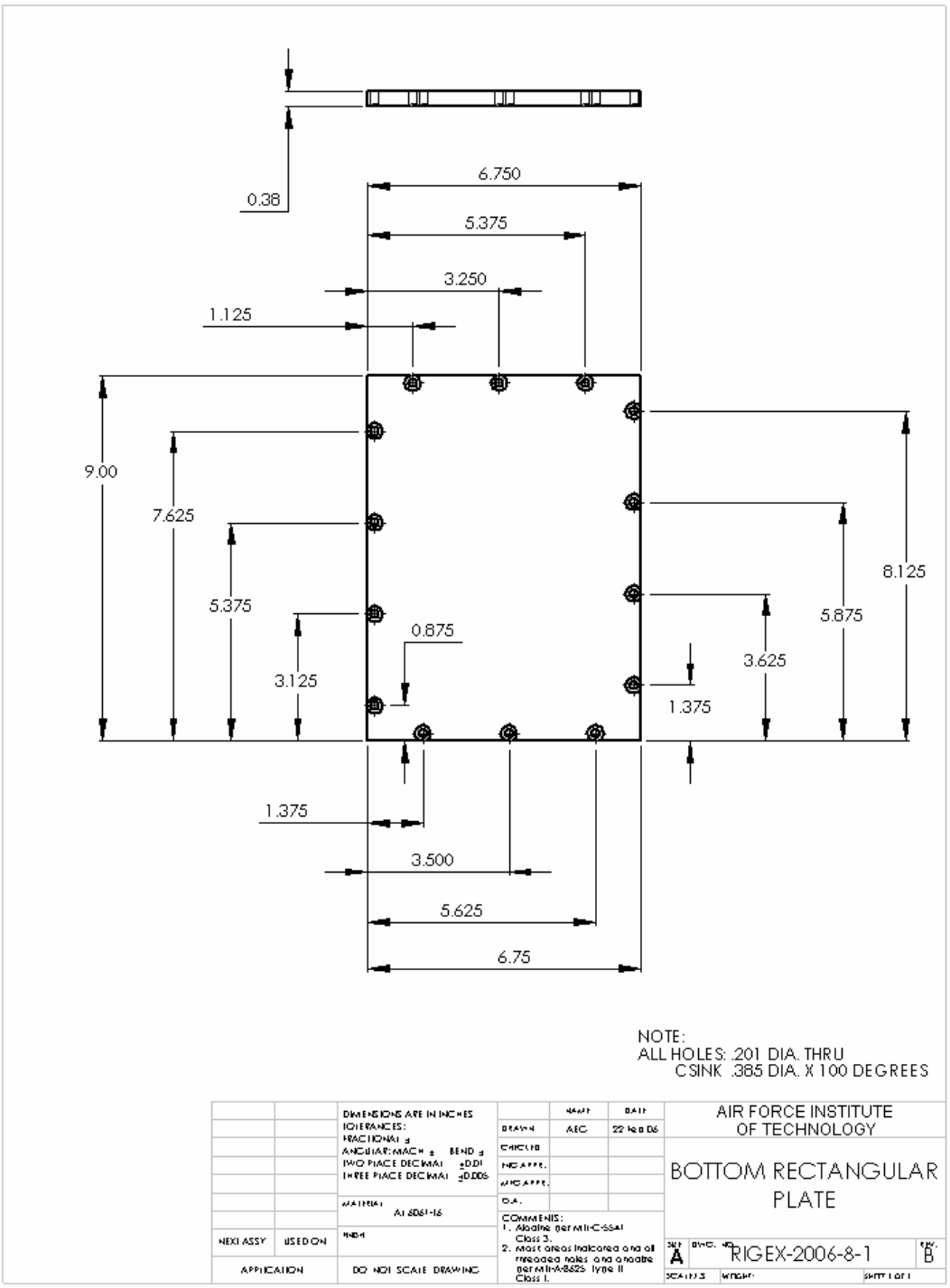

Figure D-24: Bottom Rectangular Plate

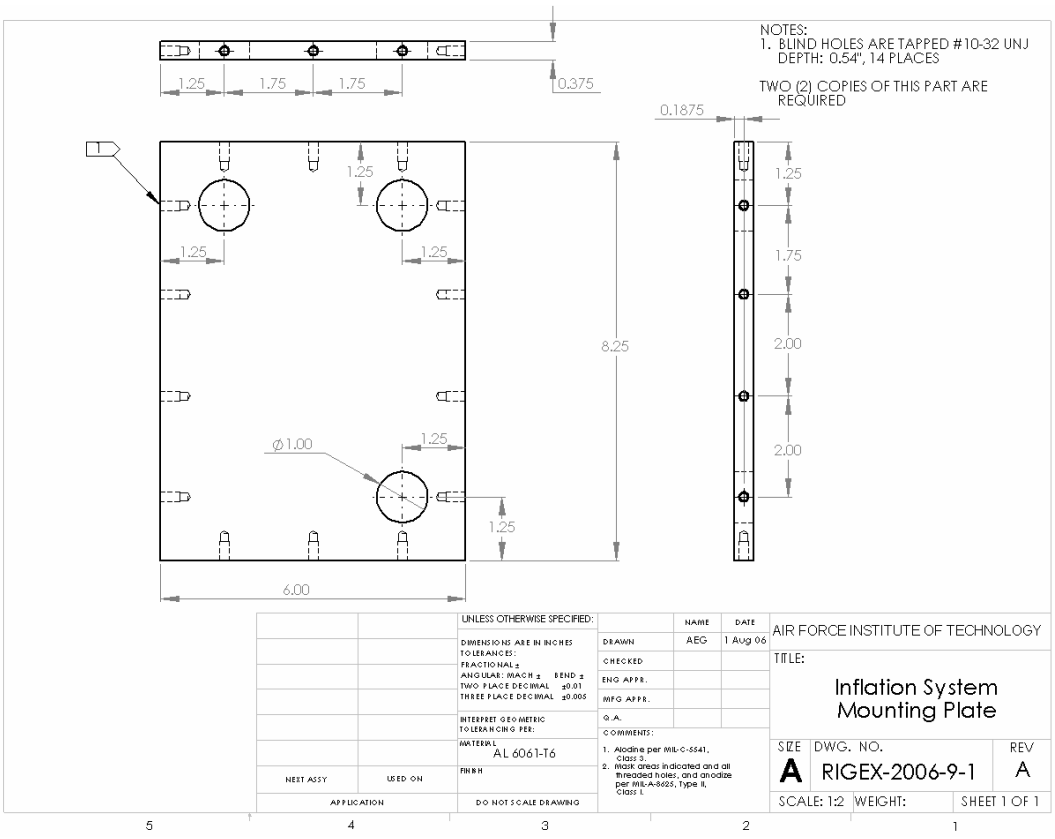

Figure D-25: Inflation Mounting Plate

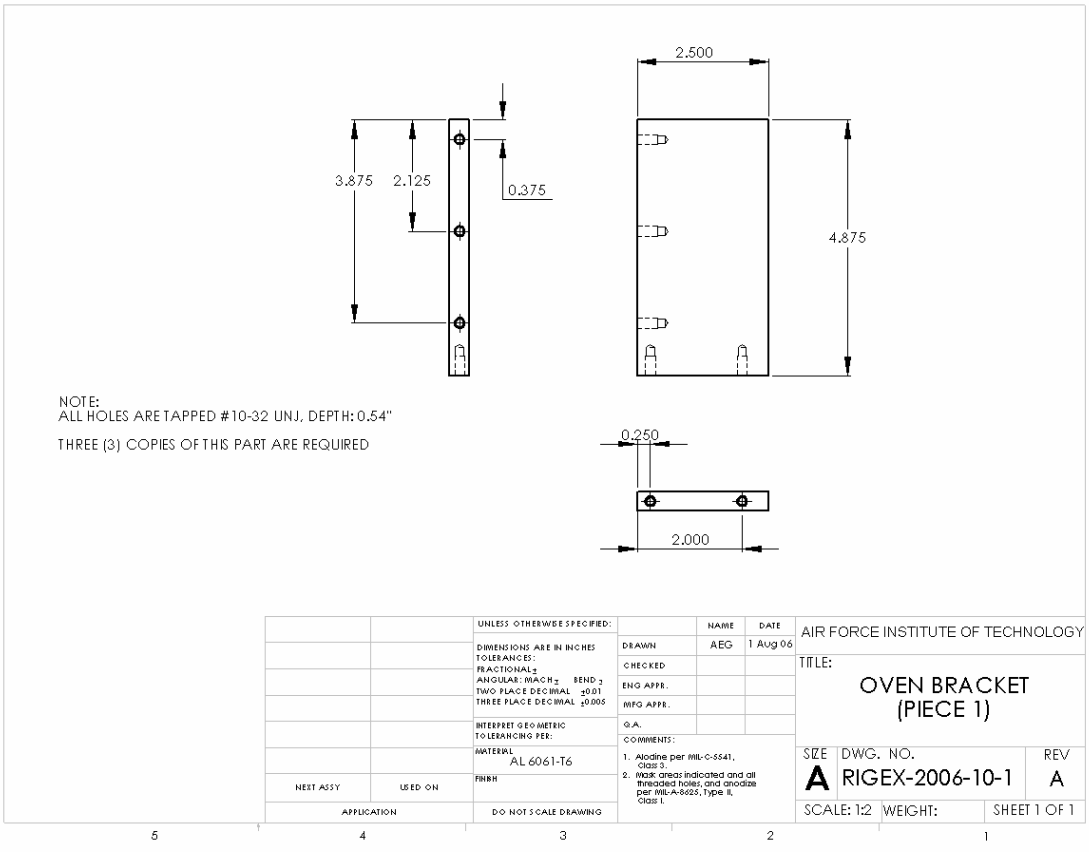

Figure D-26: Oven Bracket Piece 1

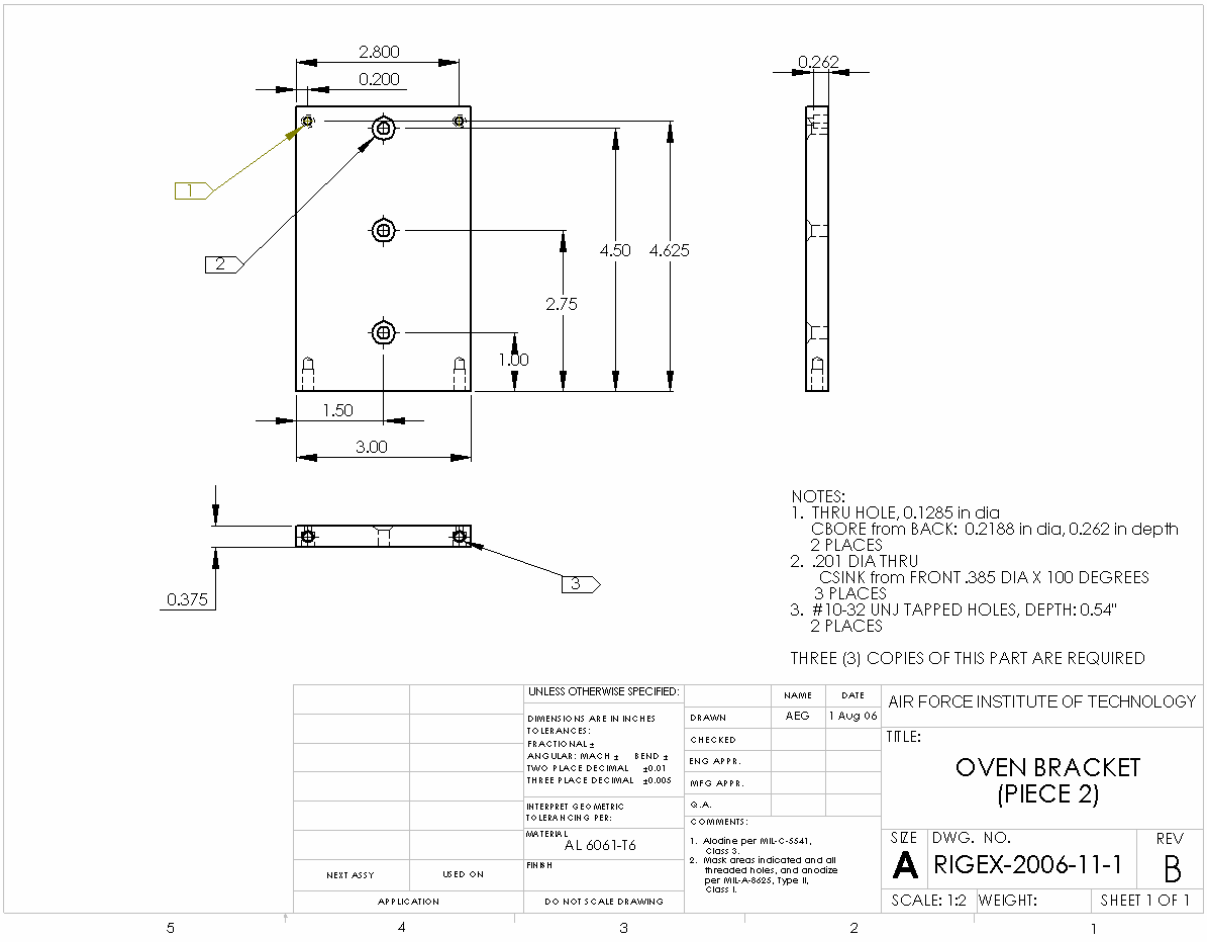

Figure D-27: Oven Bracket Piece 2

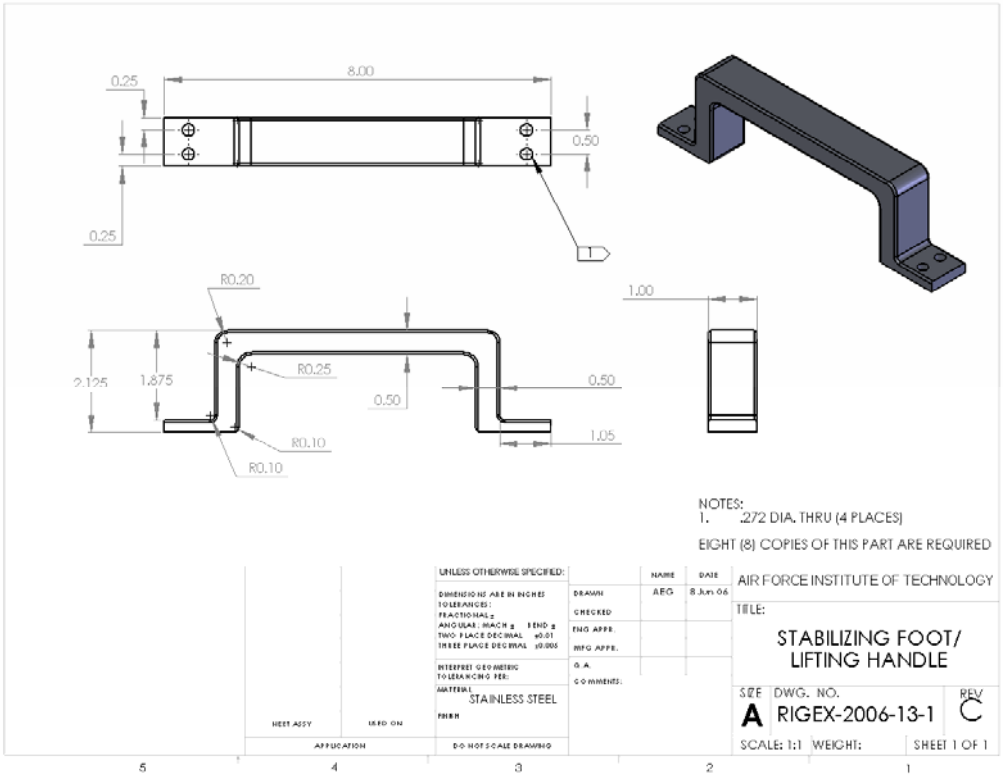

Figure D-28: Stabilizing Feet

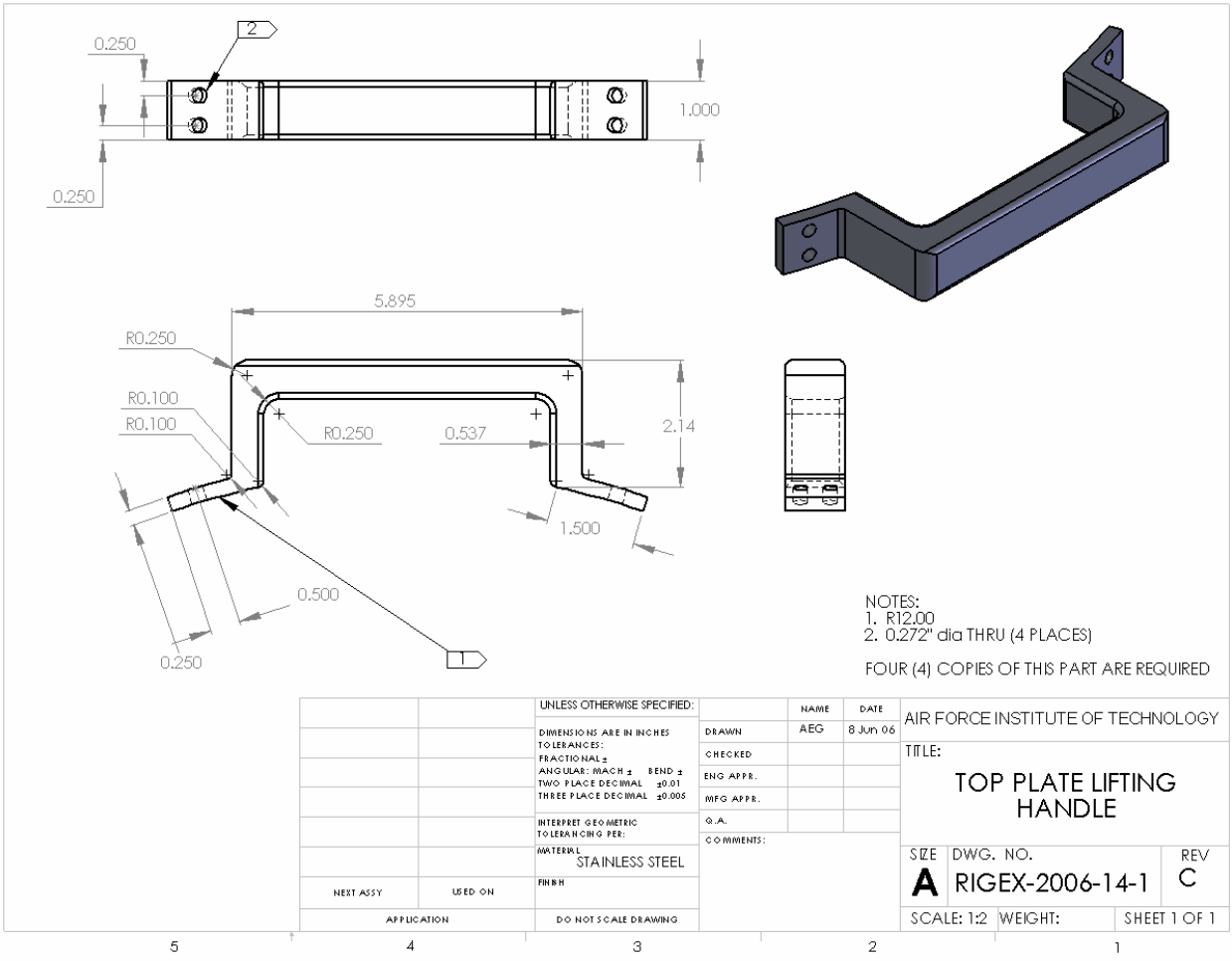

Figure D-29: Lifting Handles

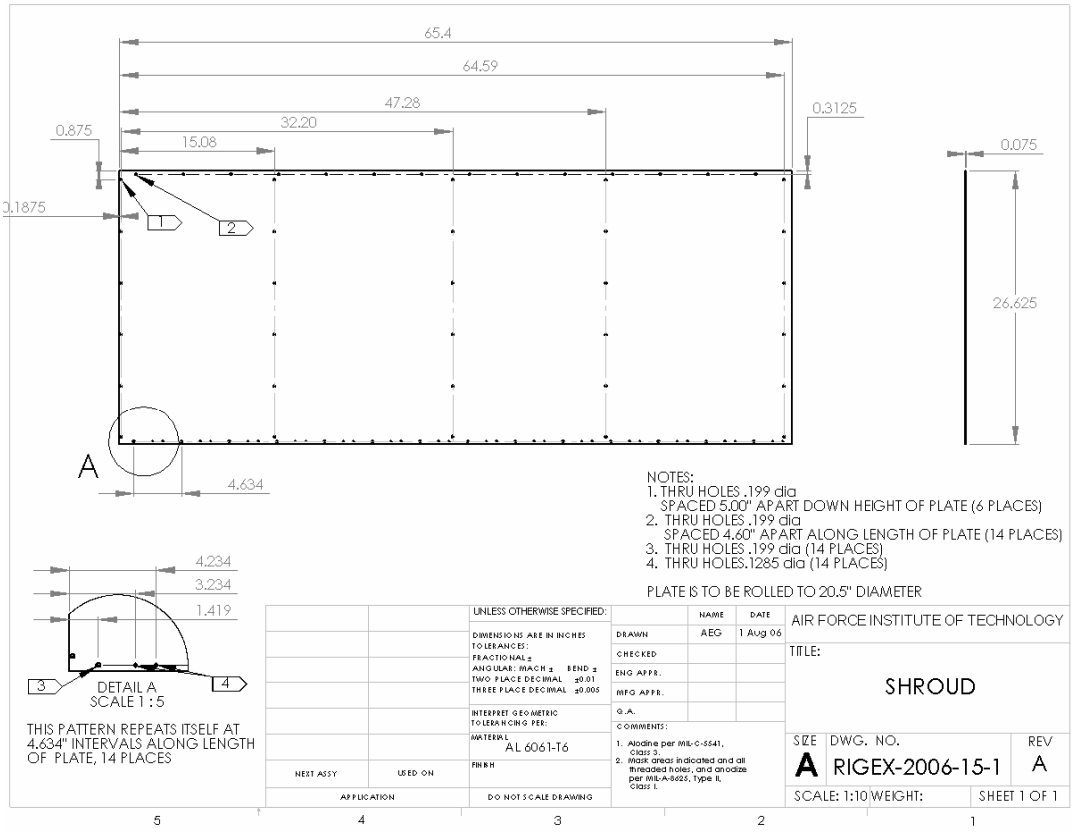

Figure D-30: Shroud

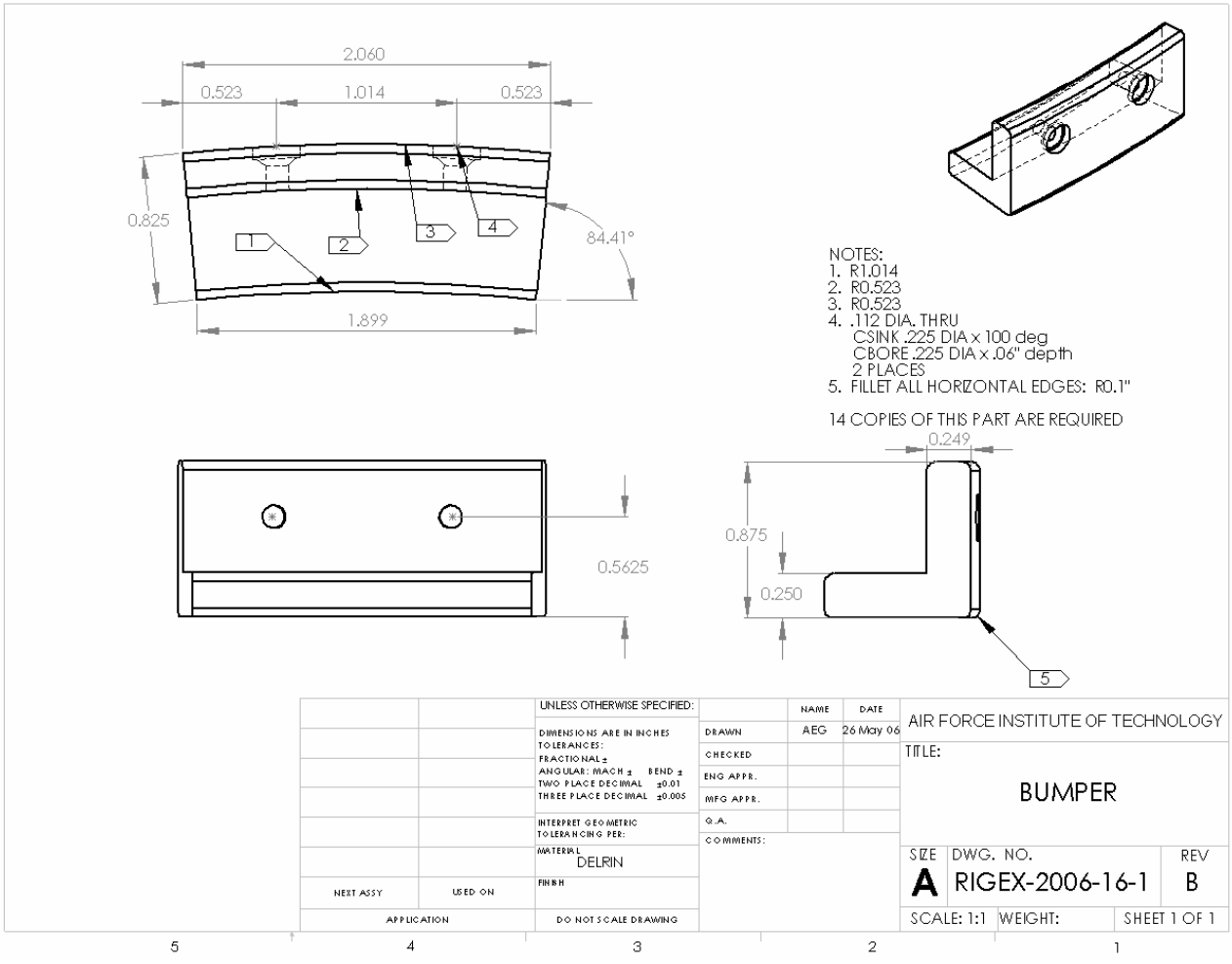

Figure D-31: Bumper

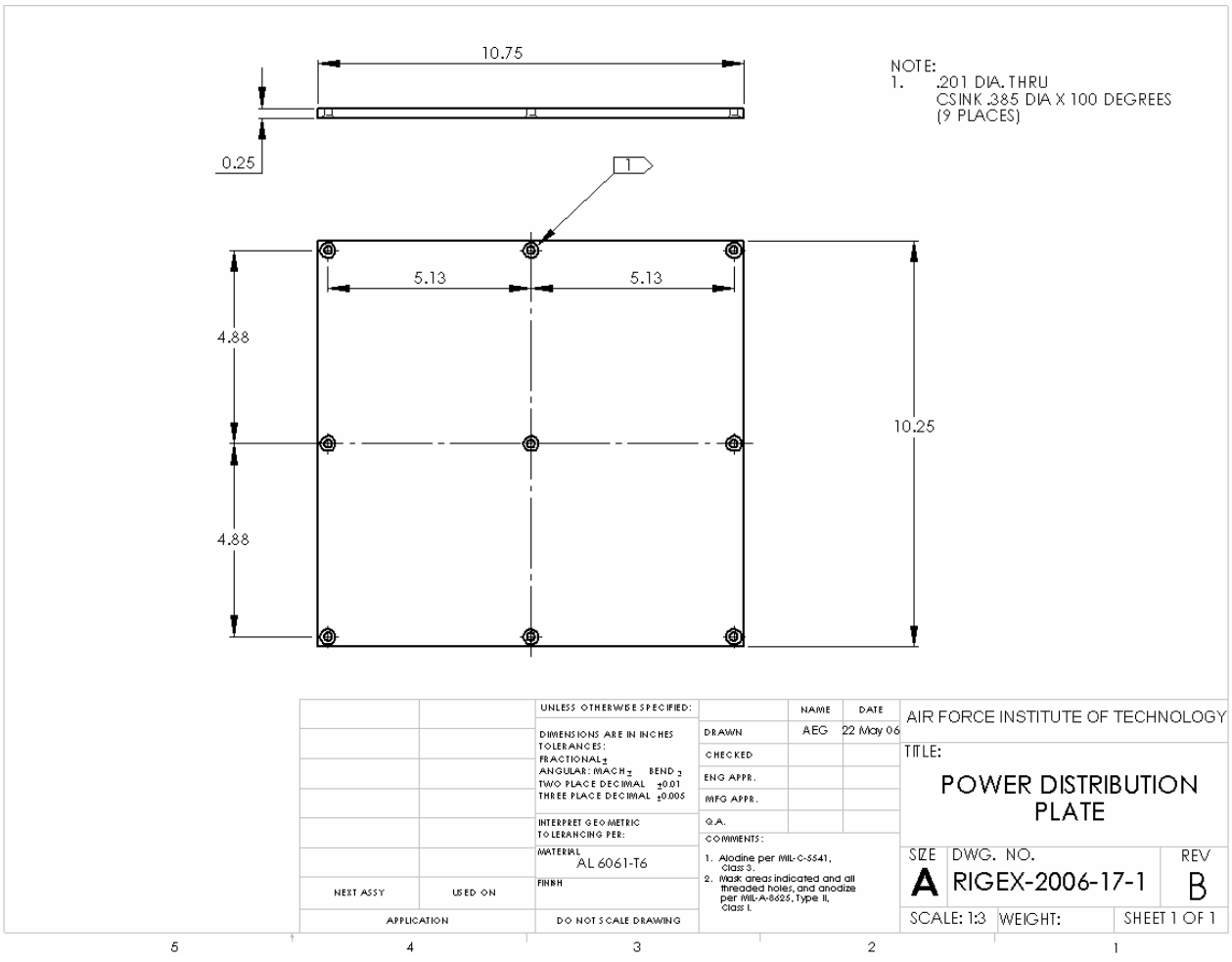

Figure D-32: Power Distribution Plate

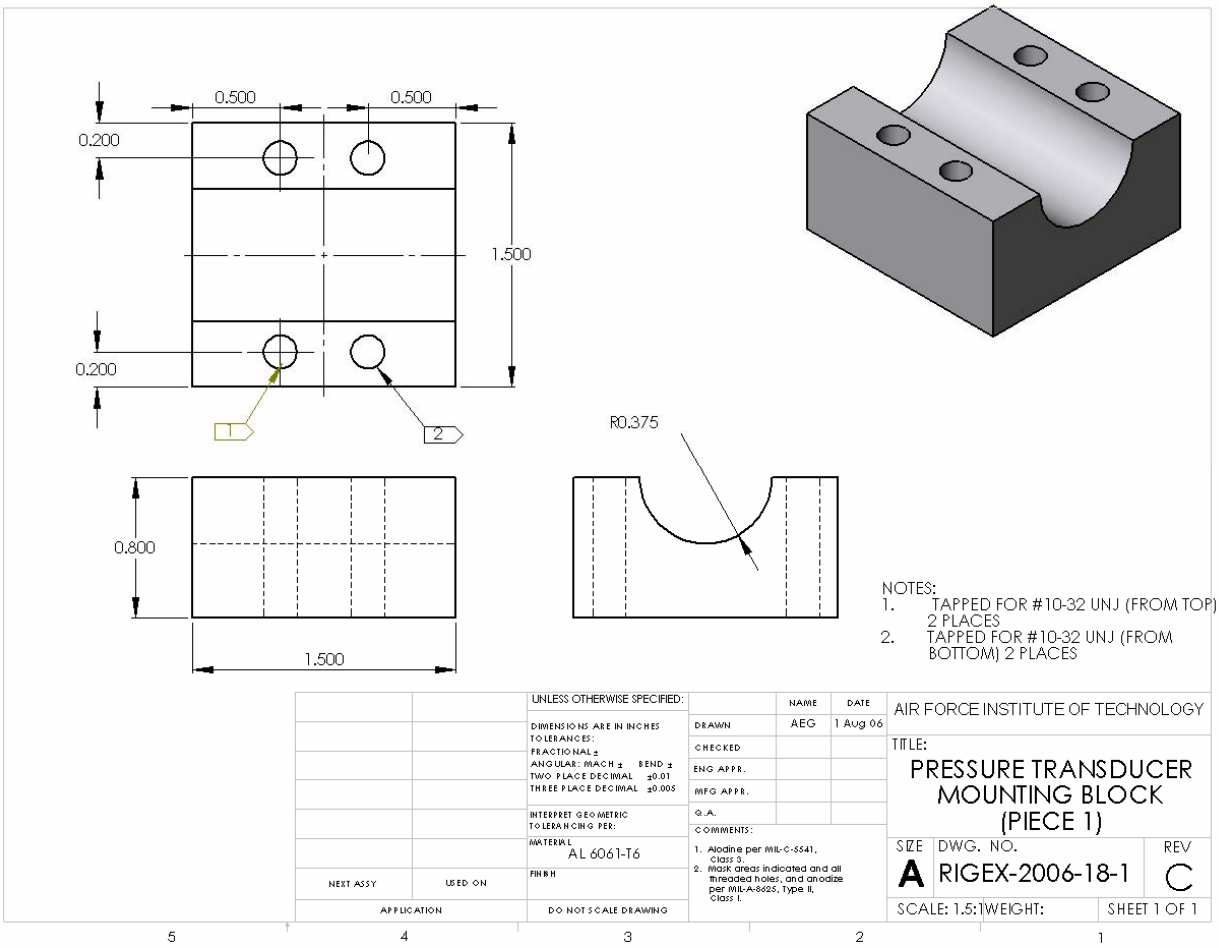

Figure D-33: Experiment Pressure Transducer Mounting Block Piece 1

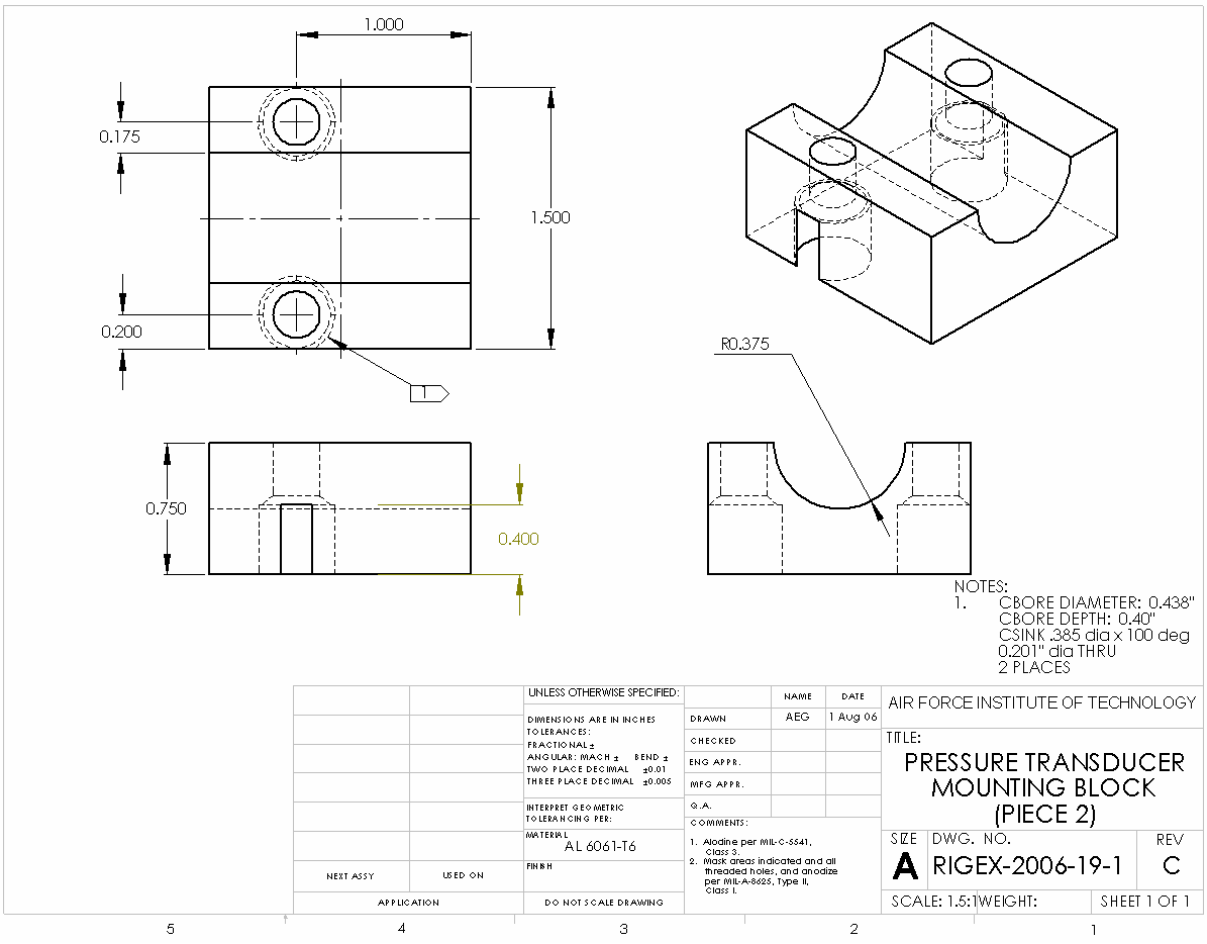

Figure D-34: Experiment Pressure Transducer Mounting Block Piece 2

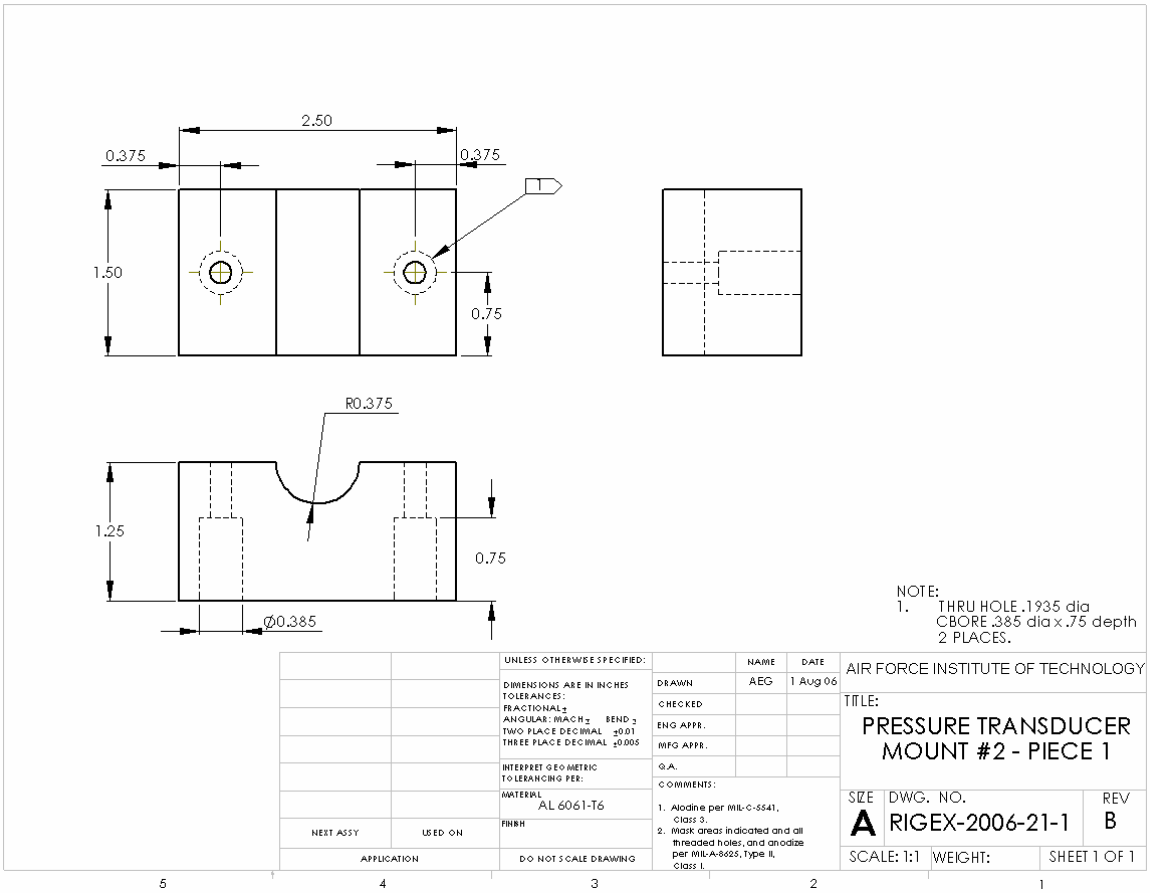

Figure D-35: Nitrogen Tank Pressure Transducer Mounting Block Piece 1

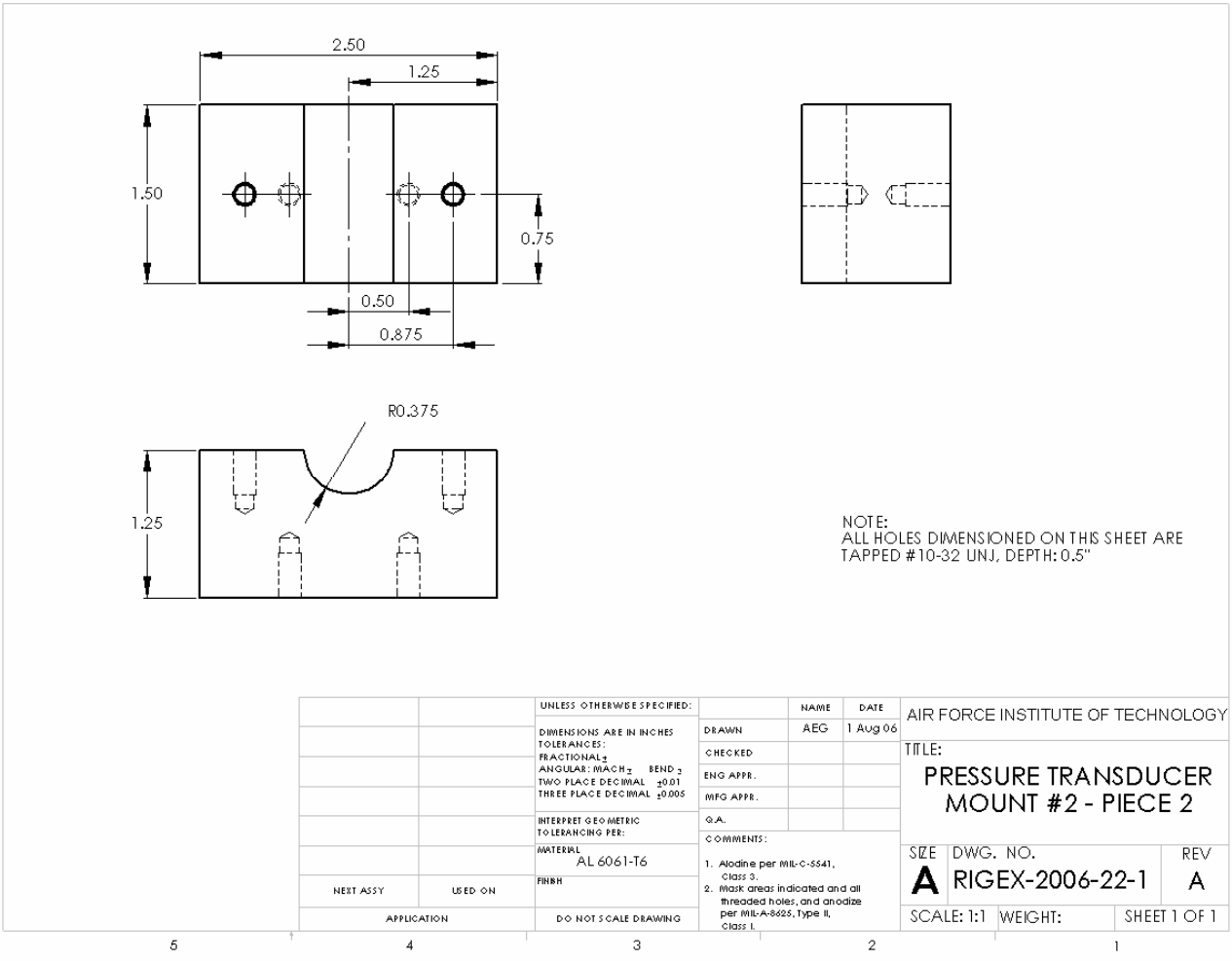

Figure D-36: Nitrogen Tank Pressure Transducer Mounting Block Piece 2

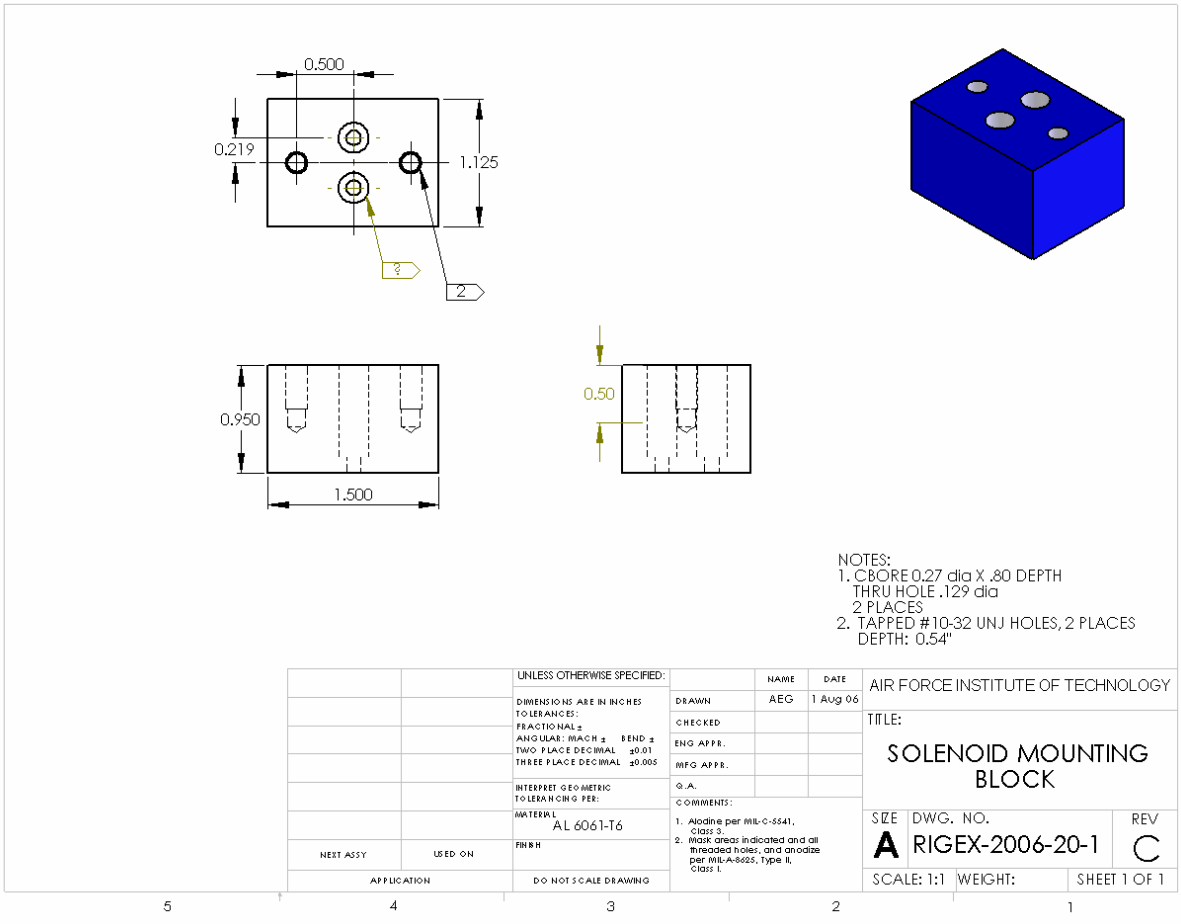

Figure D-37: Solenoid Mounting Block

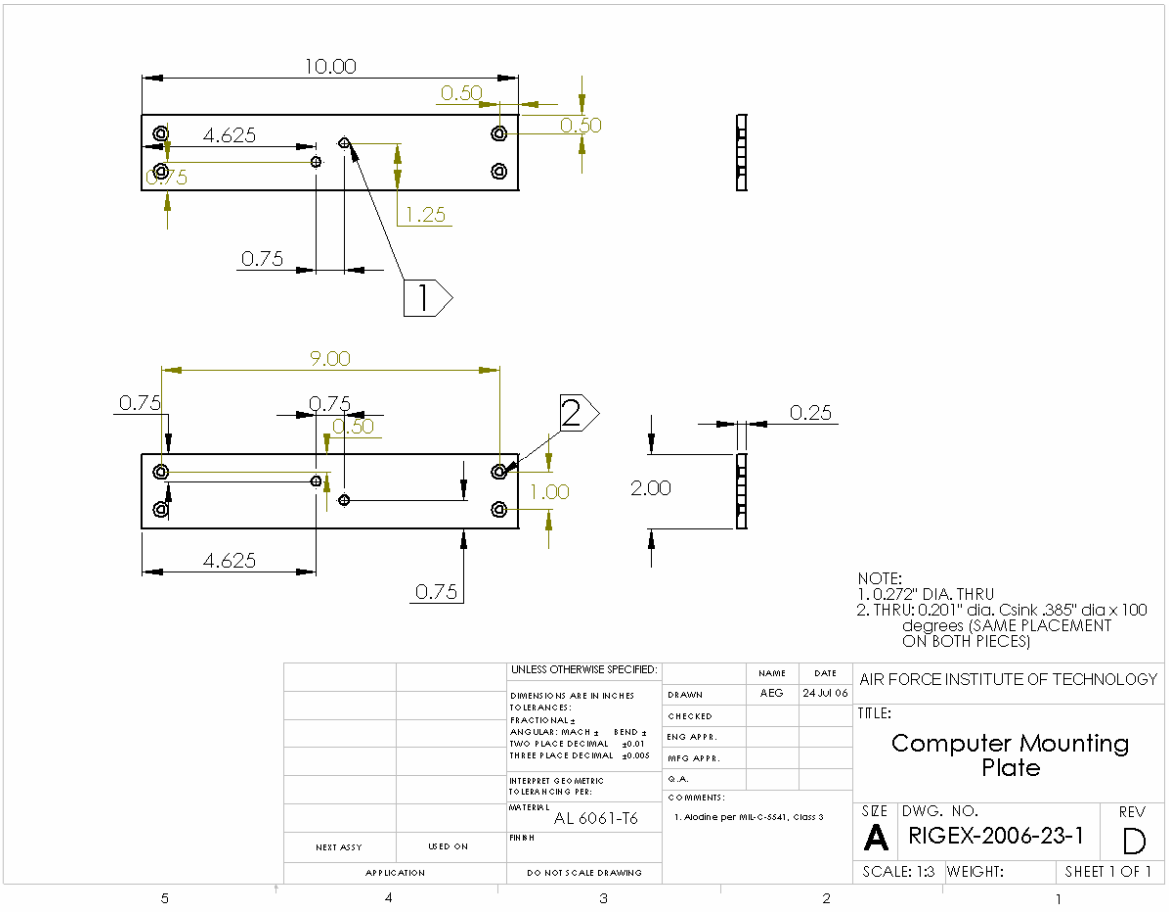

Figure D-38: Computer Mounting Plate

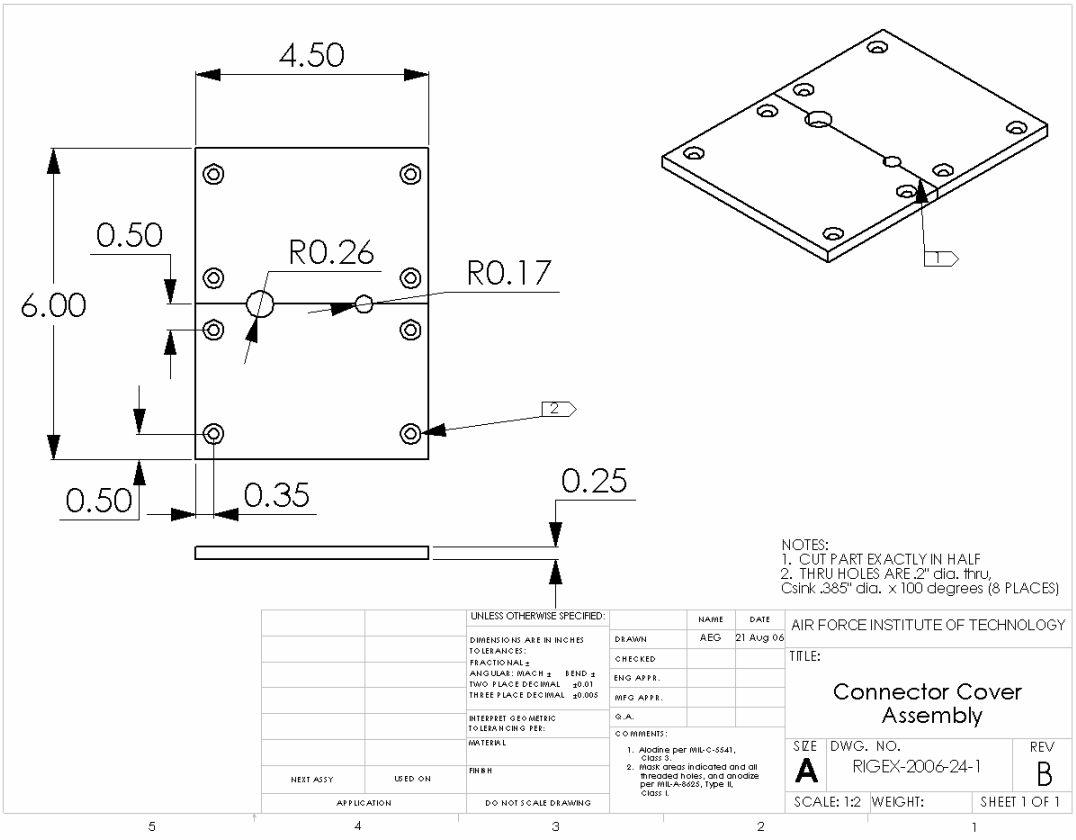

Figure D-39: Connector Hole Cover

Appendix E: Final Wire Routing Schematic

The following set of figures outline the RIGEX Wire Routing Scheme. This scheme was developed to minimize potential data noise by separating power and data wiring. It also arranges components smartly, to minimize wire usage and therefore reduce power and signal loss. This schematic will be used as a map for wiring the physical RIGEX Structure.

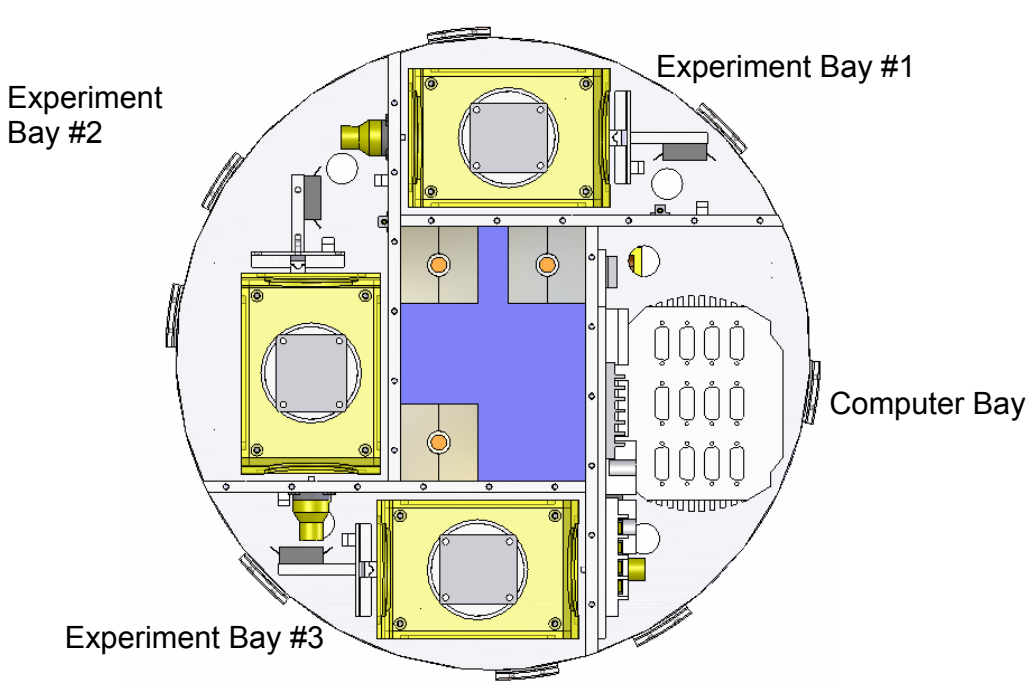

Figure E-1: Definition of RIGEX Bay Numbers

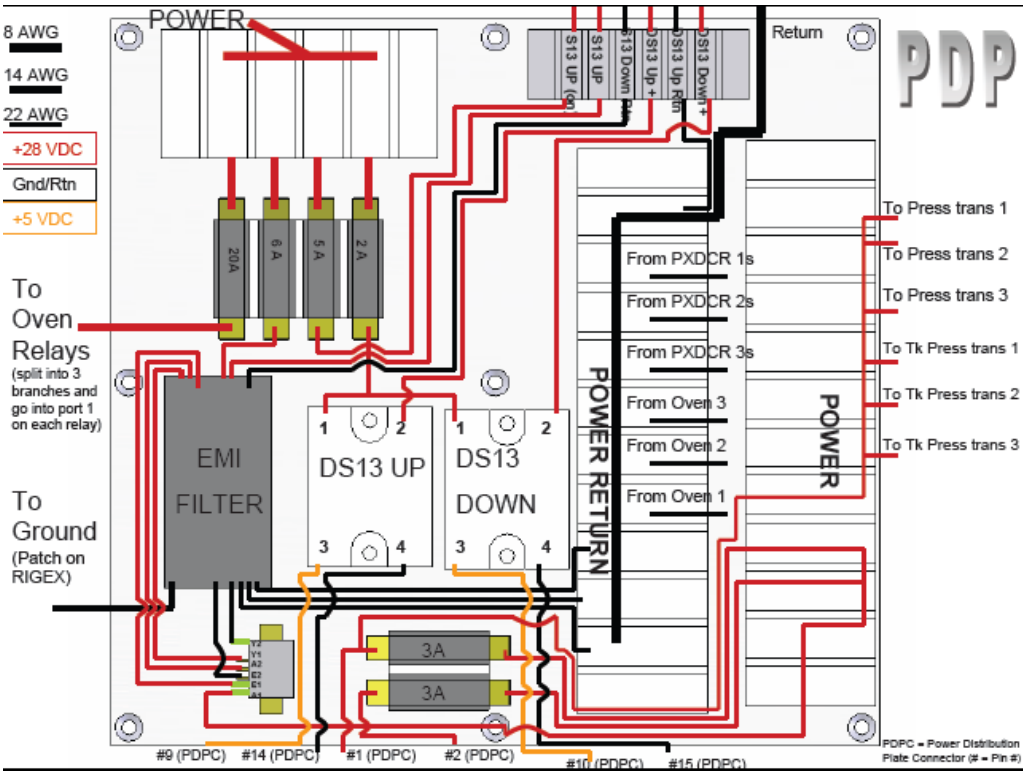

Figure E-2: Power Distribution Plate

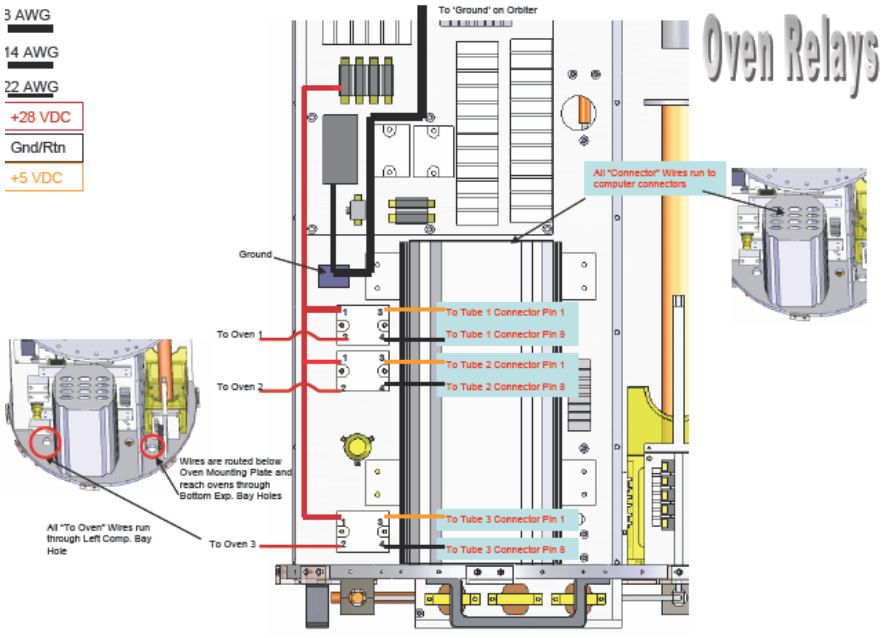

Figure E-3: Oven Relay Circuit

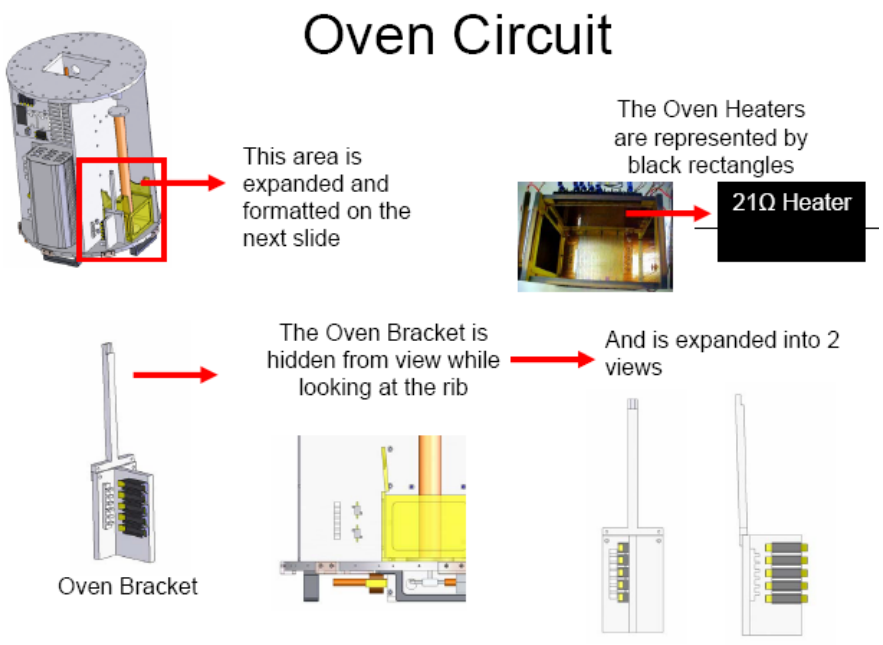

Figure E-4: Oven Circuit Explanation

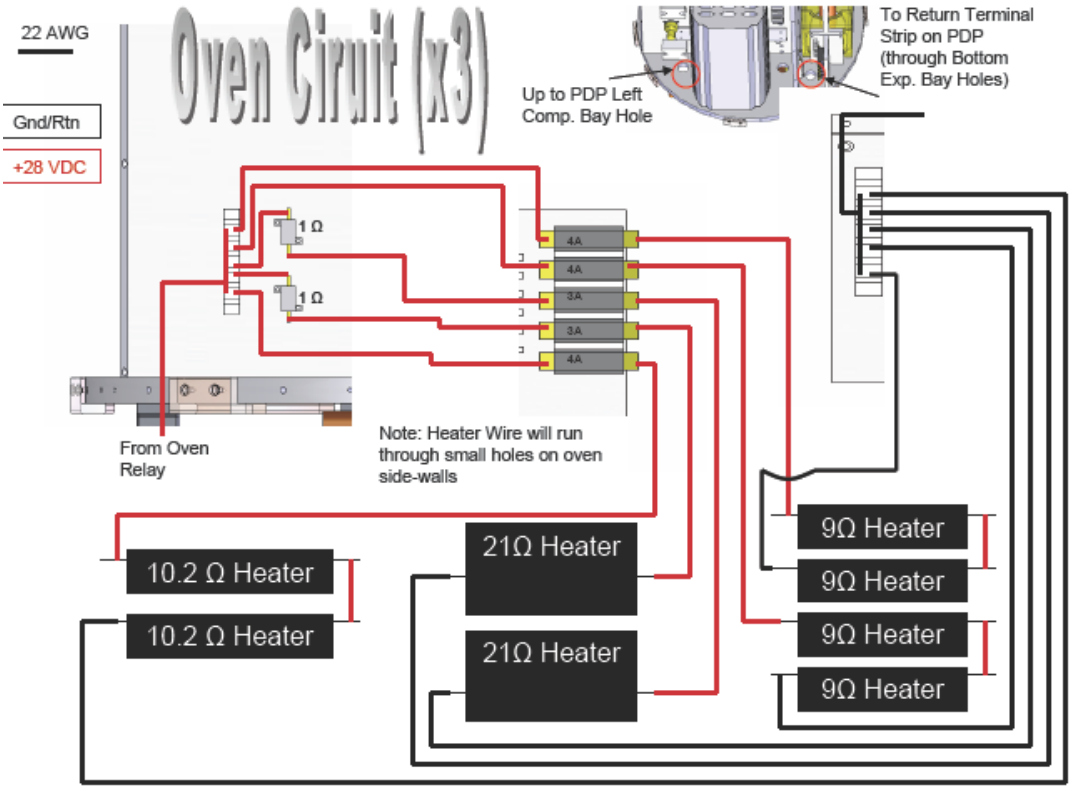

Figure E-5: Oven Circuit

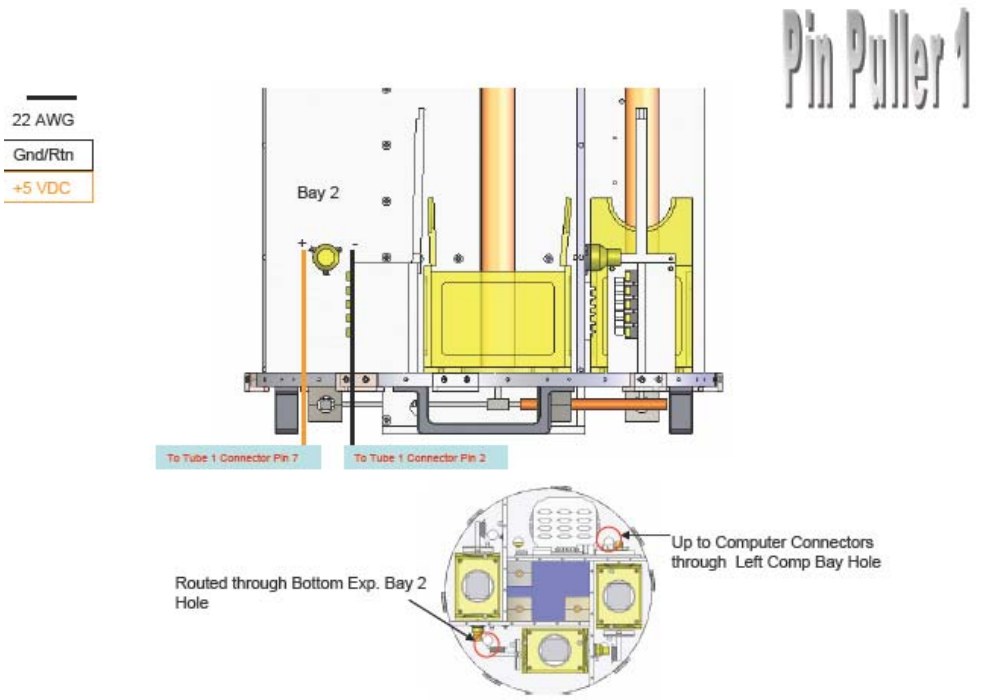

Figure E-6: Pin Puller 1

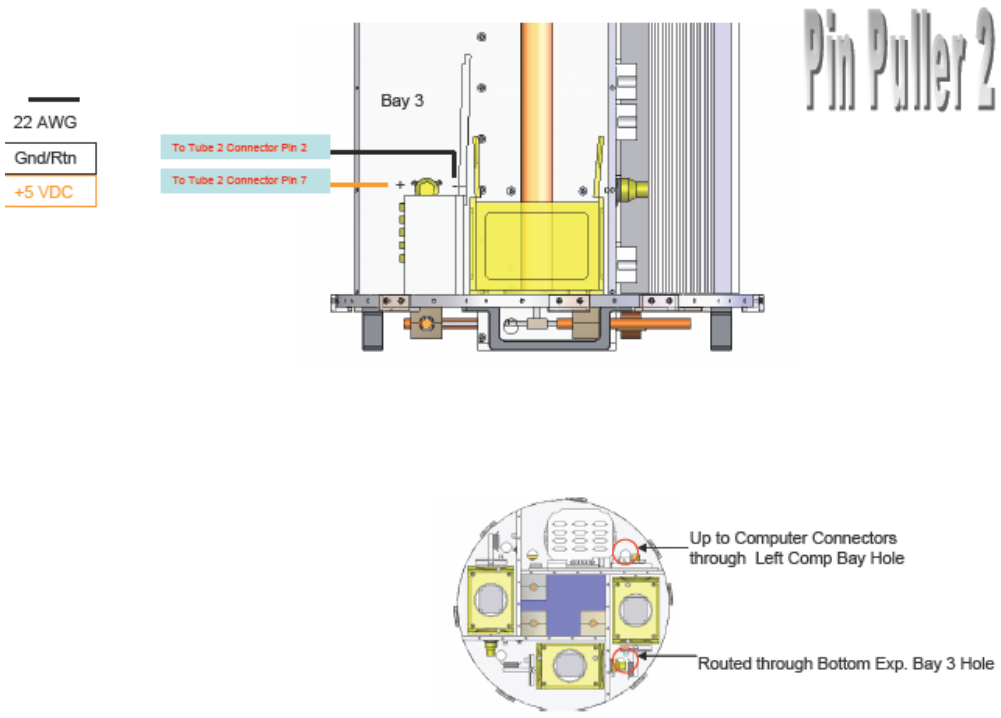

Figure E-7: Pin Puller 2

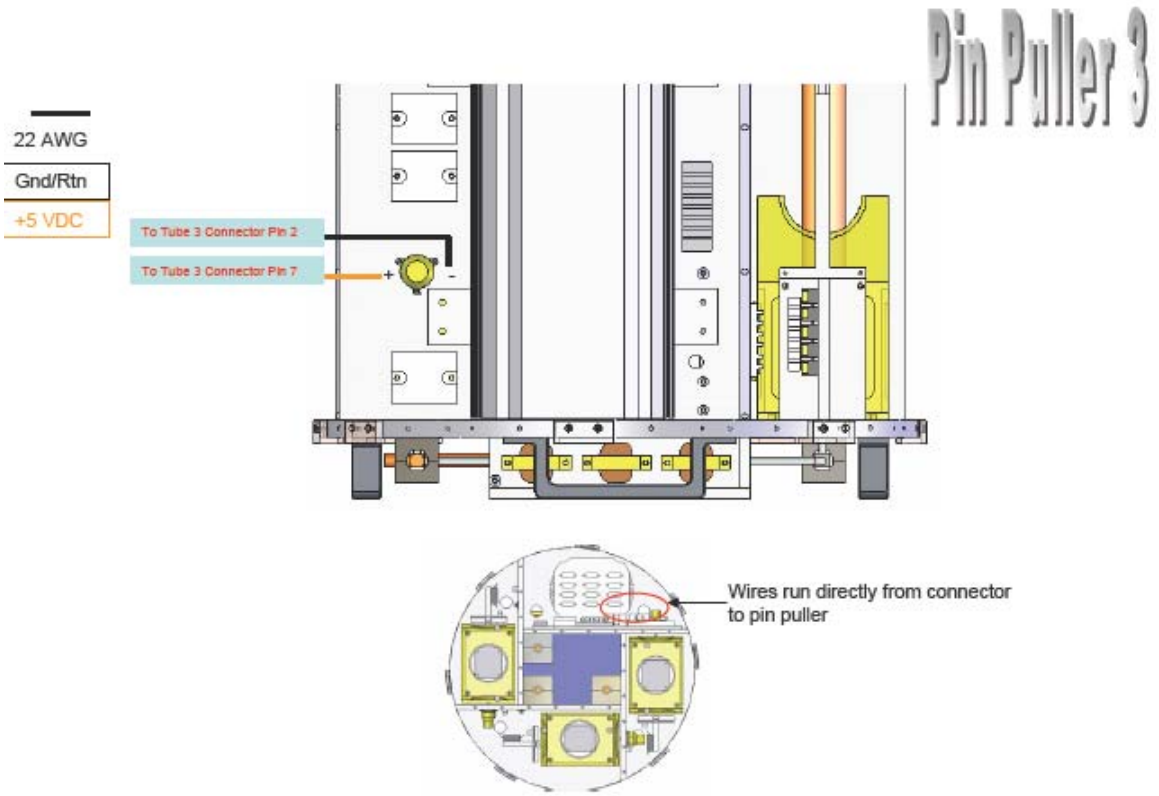

Figure E-8: Pin Puller 3

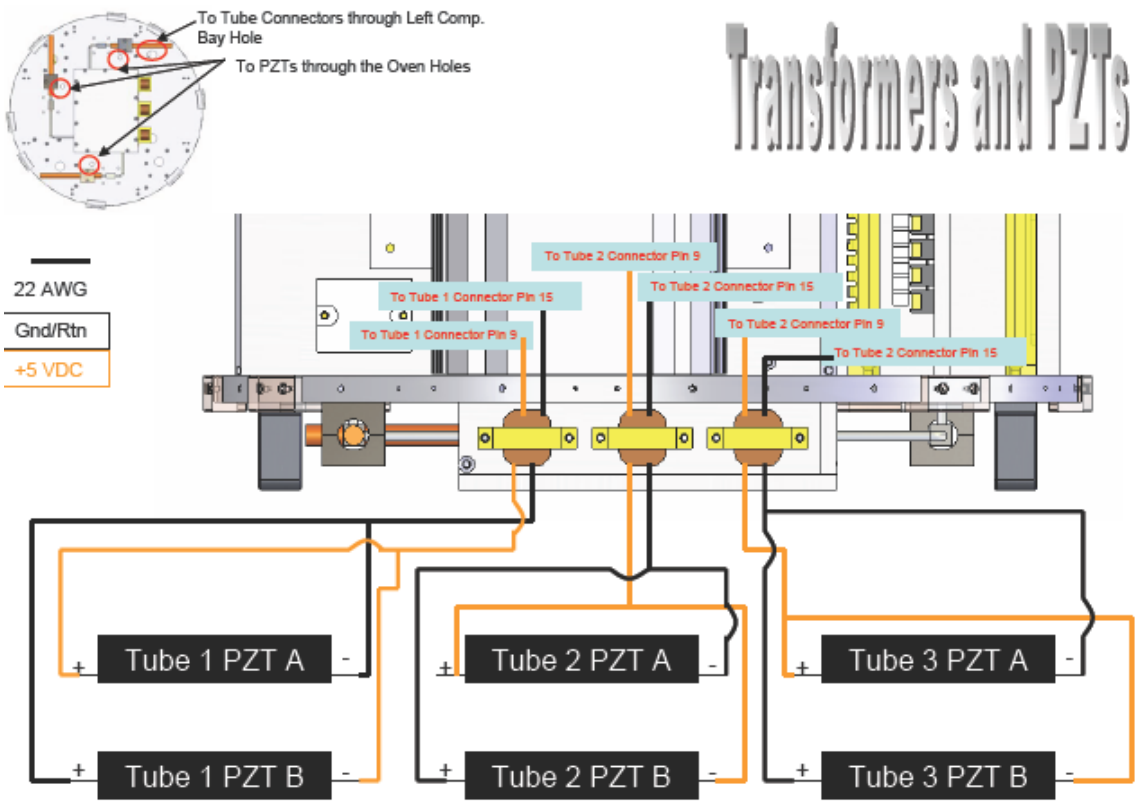

Figure E-9: Transformers and Piezoelectric Patches

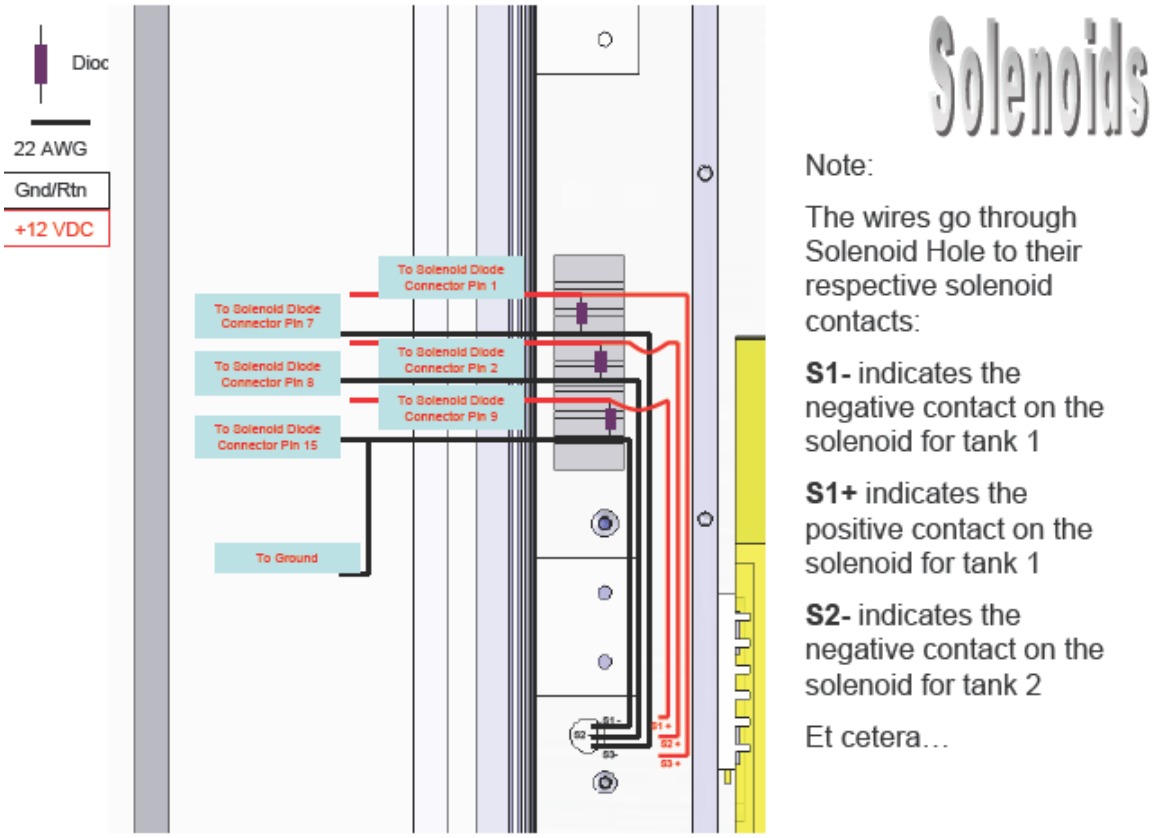

Figure E-10: Solenoids

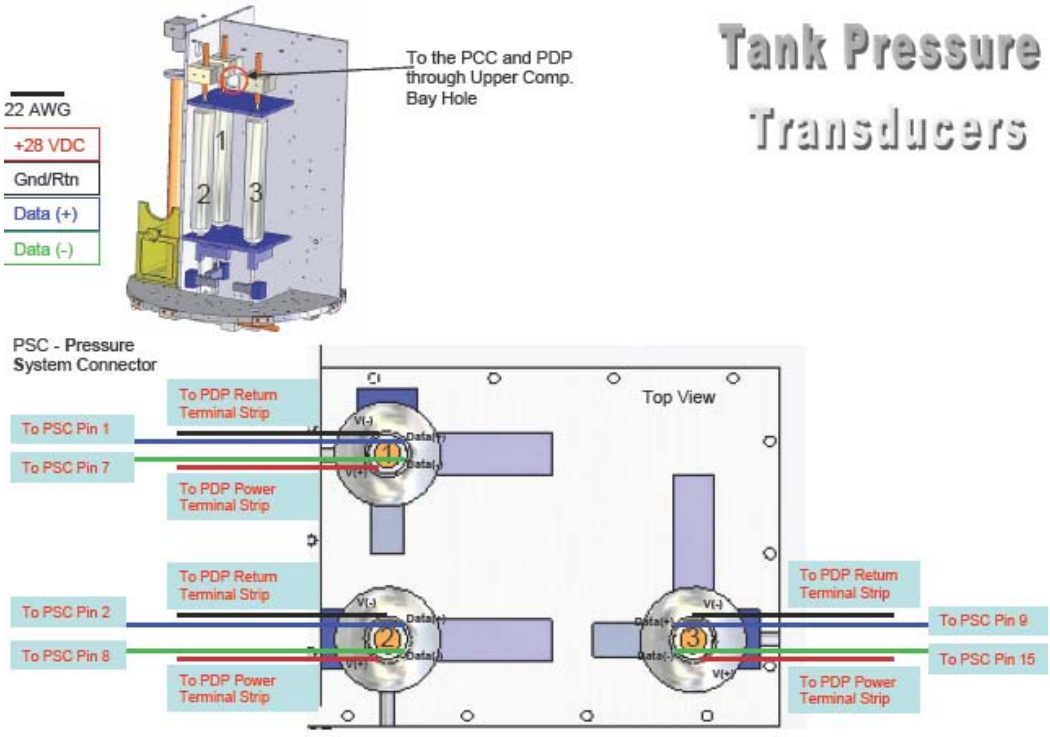

Figure E-11: Nitrogen Gas Tank Pressure Transducer

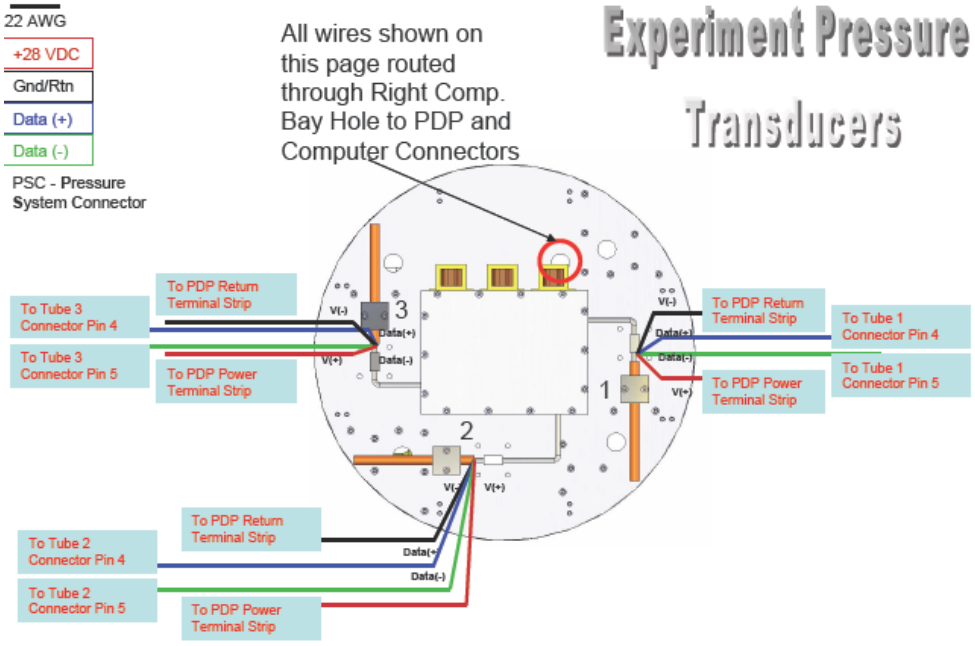

Figure E-12: Experiment Pressure Transducer

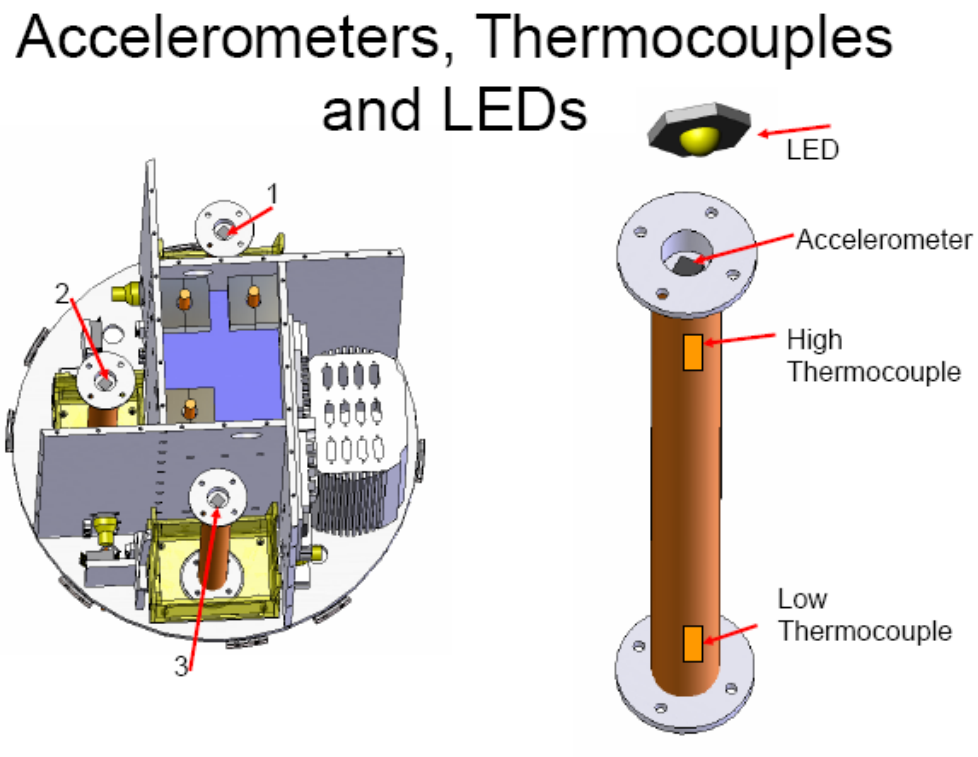

Figure E-13: Accelerometer Thermocouple and LED Explanation

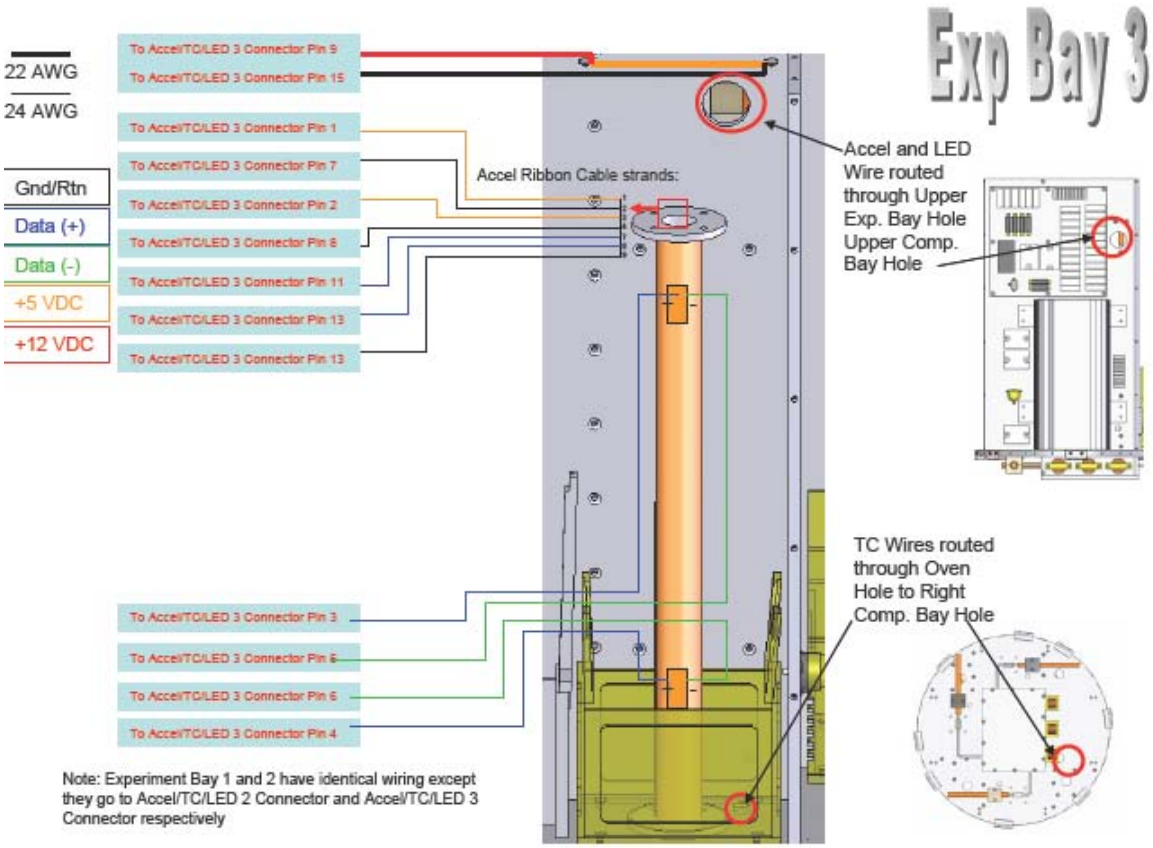

Figure E-14: Experiment Bay 3

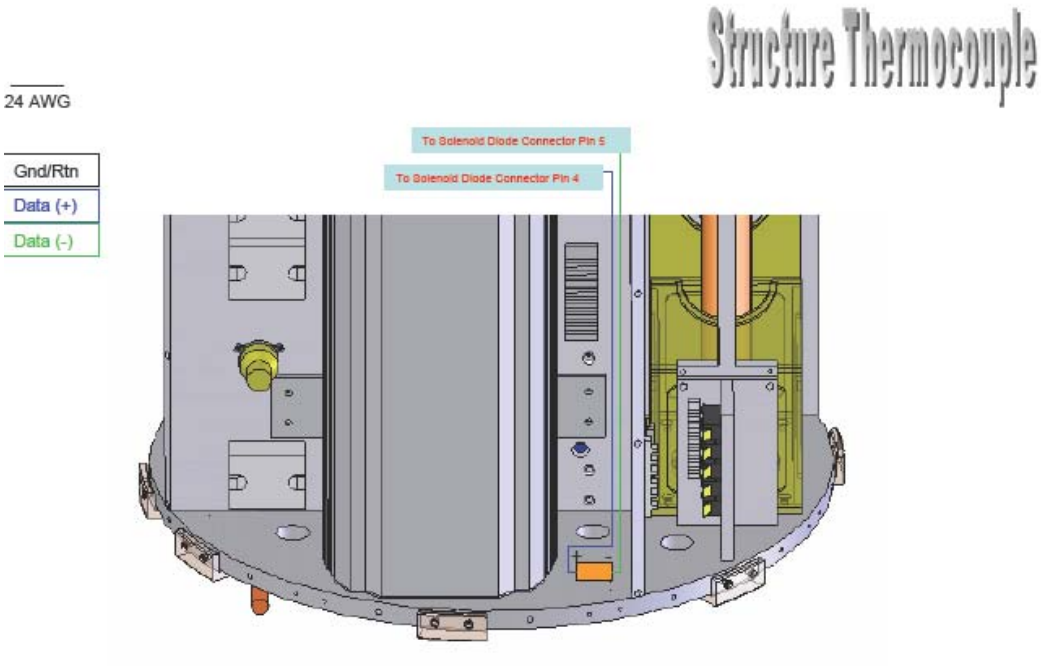

Figure E-15: Structure Thermocouple

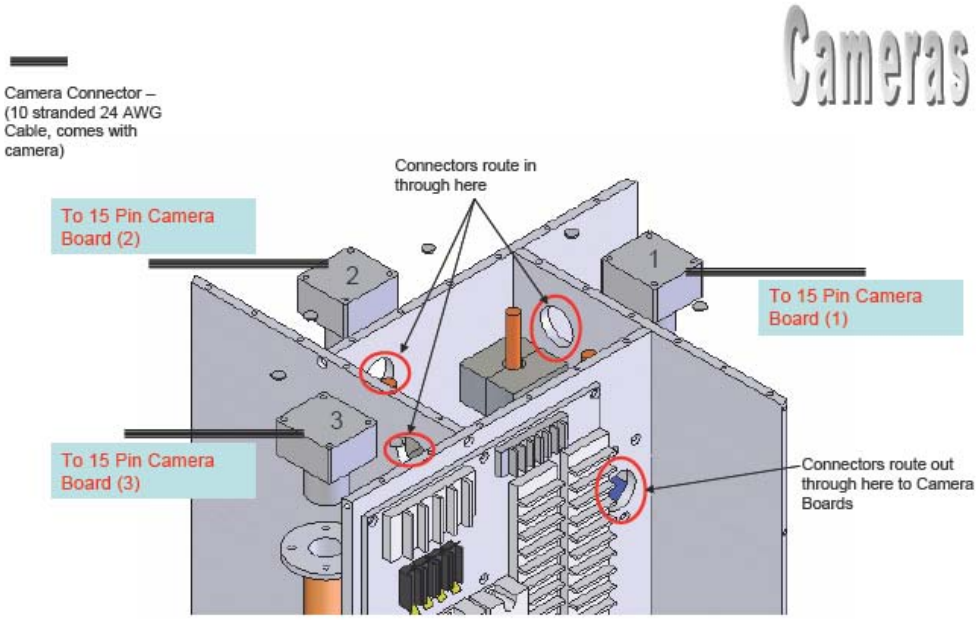

Figure E-16: Cameras

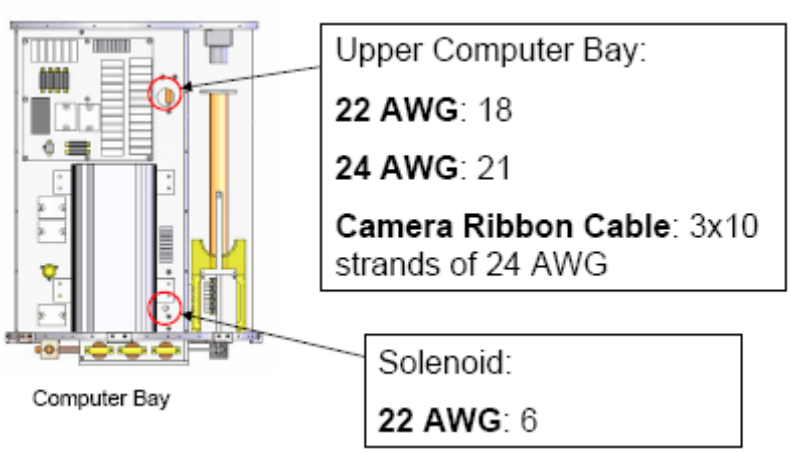

Figure E-17: Computer Bay Wire Routing Totals

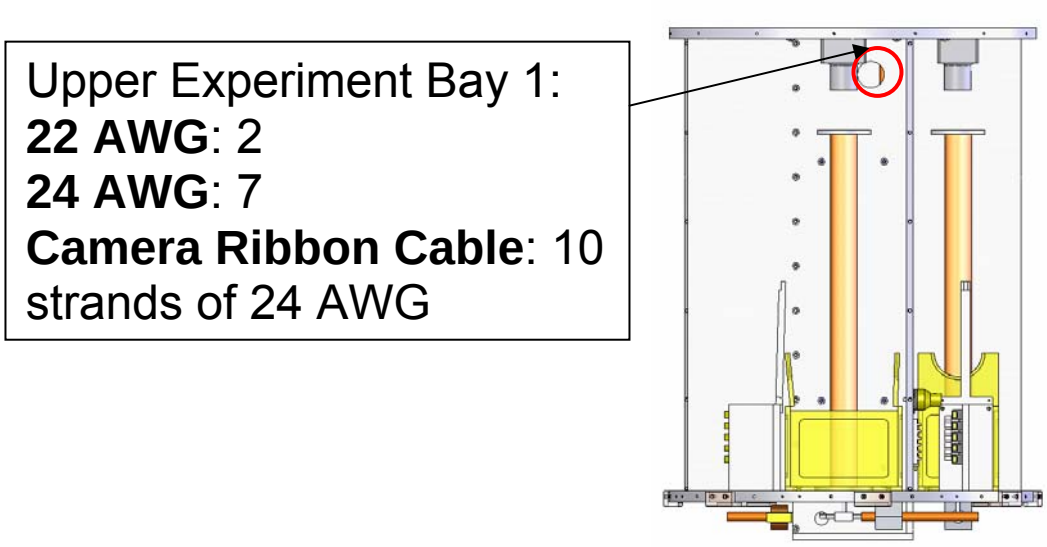

Figure E-18: Experiment Bay 1 Wire Routing Totals

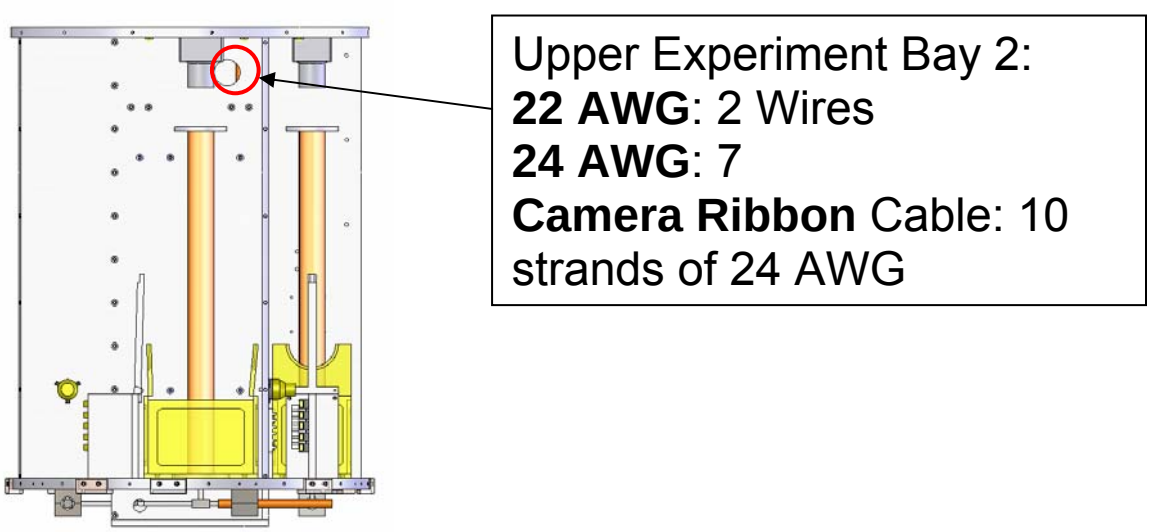

Figure E-19: Experiment Bay 2 Wire Routing Totals

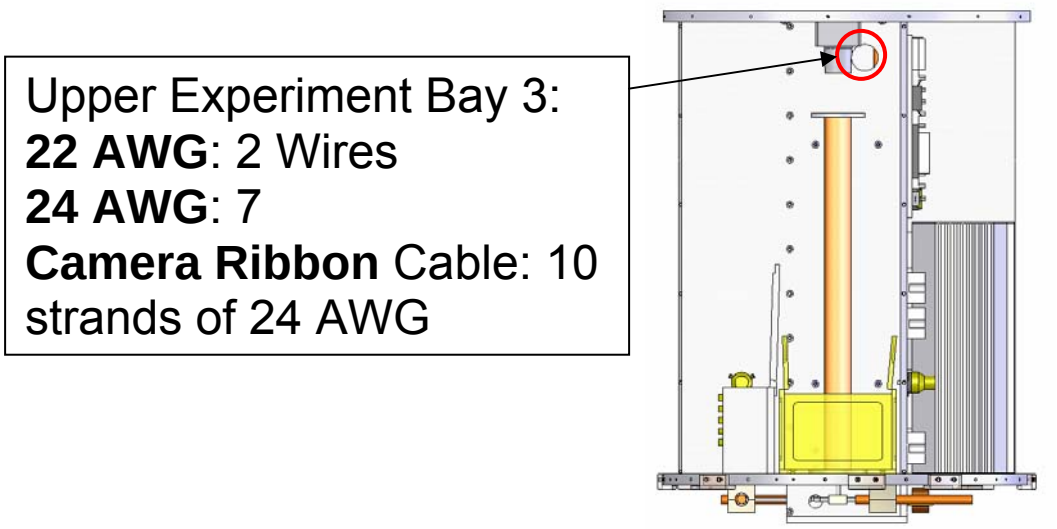

Figure E-20: Experiment Bay 3 Wire Routing Totals

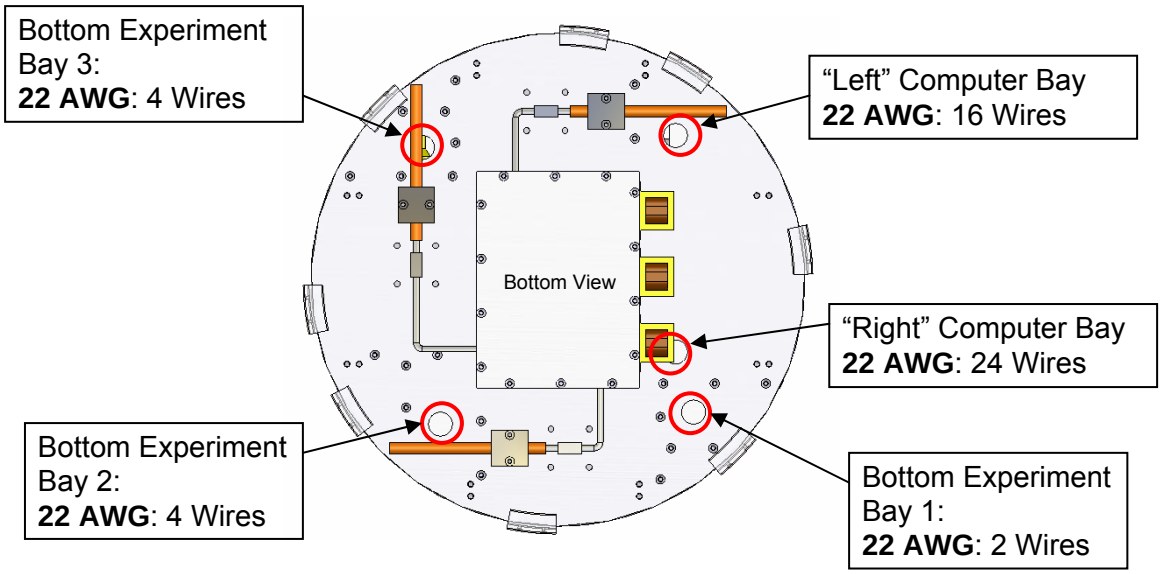

Figure E-21: Oven Mounting Plate Wire Routing Totals

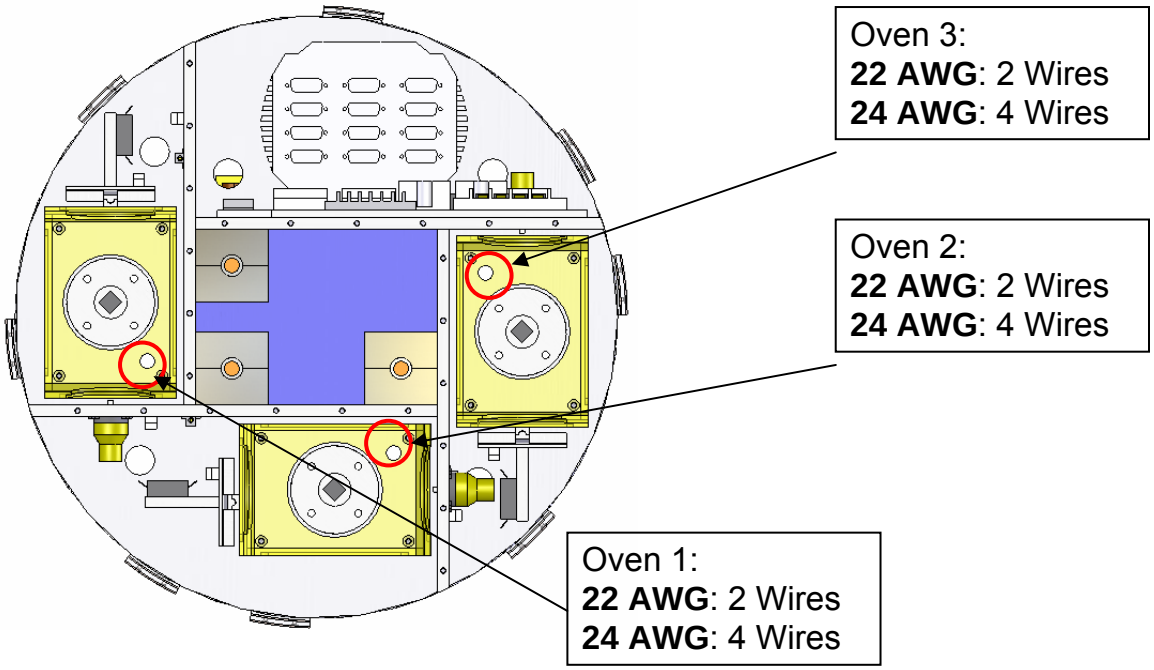

Figure E-22: Oven Wire Routing Totals

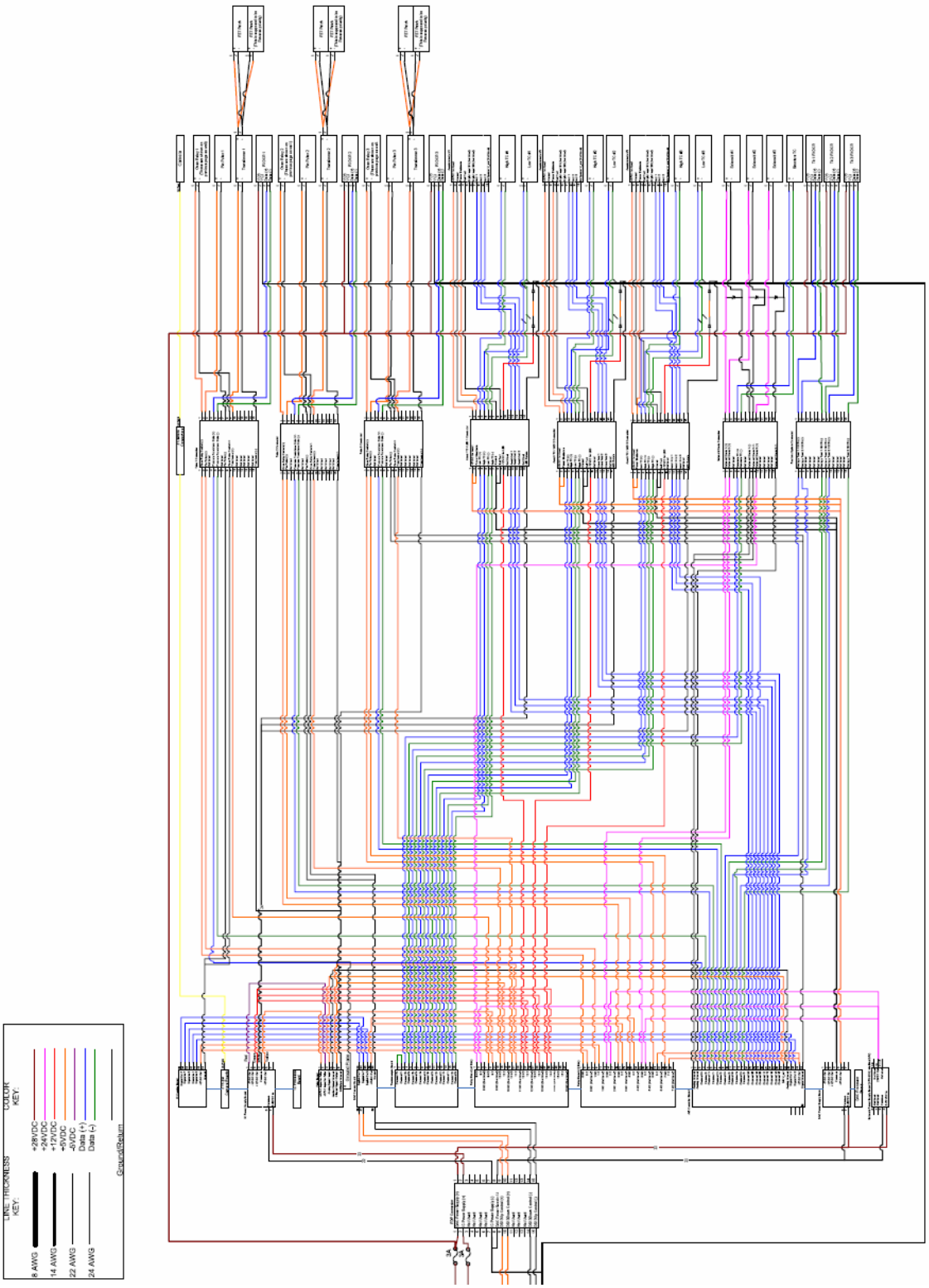

Figure E-23: Wire Routing within PC-104 Computer

Appendix F: Containment Analysis

At STP's request, a containment analysis was executed to ensure the RIGEX shroud is thick enough to contain RIGEX subsystem components should their fasteners fail. The containment analysis requirements are outlined in, and all equations are drawn from, NASA SSP 52005 Revision C (34).

F.1 Containment Methodology

The first step in the containment analysis to determine the maximum velocity a RIGEX subsystem component could obtain before striking the shroud. The velocity equation is:

$$V = \frac{A_{LF}}{2\pi f_n} + \sqrt{2aS_d} \qquad \text{(F1)}$$

where

A_{LF} = Low Frequency Transient Acceleration (m/s^2)

f_n = Minimum Natural Frequency of Vibration (s^{-1})

a = Steady State Acceleration of Orbiter (m/s^2)

S_d = Maximum Travel Distance of Component (m)

If a preloaded bolt that has a tensile yield strength less than 180,000 lb/in^2 fails, an initial velocity must be added in to the component's total velocity. This initial velocity is found from:

$$V_o = \sqrt{\frac{PLD_{\max}{}^2 l}{AEm_f}} \qquad \text{(F2)}$$

where

P = Maximum Bolt Preload (N)

l = Fastener Length (m)

A = Cross Sectional Area of Fastener (m^2)

E = Fastener Modulus of Elasticity (N/m^2)

m_f = Mass of Fastener (kg)

The *punch* equation is then used to obtain the containment shroud's required thickness:

$$T_R = \left[\frac{1}{2} m V^2 \frac{1}{d Y S_w} \right] \qquad \text{(F3)}$$

where

m = Mass of the Component (kg)

d = Perimeter of Smallest Face of Component (m)

YS_w = Yield Strength of Containment Shroud (N/m^2)

The following values were used in the analysis below:

- Low Frequency Transient Acceleration A_{LF} = 10.6g x SF = 21.2g m/s^2 (Table 2)
- Minimum Natural Frequency of Vibration f_n = 50 s^{-1} (6: 16)
- Steady State Acceleration of Orbiter a = 6.5g x SF = 13g m/s^2 (15: C-2)
- Yield Strength of Containment Shroud YS_w = 2.413 x 10^8 N/m^2 (8)

- Gravity $g = 9.8$ m/s^2

F.2 Oven Containment

The ovens that will be used to heat the thermoplastic composite tubes to their glass transition temperature were constructed prior to RIGEX being manifested on CAPE. While still in excellent condition, the oven walls are fastened together with bolts that are not in compliance with a NAS, and those bolts do not have a locking mechanism installed. The oven will by together by thirty-two of these #4-40 hex flat head cap screws. Layers of insulation will also hold the oven walls together. Finally, prior to experiment initiation, the oven will be secured to the oven mounting plate by the oven latch. Yet, the use of non aerospace standard screws presents a containment hazard. Therefore, a containment analysis was performed to show that the oven would be contained within the RIGEX shroud if the oven bolts should fail.

The maximum distance that the oven could travel within a RIGEX experiment bay before impacting the shroud is 0.687 m, therefore, Equation F1 shows that the velocity of the oven at impact would be 13.89 m/s.

The bolts constraining the oven, while they are not in conformance with a NAS, have a yield strength significantly less than 180,000 lb/in^2. Due to this low yield strength, paragraph 5.3.1.1B in SSP 52005 Revision C states the oven bolts do not have low fracture toughness and therefore an initial velocity due to preloaded bolt failure is not needed.

The oven mass is 0.643 kg, and the perimeter of its smallest face is 0.4636 m. Using these values, Equation F3 shows that the containment shroud needs to be 7.447 x

10^{-4} m thick (0.0293 in). As the shroud is already being constructed out of 0.075 in thick aluminum, oven containment is closed as a safety concern.

F.3 Computer Containment

While the computer is being secured by an intricate system of NAS compliant bolts, Heli-Coils and locknuts, STP raised concern over its containment, as it is by far the largest and heaviest RIGEX component. A containment analysis was therefore executed to alleviate concern.

As the bolts constraining the oven are in conformance with a NAS and have a yield strength less than 180,000 lb/in^2, an initial velocity due to bolt failure is not required.

The computer has two possible failure modes. The computer could detach from the computer mounting plate and strike the shroud, or the computer and computer mounting plate could, together, strike the shroud.

If the computer alone detached and struck the shroud, it could move 0.305m before impacting the shroud. Equation F1 reveals that the collision would occur at no more than 9.477 m/s. The computer's mass is 6.101 kg and its minimum perimeter is 0.5412 m. Equation F3 shows that the containment shroud must be at least 0.0014 m (0.055 in).

Should the computer detach from the rib along with the computer mounting plate, it would only be able to travel 0.077 m, making its maximum velocity 5.09 m/s. The minimum perimeter of the computer mounting plate is 0.1143 m, and the combined mass

of the computer and computer mounting plate is 6.536 kg. Using these values, Equation F3 shows that the shroud must be at least 0.00175 m (0.069 in).

While the computer and computer mounting plate together have the greatest shroud thickness requirement of all RIGEX components, that thickness still does not exceed the as built shroud dimensions, therefore computer containment is closed as a safety concern.

Appendix G: Phase II Safety Data Package

The following pages include the Phase II Safety Data Package. All RIGEX information contained within was provided by the RIGEX team at AFIT. CAPE to RIGEX interface information within this document was developed by the author, Mr. Scott Ritterhouse and Mr. Carson Taylor of STP. This package was compiled by Theresa Shaffer, STP's Payload Safety Engineer. Its contents will be presented by the RIGEX team to a NASA Safety Review Board on 19 September 2006.

Table of Contents

1 INTRODUCTION 1
1.1 Purpose 1
1.2 Scope 1
1.3 References 1
2 SAFETY CERTIFICATION 2
2.1 Safety Analysis Summary 2
2.2 Test Plan 2
2.3 Hazard Reports 2
2.4 Non-compliance Reports 3
2.5 Action Items and Agreements 3
2.6 Operational Controls 3
3 PAYLOAD OVERVIEW AND OBJECTIVES 3
3.1 RIGEX System Description 4
3.1.1 RIGEX Structure 5
3.1.1.1 RIGEX interface to CAPE 6
3.1.2 RIGEX Tube Assembly 7
3.1.3 Oven/Heater Assembly 8
3.1.4 Avionics Assembly 12
3.1.4.1 RIGEX Internal Photography 16
3.1.5 Inflation System Assembly 17
3.1.6 Survival heaters (No Longer Used) 20
3.2 Payload Control Parameters 20
3.3 Orbiter/Payload Interfaces 20
3.3.1 Structural Interface 20
3.3.2 Electrical Interface 20
4 Operational Requirements Overview 22
4.1 Pre-launch 22
4.2 On-Orbit 22
4.3 Post-flight 22
4.4 Aborted Flight 22
5 Procedures 22

6 Failure/Accident Record 23
7 NSTS 13830C Reflight Safety Assessment 23
8 Summary of Flight Safety Analysis 24
8.1 Structural Failure 24
8.1.1 CAPE Structure 24
8.1.2 RIGEX Structure 24
8.2 Sealed Containers/Pressurized Systems 25
8.3 EVA Hazards 25
8.3.1 Touch Temperature 25
8.3.2 Sharp Edges, Corners, Protrusions 25
8.4 Shatterable Material Release 25
8.5 Flammable Materials 26
8.6 Nonionizing Radiation 26
8.7 Electrical Power Distribution 26
8.8 Ignition of Flammable Atmospheres in Payload Bay 26
8.9 Mechanisms 26

Table of Figures

Figure 3: RIGEX Sub-Tg tube deployment in laboratory 4
Figure 3.1: RIGEX Assembly 5
Figure 3.1.1: RIGEX Primary Structure 6
Figure 3.1.1.1: CAPE Mounting Plate 7
Figure 3.1.2: RIGEX Sub-Tg Tube Assembly Components 8
Figure 3.1.3a: RIGEX Prototype Oven 9
Figure 3.1.3b: Minco Heaters 10
Figure 3.1.3c: RIGEX Prototype Oven/Tube Assembly 10
Figure 3.1.3d: Shape Memory Pin Puller 11
Figure 3.1.3e: Door Latch Operation 11
Figure 3.1.4a: RIGEX Computer 13
Figure 3.1.4b: RIGEX Power Distributiuon Diagram 14
Figure 3.1.4c: CAPE/RIGEX Pigtail Cable Routing 15
Figure 3.1.4.1c: Luxeon LED 16
Figure 3.1.4.1d: Electrim EDC-100U Camera 17
Figure 3.1.5a: Inflation System Block Diagram 17
Figure 3.1.5b: Inflation System Components 18
Figure 3.1.5c: RIGEX Inflation System 19
Figure 3.3.1: CAPE/RIGEX Assembly 21

Appendices

Appendix A: RIGEX Hazard Reports

Points of Contact

RIGEX Payload Manager

Maj Matt Budde
NASA/JSC/WR1
(281) 483-7576

RIGEX Safety Engineers

Theresa Shaffer
MEI/JSC/WR1
(281) 483-8669

Darren Bromwell
SAIC/JSC/WR1
(281) 483-7552

RIGEX Integration Engineers

Scott Ritterhouse
MEI/JSC/WR1
(281) 483-3529

Carson Taylor
OSS/JSC/WR1
(281) 483-3491

STP Chief Engineer

Perry Ballard
NASA/JSC/WR1
(281) 483-3490

Aerospace Oversight

Jim McLeroy
Aero/JSC/WR1
(281) 483-3540

RIGEX Principle Investigator

Dr. Richard G. Cobb
Air Force Institute of Technology
Department of Aeronautics and Astronautics
(937) 785-3636 x4559

Acronym List

AFIT ..... Air Force Institute of Technology
APC ..... Adaptive Payload Carrier
AWG..... American Wire Gauge
C..... Celsius
CE ..... Cargo Element
CG..... Center-of-Gravity
COTS .... Commercial Off The Shelf
DC ..... Direct Current
DFMR.... Design For Minimum Risk
DoD ..... Department of Defense
EDC.....
EMC ..... Electromagnetic Compatibility
EMI..... Electromagnetic Interference
EVA ..... Extravehicular Activity
FCP ..... Fracture Control Plan
FCR..... Fracture Control Report
FOS..... Factor of Safety
GAS..... Get Away Special
GSE..... Ground Support Equipment
ICD ..... Interface Control Document
ISS ..... International Space Station
IVA ..... Intravehicular Activity
IVT..... Interface Verification Test
JOP ..... Joint Operations Panel
JSC ..... Johnson Space Center
KSC..... Kennedy Space Center
LED ..... Light Emitting Diode
MSVP .... Mechanical Systems Verification Plan
MSVR.... Mechanical Systems Verification Report
MSWG... Mechanical Systems Working Group
MUA ..... Materials Usage Agreement
NASA .... National Aeronautics Space Administration
NCR ..... Non-Compliance Report
NSTS..... National Space Transportation System
PLB ..... Payload Bay
PO ..... Payload Organization
PSRP .... Payload Safety Review Panel
PZT ..... Lead Zirconium Titanate
RIGEX ... Rigidizable Inflatable Get-Away-Special Experiment
SAIC ..... Science Application International Corporation
SPA ..... Small Payload Accommodations
SSP ..... Standard Switch Panel
STS ..... Space Transportation System
SVP ..... Structural Verification Plan
SVTL ..... Safety Verification Tracking Log
Tg ..... Glass Transition Temperature
TIM ..... Technical Interchange Meeting
TBD ..... To Be Determined
TBR ..... To Be Resolved
TBS ..... To Be Supplied
TVac..... Thermal Vacuum
V ..... Volt
VDC..... Voltage Direct Current

1 INTRODUCTION

1.1 Purpose

The purpose of this Phase II Payload Flight Safety Data Package is to document the applicability of the hazards, hazard causes, controls and verifications for the Rigidizable Inflatable Get-Away-Special Experiment (RIGEX) payload configuration. This flight safety assessment is based on safety requirements outlined in NSTS 1700.7B. The data presented in this document is based on the requirements for a Phase II Safety Review as detailed in NSTS/ISS 13830C.

1.2 Scope

This Payload Flight Safety Data Package provides independent validation that the RIGEX cargo element (CE) complies with all applicable STS safety requirements; and that RIGEX can be transported on the STS and operated in a safe manner using the Canister for All Payload Ejections (CAPE) mounted to a Space Shuttle Program provided Small Payload Accommodations (SPA) /Get Away Special (GAS) Beam. The intent of this document is to assess the RIGEX hardware and identify all hazards, hazard causes, controls and verifications, as necessary.

1.3 References

The following are compliance documents (current issue), which are related to the system design, testing, processing and operation of RIGEX.

a. ICD-2-19001, Shuttle Orbiter/Cargo Bay Standard Interfaces.

b. NSTS-21000-IDD-SML-Rev C, Small Payload Accommodation Interface Definition Document.

c. MSFC-HDBK-527/JSC 09604 or (MAPTIS), Materials Selection List for Space Hardware Systems.

d. NSTS 1700.7B, Safety Policy and Requirements for Payloads Using the Space Transportation System.

e. NASA-STD-6001, Flammability, Odor, Offgassing and Compatibility Requirements and Test Procedures for Materials in Environments that Support Combustion.

f. NASA-STD-5003, Fracture Control Requirements for Payloads Using the Space Shuttle.

g. NASA-STD-5001, Structure Design and Test Factors of Safety for Spaceflight Hardware.

h. NSTS/ISS 13830C, Payload Safety Review and Data Submittal Requirements.

i. NSTS 14046E, Payload Verification Requirements.

j. NSTS/ISS 18798, Interpretations of NSTS/ISS Payload Safety Requirements.

k. NSTS 22648, Flammability Configuration Analysis for Spacecraft Systems.

l. KHB 1700.7, Space Transportation System, Payload Ground Safety Requirements.

m. NASA-STD-3000, Man-System Integration Standards.

n. MSFC-STD-3029 - Guidelines for the Selection of Metallic Materials for Stress Corrosion Cracking Resistance.

o. MIL STD 461E, Department of Defense Interface Standard, Requirements for the Control of Electromagnetic Interference Characteristics of Subsystems and Equipment.

p. JSC 23642, Rev D, JSC Fastener Integrity Plan

q. SHI-ICC-M0001 - Rev B, Integrated Cargo Carrier Payload Standard Interface Definition Document

2 SAFETY CERTIFICATION

2.1 Safety Analysis Summary

The RIGEX hardware is new and has been reviewed for all applicable hazards and hazard causes. The CAPE hardware is reflight hardware. The reflight assessment of the CAPE is included in Section 7.

The hazard assessment has been conducted on the payload system and subsystem level. In addition, all interfaces have been assessed and the applicable hazards have been documented to ensure that the safety requirements established in NSTS 1700.7B have been met. The CAPE is a reusable launcher and will fly on STS-116 as part of the STP-H2 complement.

The RIGEX Flight Payload Standardized Hazard Report and the RIGEX Flight Unique Hazard Reports are located in Appendix A. There are no Reflight hazard reports being used for the RIGEX project. All hazard reports are being presented as "new".

2.2 Test Plan

The CAPE/RIGEX assembly will undergo an integrated vibration test to sidewall protoflight levels as outlined in the CAPE/RIGEX Structural Verification Plan (SVP). RIGEX hardware will undergo qualification and acceptance level environmental testing including thermal vacuum and subsystem random vibration. Additional testing will include sharp edge inspection of the CAPE/RIGEX assembly. Other tests not listed may also be performed per the SVP or the Fracture Control Plan (FCP). An Interface Verification Test (IVT) will be performed to ensure compatibility with Orbiter electrical systems.

2.3 Hazard Reports

Since the CAPE is a reusable payload carrier, hazard reports pertaining to the CAPE/payload assembly are noted as "CAPE" hazard reports. Hazard reports specific to the RIGEX payload are noted as "RIGEX" hazard reports.

2.4 Non-compliance Reports

There are no Non-compliance Reports (NCRs) associated with RIGEX.

2.5 Action Items and Agreements

From the Phase 0/I Flight Safety Review 14 Dec 2005:

3.1 The PO agreed to update the safety data packet to note that the high voltage sources are inaccessible.

> There are no high voltage sources in the CAPE/RIGEX assembly. The highest voltage is 28VDC +/- 4VDC from the Orbiter.

2.6 Operational Controls

There are no Operational Controls associated with RIGEX.

3 PAYLOAD OVERVIEW AND OBJECTIVES

RIGEX is a Cargo Bay Payload experiment exploring the use of inflatable and rigidizable structures for use on operational space systems. RIGEX is being developed by graduate students at the Air Force Institute of Technology (AFIT). RIGEX will be contained within the STP-provided CAPE which will be mounted to the Cargo Bay sidewall via the SPA/GAS Beam assembly. Integration of RIGEX into CAPE and of CAPE to the SPA/GAS Beam will be performed by STP.

RIGEX consists of inflatable tubes that become flexible when heated, expand with air pressure (supplied by the experiment), and then rigidize by cooling. RIGEX is a step in the development of inflatable, rigidizable space structures. Photographs from a 1-g tube deployment can be seen in Figure 3.

The Orbiter crew will initiate the experiment and one tube at a time will heat, inflate, cool/rigidize, and vent. Data and video will be collected and stored internally. Mechanical properties of the rigidized structure will be assessed by exciting each tube using piezoelectric patches mounted to the tubes to obtain modal characterization data.

RIGEX was originally developed to fly as a GAS payload. The design has been adapted for use with the CAPE canister. The original design was battery powered and had no interaction with the Orbiter systems other than to be powered on through the GAS interface.

Note: This experiment is contained within the CAPE canister for the duration of the shuttle mission and once initiated operates autonomously.

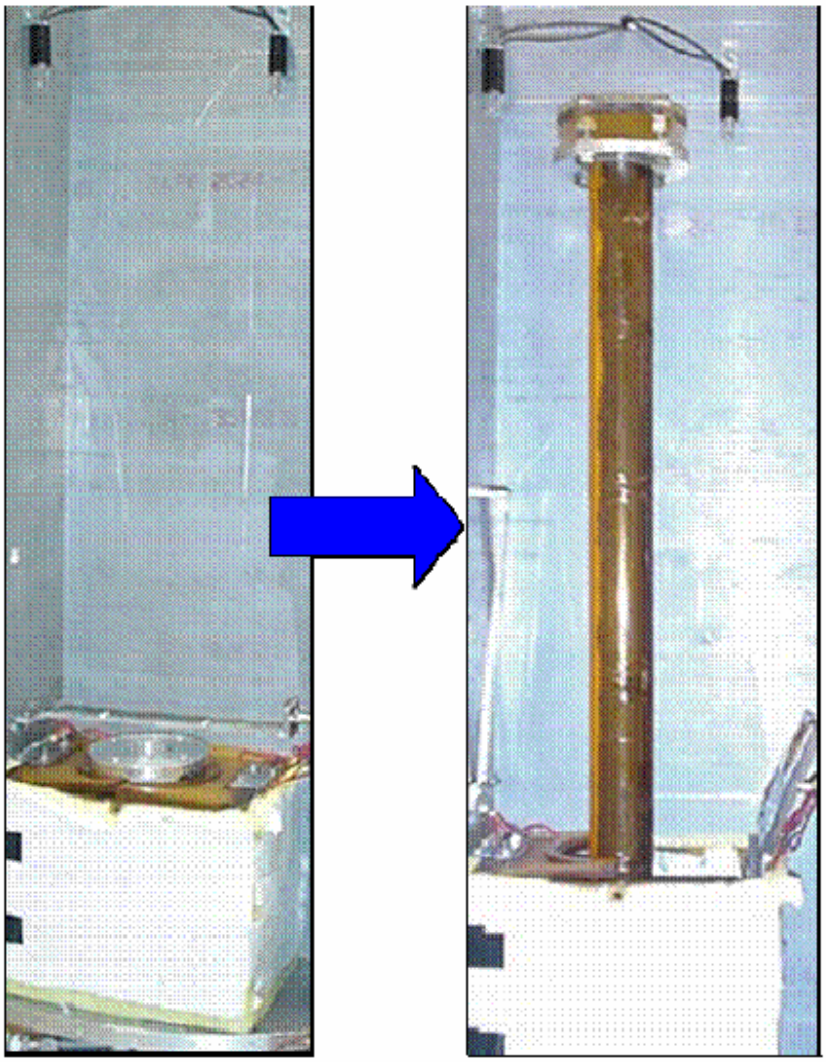

Figure 3: RIGEX Sub-Tg tube deployment in laboratory

3.1 RIGEX System Description

RIGEX consists of a the RIGEX primary structure, the CAPE Mounting Plate/Lid, the command and control computer, three inflatable tubes, three ovens, three inflation systems, and the necessary instrumentation to capture the experimental data. A picture of the RIGEX assembly showing components can be seen in Figure 3.1.

RIGEX consists of three inflatable tubes as well as heating, inflation, and data collection systems for each tube. The RIGEX tubes become flexible at a transition temperature of 125 °C, expand with gaseous nitrogen pressure (supplied by the experiment), rigidize by cooling, and are vented to obtain internal ambient pressure. After the Shuttle astronauts initiate the experiment computer, each tube in turn will be heated past its transition temperature, inflated, re-cooled to a structurally-stiff state, and vented. Environmental sensors

and cameras record the inflation and cooling process to verify proper deployment. After the tube is vented, a modal analysis using an excitation device (piezoelectric patch) at the cantilevered end of the tube will then be done to characterize the mechanical properties of the rigidized structure. During the excitation cycle, accelerometers mounted at the free end of the tube are used to collect data on its modal response. The entire process is repeated sequentially for each of the three tubes.

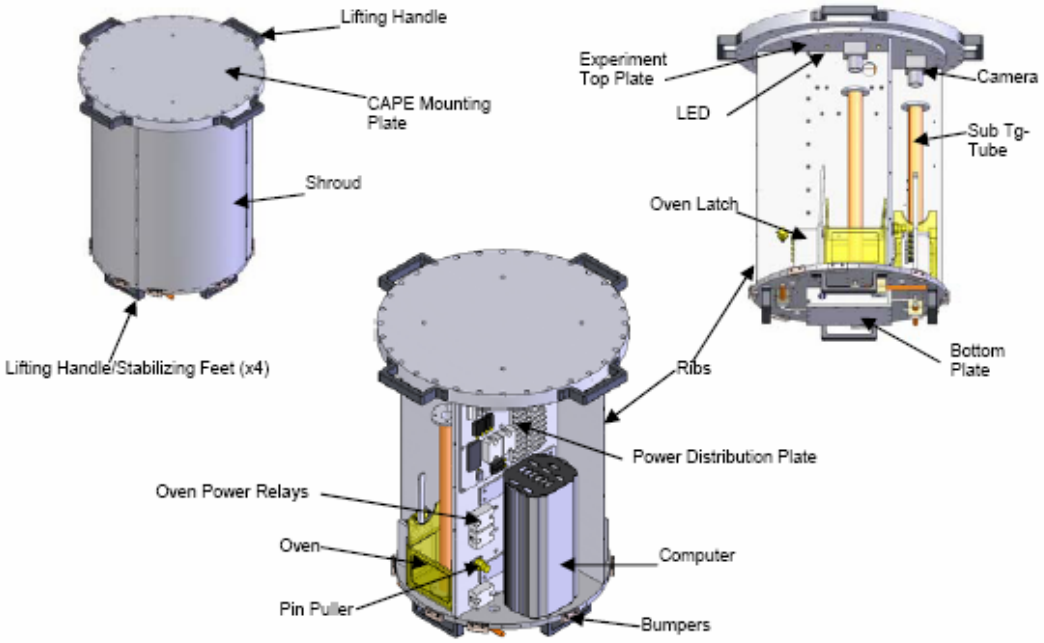

Figure 3.1: RIGEX Assembly

3.1.1 RIGEX Structure

The RIGEX structure was originally designed to fit in a GAS can. The interface has been modified to fly in the CAPE canister.

The RIGEX primary structure consists of a top and bottom plate and four vertical outside compartments surrounding an inner compartment as shown in Figure 3.1.1. The Top Plate and Oven Mounting Plate are 0.625" 6061-T6 aluminum. The remaining structural components are comprised of Al 6061-T6 plate of 0.375" thickness. The RIGEX Top Plate is held to the CAPE Mounting Plate by 28 3/8-24 NAS1189 Patchlock screws and the other structural components are held together by #10-32 NAS1189 Patchlock screws. Three of the outer compartments house an individual tube/oven assembly and the fourth outer compartment houses the avionics. The nitrogen gas storage cylinders are housed in the inner compartment.

In order to protect RIGEX during ground processing and protect the inner coating of the CAPE canister, a Shroud will enclose the outer diameter of RIGEX experiment from the top plate to the bottom plate. The Shroud is comprised of 0.075" 6061-T6 aluminum. The Shroud will be attached to the RIGEX structure

using 52 #8-32 NAS8402 screws with Heli-coil inserts. Soft bumpers of Delrin will be attached to the bottom plate of the RIGEX experiment in order to protect the CAPE inner coatings during ground processing. GSE handles are mounted to the CAPE Mounting Plate and the Oven Mounting Plate for ground operations and to provide a stable footing for RIGEX ground operations outside of the CAPE. Handles will be removed for flight.

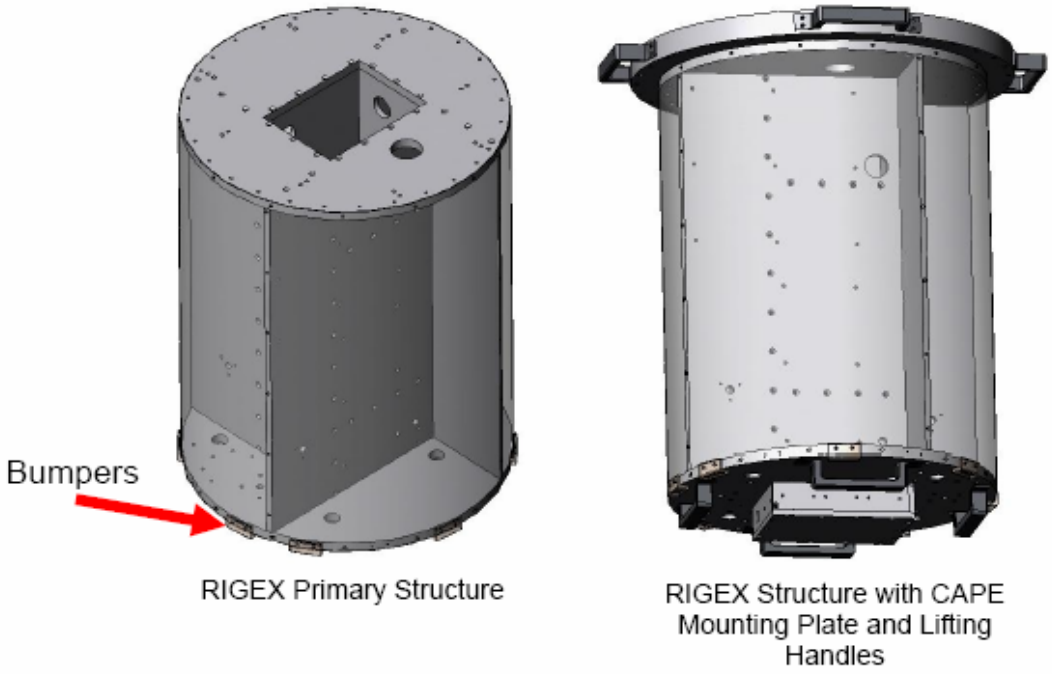

Figure 3.1.1: RIGEX Primary Structure

3.1.1.1 RIGEX interface to CAPE

RIGEX will be attached to the CAPE via the CAPE Mounting Plate which will also serve as the Lid. The CAPE Mounting Plate can be seen in Figure 3.1.1.1. The Mounting Plate will be attached to the CAPE via 32 1/4-28 NAS1352N4 bolts using locknuts for backout prevention. The mounting plate will be attached to the RIGEX Top Plate using 28 3/8-24 NAS1189 bolts using patchlock for backout prevention.

The CAPE Avionics Box will not be used for the RIGEX flight. RIGEX will provide two pigtails through an access port in the CAPE Mounting Plate. The cables will be attached to the CAPE Mounting Plate using P-clamps and will be constrained along one of the CAPE Cable Guides and Shear Plate.

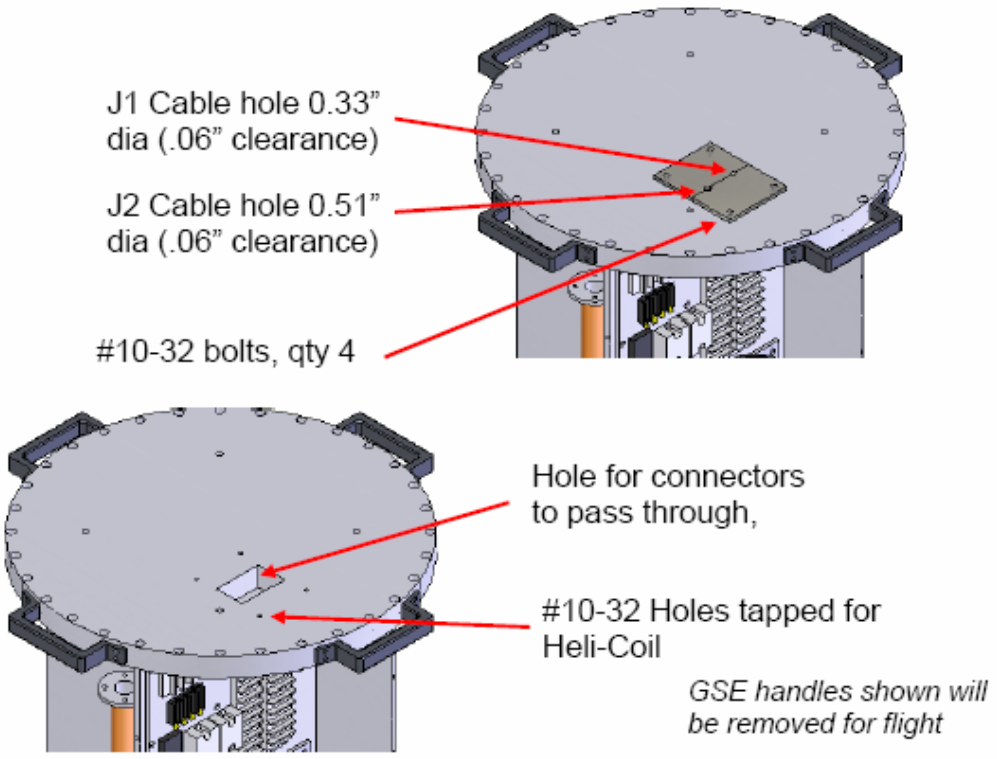

Figure 3.1.1.1: CAPE Mounting Plate

3.1.2 RIGEX Tube Assembly

The RIGEX tubes are referred to as "Sub-Tg" tubes due to their rigidity below the glass-transition temperature (Tg). The body of the tubes is composed of Kevlar fibers in a polyurethane resin and the entire tube is covered with Kapton tape. The tubes are 1.5 inches in diameter, 15 mils thick, and 20 inches long when deployed.

The tubes are capped with end caps machined from 6061-T6 Aluminum.

Two piezoelectric patches are attached 180 degrees apart at the base of each tube. These Lead Zirconium Titanate (PZT) patches were developed by Langley Research Center and are flying for the first time. After the tube has inflated, cooled and vented, the piezoelectric patches are excited to induce vibration which is recorded via a Kionix KXPA-4 accelerometer attached to the end cap.

The Sub-Tg tube components can be seen in Figure 3.1.2.

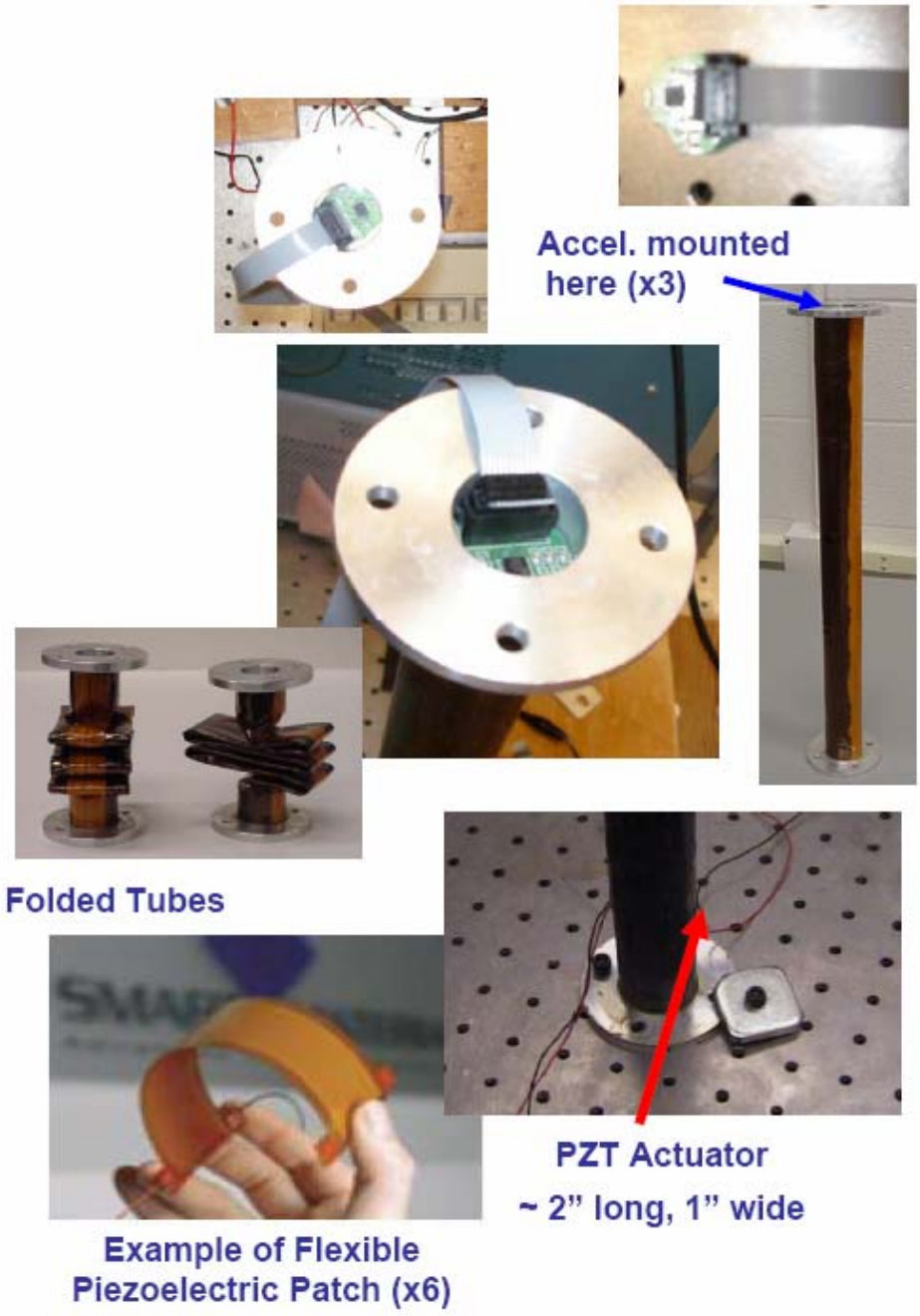

Figure 3.1.2: RIGEX Sub-Tg Tube Assembly Components

3.1.3 Oven/Heater Assembly

There are three oven/tube assemblies within the RIGEX experiment. Each oven is 5" tall, 4.25" wide, and 6" long. Each oven is made of .25" thick Ultem 1000 PEI Polyetherimide material, and contain eight foil-backed Minco resistive

heaters of various sizes to provide heat (flat black paint is applied to each heater in order to increase surface emissivity). Figure 3.1.3a shows a prototype oven without the experiment tube. Figure 3.1.3b shows the Minco heaters. Figure 3.1.3c shows an oven/tube prototype assembly.

Thermal analysis shows that one or two ovens can fail on without creating a hazard. Thermal-Vacuum (TVac) testing is planned to confirm the thermal analysis. If all three ovens were fail on, the 20 Amp fuse would blow.

Each oven has hinged doors which open in the middle to allow the expanding tube out of the oven assembly. The oven doors are held closed by the top of the tube assembly. The tube assembly is held in place by the door latch which is held closed by a shape-memory alloy pin puller developed at Glenn Research Center. Figure 3.1.3d shows the shape-memory pin-puller. Figure 3.1.3e shows the operation of the door latch. The door latch is not spring-loaded, it will be pushed out of the way by the expanding tube.

Oven insulation remains to be selected and will be selected from A-rated materials.

Oven with Doors Closed **Oven with Doors Open**

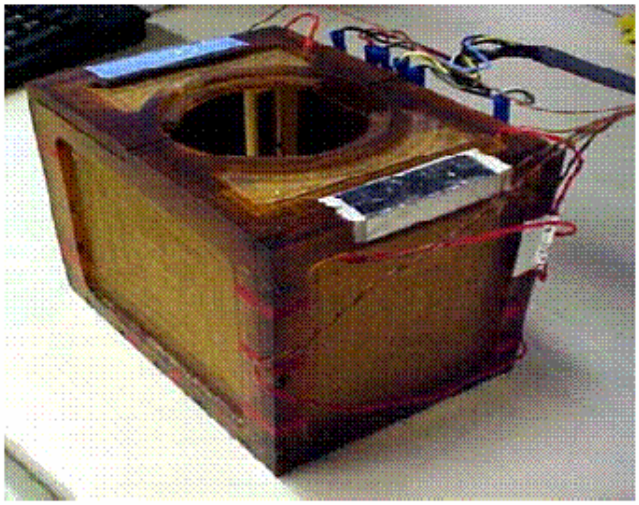

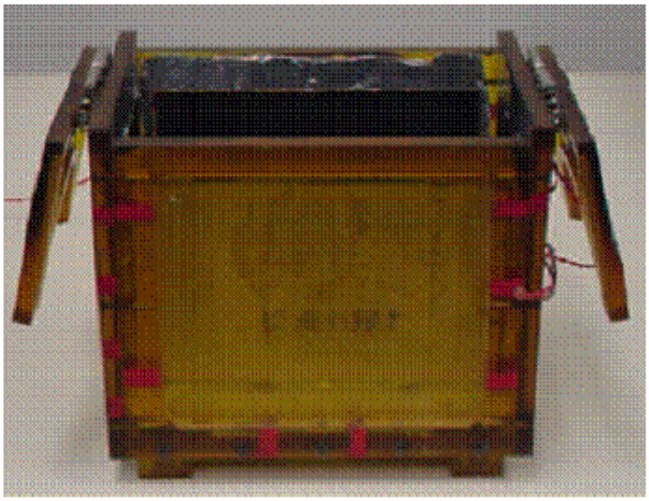

Note: Prototype oven shown without insulation

Figure 3.1.3a: RIGEX Prototype Oven

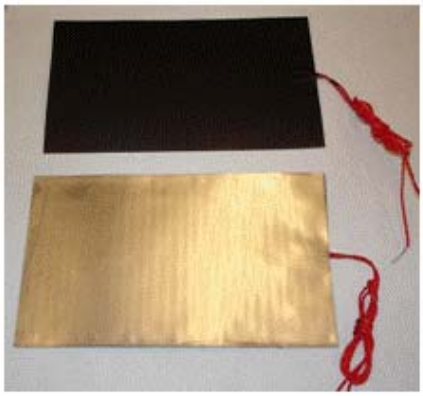

Figure 3.1.3b: Minco Heaters

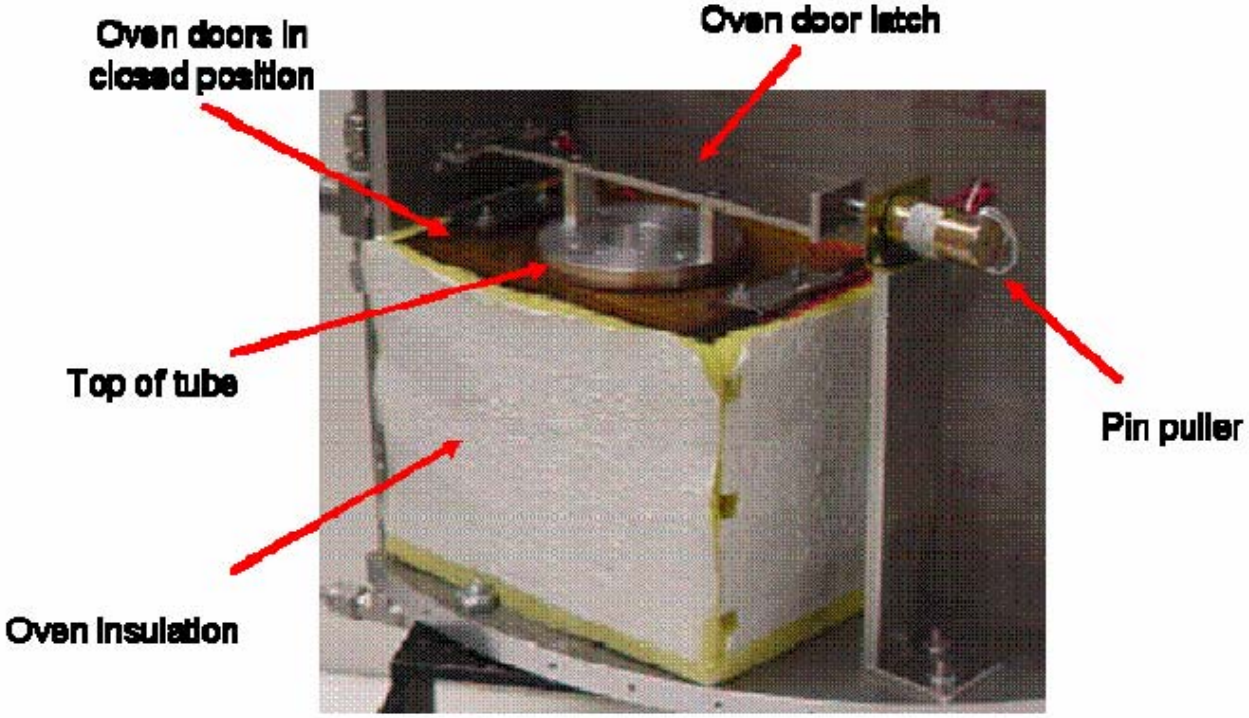

Figure 3.1.3c: RIGEX Prototype Oven/Tube Assembly

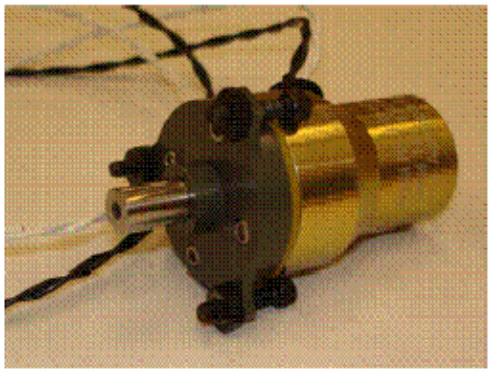

Figure 3.1.3d: Shape Memory Pin Puller

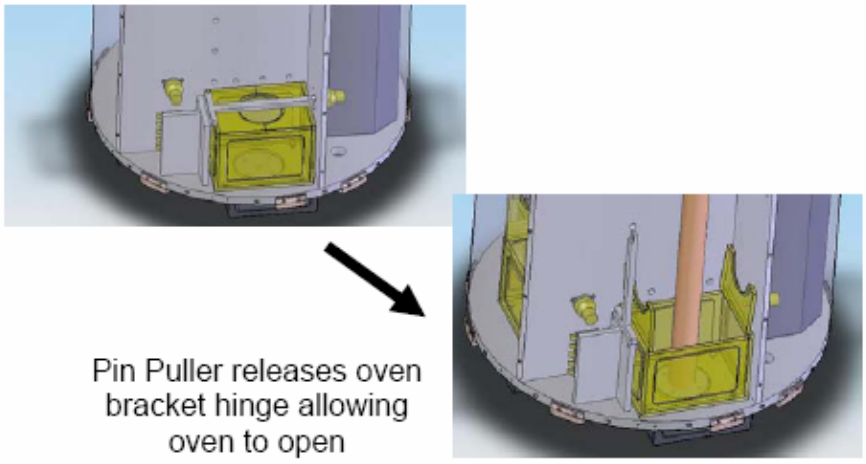

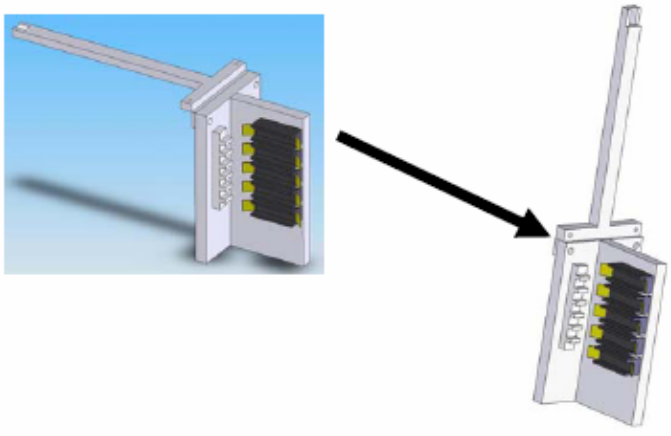

Figure 3.1.3e: Door Latch Operation

3.1.4 Avionics Assembly

RIGEX requires a 24-32 VDC power source. This power is fused and then routed to the experiment via four buses:

1) The Oven bus provides power through a 20 Amp fuse to the oven heaters. The oven heaters are activated via the RIGEX computer through solid state relay control.
2) The Control bus provides power through the Standard Switch Panel (SSP) S13 switch through through a 5 Amp fuse. Once flipped by the Orbiter Crew, this switch enables a return that is sent through the internal RIGEX EMI filter, which then enables the YCL Latching Relay and powers the experiment control system.
3) The Display bus provides power through a 2 Amp fuse to the SSP Display via the DS13 UP and DS13 DOWN relays. When initiated by the computer, these relays will send a signal to the orbiter that will trigger a DS13 UP or DOWN indication.
4) The Main Power bus provides power through a 6 Amp fuse and the EMI filter to the 3 PC-104 High Efficiency Power Supply Boards and the 6 pressure transducers.

Within the PC-104 Computer (Figure 3.1.4a), the Data Acquisition Computer (DAC) power supply board is the main power source for the experiment, while the Imaging Computer (IC) power supply board powers the imaging systems and the Solenoid power supply board provides the +24VDC required to activate the three inflation solenoids.. Both the DAC and IC power supply boards provide stepped down power of +/- 12VDC and +/- 5VDC to power other parts of the experiment.

Control Power will enter the computer through the power pigtail cable, and will be distributed through a harness to each experiment bay. For each of the three tube assemblies, there is one relay inside the computer that controls power to a solid state relay outside the computer, which in turn controls the power supplied to the heater assembly. Everything is provided with a common ground.

The RIGEX computer controls the experiment operation which includes the oven heaters, the tube inflation and venting, the data acquisition, the accelerometers, and the imaging system. The RIGEX provides notification through a SSP display (DS13) that the experiment is completed.

A power distribution diagram is shown in Figure 3.1.4b.

Two pigtail cables will be provided by RIGEX for connection with the Orbiter. The "Power" pigtail cable will terminate with a P501 connector. The "Switches and Displays" pigtail cable will split to the P103 connecting to SSP S13 and P108 connecting to SSP DS13.

Planned cable routing from the CAPE Mounting Plate to the Orbiter is illustrated in Figure 3.1.4c.

PC-104 Computer Boards
(14 boards)

Computer Housing

Figure 3.1.4a: RIGEX Computer

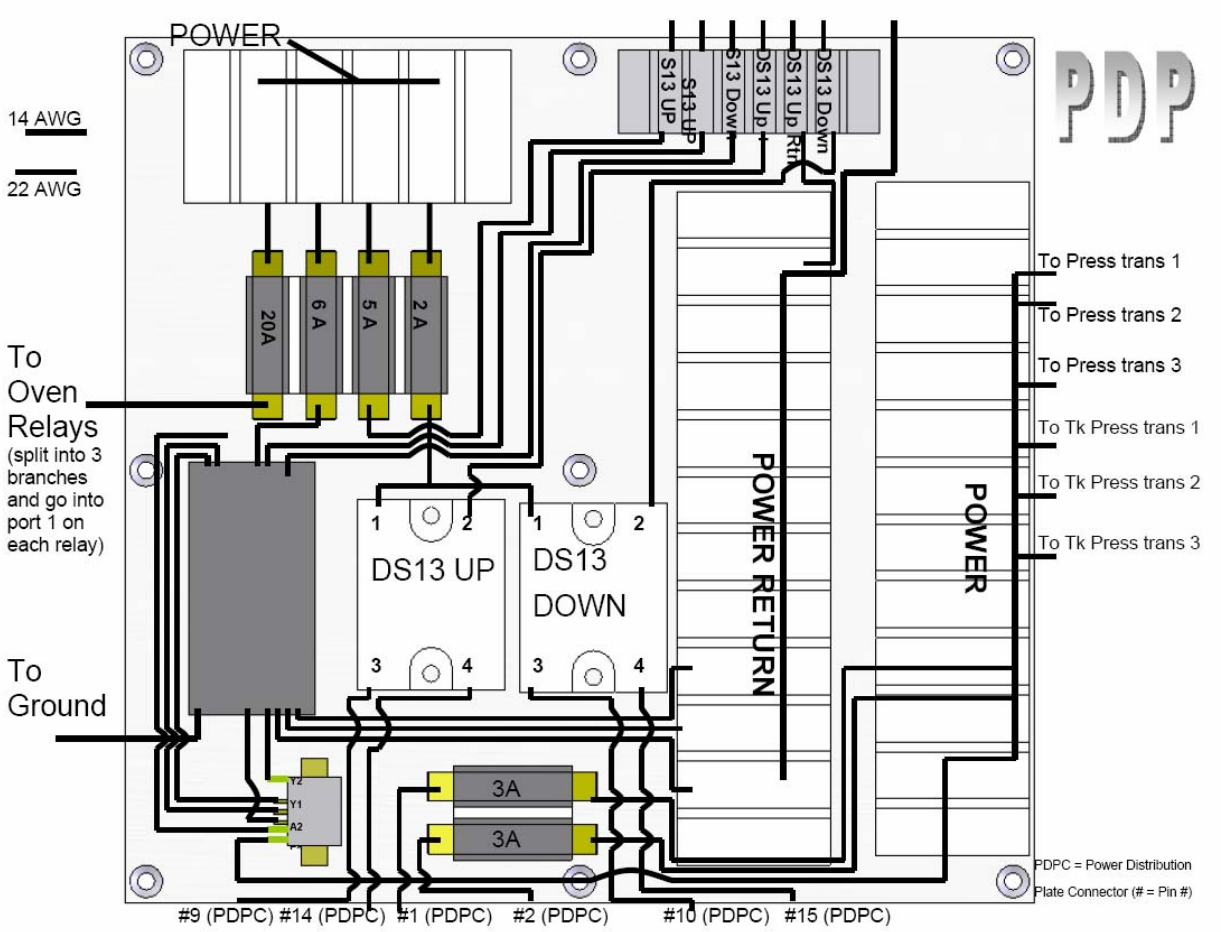

Figure 3.1.4b: RIGEX Power Distributiuon Diagram

Page 14

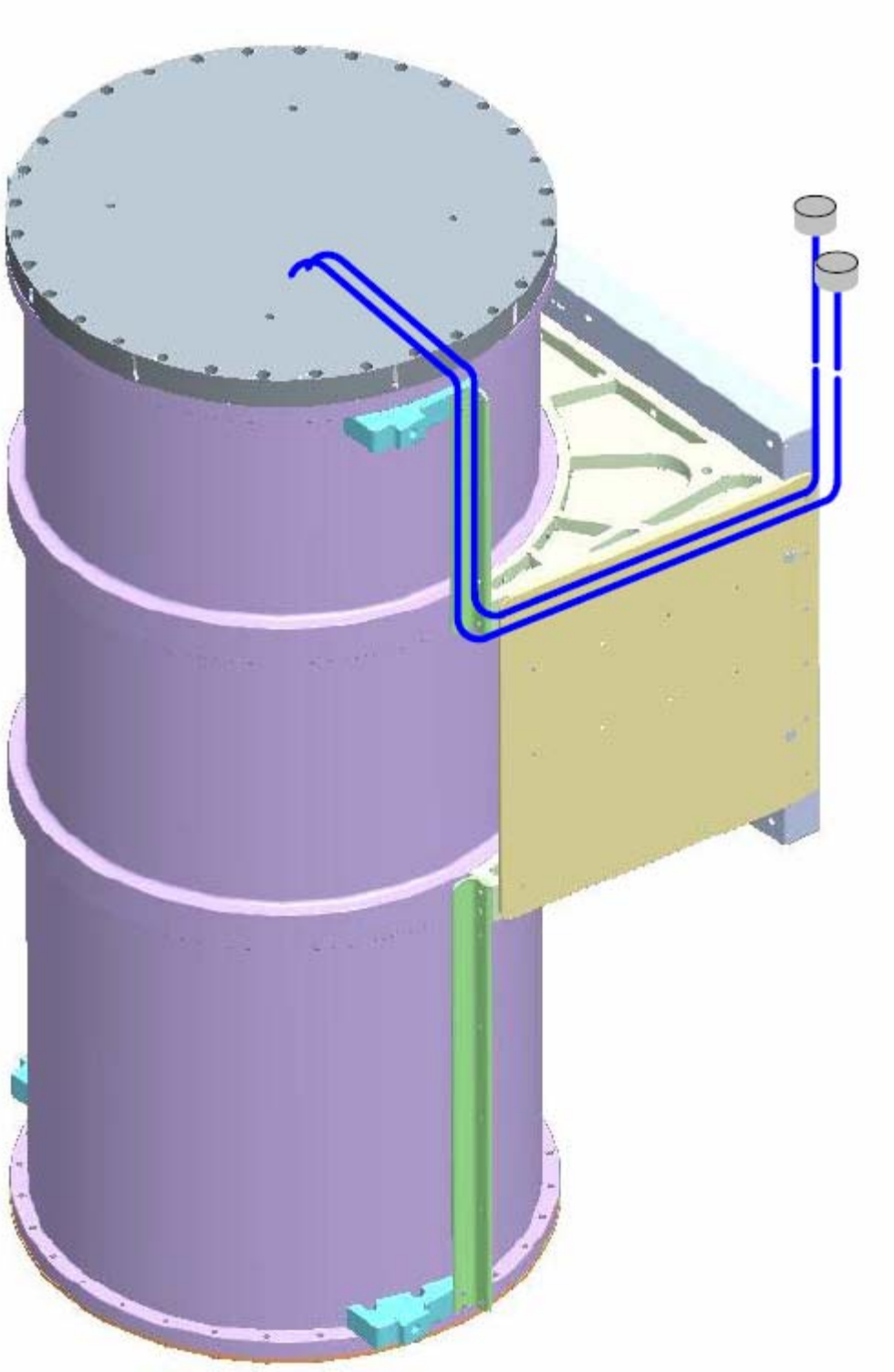

Figure 3.1.4c: CAPE/RIGEX Pigtail Cable Routing

3.1.4.1 RIGEX Internal Photography

Each of the three tube compartments will contain a digital camera and LED lighting to record the deployment experiment. The still images will be used to record the tube orientation. The cameras are Electrim cameras model EDC-100U with Kintronics Computar lenses (one lens is model EX2C and the other two are model M1614MP). The LED lights are Luxeon Model LXHL-L5WC and are shown in Figure 3.1.4.1c. The cameras are connected to the RIGEX avionics via a board supplied with the camera. The photos will be stored on the experiment in on the computer's hard drive and retrieved from the RIGEX computer during post-flight ground processing at AFIT. The Electrim camera can be seen in Figure 3.1.4.1d.

Figure 3.1.4.1c: Luxeon LED

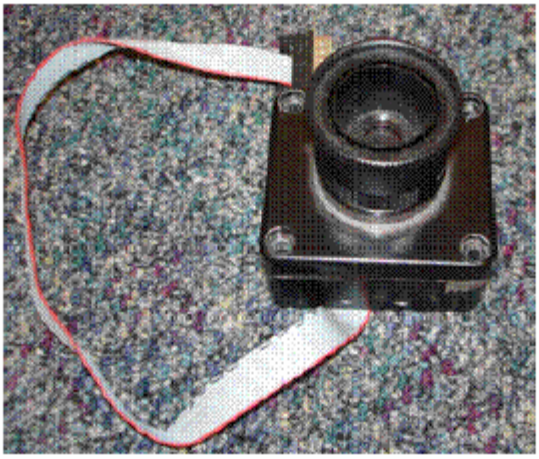

Figure 3.1.4.1d: Electrim EDC-100U Camera

3.1.5 Inflation System Assembly

In order to provide redundancy, each tube has its own inflation system. Each inflation system consists of a pressure cylinder, a solenoid valve (to control airflow into and out of the tube), a fill/purge valve (not shown in the block diagram), two pressure transducers (one to measure tank pressure and one to measure tube pressure), and tubing to connect each part. The bulk of each system lies in the center compartment of RIGEX, with just a small amount of tubing on the bottom to connect to the inflatable tubes. A block diagram of the inflation system is shown in Figure 3.1.5a. Key components of the inflation system are shown in Figure 3.1.3b. The physical configuration of the inflation system is shown in Figure 3.1.3c.

The RIGEX inflation system cylinders will be filled with nitrogen gas at 1 atmosphere (14.7 psia). On-orbit, worst case temperatures are estimated to be no higher than 74°C, which would result in a MDP of less than 18 psia.

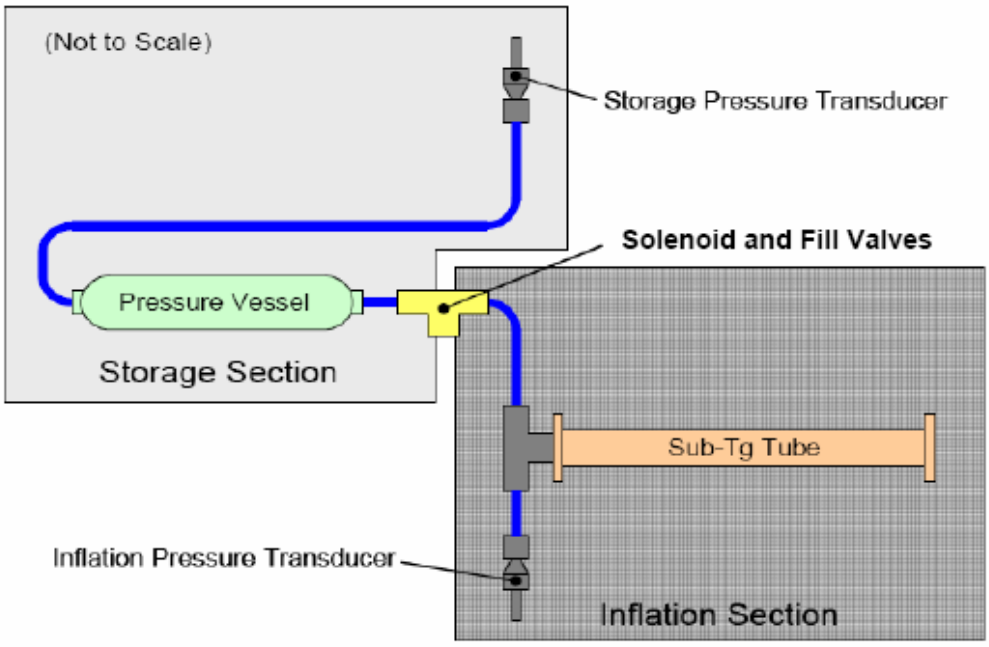

Figure 3.1.5a: Inflation System Block Diagram

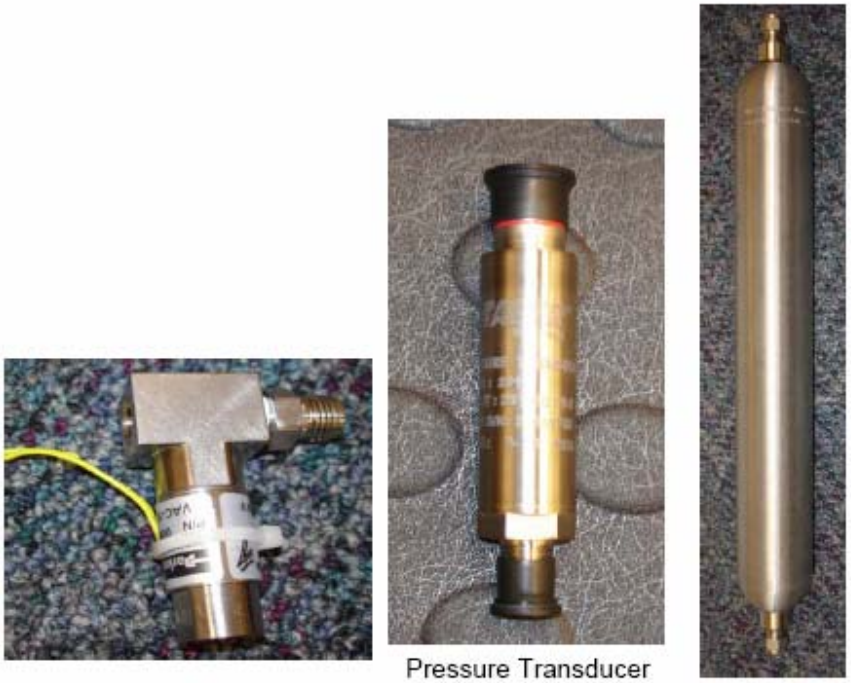

Solenoid Valve
(x3)

Pressure Transducer
(x6)

Inflation Cylinder
(x3)

Figure 3.1.5b: Inflation System Components

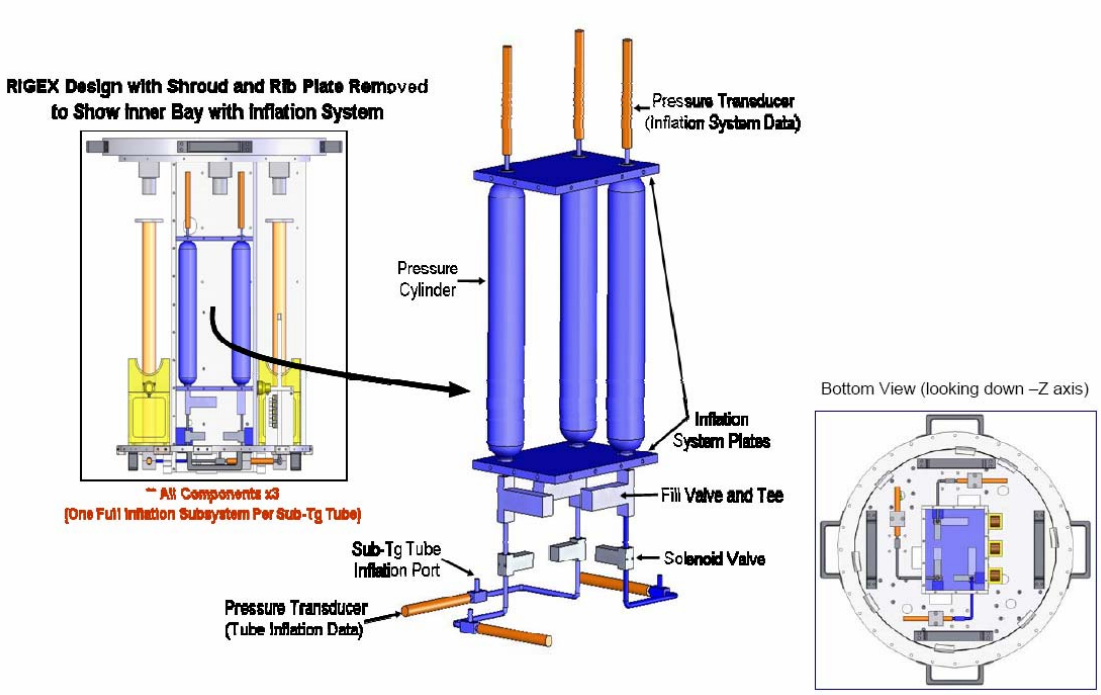

Figure 3.1.5c: RIGEX Inflation System

Page 19

3.1.6 Survival heaters (No Longer Used)

The survival heaters present in the Phase 0/I FSDP are no longer required. A computer board has been selected with a survival temperature range that will not require heaters.

3.2 Payload Control Parameters

The RIGEX Avionics Assembly (Section 3.1.3) is powered by the Orbiter 28-VDC via the Standard Switch Panel (SSP). The CAPE/RIGEX has a combined weight of 190 kg (420 lbs.) Max.

3.3 Orbiter/Payload Interfaces

The Orbiter/CAPE interfaces are structural and electrical.

3.3.1 Structural Interface

The CAPE will mount to a SPA/GAS Beam assembly that is mounted to the Orbiter sidewall via the CAPE SPA/GAS Beam Mounting Plate. The CAPE Assembly can be seen in Figure 3.3.1.

3.3.2 Electrical Interface

The RIGEX will be powered by the SSP via the RIGEX pigtails. The SSP will provide RIGEX avionics and experiment power, talkback to the crew that the experiment has received power and an indication when the experiment is completed.

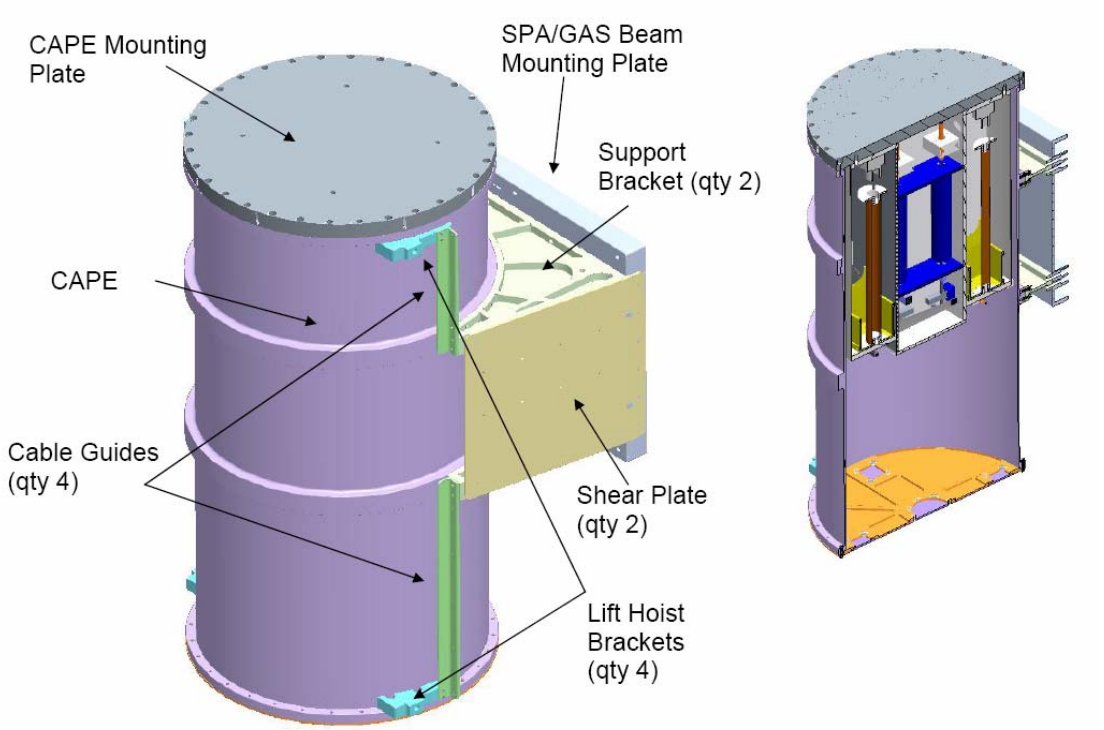

Figure 3.3.1: CAPE/RIGEX Assembly

4 Operational Requirements Overview

4.1 Pre-launch

The CAPE and RIGEX experiment will be delivered to KSC separately. Post delivery checkout operations include unpacking the CAPE and RIGEX, functional verification of the RIGEX, and installation of the RIGEX inside the CAPE. Filling of the inflation gas cylinders is planned to be performed prior to shipping from AFIT. Once the hardware is mounted in the payload bay, an IVT will be performed. After the IVT, no other pre-launch activities are required. All KSC ground operations will comply with KHB 1700.7.

4.2 On-Orbit

RIGEX will be initiated via the SSP. After the RIGEX computer boots, the SSP display will transition from Stripes to Up and then to Down after approximately 380 seconds and then after approximately 360 seconds will go back to the Up position. The sequence of events is driven by the need to verify all interfaces during the Orbiter IVT. Operations within the RIGEX experiment are autonomous once power is applied. Since RIGEX science during inflation and vibration are sensitive to external loads, the PO has requested minimal Orbiter thruster burns during RIGEX operation.

RIGEX will send a talkback to the crew via the SSP Down display that the experiment is complete. At this time, or after a maximum time of TBD, the crew may remove all power from the RIGEX via the SSP switch.

4.3 Post-flight

After landing, the CAPE/RIGEX hardware will be removed from the orbiter, during standard deintegration processing, and turned over to the appropriate payload representative.

4.4 Aborted Flight

After the orbiter is returned to KSC, the CAPE/RIGEX hardware will be removed from the orbiter and turned over to the appropriate payload representative.

5 Procedures

At the appropriate time in the timeline, the crew will activate the RIGEX via the SSP. Operations within the RIGEX experiment are autonomous once power is applied. RIGEX science during inflation and vibration are sensitive to external loads, so the PO has requested minimal Orbiter thruster burns during the RIGEX experiment.

RIGEX will send a talkback to the crew via the SSP Down display that the experiment is complete. At this time, or after a maximum time of TBD, the crew may remove all power from the RIGEX via the SSP switch.

6 Failure/Accident Record

There are no failures or accidents associated with the CAPE/RIGEX hardware.

7 NSTS 13830C Reflight Safety Assessment

The CAPE hardware for this mission has been evaluated as reflight hardware in accordance with NSTS 1700.7B Paragraph 216. The statuses of all the safety verifications from the baseline CAPE hazard reports from the STP-H2 Flight Safety Data Package for STS-116 were reviewed. The following paragraphs provide all of the information required by NSTS/ISS 13830C, and follow the general template established in Section 9 (a through n) for reflight payload data.

a. The baseline safety analysis for the CAPE hardware is part of the STP-H2 Complement analysis for STS-116. The CAPE reflight hardware consists of: The CAPE Canister (which includes 4 Cable Guides, 4 Lift Hoist Brackets, and an End Cap), the Support Brackets (2), the GAS Beam Mounting Plate, and the Shear Plates (2).

b. The proposed use of all reflown CAPE payload elements for CAPE/RIGEX remains the same as what was approved for the previous CAPE mission (STP-H2) with the exception that STP-H2 was mounted on ICC via the STP-H2 wedge, and CAPE/RIGEX will be mounted on the sidewall via the SPA/GAS beam.

c. The only applicable hazard reports from the STP-H2 use of CAPE on STS-116 are the Standard Hazard Report, STD-CAPE-01, and the structural hazard report, CAPE-02. These were adapted for the RIGEX payload and presented at the Phase I Safety Review as STD-RIGEX-F01 and CAPE-F07, respectively.

d. There are no previously baselined hazard reports being used for the RIGEX project.

e. A CAPE/RIGEX Safety Verification Tracking Log (SVTL) will be provided in the CAPE/RIGEX Phase III FSDP.

f. The are no CAPE noncompliance reports.

g. There are no limited life items in CAPE.

h. The CAPE reflight hardware will be visually inspected and refurbished if necessary. A CAPE/RIGEX integrated random vibration test will be performed to sidewall protoflight levels.

i. The CAPE hardware has not experienced in-flight or ground anomalies.

j. There are no pyrotechnic initiators with the CAPE hardware.

k. CAPE does not contain any sources of ionizing radiation.

l. The CAPE hardware is scheduled to fly on STS-116 as part of the STP-H2 Complement.

m. Not Applicable.

n. A Flight Certificate of NSTS/ISS Payload Safety Compliance will be provided at Phase III.

8 Summary of Flight Safety Analysis

RIGEX as mounted in the CAPE Canister in the Payload Bay has been assessed for hazards related to inadvertent activation. No credible hazard has been found as result of the experiment inadvertently activating. As such, no fault tolerance to inadvertent activation has been provided. One SSP switch and associated display has been requested from the shuttle program.

Talkback display to the crew, indicating that the experiment has begun, is provided for the convenience of the crew. Talkback display to the crew that the experiment is complete is provided to prevent premature deactivation of the experiment since the exact duration will depend on the temperature conditions in the payload bay during experiment operations and cannot be accurately predicted prior to the mission.

8.1 Structural Failure

An integrated CAPE/RIGEX structural failure hazard report, CAPE-F07, is provided in Appendix A.

8.1.1 CAPE Structure

The CAPE structure was designed in accordance with NSTS 14046 to a FOS of at least 1.25 times the limit loading on yield and 1.4 on ultimate. Limit loads will consist of combined loads including thermal and other environmental effects.

CAPE was designed in accordance with NASA-STD-5003 for fracture control. Structural materials were selected in accordance with MSFC-STD-3029, Table 1.

The CAPE was designed to withstand differential pressure during ascent and descent. A venting analysis will be performed to assure all compartments are adequately vented.

CAPE Fasteners meet the applicable Military Specifications and will be traceable to manufacturer's lot testing. Fastener back-off prevention (Military Standard MS21209 helical inserts, NAS1805 lock nuts, or NAS1791 nut plates) were used on CAPE safety critical fasteners. Fasteners have been selected in accordance with the JSC fastener integrity plan.

8.1.2 RIGEX Structure

The RIGEX structure will be designed in accordance with NSTS 14046 to a FOS of at least 1.25 times the limit loading on yield and 1.4 on ultimate. Limit loads will consist of combined loads including thermal and other environmental effects.

The RIGEX will be designed to withstand differential pressure during ascent and descent. A venting analysis will be performed to assure all compartments are adequately vented.

RIGEX will be designed in accordance with NASA-STD-5003 for fracture control. Structural materials will be selected in accordance with MSFC-STD-3029, Table 1, or a Materials Usage Agreement (MUA) will be submitted.

RIGEX will be completely contained within the CAPE and the CAPE Mounting Plate for the duration of the mission. Fasteners have been selected in accordance with the JSC fastener integrity plan. Lock nuts will be used as back-out prevention for the CAPE/CAPE Mounting Plate fasteners.

Note: The Sub-Tg tubes are not expected to survive re-entry. The tubes are expected to collapse, but not come apart, allowing the tube end caps to bounce around but remain attached to the tube. A punch equation has been performed to verify the tube end caps will be contained by the RIGEX shroud.

8.2 Sealed Containers/Pressurized Systems

The RIGEX inflation system has a very low delta-pressure. With the exception that the system has multiple components, it would qualify as a "sealed container" per NASA-STD-5003. The gas is non-hazardous (nitrogen), all components (except the Sub-Tg tubes) are made from metal alloys typically used for sealed containers, the system is pressurized to less than 1.5 atmospheres at worst-case environmental conditions. All components meet the Factor of Safety Requirements defined in NSTS 1700.7b, Par. 208.4c.

The Sub-Tg tubes cannot be shown to have FOS. Containment by the RIGEX structure will be shown. Intuitively, the tubes should leak-before-burst, but it is not possible to rigorously verify by analysis or test.

The Inflation System is addressed in the unique hazard report RIGEX-F02, located in Appendix A.

8.3 EVA Hazards

8.3.1 Touch Temperature

The CAPE/RIGEX payload will meet the EVA touch temperature requirements of NSTS 07700 Volume XIV, Appendix 7. This hazard is addressed on the RIGEX Flight Payload Standardized Hazard Control Report, STD-RIGEX-F01, located in Appendix A.

8.3.2 Sharp Edges, Corners, Protrusions

The CAPE/RIGEX payload will meet the intent of the sharp edge requirements of NSTS 07700 Vol. XIV, App. 7. All crew accessible areas will be designed and inspected to verify compliance with the human factors requirements in NASA-STD-3000. This hazard is addressed on the RIGEX Flight Payload Standardized Hazard Control Report, STD-RIGEX-F01, located in Appendix A.

8.4 Shatterable Material Release

There are no shatterable materials on the exterior of the CAPE/RIGEX assembly.

The RIGEX cameras have glass lenses, but are contained within the RIGEX/shroud assembly which in turn is contained within the CAPE/RIGEX mounting lid assembly. This hazard is addressed on the RIGEX Flight Payload Standard Hazard Report, STD-RIGEX-F01, located in Appendix A.

The RIGEX experiment tubes are not shatterable. They are comprised of Kevlar fibers is a polyurethane resin, encapsulated in Kapton tape. The RIGEX experiment is illuminated by LEDs which have Lexan covers and are non-shatterable.

8.5 Flammable Materials

The CAPE/RIGEX payload materials will be selected to meet the flammability requirements as outlined in MSFC-HDBK-527/JSC 09604 or MAPTIS. An MUA will be generated if non-A-rated materials are used. The materials list and MUA, if necessary, will be submitted to JSC Materials Branch for review and approval. This hazard is addressed on the RIGEX Flight Payload Standardized Hazard Control Report, STD-RIGEX-F01, located in Appendix A.

8.6 Nonionizing Radiation

The CAPE/RIGEX payload will meet the EMI/EMC requirements of ICD-2-19001, 10.7.3.2.2. RIGEX will be tested in accordance with JSC 27743. The EMI/EMC test results will be submitted to JSC EEECTP for review and approval. This hazard is addressed on the RIGEX Flight Payload Standardized Hazard Control Report, STD-RIGEX-F01, located in Appendix A.

8.7 Electrical Power Distribution

The CAPE/RIGEX will meet the wire sizing and circuit protection requirements of NSTS/ISS 18798, Interpretation Letter TA-92-038. This hazard is addressed on the RIGEX Flight Payload Standardized Hazard Control Report, STD-RIGEX-F01, located in Appendix A.

The RIGEX avionics will be powered via a pair of pigtails through an access port in the CAPE Mounting Plate/Lid. The cables will be attached to the CAPE Mounting Plate using P-clamps and will be constrained along one of the CAPE Cable Guides and Shear Plate. The CAPE Avionics Box will not be used for the RIGEX flight.

8.8 Ignition of Flammable Atmospheres in Payload Bay

The RIGEX will be unpowered during launch and landing.

8.9 Mechanisms

There are no safety critical mechanisms in the CAPE/RIGEX assembly. All operations are contained within the CAPE/RIGEX structure.

Bibliography

1. Bickford, John H. *An Introduction to the Design and Behavior of Bolted Joints, 3rd Edition*. New York: Marcel Dekker, Inc., 1995.

2. Boeing. "STS-114, ISS-LF1, MPLM, ESP2, LMC OV-103, Discovery Flight 31". http://www.boeing.com/defense-space/space/returntoflight/sts-114/images/cargobay.gif

3. Boeing North American, Inc. Reusable Space Systems. *Space Flight Operations Contract: Shuttle Orbiter/Small Payload Accommodation Interfaces.* NSTS-21000-IDD-SML. Revision C. United Space Alliance, 19 February 1998.

4. Bong, Duane. "Finite Element Analysis," *VisionEngineer – Finite Element Analysis*. 27 January 2004. http://www.visionengineer.com/mech/tools_fea.shtml.

5. *Container for All Payload Ejections (CAPE) Hardware Users Guide (CHUG).* DoD Shuttle/ISS Payload Support Contract. Johnson Space Center, Houston: Muniz Engineering, Inc., 10 March 2003.

6. Bromwell, Darren. *Canister for All Payload Ejections/Internal Cargo Unit (ICU) Structural Verification Plan.* CAPE-SVP-0002. Revision D. DoD Shuttle/ISS Human Spaceflight Payloads. Johnson Space Center, Houston, December 2005.

7. Cook, Robert D., David S. Malkus, Michael E. Plesha, and Robert J. Witt. *Concepts and Applications of Finite Element Analysis* (Fourth Edition). New York: John Wiley & Sons, Inc., 2002.

8. Department of Defense. *Military Handbook 5H (MIL-HDBK-5H)*. December 1998.

9. Department of Defense. *Fastener Element, Self-Locking, Threaded Fastener, 250F Maximum*. Mil-F-18240E. 1 December 1989.

10. DiSebastian, John D., Captain, USAF. *RIGEX: Preliminary Design of a Rigidizable Inflatable Get-Away-Special Experiment*. Master's Thesis, Air Force Institute of Technology (AFIT), Wright-Patterson AFB OH, March 2001.

11. Engineering Fundamentals. Unified Screw Threads – UNF Fine. *http://www.efunda.com/designstandards/screws/screwunf.cfm*

12. *FEMAP v9.0 User's Guide.* Plano TX: UGS Corporation, 2004.

13. Freeland, R. E., G. D. Bilyeu, G. R. Veal, and M. M. Mikulas. "Inflatable Deployable Space Structures Technology Summary." http://www.lgarde.com/people/papers/iaf-98-I501.pdf.

14. Gamblin, Charles R. *Spacecraft Structural Analysis Today and Yesterday*. Huntsville AL: Teledyne Brown Engineering.

15. Goodwin, Jeremy S., Captain, USAF. *Detailed Design of the Rigidizable Inflatable Get-Away-Special Experiment*. Master's Thesis, Air Force Institute of Technology (AFIT), Wright-Patterson AFB OH, March 2006.

16. Heli-Coil Inc. *Heli-Coil Screw Lock Torque Data*. Shelton CT: Emhart Teknologies.

17. Helms, Sarah K., 2nd Lieutenant, USAF. *Development and Testing of an Inflatable, Rigidizable Space Structure Experiment*. Master's Thesis, Air Force Institute of Technology (AFIT), Wright-Patterson AFB OH, March 2006.

18. Holstein III, Raymond G., Captain, USAF. *Structural Design and Analysis of a Rigidizable Space Shuttle Experiment*. Master's Thesis, Air Force Institute of Technology (AFIT), Wright-Patterson AFB OH, March 2004.

19. Huang, John, Houfei Fang, Richard Lovick, and Michael Lou. "The Development of Large Flat Inflatable Antenna for Deep-Space Communications." *AIAA 2004-6112. American Institute of Aeronautics and Astronautics, Inc. Space 2004 Conference and Exhibit*. San Diego CA, 28-30 September 2004.

20. Kendall, Randy. "EELV: The Next Stage of Space Launch". *The Aerospace Crosslink*. http://www.aero.org/publications/crosslink/winter2004/07.html

21. Lichodziejewski, David, Gordon Veal, and Billy Derbes. "Spiral Wrapped Aluminum Laminate Rigidization Technology." AIAA 2002-1701. *American Institute of Aeronautics and Astronautics, Inc*. 2002.

22. Lindemuth, Steven N., Captain, USAF. *Characterization and Ground Test of an Inflatable Rigidizable Space Experiment*. Master's Thesis, Air Force Institute of Technology (AFIT), Wright-Patterson AFB OH, March 2004.

23. Liu, Thomas. Chief Engineer, Field Emission Get Away Special Investigation, Student Space Systems Fabrication Laboratory, University of Michigan. Electronic Correspondence. 29 June 2006.

24. Moeller, Chad R., Captain, USAF. *Design and Ground-Testing of an Inflatable-Rigidizable Structure Experiment in Preparation for Space Flight*. Master's

Thesis, Air Force Institute of Technology (AFIT), Wright-Patterson AFB OH, June 2005.

25. Moody, David C., 1st. Lieutenant, USAF. *Microprocessor-Based Systems Control for the Rigidized Inflatable Get-Away Special Experiment*. Master's thesis, Air Force Institute of Technology (AFIT), Wright-Patterson AFB OH, March 2004.

26. National Aerospace Standards Committee. *Screw, Machine, Washer Head, Full Thread, Phillips Recess, A286 CRES*. NAS 8402 thru 8404. Aerospace Industries Association of America, Inc. 1988.

27. National Aerospace Standards Committee. *Screw, Cap, Socket Head Undrilled and Drilled, Plain and Self-Locking Alloy Steel, Corrosion-Resistant Steel and Heat-Resistant Steel, UNRF-3A*. NAS 1351. Aerospace Industries Association of America, Inc. 1998.

28. National Aerospace Standards Committee. *Screw, Cap, Socket Head Undrilled and Drilled, Plain and Self-Locking Alloy Steel, Corrosion-Resistant Steel and Heat-Resistant Steel, UNRC-3A and UNRC-2A*. NAS 1352. Aerospace Industries Association of America, Inc. 1998.

29. National Aerospace Standards Committee. *Screw, Self-Locking, Flat 100 Deg Head, Full Thread*. NAS 1189. Aerospace Industries Association of America, Inc. 2003.

30. National Aeronautics and Space Administration. *JSC Fastener Integrity Testing Program*. JSC 23642 Revision D. Houston: Lyndon B. Johnson Space Center, 26 January 2000.

31. National Aeronautics and Space Administration. *Load Analyses of Spacecraft and Payloads.* NASA-STD-5002. Marshall Space Flight Center Alabama, 21 June 1996.

32. National Aeronautics and Space Administration. *Space Shuttle Criteria for Preloaded Bolts*. NSTS 08307 Rev. A Space Shuttle Program. Houston: Lyndon B. Johnson Space Center, 6 July 1998.

33. National Aeronautics and Space Administration. *Saturn*. N66-82740. Marshall Space Flight Center. http://ntrs.nasa.gov/archive/nasa/casi.ntrs.nasa.gov/19660083255_1966083255.pdf

34. National Aeronautics and Space Administration. *SSP 52005 Revision C*, December 2002.

35. National Aeronautics and Space Administration. *Torque Limits for Standard, Threaded Fasteners*. MSFC-STS-486B. Marshall Space Flight Center, November 1992.

36. Naval Research Laboratory. "Project ANDE Assembly and Testing Nears Completion at NRL for Fall Delivery to NASA". http://www.nrl.navy.mil/pao/pressRelease.php?Y=2005&R=22-05r. 12 May 2005.

37. Philley, Thomas Lee, 1st Lieutenant, USAF. *Development, Fabrication, and Ground Test of an Inflatable Structure Space-Flight Experiment*. Master's thesis, Air Force Institute of Technology (AFIT), Wright-Patterson AFB OH, March 2003.

38. Popov, E.P. *Mechanics of Materials*. Prentice-Hall, 1958.

39. SAE Aerospace. *Screw Threads – UNJ Profile, Inch Controlled Radius Root with Increased Minor Diameter*. AS8879. SAE International, August 2004.

40. Shaffer, Theresa M. *Phase II Safety Data Package*. August 2006.

41. Sakoda, Daniel. The Petite Amateur Navy Satellite (PANSAT) Hitchhiker Ejectable. Monterey CA: Naval Postgraduate School, 1995

42. Single, Thomas G., Captain, USAF. Experimental Vibration Analysis of Inflatable Beams for an AFIT Space Shuttle Experiment. Master's thesis, Air Force Institute of Technology (AFIT), Wright-Patterson AFB OH, March 2002.

43. University of Michigan. *NASA Small Self-Contained Program Getaway Special G-187 Preliminary Structural Verification Document*. 26 July 2003.

44. University of Michigan. *Field Emission Get-Away-Special Investigation*. Student Space Systems Fabrication Laboratory. http://data.engin.umich.edu/s3fl/fegi/

45. University of Missouri. *Introduction to Mechanics and Finite Element Analysis*. http://campus.umr.edu/mfge/ugumrmfge/FEMwebpage/Projecta.htm

46. VORTEX Project Team. *Get Away Special Payload G-093: The Vortex Ring Transit Experiment (VORTEX) Flights*. University of Michigan Students for the Exploration and Development of Space.

47. VORTEX Project Team. *NASA Self-Contained Payload Program Get Away Special G-093 Structural Verification Document*. University of Michigan. 4 August 1997.

48. Welsh, J.S. and Sanford, G.E. "EELV Secondary Payload Adapter Static Qualification Tests". *Experimental Techniques*. January/February 2004.

Vita

Second Lieutenant Anna Gunn-Golkin graduated from Cherry Hill High School West in Cherry Hill New Jersey in June 2001. One week later, she entered undergraduate studies at the United States Air Force Academy. While at the Academy, she was a member of the 24th and 25th Cadet Squadrons as well as an exchange cadet serving in Delta Company at the United States Coast Guard Academy. At the Academy, she flew the TG-10B as a Formal Training Unit Instructor Pilot for the 94th Flying Training Squadron and commanded the Instructor Upgrade Program. She was commissioned and graduated with military distinction and a Bachelor of Science degree in Astronautical Engineering in June 2005.

In September 2005, Lt. Gunn-Golkin entered the Air Force Institute of Technology's Graduate School of Engineering and Management in pursuit of her Master of Science degree in Astronautical Engineering. Her studies include specialty sequences in structures and advanced astrodynamics. After graduation in September 2006, she will be assigned to the 1st Air and Space Test Squadron at Vandenberg Air Force Base, California.

REPORT DOCUMENTATION PAGE

Form Approved
OMB No. 074-0188

1. REPORT DATE *(DD-MM-YYYY)*	**2. REPORT TYPE**	**3. DATES COVERED** *(From – To)*
14-09-2006	**Master's Thesis**	Sept 2005 – Sept 2006

4. TITLE AND SUBTITLE

Structural Analysis of the Rigidizable Inflatable Get-Away-Special Experiment

5a. CONTRACT NUMBER

5b. GRANT NUMBER

5c. PROGRAM ELEMENT NUMBER

6. AUTHOR(S)

Anna E. Gunn-Golkin, Second Lieutenant, USAF

5d. PROJECT NUMBER

5e. TASK NUMBER

5f. WORK UNIT NUMBER

7. PERFORMING ORGANIZATION NAMES(S) AND ADDRESS(S)

Air Force Institute of Technology
Graduate School of Engineering and Management (AFIT/EN)
2950 Hobson Way
WPAFB OH 45433-7765

8. PERFORMING ORGANIZATION REPORT NUMBER

AFIT/GA/ENY/06-S01

9. SPONSORING/MONITORING AGENCY NAME(S) AND ADDRESS(ES)

N/A

10. SPONSOR/MONITOR'S ACRONYM(S)

11. SPONSOR/MONITOR'S REPORT NUMBER(S)

12. DISTRIBUTION/AVAILABILITY STATEMENT

APPROVED FOR PUBLIC RELEASE; DISTRIBUTION UNLIMITED.

13. SUPPLEMENTARY NOTES

14. ABSTRACT

The purpose of this research was to validate the structural integrity of the Rigidizable Inflatable Get-Away-Special Experiment (RIGEX) and make appropriate improvements to the design, motivated by static and dynamic analysis results. RIGEX is designed to advance the use of rigidizable inflatable structures in the space environment by providing three sets of on-orbit test data on the structural characteristics of three thermoplastic composite tubes. This thesis discusses the RIGEX structural analysis. The term structural analysis refers to the development of a detailed finite element model and the tests for which the model was used. The finite element model provided an acceptable estimation of RIGEX's natural frequencies, the structural integrity of the fastener system, the maximum stress seen by the aluminum primary structure, and the maximum possible displacements at various locations around the RIGEX structure for various load conditions. These three analyses motivated numerous design changes, which are discussed in detail in this thesis. The analysis process was repeated following each design change until all structural integrity and design criteria were met. In addition to the structural analysis and associated design changes, this thesis presents the *as built* RIGEX drawing package and wiring schematic.

The results presented in this thesis are the first step towards passing the structural integrity requirements set forth by the National Aeronautics and Space Administration (NASA) for manned spaceflight. Recommendations of appropriate construction and testing techniques to ensure the actual structure matches the computer model are discussed.

15. SUBJECT TERMS

Inflatable Structures, Space Systems, Space Shuttle Payload, Rigidizable Structures, Bolt Analysis, Fastener Analysis, Finite Element Analysis, Structural Strength Verification, Structural Analysis, Canister for All Payload Ejections, Get-Away-Special

16. SECURITY CLASSIFICATION OF:			**17. LIMITATION OF ABSTRACT**	**18. NUMBER OF PAGES**	**19a. NAME OF RESPONSIBLE PERSON**
REPORT	**ABSTRACT**	**c. THIS PAGE**			Richard G. Cobb, PhD, AFIT/ENY
U	**U**	**U**	**UU**	237	**19b. TELEPHONE NUMBER** *(Include area code)* (937) 255-3636, ext 4559; e-mail: Richard.Cobb@afit.edu